

Patient-Prosthesis Interaction: Control through the Healthy Leg

DOCTORAL THESIS

submitted in partial fulfillment of the requirements for the degree of

Doktor der Technischen Wissenschaften (Dr. techn.)

in

Doctoral Program in Natural Science Electrical Engineering

by

Michael Tschiedel

Registration Number 01326357

to the

Faculty of Electrical Engineering and Information Technology at the TU Wien

Advisor: Dipl.-Ing. Michael Friedrich Russold, PhD, MBA
Ao.Univ.Prof. Dipl.-Ing. Dr.techn. Eugenijus Kaniusas

Vienna, 22.02.2022

Michael Tschiedel



Die approbierte gedruckte Originalversion dieser Dissertation ist an der TU Wien Bibliothek verfügbar.
The approved original version of this doctoral thesis is available in print at TU Wien Bibliothek.

Patienten-Prothesen Interaktion: Steuerung durch das gesunde Bein

DISSERTATION

zur Erlangung des akademischen Grades

Doktor der Technischen Wissenschaften (Dr. techn.)

im Rahmen des Studiums

Doktoratsstudium der Technischen Wissenschaften Elektrotechnik

eingereicht von

Michael Tschiedel

Matrikelnummer 01326357

an der

Fakultät für Elektrotechnik und Informationstechnik der Technischen Universität Wien

Betreuer: Dipl.-Ing. Michael Friedrich Russold, PhD, MBA
Ao.Univ.Prof. Dipl.-Ing. Dr.techn. Eugenijus Kaniusas

Wien, 22.02.2022

Michael Tschiedel



Die approbierte gedruckte Originalversion dieser Dissertation ist an der TU Wien Bibliothek verfügbar.
The approved original version of this doctoral thesis is available in print at TU Wien Bibliothek.

Erklärung zur Verfassung der Arbeit

Michael Tschiedel
1200 Wien, Österreich

Hiermit erkläre ich, dass ich diese Arbeit selbständig verfasst habe, dass ich die verwendeten Quellen und Hilfsmittel vollständig angegeben habe und dass ich die Stellen der Arbeit - einschließlich Tabellen, Karten und Abbildungen -, die anderen Werken oder dem Internet im Wortlaut oder dem Sinn nach entnommen sind, auf jeden Fall unter Angabe der Quelle als Entlehnung kenntlich gemacht habe.

(Ort, Datum)

(Unterschrift Verfasser)



Die approbierte gedruckte Originalversion dieser Dissertation ist an der TU Wien Bibliothek verfügbar.
The approved original version of this doctoral thesis is available in print at TU Wien Bibliothek.

“Education isn’t something you can finish.”
-Isaac Asimov-



Die approbierte gedruckte Originalversion dieser Dissertation ist an der TU Wien Bibliothek verfügbar.
The approved original version of this doctoral thesis is available in print at TU Wien Bibliothek.

Abstract

The loss of a lower limb is an irreversible and traumatic event in the life of the affected person. Although modern prostheses can restore the function of the missing body parts to a high extent, commercial state-of-the-art lower limb devices neither measure nor incorporate environmental information for intent recognition or for device control. This inevitably leads to the problem that the patient adapts to the behavior of the prosthesis rather than the system to the amputees' needs. Unphysiological gait patterns and increased compensatory movements are just some of the known consequences.

This thesis offers a concept for improving patient-prosthesis interaction. The device control is enhanced by measuring and evaluating the position of the unimpaired residual contralateral leg. This leads to an even more lifelike replication of the physiological gait pattern.

First, an extensive literature survey was conducted to find out which modalities of environmental sensors are already being used and how they improve the control of lower limb prostheses. During this review, five control approaches were identified, as to how “next generation prostheses” could be optimized. Overall, there is a clear trend towards more upcoming terrain or object estimation, with the basic idea of delivering switching probabilities between different activities. Most relevant to this work, however, was the conclusion that even a single sound-leg measurement can significantly reduce the error rate in detecting the amputees' intent correctly.

Based on these findings, a first depth camera-based system was developed. This contralateral limb tracking (CoLiTrack) approach, combines a single depth camera with an inertial measurement unit, both mounted on the ipsilateral leg, which is able to estimate the shank axis of the contralateral side. Initially, the scene captured by the camera was transformed into a stabilized world coordinate system. In order to achieve real-time performance, the subsequent shank-estimation process was split into two less computationally intensive steps: First, circular models were fitted against 2D projections of the input using the iterative closest point algorithm. Second, the final shank axis was determined by applying the random sample consensus method. In three experiments, data from five able-bodied subjects was evaluated. The results demonstrated a trackability of the shank axis over one sixth of the entire human gait cycle for dynamic situations.

In order to overcome the limitations of the previous depth camera-based approach, a second contralateral limb ranging (CoLiRang) system was developed. Using four novel ultrasonic time-of-flight sensors on the ipsilateral leg, the position of the other contralateral leg was estimated.

ABSTRACT

Initially, each sensor measured the respective distances to the contralateral side. These distances were then triangulated to determine the directional information of the other leg. In order to evaluate the system as a whole, several tests were performed and experiments with two healthy participants were conducted. The results showed a mean triangulation deviation of less than 30 mm and a divergence in detecting the moment of passing even below 1° . Most importantly, this novel approach was able to track the state of the other leg correctly in dynamic situations throughout the entire human gait cycle.

Finally, the ultrasonic-based concept was integrated into an enhanced seeing prosthesis (SEP) system. For the first time, it was possible to control the damping behavior, walking resistance of the device, via the state of the patient's unimpaired contralateral residual leg in real time. In order to evaluate the novel system, a prospective pilot clinical study was designed, approved, and conducted with five transfemoral amputees. Closed-loop optimization sessions were conducted first, followed by a clinical biomechanical gait analysis with each participant. The results revealed a more physiological gait pattern and a distinct facilitation of the remaining musculoskeletal system for yielding activities. In particular, the interception on the contralateral healthy leg was reduced on average by about 25% for going down the ramp and even by about 40% for the staircase task, respectively.

This work has demonstrated that environmental sensing technologies can successfully improve the patient-prosthesis interaction. Taking these findings into account for further development, prostheses of the next generation would be able to truly adapt to patients' needs.

Kurzfassung

Der Verlust einer unteren Extremität ist ein irreversibles und traumatisches Ereignis im Leben des Betroffenen. Moderne Prothesen ersetzen die fehlenden Körperfunktionen bereits weitgehend, jedoch verwenden derartige kommerzielle Systeme nach dem Stand der Technik ausschließlich interne Messwerte und Systemparameter, um die Bewegungsintention ermitteln und die Prothese entsprechend steuern zu können. Dies führt allerdings zwangsläufig zu der Problematik, dass sich die Patienten an das Prothesenverhalten anpassen und nicht die Systeme an die Bedürfnisse der Amputierten. Unphysiologische Gangmuster und verstärkte kompensatorische Bewegungen sind nur einige der bekannten Folgen davon.

Diese Arbeit bietet ein Konzept zur Verbesserung der Patienten-Prothesen-Interaktion. Durch die Messung und Auswertung der Position des gesunden kontralateralen Beines wird die Gerätesteuerung verbessert und dadurch eine noch naturgetreuere Nachbildung des physiologischen Gangbildes erreicht.

Um den Forschungsfortschritt der letzten Jahre zu ermitteln, wurde in einem ersten Schritt eine detaillierte Literaturrecherche durchgeführt. Ziel war es dabei herauszufinden, welche Umgebungssensoren bereits zur Anwendung kommen und wie deren Signale zur Erweiterung der bestehenden Prothesensteuerungen verwendet werden. Anhand der gewonnenen Erkenntnisse wurden fünf Steuerungsansätze ermittelt, wie "zukünftige Prothesen" erweitert werden könnten. Insgesamt zeigt sich ein deutlicher Trend hin zu Systemen für Gelände- oder Objekterkennung mit der Grundidee, eine Wahrscheinlichkeit für einen möglichen Terrainübergang frühzeitig abzuschätzen. Maßgeblich für den Erfolg dieser Arbeit war die Erkenntnis, dass bereits die Messung eines einzelnen kontralateralen Beinparameters die Fehlerrate der korrekten Erkennung der Anwenderintention signifikant reduzieren kann.

Basierend auf diesen Erkenntnissen wurde ein erstes tiefenkamerabasiertes System entwickelt. Das System namens CoLiTrack kombiniert eine Tiefenkamera mit einer inertialen Messeinheit, beide angebracht auf dem einen ipsilateralen Bein, um die Achse des anderen kontralateralen Unterschenkels zu schätzen. Initial wurde die von der Kamera erfasste Szene in ein stabilisiertes Weltkoordinatensystem transformiert. Durch die Zerlegung des nachfolgenden Achsenermittlungsverfahrens in zwei weniger rechenintensive Abschnitte wurde die Verarbeitungszeit deutlich reduziert: Hierbei wurden zuerst kreisförmige Modelle mithilfe des Iterative Closest Point Algorithmus an 2D-Projektionen aus dem Tiefenbild angenähert und dann mittels des Random Sample Consensus Verfahren die endgültige Beinachse ermittelt. Insgesamt wurden drei Experimente

KURZFASSUNG

mit fünf gesunden Probanden durchgeführt. Die Resultate haben gezeigt, dass die entwickelte Methode in dynamischen Situationen die kontralaterale Unterschenkelachse über ein Sechstel des gesamten menschlichen Gangzyklus hinweg korrekt verfolgen kann.

Um die Limitierungen des vorherigen tiefenkamerabasierten Ansatzes zu überwinden, wurde ein zweites System namens CoLiRang entwickelt. Mittels vier neuartiger Ultraschalllaufzeit-Sensormodule auf dem ipsilateralen Bein wird die Position des anderen kontralateralen Beines geschätzt. Initial wird mit jedem Sensor der Abstand zur kontralateralen Seite gemessen. Durch die nachfolgende Triangulation der gewonnenen Entfernungen wurde auch die Richtungsinformation des anderen Beins abgeleitet. Zur Beurteilung des Gesamtsystems wurden verschiedene Untersuchungen sowie Experimente mit zwei gesunden Probanden durchgeführt. Die Resultate haben gezeigt, dass die entwickelte Methode in dynamischen Situationen den Zustand des anderen Beines über den gesamten menschlichen Gangzyklus hinweg korrekt verfolgen kann, wobei insbesondere die korrekte Erkennung des Zeitpunktes des Vorbeischwingens von Relevanz ist.

Schließlich wurde das ultraschallbasierte Konzept in ein verbessertes Prothesensystem namens SEP integriert. Dies ermöglichte es erstmalig, das Dämpfungsverhalten, den Gehwiderstand des Geräts, in Echtzeit über den Zustand des gesunden kontralateralen Beines des Patienten zu steuern. Um das neuartige System mit fünf Oberschenkelamputierten zu evaluieren, wurde eine klinische Pilotstudie konzipiert, genehmigt und durchgeführt. Zunächst wurden mehrere Optimierungsmessungen des geschlossenen Regelkreises durchgeführt und nachfolgend alle Probanden einer klinischen Gang- und Bewegungsanalyse unterzogen. Die Ergebnisse zeigten besonders beim Hinabgehen einer Rampe oder einer Stiege ein physiologischeres Gangbild und eine Entlastung des übrigen Bewegungsapparates. Insbesondere das Abfangen auf dem kontralateralen gesunden Bein war deutlich reduziert.

Diese Arbeit hat gezeigt, dass moderne Umgebungssensoren die Patienten-Prothesen-Interaktion grundlegend verbessern können. Unter Berücksichtigung diese Erkenntnisse bei zukünftigen Entwicklungen, würden sich Prothesen der nächsten Generation tatsächlich an die Bedürfnisse der Patienten anpassen.

Acknowledgements

My special thanks go first and foremost to my university supervisor, **Prof. Eugenijus Kaniusas**, and to my boss at Ottobock, **Dr. Friedrich Russold**, for teaching me *how to become a researcher* and *how to ask the right questions*.

Furthermore, I would like to express my gratitude for being able to work in a world-leading company for the past few years. Without the pleasant and fruitful cooperation with all **my colleagues**, this work would not have been possible at all. Special thanks go to ANNA MEIXNER, DIRK SEIFERT & SVEN ZARLING: Without their efforts, the prosthesis integration and control improvement would have been impossible. I would like to thank ANDREAS BOHLAND, CHRISTOPH ZAHALKA & WOLFGANG SAUBERER for our valuable technical discussions, ROLAND AUBERGER, RICHARD WOODWARD & THOMAS PICKERILL for challenging and reviewing my work, and FABIAN OSSWALD & RAPHAEL SCHEFFEL for manufacturing the prosthetic test fittings. The clinical pilot study would not have been possible without the support from my colleagues JOHANNES ZAJC & EUGENIA SCHWARZKOPF and our clinical partner ANDREAS KRANZL with his team from the *Orthopädisches Spital Speising*.

I also want to thank **my friends** for giving me the courage and emotional support over the last years. The good memories we share always help me to get back on track when I struggle.

Last, but by no means least, my deepest gratitude goes to **my family** for supporting me in any decision of my life and for always standing behind me, no matter what happens.

This dissertation is produced in cooperation with *Otto Bock Healthcare Products GmbH* in Vienna and partially funded by the *Austrian Research Promotion Agency (FFG)* program “Industriennahe Dissertationen”.



Die approbierte gedruckte Originalversion dieser Dissertation ist an der TU Wien Bibliothek verfügbar.
The approved original version of this doctoral thesis is available in print at TU Wien Bibliothek.

Contents

1	Introduction	1
1.1	Lower Limb Prosthetics	1
1.1.1	Loss of the Lower Limbs	1
1.1.2	Modern Lower Limb Protheses	3
1.1.3	Control of Lower Limb Protheses	7
1.2	Environmental Sensing Technologies	9
1.2.1	Physical Foundations	9
1.2.2	Time-of-Flight Principle	13
1.3	Aim of Work	17
2	Methods	19
2.1	Current State of Research	19
2.1.1	Snowballing on Reference	20
2.1.2	Systematic Database Search	20
2.2	Depth Camera-based Contralateral Limb Tracking	22
2.2.1	System Overview	22
2.2.2	Image-Processing Chain	24
2.2.3	Experimental Plan	28
2.3	Ultrasonic-based Contralateral Limb Ranging	31
2.3.1	System Overview	31
2.3.2	Signal-Processing Chain	34
2.3.3	Experimental Plan	38
2.4	Enhanced Prosthesis Control System	43
2.4.1	System Integration	43
2.4.2	Clinical Pilot Study	46
2.4.3	Experimental Plan	48
3	Results	53
3.1	Current State of Research	53
3.1.1	Implicit Environmental Sensing	53
3.1.2	Explicit Environmental Sensing	56

CONTENTS

3.2	Open-Loop Depth Camera Tracking	60
3.2.1	Static Evaluation	60
3.2.2	Dynamic Evaluation	62
3.2.3	Real-World Evaluation	64
3.3	Open-Loop Ultrasonic Ranging	65
3.3.1	Static Evaluation	65
3.3.2	Behavior Simulation	68
3.3.3	Dynamic Evaluation	71
3.4	Closed-Loop Prosthesis System	74
3.4.1	Optimized Parameters	74
3.4.2	Biomechanical Analysis	75
3.4.3	Satisfaction Questionnaire	104
4	Discussion	107
4.1	Current State of Research	107
4.1.1	Control Strategy Landscape	107
4.1.2	Development Considerations	110
4.2	Open-Loop Depth Camera Tracking	113
4.2.1	Advantages	113
4.2.2	Limitations	114
4.2.3	Future Work	114
4.3	Open-Loop Ultrasonic Ranging	116
4.3.1	Advantages	116
4.3.2	Limitations	117
4.3.3	Future Work	117
4.4	Closed-Loop Prosthesis System	119
4.4.1	Advantages	119
4.4.2	Limitations	120
4.4.3	Future Work	120
5	Conclusion	123
	Appendix	127
Publication A	RELYING ON MORE SENSE FOR ENHANCING LOWER LIMB PROSTHESES CONTROL: A REVIEW	127
Publication B	REAL-TIME LIMB TRACKING IN SINGLE DEPTH IMAGES BASED ON CIRCLE MATCHING AND LINE FITTING	141
	Author's Publications	153
	List of References	155

Acronyms

ADC	A nalog-to- D igital C onverter
aMPK	a ctive M icro P rocessor-controlled K nee
CMOS	C omplementary M etal- O xide- S emiconductor
COM	C OMmunication port
CoLiRang	C ontralateral L imb R anging (using sonar sensors)
CoLiTrack	C ontralateral L imb T racking (using a depth camera)
DSP	D igital S ignal P rocessor
EMG	E lectro M yo G raphy
EES	E xplicit E nvironmental S ensing
EV	E xtension V alve (of hydraulic damper unit)
FV	F lexion V alve (of hydraulic damper unit)
GONIO	G ONIOmeter
I²C	I nter- I ntegrated C ircuit
ICP	I terative C losest P oint
IES	I mplicit E nvironmental S ensing
IMU	I nertial M easurement U nit
LIDAR	L Ight D etection A nd R anging
MEMS	M icro- E lectro- M echanical S ystem
MPK	M icro P rocessor-controlled K nee

ACRONYMS

pMPK	passive MicroProcessor-controlled Knee
RANSAC	RANdom SAmples Consensus
RADAR	RAdio Direction And Ranging
RX	Receiver
SEP	SEeing Prosthesis (using sonar sensors)
TOF	Time Of Flight
TX	Transmitter

Introduction

The aim of this chapter is to provide the necessary background knowledge for this thesis. First, an introduction into *Lower Limb Prosthetics* is given. Next, main concepts of *Environmental Sensing Technologies* are introduced, followed by a final section defining the *Aim of Work*.

1.1 Lower Limb Prosthetics

1.1.1 Loss of the Lower Limbs

The amputation of a limb is an irreversible intervention into the physical and psychological integrity of a human being. This event fundamentally changes the life of amputees in terms of their perception by others, their independence and also with regards to their occupational life. Furthermore, studies have shown a high risk of death [1] or reamputation [2]. Moreover, approximately 30% of amputees are affected by depression [3]. Therefore, an amputation should always be the last option, when conservative therapies are no longer applicable.

Prevalence. In general, it is difficult to determine the number of amputees because most countries do not keep a central register of amputations. Especially for the United States of America, where health insurance is not compulsory, it is difficult to obtain reliable information. Studies estimate that there are nearly two million people living with limb loss [4] and approximately 185,000 new amputees each year [5] in the United States. In Germany, approximately 55,000 lower limb amputations were performed in 2015, according to national hospital discharge data [6]. Overall, amputation of the lower limb accounts for 85% of all amputations [7], and recent projections indicate that the number of lower limb amputations will increase substantially in the next years [4].

Reasons for amputation. The main goal of an amputation is to remove diseased or damaged tissue and to allow healing. In terms of lower limbs, the main reason (75-80%) for an amputation are peripheral vascular diseases with or without diabetes [8,9]. Other nonischemic indications

1. INTRODUCTION

include trauma (<5%), infection (3-5%), congenital anomaly (<3%) or other reasons, including tumor (5%). In contrast, amputation of upper limbs are mostly caused by traumata (>90%). However, there are quantifiable differences between different regions of the world. For example, the risk of an amputation caused by infection is about five times higher in developing countries than in the industrialized nations. [10]

Amputation level. The minimum amputation level is defined as the lowest level at which an amputation will heal. In general, a balance needs to be maintained between a decreased complication rate of a more proximal amputation and increased function of a more distal one [7]. Surgical procedures performed at the level of the ankle and below are known as *minor amputations*. In contrast, any operation above the ankle is classified as *major amputation*. The levels of amputation of the lower limb are depicted in figure 1.1. The foot amputation may occur below the ankle at any part of the foot [11]. The transtibial amputation is the most common type of lower limb amputation. The surgical procedure is performed between ankle and knee and has reported success rates of more than 85% [7]. In a disarticulation of the knee, the amputation is carried out at the knee joint. This does not require a separation of bone or muscle tissue, thus minimizing the risk of haemorrhage or infection and ensuring that the muscles and the thigh are entirely preserved, which is advantageous for loading the residual limb [12]. Further up, the transfemoral amputation, performed between knee and hip, is the second most common type of amputation [7]. In this case, most leg muscles and bones are lost, and a prosthetic device is needed to replace the natural movements of the knee and the ankle. In order to provide a strong lever arm for interaction with the prosthesis, the residual stump should be left as long as possible [13]. Finally, the hip disarticulation refers to the amputation of the entire lower limb through the hip joint.

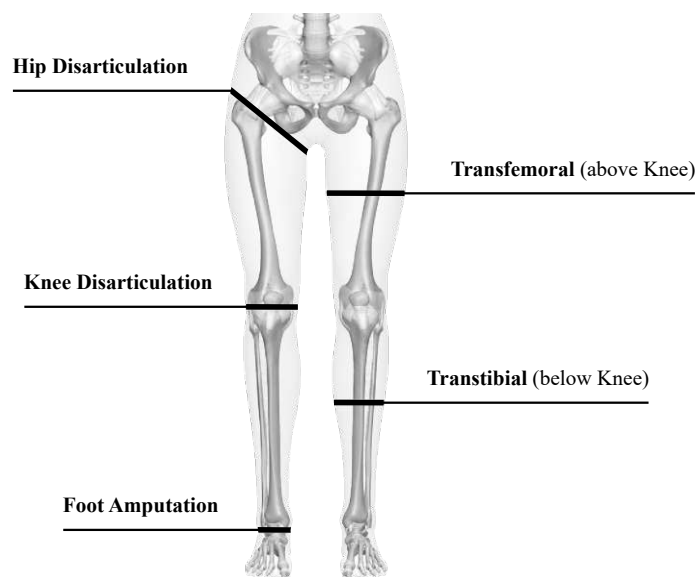


Figure 1.1: Different levels of lower limb amputation, adapted from [11].

1.1.2 Modern Lower Limb Prostheses

Modern prostheses can replace the functionality of missing body parts to a high degree and, thus, improve patients' independence and mobility. One of the most important aims of lower limb prosthetic systems is the imitation of the physiological gait pattern [14]. In comparison to prostheses for upper extremities, visual replacements of the lost body parts with cosmetic prostheses are less common for the lower extremities [15]. Generally, the higher the amputation level, the more sophisticated prosthetic systems are required in order to restore motion functionality.

A schematic of a transfemoral prosthesis system is presented in figure 1.2. The socket is an important part of any system, as it is the customized interface between the residual limb and the prosthetic device. A crucial factor for the overall performance and the rehabilitation success is, therefore, the socket design – formerly crafted by hand, today computer-aided and based on conditions of the patient's stump. A standardized pyramid adapter connects the socket with a prosthetic knee joint, which mimics the functions of the knee, thus providing mobility and safety. Finally, a prosthetic foot is connected with the help of a tube adapter; its length is adapted to the patient's body size. Modern feet are made of carbon fiber to absorb shocks, stabilize while walking and return energy through their spring designs. [16, 17]

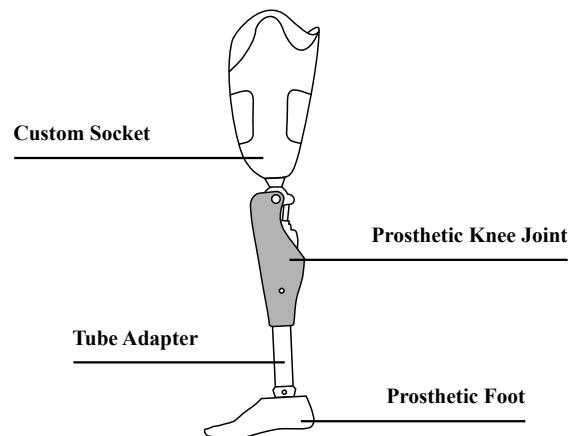


Figure 1.2: Parts of a transfemoral prosthesis system, adapted from* [MT1, 16].

K levels. The correct selection of prosthetic components is a very complex and responsible task, which needs to fit the patient's situation. Obviously, the higher the level of biomechanical imitation, the higher its complexity and, thus, its price. Costs can rise up to € 60,000 or even more for advanced systems [18]. The United States' Health Care Financing Administration established a 5-level functional classification concept [19]. This system, called K levels, is a rating from 0 to 4 and it indicates a patient's ability to reach a certain functional state within a given period of time. A description of the individual levels is given in table 1.1 on the next page.

***Note:** Author's own publications are referenced as [MT1] to [MT4] while external works as [1] to [129].

1. INTRODUCTION

K Level	Description
Level 0	Does not have the ability or potential to ambulate or transfer safely with or without assistance, and a prosthesis does not enhance their quality of life or mobility.
Level 1	Has the ability or potential to use a prosthesis for transfers or ambulation on level surfaces at fixed cadence. Typical of the limited and unlimited household ambulator.
Level 2	Has the ability or potential for ambulation with the ability to traverse low level environmental barriers such as curbs, stairs, or uneven surfaces. Typical of the limited community ambulator.
Level 3	Has the ability or potential for ambulation with variable cadence. Typical of the community ambulator who has the ability to traverse most environmental barriers and may have vocational, therapeutic, or exercise activity that demands prosthetic utilization beyond simple locomotion.
Level 4	Has the ability or potential for prosthetic ambulation that exceeds basic ambulation skills, exhibiting high impact, stress, or energy levels. Typical of the prosthetic demands of the child, active adult, or athlete.

Table 1.1: Definition of K levels, adapted from [19].

Today, many health insurance companies around the world still use this evaluation system to determine eligibility for reimbursement. However, in 2016, a survey found that 67% of prosthetists criticised the K levels for not accurately assessing the patient's rehabilitation potential [20]. Therefore, clinical outcome measures like the amputee mobility predictor [21] or standardized tests (e.g. timed up-and-go or timed walk test) are currently gaining more and more importance [22,23].

Knee classification. Prosthetic knee joints can be divided into three different types, namely mechanical knees, microprocessor-controlled passive knee joints (pMPK) and microprocessor-controlled active prosthetic knees (aMPK) [14]. Mechanical, non-microprocessor knees are limited in functionality and safety and use only a friction-based hinge to replace the knee joint [25]. Instead, modern passive as well as active microprocessor-controlled prostheses evaluate embedded sensors to enable real-time control of joint movement, which attempts to imitate the normal biological knee function for transfemoral amputees. pMPKs are energy dissipating devices. The movement of the device is caused only by the energy generated by the hip, and the actuators of such pMPKs adjust the damping behavior.

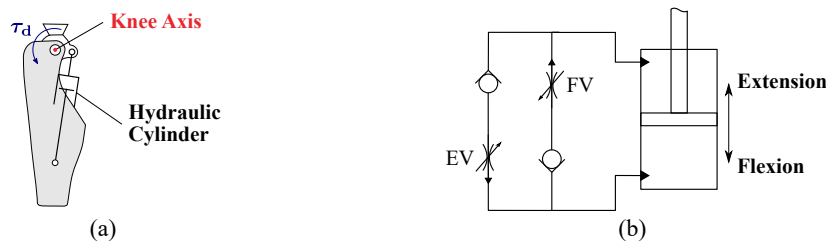


Figure 1.3: (a) pMPK with a hydraulic damper unit. (b) Schematic of hydraulic circuit with valves for flexion (FV) and extension (EV), adapted from [MT1, 24].

The well-known Ottobock C-Leg[®] prosthesis [26], first introduced around the turn of the millennium, uses a hydraulic damper unit to adjust the knee impedance. As shown in figure 1.3 on the facing page, the damper consists of a piston, which causes a hydraulic fluid to move in a cylinder. Two valves control the flow of fluid, generating a damping torque τ_d around the knee axis and thus changing the damping resistances for extension and flexion [24]. In contrast, aMPKs have the capability to provide net positive work, enabling the performance of more energy demanding tasks with less effort, like stair negotiation [27] or sit-to-stand transfer [28]. Although numerous research aMPKs with powerful actuators are known [14, 29], so far Össur's Power Knee[™] [30] and Rebocon Bionic's IntelLeg [31] are the only commercially available devices.

Gait functionality. Mimicking normal biological leg functionality is a major requirement for prostheses, as regaining mobility is an urgent desire of lower limb amputees. Humans use upright gait on two legs for efficient locomotion, known as level-ground walking. Therefore, walking can be described as a repetitious sequence to move forward: While one leg serves as support, the other shifts itself to the new site. This is repeated, until the final destination (in space) is reached. One single leg sequence is called *gait cycle*, consisting itself of two periods: stance and swing. Stance refers to the period of the foot being on the ground. It begins with the heel strike, also known as initial contact, when the heel touches the ground, before the foot is lifted off the ground at toe off. Then it swings freely in the air for the rest of the gait cycle. In between, there is a short phase, referred to as double support, in which both feet are on the ground. The stance-to-swing proportion was found to be about 60 : 40 for healthy people. Typical sagittal plane motion of hip, thigh, knee, shank and ankle is depicted in figure 1.4 on the next page. The sagittal plane is a vertical plane across the body dividing it into left and right parts. [32]

Since walking is a repetitive alternating motion that results in forward progression of the body, spatial (distance) and temporal (time) parameters are commonly used to characterize it [33]:

- **Step length** (m): Distance between the heel contacts of the opposite feet.
- **Cadence** (1/s): Number of steps per unit time.
- **Velocity** (m/s): Product of *cadence* and *step length*.

All these parameters are dependent on each other and vary with age, height and gender [33]. In addition, Newton's¹ third law states that when a force acts on a body (action), an opposite and equal force must act back (reaction) [34]. Therefore, the "ground reaction force" is the force exerted by the ground on a body in contact with it. For example, if a person is standing motionless on the ground, the force corresponds with the person's weight. During dynamic motion, the ground reaction force also has a component parallel to the ground: When the person is walking, there is an exchange of horizontal (frictional) forces with the ground. Normally, spatio-temporal parameters and ground reaction forces should be similar for the right or left (limb) side, and any deviation in these measures is an indicator for a pathological gait. Even pMPKs, which replace the missing body parts to a high degree, lead to measurable disturbances in gait pattern and, thus, to an increase in energy expenditure during walking [35].

¹Isaac Newton (1642 – 1727), English mathematician and physicist.

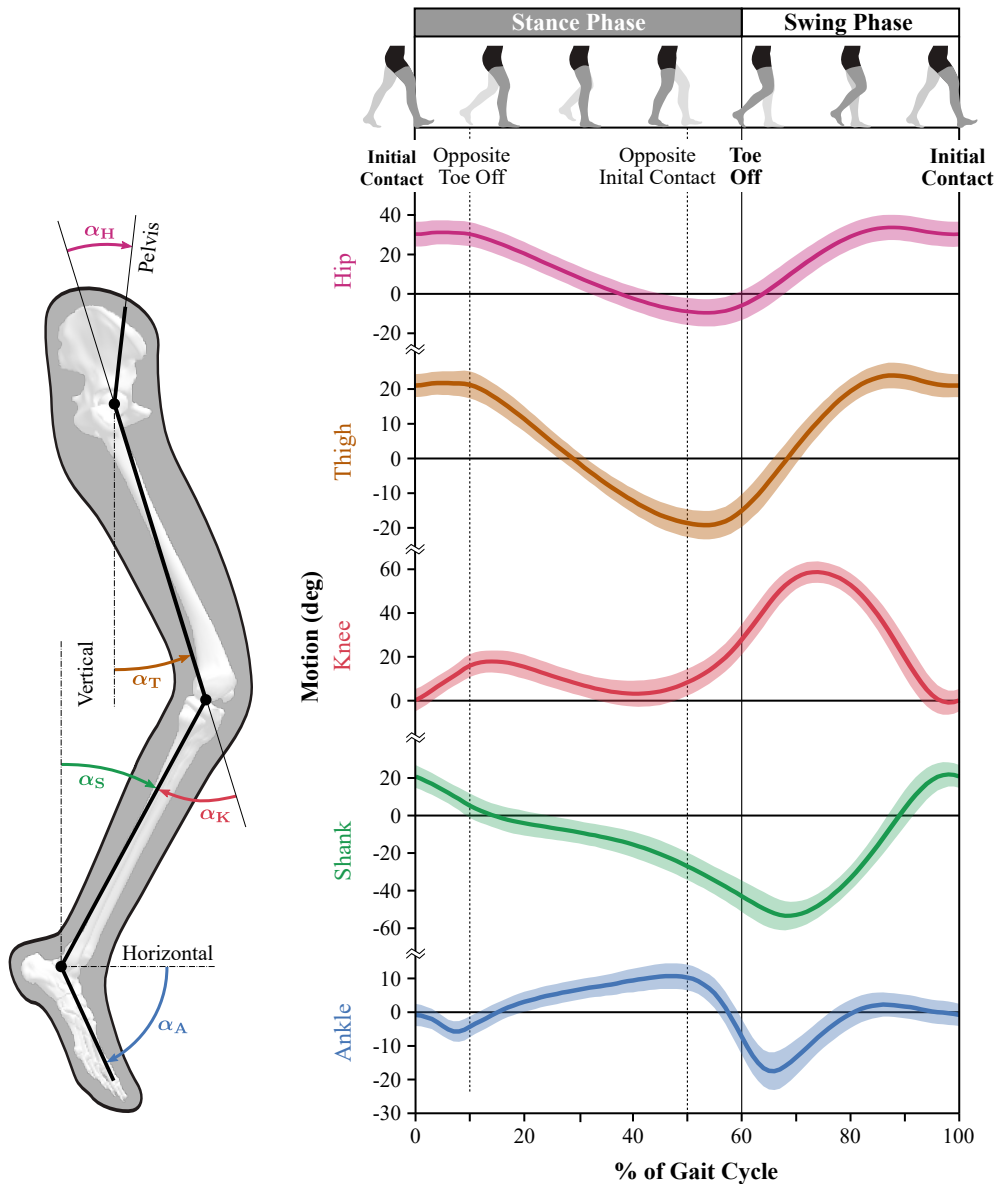


Figure 1.4: Sagittal plane motion during free level-ground walking. (left schematic) Definition of joint angles: thigh angle (α_T) and shank angle (α_S) relative to vertical, ankle angle (α_A) relative to horizontal, knee angle (α_K) between thigh and shank, and hip angle (α_H) relative to pelvis. (right diagrams) Heel strike is the first inertial contact when the foot touches the ground. At about 60% of the entire gait cycle, toe off is the end of the stance phase, initiating the swing phase. Then, the leg swings freely in the air until the next heel strike, before repeating the cycle. The plots show nominal angles with standard deviation in light-colored band, data from [32].

1.1.3 Control of Lower Limb Prostheses

Advanced lower limb devices are able to adapt autonomously to the patients' needs with the help of numerous embedded sensors. Among those, knee angle and angular velocity sensors, shank (axial) load cells or inertial measurement units (IMU) are commonly used. All these sensors are typically sampled with 100 Hz or higher to offer auto-adaptive control and to (re)act on a perceived real-time basis. [14]

Generalized framework. The idea for a control framework stems from Varol et al. [36] and was extended by Tucker et al. in 2015 [37]. This generalized control framework concept – dedicated to lower limb prostheses control – consists of four major sub-blocks, namely the controller, the device, the user and the environment, as shown in figure 1.6 on the following page.

In this framework, the *Controller* itself is represented as a three-level hierarchy. The high-level layer is responsible for the correct estimation of the patient's locomotive intent. Thereby, various terrains like level ground, stairs or ramps are related to different modes of locomotion. For this, identifying transitions between different forms of locomotion correctly is the most challenging task. Furthermore, volitional control allows the patient to consciously manipulate the state of the prostheses (e.g. mode of the device or only parameters, like damping resistance). It is also possible to combine both of these, so that the behavior of the device can be modulated with direct volitional control only within a given activity. Next, the mid-level layer maps the patient's estimated motion intent from the high-level to the desired state outputs of the device for the low-level to track. Impedance, admittance, position/velocity or torque controllers are typically used here. Finally, for the low-level layer, feedforward and feedback controllers send commands to the actuator(s) to minimize the error with respect to the current state, actuating the device and thus closing the control loop.

The controller is directly linked to the *Device* that provides the mechanical and actuator structure to restore or support normal biological functionality, assisting the *User* in an intuitive and synergistic way. From the device's point of view, everything else is *Environment*.

Finite-state machine. Although “artificial intelligence” is receiving much attention in the media, almost all commercial lower limb prosthetic devices use finite-state machines [14]. In accordance to the generalized framework, such a system represents the high-level layer of the controller to accurately reproduce the biomechanical aspects of gait.

The gait is decomposed into a series of distinct phases (states) characterized by a discrete set of parameters (e.g. specific impedance setting). Based on a fixed set of rules (transitions), the finite-state machine can switch between a pair of states [38], as depicted in figure 1.5 on the next page. Typically, transitions are based on sensor signals (e.g. axial force or knee angle) or combinations thereof, and corresponding threshold levels [14]. Ottobock, for example named its finite-state machine *RuleSet*. The “simple” level-ground walking activity consist already of up to ten states, called rules, depending on the mobility level of the patient [39].

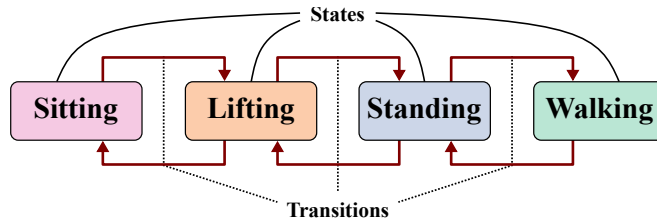


Figure 1.5: Example diagram of finite-state machine for lower limb prosthetic device control.

The simplicity and flexibility of finite-state machines allows them to be used for devices with very limited processing power. Moreover, such heuristic rule-based approaches benefit from their deterministic behavior, which lowers error rates well below the per mille range. In contrast, assuming a performance of about 99% of advanced “machine learning” approaches and calculating with about 3000 steps per day [40], and further expecting only every tenth misclassification to be serious, there would still be three tumbles per day, which does not seem very promising.

Environmental sensing. The environment is in ongoing interaction with the user and the prosthetic device – ground reaction forces provide balance, support and propulsion. Beside the generalized controller framework, Tucker et al. [37] coined the terms: *implicit environmental sensing* (IES) and *explicit environmental sensing* (EES). On the one hand, IES tries to create an understanding of the current mode of locomotion by measuring the state of the residual user’s body. EES, on the other hand, directly estimates terrain features, as shown in figure 1.6.

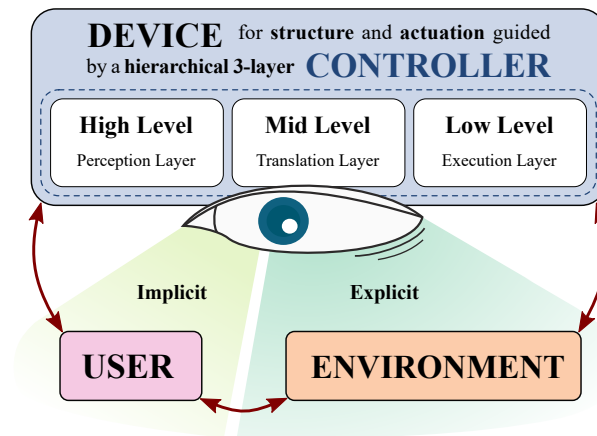


Figure 1.6: Control framework. Dynamics between a prosthetic device, a user, and his environment. The hierarchical controller estimates the patient’s intent at the high-level, translates it into device states at the mid-level and finally executes these commands at the lower level. Environmental awareness is achieved by observing the user (IES) or the environment (EES), adapted from [MT2, 37].

1.2 Environmental Sensing Technologies

In recent years, the robotic and automotive industry have driven innovation and development of environmental sensor systems. For example, (fully) autonomous vehicles need an almost seamless 360° perception of their surroundings in order to navigate safely and to be able to (re)act with foresight [41]. In general, there is a variety of approaches and technologies for distance detection of obstacles, and it is beyond the scope of this thesis to give a complete overview of all of them. Essential for this work, however, are the so-called time-of-flight (TOF) sensors, which measure the pulse reflection duration. Based on the type of signal wave used, TOF sensors can be categorized as shown in figure 1.7.

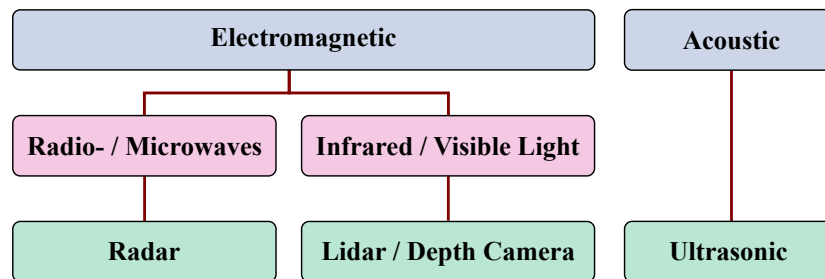


Figure 1.7: Categorization of TOF sensors (green) based on the type of wave (blue) and range of frequency (pink), adapted from [42].

1.2.1 Physical Foundations

Wave propagation. The propagation of waves, such as sound or light, can be described mathematically by the wave equation. Historically, d’Alembert² discovered this partial differential equation in the 18th century to describe the problem of a vibrating string of a musical instrument. Nowadays, the wave equation is used to describe a variety of different physical problems [34]. The wave equation for a plane wave traveling in one space dimension x can be written as follows:

$$\frac{\partial^2 u}{\partial t^2} = v^2 \frac{\partial^2 u}{\partial x^2} \quad (1.1)$$

where u represents the dependent variable, which is changing as the wave passes with the velocity v over time t . In terms of electromagnetic waves, u is substituted by the electric field E . Instead, when considering sound waves, the sound pressure p replaces u in the wave equation. In general, the simplified solution to this one-dimensional wave equation in positive space dimension x is:

$$u(x, t) = A \sin(\omega t - kx + \phi) \quad (1.2)$$

²Jean le Rond d’Alembert (1717 – 1783), French mathematician, physicist, philosopher, and music theorist.

1. INTRODUCTION

where A is the amplitude, $\omega = 2\pi f$ is the angular frequency, and ϕ is the initial phase. The wave number k is given by:

$$k = \frac{2\pi}{\lambda} \quad (1.3)$$

where λ is the wavelength, and the propagation velocity v of the wave corresponds to the product of the wavelength and the frequency:

$$v = \lambda f. \quad (1.4)$$

As depicted in figure 1.7, radar, lidar and depth cameras use electromagnetic waves but with different frequencies. RADAR, as the full name *RA*dio *DE*tectio*N* *AN*d *RA*nging already indicates, uses radio waves with frequencies of 300 kHz up to 300 GHz. Instead, LIDAR, short for *LI*ght *DE*tectio*N* *AN*d *RA*nging, uses electromagnetic waves in the optical and infrared spectrum ranging from 6 THz up to 1 PHz. [34, 42] Derived from Maxwell's³ equations, electromagnetic waves are generated when an electric field comes in contact with a magnetic field. Therefore, this type of wave does not need a medium to propagate. The electric and magnetic components are perpendicular to each other, and also perpendicular to the propagation direction, as shown in figure 1.8(a). In vacuum, the velocity of an electromagnetic wave is limited by the distributed capacitance and inductance, respectively known as the electric constant ε_0 and the magnetic constant μ_0 :

$$v_{\text{vacuum}} = \frac{1}{\sqrt{\varepsilon_0 \mu_0}} \quad (1.5)$$

resulting in 299,792,458 m/s. In a medium, however, the electromagnetic wave usually does not propagate at a speed of vacuum, as the two field constants are modified by the material. This is given by the factors of relative permittivity ε_r and the relative permeability μ_r , respectively, both depending on the frequency of the wave [43]. Therefore, the velocity of an electromagnetic wave in the medium v_{medium} is lower than in vacuum, accordingly:

$$v_{\text{medium}} = \frac{1}{\sqrt{\varepsilon_0 \varepsilon_r \mu_0 \mu_r}} = \frac{v_{\text{vacuum}}}{\sqrt{\varepsilon_r \mu_r}}. \quad (1.6)$$

Instead, ultrasonic sensors are based on acoustic waves, using frequencies which start in the audible frequency range for humans of below 20 kHz and go up to 200 kHz [34, 42]. Mechanical waves like these need a medium to travel, as propagation is based on the oscillation of molecules. In general, the surrounding medium is compressed (local high-pressure regions) and expanded (local low-pressure regions). As depicted in figure 1.8(b), molecules vibrate longitudinally to the propagation direction of the traveling wave [34]. This manifests that the velocity of an acoustic wave varies greatly in different media. In a perfect vacuum, where by definition there is nothing,

³James Clerk Maxwell (1831 – 1879), Scottish scientist in the field of mathematical physics.

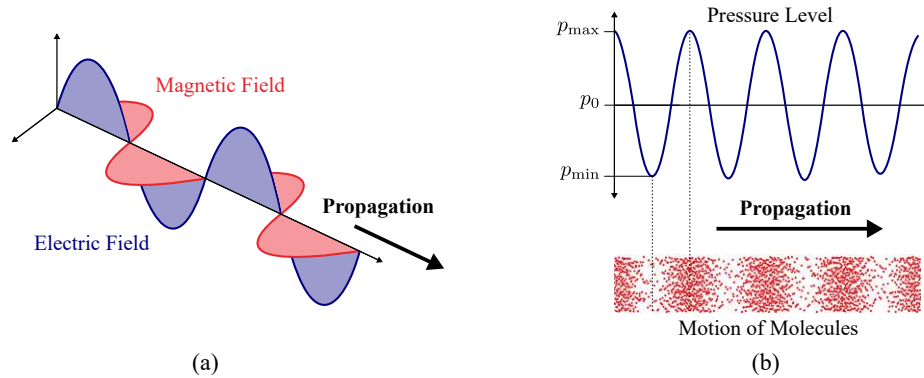


Figure 1.8: Schematic representation of (a) an electromagnetic wave and (b) a sound wave.

nothing can vibrate, and therefore the speed of sound is zero. The velocity of an acoustic wave v_{acoustic} is a function of the medium's density ρ and its rigidity (or compressibility in gases) K :

$$v_{\text{acoustic}} = \sqrt{\frac{K}{\rho}}. \quad (1.7)$$

The less stiff (or more compressible) the medium, the slower the velocity. Typically, in gases, sound propagates at the slowest rate. In liquids, sound is faster, and even faster in solids because they are relatively rigid and difficult to compress. Furthermore, there is a strong dependence on the medium's temperature, but only a weak dependence on the wave's frequency. At 20 °C, the speed of sound in ordinary air is about 343 m/s and almost 4.3 times faster in water of about 1,484 m/s [44].

Attenuation behavior. A disadvantage of using TOF sensors is the fact, that the intensity of an emitted wave continuously decreases. Assuming a sensor as a point source, the inverse-square law describes that intensity I is inversely proportional to the square of the distance d to the sensor [34]:

$$I(d) \propto I(0) \frac{1}{d^2}. \quad (1.8)$$

In addition to this geometric dilution, scattering, absorption, and other mechanisms of energy dispersion reduce the intensity of the original signal even further [43]. This attenuation in a homogenous medium is described by the Beer–Lambert⁴ law:

$$I(d) = I(0)e^{-\alpha d} \quad (1.9)$$

where α depends on the medium properties and the frequency. The higher the frequency, the shorter the distances that waves can travel, before exhausting all their energy. In general, these

⁴Pierre Bouguer (1698 – 1758), French mathematician and Johann Heinrich Lambert (1728 – 1777), Swiss polymath.

effects occur simultaneously during both the TOF signal transmission and the reflected return.

Reflection and transmission. Reflection and transmission play a decisive role depending on the material properties of the object as well as on its surface structure and geometry [43].

When a wave reaches the boundary between one medium and another, part of the incident wave is reflected and part of the wave is transmitted across the boundary, as depicted in figure 1.9(a). If the irregularities of the object surface are larger than the wavelength of the signal, the wave is reflected specularly – the angle of incidence equals the angle of reflection, known as law of reflection. Otherwise, the reflection is scattered diffusely in all directions, as shown in figure 1.9(b). In general, objects with large, dense, and flat surfaces at 90° to the incident wave yield strong echoes, while objects with small, round, and soft surfaces reduce the reflection response. [43, 45]

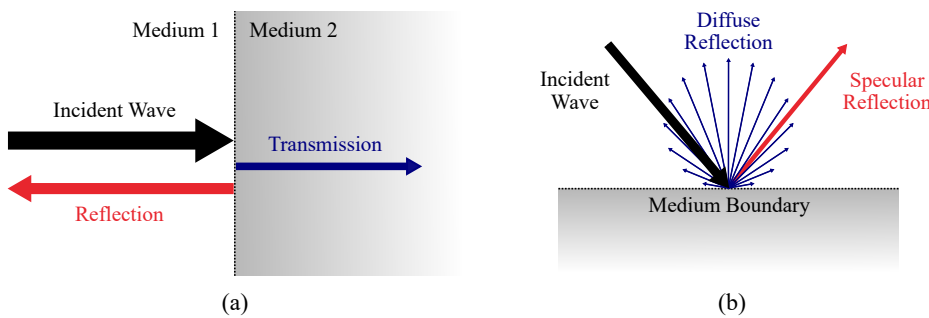


Figure 1.9: (a) Visualization of reflection and transmission of an incident wave at medium boundaries. (b) The reflection can be specular (at a definite angle) or diffuse (in all directions).

Signal modulation. Correct distinction between the transmitted and the reflected wave is essential for TOF sensors. Therefore, one or more properties of the basic wave equation are modulated. In general, a low-frequency modulation signal varies the amplitude, frequency or phase of the periodic high-frequency carrier signal. [42]

In terms of *amplitude modulation*, the carrier amplitude is varied in accordance with the amplitude of the modulating signal. The most practical way is to use a rectangular pulse wave as modulation basis. In this case, the amplitude of the carrier alternates between a fixed minimum, typically zero, and a maximum, as shown in figure 1.10(a) on the next page. The period of the carrier signal T_C as well as the period of the modulation signal T_M remain unchanged. They are both reciprocal to the corresponding frequency. The “on time” of the wave correlates with the pulse-width period T_{PW} of the pulse wave, followed by the “off time” until the next (periodic) repetition. [42]

Instead of modulating the amplitude, *frequency modulation* alters the frequency of the carrier. The carrier period (reciprocal to the frequency) varies in accordance with the amplitude of the modulating signal. Again, a modulation with a rectangular pulse wave is very common. As shown

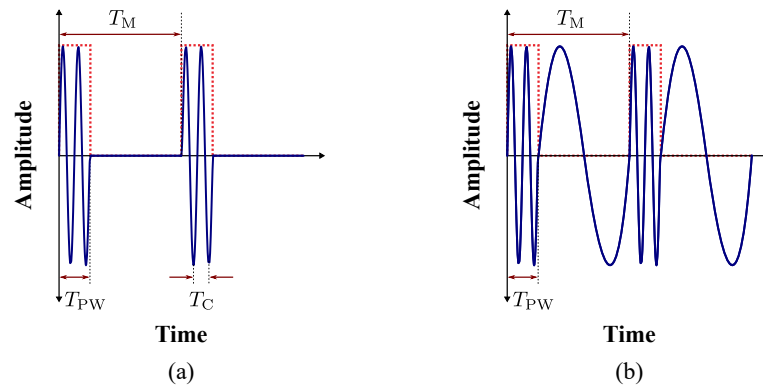


Figure 1.10: Illustration of signal modulation. (a) Amplitude modulation and (b) frequency modulation using a rectangular pulse wave (red dotted) as modulating signal, adapted from [42].

in figure 1.10(b), this varies the frequency of the carrier, while the period of the modulation signal T_M remains constant. [42]

1.2.2 Time-of-Flight Principle

Time-of-flight (TOF) refers to the time taken by a wave (acoustic or electromagnetic) to travel a distance through a specific medium [42]. In terms of TOF sensors, a wave is emitted, then reflected by surrounding objects and received again by the sensor. This sensor measures the delay between the emitted and the received echo t_{TOF} , as depicted in figure 1.11.

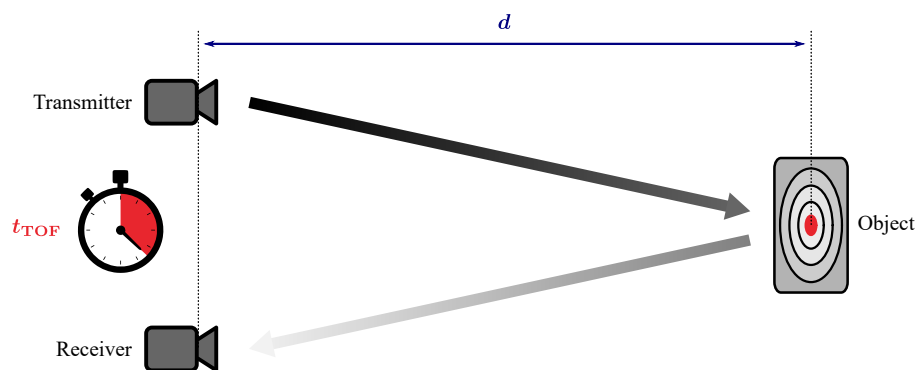


Figure 1.11: Time-of-flight principle. A wave is emitted by a transmitter, reflected by an object and received again by the receiver, whereby the sensor measures the total round-trip time t_{TOF} . The gradient arrows indicate the continuous decrease of intensity.

1. INTRODUCTION

By knowing the velocity of propagation v , the measured round-trip time t_{TOF} can be used to calculate the distance d between the sensor and the object:

$$d = v \frac{t_{\text{TOF}}}{2}. \quad (1.10)$$

Since the wave (acoustic or electromagnetic) must propagate forth (transmitter \Rightarrow object) and back (object \Rightarrow receiver) again, a division by 2 is necessary.

Range. The simplest version of TOF sensors uses amplitude pulse wave modulated signals, as shown in figure 1.10(a) on page 13. In most applications, the transmitter and the receiver are combined into one sensor, called transceiver [42, 45]. However, this has the disadvantage of creating a blind zone that limits the *minimum detection range*. The minimum detectable distance d_{min} corresponds with the pulse-width period T_{PW} of the pulse by:

$$d_{\text{min}} = v \frac{T_{\text{PW}}}{2}. \quad (1.11)$$

In general, the shorter the pulse-width period, the smaller the blind zone.

The *maximum detection range* is determined by the period of the complete pulse T_{M} . This maximum unambiguous range d_{max} to avoid interference of decisive echoes is given by:

$$d_{\text{max}} = v \frac{T_{\text{M}}}{2}. \quad (1.12)$$

In general, the longer the period of the modulation, the larger the detection range.

Resolution. Another important characteristic of a TOF sensor is its resolution. Theoretically, the minimum difference in range which is required between two objects, so that they can be distinguished as separate bodies, directly correlates with the minimum detectable distance, compare equation 1.11. Below this (range) threshold, different bodies are registered as a single object. [42]

Detectability. The size of the target is a crucial factor for the sensor's detectability. If the object is too small, the reflected wave is too weak to be registered by a sensor. Moreover, it is also influenced by the surface structure and the geometry of the objects as well as by the properties of the medium itself. In addition, external influences (e.g. sunlight or wind) can have a negative effect on the use of TOF sensors. [43, 45]

Field of View. The TOF sensor's field of view is another important property for selecting the right type of sensor for a specific application [46]. For example, laser distance sensors measure only in the specific direction of the laser beam. In contrast, the emitted acoustic wave by ultrasonic sensors is far less directed, resulting in broad field of views of up to 180° . However, measurements within these semicircular beam patterns provide only distance (radial) information, but no directional (angular) information [MT2]. Therefore, most manufacturers offer horns for their ultrasonic sensors to focus the beam mechanically in a specific direction [45]. Instead, TOF-based depth cameras incorporate optics to capture depth information from a whole scene.

Similar to color cameras, an array of individual TOF receivers is coupled to a lens system: each pixel receives the echoed wave of a specific point within the scene. This measurement matrix is also called a depth map and provides all the distance measurements between the sensor and the imaged scene at once, updating at the frame rate of the camera. [46]

Comparison. In general, each type of sensor presented in figure 1.7 on page 9 has their own advantages and disadvantages, summarized in figure 1.12 on the following page. Note: Technical parameters were extracted from the publications reviewed in author's work [MT2], where missing information was completed with the help of the manufacturer's data sheet. Instead of absolute values, a rating scale (low, medium and high) is used. The "Unobstructed Field of View" field indicates, whether the sensor functionality requires an unobstructed field of view or not: yes/no.

Ultrasonic sensors are based on acoustic waves, usually using frequencies that are above the range of human hearing. Typically, piezoelectric transceivers, which are able to convert electrical signals into ultrasound and vice versa, are used. As the speed of sound is far lower than the speed of light, nature limits the maximum update rate of these sensors. For example, the round trip time of an object at a distance of 1 m is approximately 6 ms. Although these sensors can have a very wide field of view, directional resolution is not given. However, ultrasonic sensors are common for close-range applications because they can detect even transparent materials, such as glass.

Instead, sensors that operate on any type of light are based on electromagnetic waves. Since the speed of light is much higher, the round trip time is usually negligible. Therefore, the update rate of such sensors is only limited by the processing rate of the internal hardware. For example, infrared-based distance sensors emit below the visible light range, while laser sensors are typically in the visible range (red or green light) or above (invisible ultraviolet range). *Lidar* systems combine 1D laser distance sensors with a sophisticated (mechanical) mirror system to capture 2D scene scans. However, the moving parts in devices like these can be damaged by shocks or vibrations. Historically, lidar sensors used to be very expensive, whereas today the industry has moved towards developing low-cost solid-state versions for a broad application.

Depth cameras try to estimate the surrounding world in 3D – something that nature (human eyes) has perfected over millions of years. In the past, color cameras with passive light sensors were combined into stereo vision systems to calculate depth information. The performance of these systems depends primarily on the underlying calculation method (stereo correspondence algorithm) that attempts to match pixels of the two individual color images. Nowadays, depth cameras also use the TOF principle, illuminating the scene with a light impulse and capturing the reflection simultaneously by multiple elements. Thus, a full 3D perception is generated at once. Modern TOF-based depth cameras provide resolutions of up to 640 x 480 pixels, with update rates of up to 60 (depth) frames per second and are small enough to be implemented into a smartphone [47]. However, all these concepts based on infrared, visible or even ultraviolet light are limited by the fact that they explicitly require an unobstructed field of view, as depicted in figure 1.12 on the next page.

1. INTRODUCTION

The only type of sensor not limited by an unobstructed field of view is *radar*. Although this technology also uses electromagnetic waves, thanks to the high-frequency range of up to 300 GHz, certain materials, such as fabrics or plastics, typically appear transparent. On the one hand, this allows to “look through” these materials. On the other hand, objects or barriers made of these materials remain invisible, which may cause problems. Whether an object can be detected, depends in turn on the material properties of the target as well as its size and geometry [48]. Another positive aspect of radar sensors is that they can operate regardless of harsh outdoor conditions, such as heavy rain, snow, or fog. Although radar technology was discovered in the early 20th century, new super near-field radar sensors that can detect human gestures have only recently become available. Recent advances include Google’s radar-based gesture recognition technology for touchless interaction (Project Soli), which is implemented in their Pixel 4 smartphone, [49].

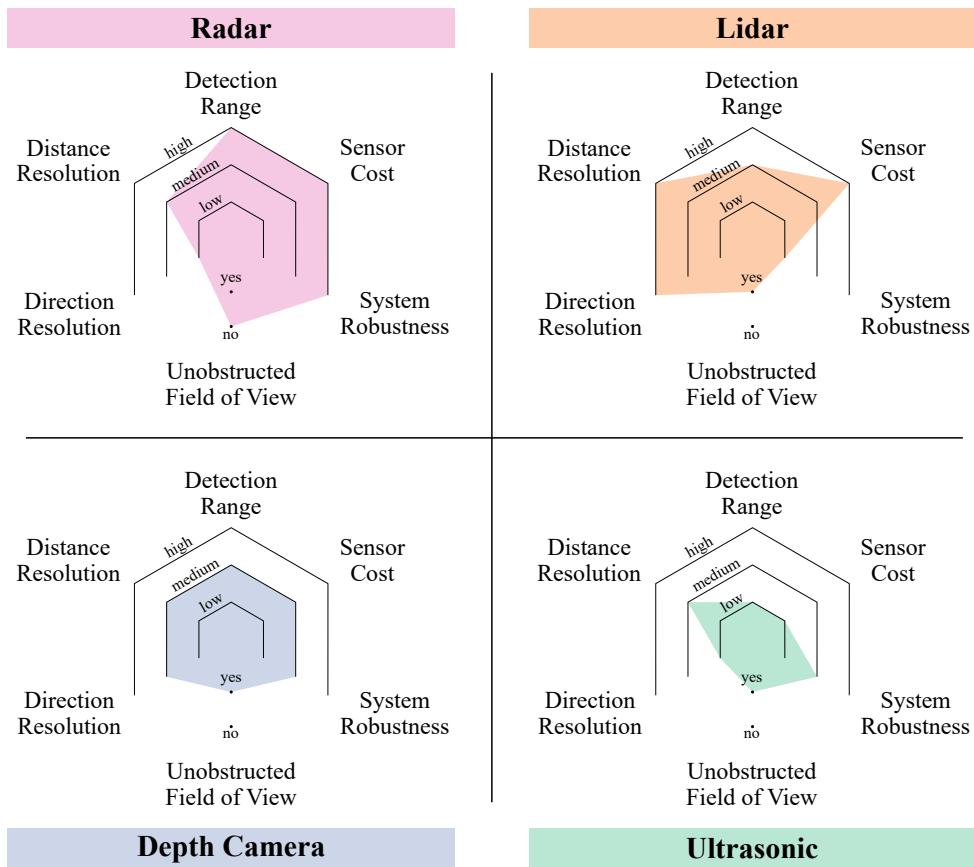


Figure 1.12: Comparison of TOF sensors, data from [MT2].

1.3 Aim of Work

The aim of this thesis is to improve patient-prosthesis interaction towards a more lifelike replication of the physiological gait pattern. Especially in situations such as walking down ramps or stairs, the lack of sound-side control on all commercially available devices resulted in an asymmetrical gait and thus increased stress on other joints.

First, the in-depth analysis of the current state of research in lower limb prostheses, which is presented in the subsequent chapter, helped to identify areas where further research could make “next generation prostheses” more user-friendly, functional and safe. Overall, there is a clear trend towards more upcoming terrain or object estimation systems using all types of TOF-based sensors. However, due to a relatively broad patent that was discovered through the freedom-to-operate research, EES approaches like these are highly interesting in theory, but not exploitable in a commercial way. To mitigate the patent risk, other concepts focused on IES have been investigated. Subsequently, a proper patent was filed by the author, covering the idea of enhancing the lower-limb prosthetic device control through the state of the sound side.

From this novel perspective, two completely new contralateral limb estimation systems were designed, integrated and open-loop tested: a depth camera-based approach named CoLiTrack and an ultrasonic-based system referred to as CoLiRang. Finally, the latter one was integrated into a prosthesis system, identified as SEP, and underwent a closed-loop evaluation throughout a prospective clinical pilot study.

The remainder of the thesis is organized as follows: Chapter 2 gives a thorough description of the methodology. Chapter 3 provides the experimental results, which are then discussed in Chapter 4. A conclusion of the lessons learned throughout the process is given in Chapter 5.



Die approbierte gedruckte Originalversion dieser Dissertation ist an der TU Wien Bibliothek verfügbar.
The approved original version of this doctoral thesis is available in print at TU Wien Bibliothek.

CHAPTER 2

Methods

As a basis for this thesis, a *Current State of Research* survey was conducted. From a novel perspective, two different contralateral limb estimation systems for enhanced patient-prosthesis interaction were evaluated. Within this chapter, the methodology of the *Depth Camera-based Contralateral Limb Tracking* approach, called CoLiTrack, and the *Ultrasonic-based Contralateral Limb Ranging* system, referred to as CoLiRang, are presented. First, a detailed system overview and the methodology for each concept are given. Next, the open-loop experimental trials are outlined. Finally, the CoLiRang approach is integrated into an *Enhanced Prosthesis Control System*, identified as SEP, and closed-loop evaluated throughout a prospective clinical pilot study. The outcome of all performed trials can be found in the following chapter *Results*.

2.1 Current State of Research

Modern prostheses are powerful devices that can replace missing limbs already to a great extent. However, the lack of environmental information – either IES or EES – often makes smooth transition between different forms of locomotion difficult. In the field of environmental sensing technologies, industry has driven innovation and development resulting in reduced prices for evaluation kits with powerful computer vision tools. As a basis for further research, it is now important to know which types of environmental sensors are already used in lower limb prostheses and how they improve device control.

In order to identify the progress made in this area, a detailed literature search was conducted. The related sections are largely based on my published survey titled *Relying on more sense for enhancing lower limb prostheses control: a review* by Michael Tschiedel, Michael Friedrich Rus-sold and Eugenijus Kaniusas, published in the *Journal of NeuroEngineering and Rehabilitation* on July 17, 2020, which is referred to as [MT2] and appended as Publication A.

2. METHODS

2.1.1 Snowballing on Reference

The search process for identifying the current state of research combined different strategies. A very common starting-point is to use a well-known, frequently cited publication. From here, the idea is to review the reference list as well as going forward by identifying articles citing this paper. In academia, this approach is known as snowballing [50]. For this review, the comprehensive survey by Tucker et al. from 2015 [37], which also introduced the generalized control framework described in section 1.1.3 on page 7, was used as basis.

2.1.2 Systematic Database Search

A systematic (database) search is helpful to find publications within a field of interest. This approach, defined by the PRISMA guidelines [51], was applied on two Internet databases, *IEEE Xplore* and *PubMed.gov*. In order to find publications of interest, search strings were defined. The first term was either “prothe*”, “extremity” or “limb” combined with either “radar”, “lidar”, “time-of-flight” or “depth” via a logical AND for focusing on dedicated sensor expressions, or with “terrain”, “environment” or “locomotion” for more holistic synonyms.

Within the publications found with this first two approaches, duplicates were removed and title, abstract as well as full publication were screened. Then, the following criteria were applied to include or exclude publications:

Inclusion:

- + Concepts for estimating environmental information
- + Strategies for all types of locomotion modes
- + Application for enhancing “prosthesis control” must be mentioned
- + Only articles published in English
- + Only articles from the previous ten years (2009 – 2019)

Exclusion:

- Systematic reviews or literature reviews
- Any kind of upper extremity solution
- All types of exoskeletons or orthotics-related papers
- IMU-based gait analysis systems without any link to prosthesis control
- Studies focusing only on neuromuscular or mechanical signals from the device
- Concepts focusing only on the residual (ipsilateral) limb
- Computer vision papers without any link to prosthesis control

Finally, an author cross-check was done. For this purpose, the publication lists of all named authors within the previously selected publications were retrieved using ORCID, Google Scholar, or private and institutional websites. If individual publications fulfilled the inclusion criteria, they were also included. For example, if the database search detected an earlier conference paper, but the same author had also published an article on the topic that had not been found before, it was also included.

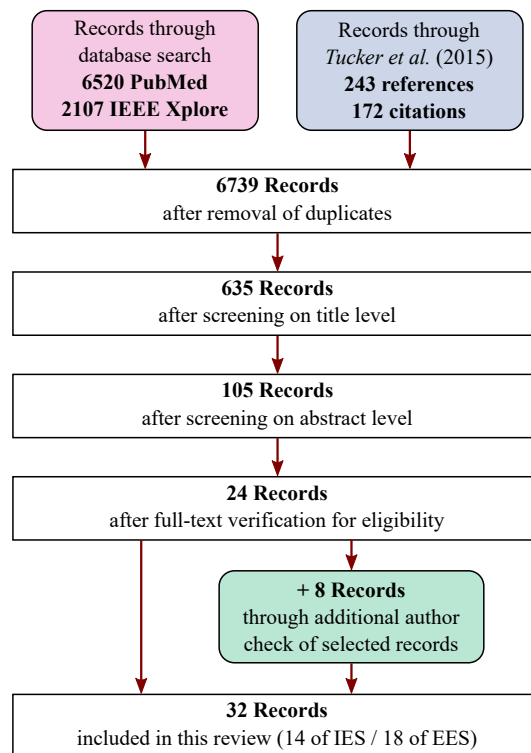


Figure 2.1: Flow diagram of database search and paper selection based on inclusion and exclusion criteria throughout the different phases of the search process, adapted from [MT2].

2.2 Depth Camera-based Contralateral Limb Tracking

In order to identify the potential of low-cost, high-resolution cameras for prosthetic applications, a first depth camera-based contralateral limb tracking approach named CoLiTrack was designed, developed and validated. For this, the system proposed by Hu et al. [52] using only a depth camera to predict bilateral gait events served as source of inspiration. However, although their approach was interesting, several limitations were mentioned. To begin with, only the results of walking on level ground by one healthy subject were analyzed, in addition, initiation and termination steps were excluded due to the difference in kinematics. Moreover, there were no experiments that evaluated robustness to reflection and clutter or the behavior of the system with regards to unknown objects in the field of view. The most limiting aspect, however, was the fact that their methodology was not optimized for timing. The high processing time of more than 1 s prevented any real-time implementation.

The related sections are largely based on my publication titled *Real-time limb tracking in single depth images based on circle matching and line fitting* by Michael Tschiedel, Michael Friedrich Russold, Eugenijus Kaniusas and Markus Vincze, published in the Journal *The Visual Computer* on April 25, 2021, which is referred to as [MT4] and appended as Publication B.

2.2.1 System Overview

The basic idea behind the CoLiTrack approach is as follows: A unilaterally-worn depth camera is used to estimate the axis and the respective shank angle of the contralateral shank, as illustrated in figure 2.2 on the next page. Since the shank kinematics are usually independent of the ankle kinematics [53, 54], this is an interesting feature, which can play a crucial role in motion-dependent control applications. Hence, the question arises of how the shape of the human leg can be identified correctly.

In principle, the shank of a human being can be modeled fairly well by the rudimentary shape of a cylinder. However, fitting a deformed and incomplete point cloud that was captured with a depth camera to such a model is challenging. Simple methods using surface normals [55] cannot be used due to noise caused by wrinkles on the pants, and well-known least square methods [56] fail due to outlier points. Furthermore, complex object matching approaches [57] are also unsuitable because the high processing time prevents real-time evaluation.

In order to overcome these limitations, the CoLiTrack approach divides this modeling problem into four parts. First, the captured point cloud is preprocessed in the camera coordinate system. Second, this scene is transformed into a ground coordinate system using the orientation information from the IMU. Next, layers from the transformed points are projected in 2D, before predefined circle models are fitted using the iterative closest point (ICP) algorithm. Finally, a 3D line is fitted through the centers of the circles using the random sampling consensus (RANSAC) method. Overall, this segmentation has significantly reduced computation time, making it fast enough for real-time applications. Moreover, compared to machine learning methods, this depth

camera CoLiTrack approach is unsupervised and has no training-induced bias. Consequently, it could appear attractive for a variety of applications in many domains, including human-device interaction, healthcare, or gaming.

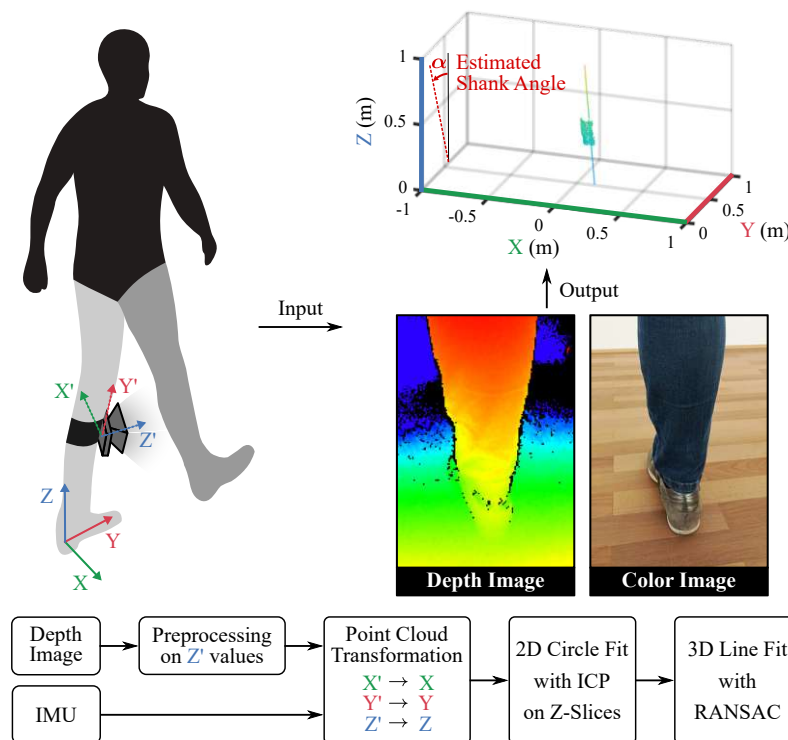


Figure 2.2: Overview of CoLiTrack. An IMU and a depth camera are fused to estimate the axis of the uninstrumented contralateral shank. (X', Y', Z') represents the camera coordinate system and (X, Y, Z) the stabilized world coordinate system. Mounting is depicted in detail in figure 2.3(a). The colors of the *Depth Image* correspond to the distance between an object and the camera: Red parts are close to the sensor, blue parts are further away. The *Color Image* was taken with a mobile phone and is for demonstration purpose only, adapted from [MT4].

2.2.2 Image-Processing Chain

Configuration. The CoLiTrack sensor configuration utilized a 3D time-of-flight depth camera (model CamBoard pico flexx with a resolution of 171 x 224 pixels manufactured by Pmd Tech, Germany) and an IMU (model BNO055 manufactured by Bosch Sensortec, Germany). In general, the depth camera measures the 3D position of objects relative to the camera origin, as described in detail in section 1.2 on page 9, while the IMU estimates the orientation and acceleration. In order to obtain a reliable reference signal of the subject’s contralateral shank, a second IMU (identical model) was worn in a modified support stocking on the subject’s sound side, as depicted in figure 2.3(a). The depth camera and the IMU were combined on a wearable support for quick and easy mounting on the subject’s leg. More importantly, this configuration allowed the visual information to be fused with the orientation information, thus stabilizing the input.

Nevertheless, the initial rotation of the camera after mounting it at the wearable support had to be corrected. For this, the kit which carries the IMU and the depth camera, shown in detail in the zoomed area of figure 2.3(a), was positioned in an upright orientation with a calibration object in its field of view. The known object itself was also mounted in a predefined position, as shown in figure 2.3(b) in pink. The initial rotation could be determined by taking a single scene shot, represented in green. This rigid transformation was computed using the coherent point drift algorithm [58] available within the Matlab Computer Vision Toolbox, stored and applied each time before proceeding with the proposed algorithm.

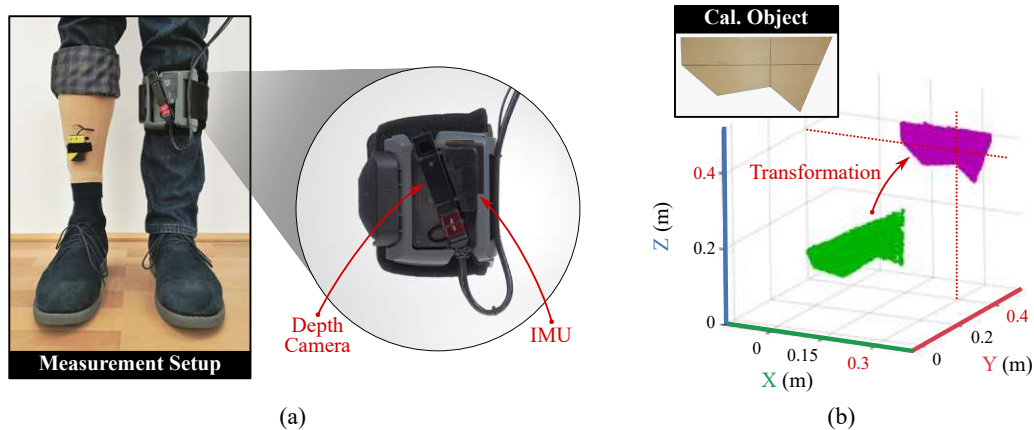


Figure 2.3: Measurement setup (a) worn by a participant and the calibration step (b) of the depth camera. IMU and depth camera were fixed on a wearable support, attached to the shank of the participant. The second IMU, mounted within a modified support stocking on the contralateral side, served as reference. Trousers were rolled up only for the photo. For calibration, the camera was placed in the origin of the world coordinate system. The true (pink) position of the calibration object was known. The transformation matrix could be calculated out of the captured (green) image, adapted from [MT4].

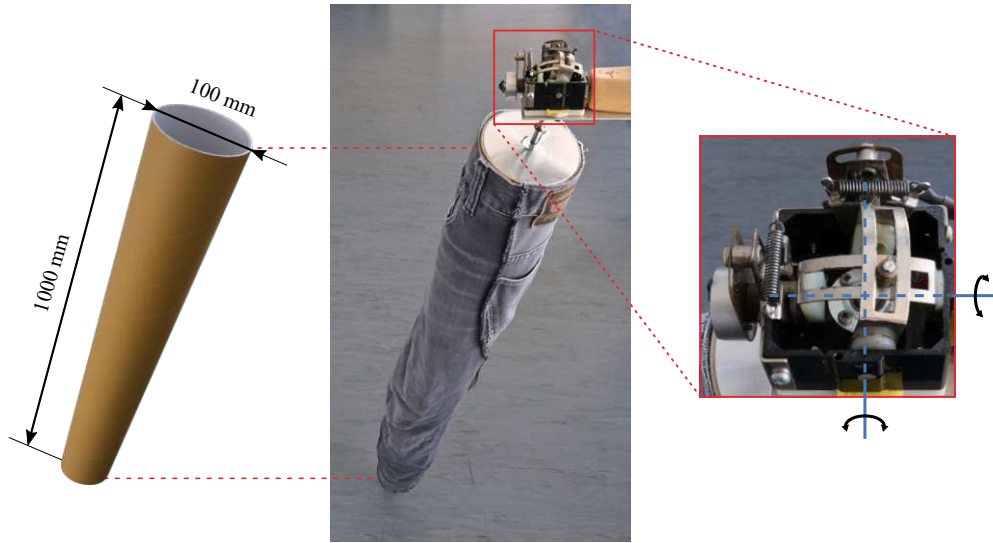


Figure 2.4: Overview of the development (leg) test bench. System consists of a carton cylinder, representing the “human leg” (shank and thigh with permanently stretched knee), which is covered by conventional jeans (cut to just one pant leg and sewn accordingly). This setup is inversely mounted on a two axis potentiometer joystick, which allows to tilt in each direction.

For algorithm development and optimization, a special “leg test bench” was designed and built. As depicted in figure 2.4, a carton cylinder which can swing about 45° in each direction simulates the human leg.

Data acquisition and analysis were performed using Matlab R2018b and a wrapper library provided by the camera manufacturer, running on a business laptop with 8 GB memory size and an Intel Core i5-8250U.

Preprocessing. After capturing, the depth data is preprocessed in the camera coordinate system, as illustrated in the processing chain in figure 2.2 on page 23. First, points (pixels) without any depth information are removed. Next, in order to remove (depth) noise, the point cloud is blurred with a Gaussian blur. If the sound-side leg is in the depth camera’s field of view, it can be assumed that the closest point also belongs to the contralateral leg. This point is then selected as “point of interest”. In combination with the confidence map, which was also retrieved from the depth sensor representing the confidence of a measured distance (Z') for every pixel (X' , Y') of the input, points below a certain threshold relative to confidence of the point of interest are deleted: the farther away, the lower the corresponding confidence. This made it possible to select only points that belonged to the sound-side leg. In order to reduce the processing effort even further, the preprocessed point cloud was downsampled using a 10 mm grid filter.

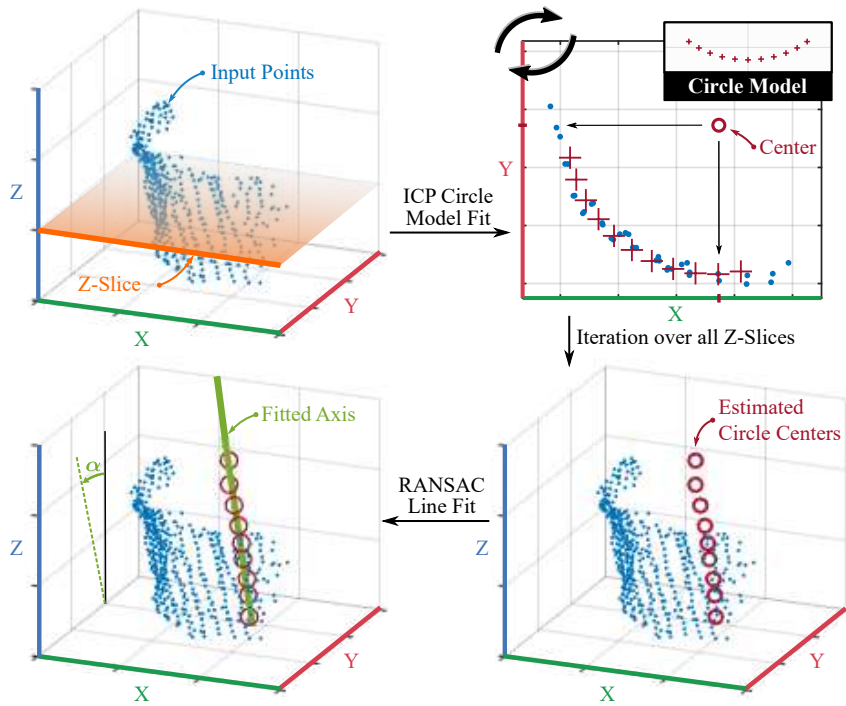


Figure 2.5: Visualization of the CoLiTrack algorithm. The point cloud after preprocessing and transforming is taken as input. Z-slices are extracted, and a 10-point circle model is fitted iteratively by using the ICP algorithm in 2D (X/Y-plane). All model circle center points are then used to estimate the shank axis correctly by using the RANSAC method in 3D. Finally, the contralateral shank angle α is calculated with respect to the sagittal plane (Y/Z-plane), adapted from [MT4].

Transformation. Within the gait cycle, the subject’s shank can swing, as shown in figure 1.4 on page 6. In order to transform the preprocessed input of camera coordinates into a stabilized world coordinate system, the motion must be registered. With the help of the IMU, the pitch-angle (rotation around the Y-axis), roll-angle (rotation around the X-axis) as well as the yaw-angle (rotation around the Z-axis) are measured. However, since the latter is often unstable, only roll and pitch angles are considered when applying Euler’s rotation angle matrix, while rotation about the Z-axis is ignored. The stabilized world coordinate system is defined as the IMU reference frame, calibrated to the ipsilateral foot, as depicted in figure 2.2 on page 23.

ICP circle fit. A visualization of the CoLiTrack algorithm with the ICP and the subsequent RANSAC fitting process is depicted in figure 2.5 on the facing page. After transforming the input into a stabilized world coordinate system, Z-layers with a height of 30 mm and 10 mm overlapping on both sides are extracted in 2D. With the help of the ICP algorithm [59, 60], predefined circular models are fitted to match the input in the best way possible. The principle of this ICP algorithm is depicted in figure 2.6.

For the CoLiTrack approach, a circle model of 10 points, evenly distributed over 90° in a radius of 50 mm, is rigidly transformed (translated and rotated) to minimize the error metric. The algorithm reiterates, until the sum of squared differences between the coordinates of the matched points fall below a certain threshold. This was repeated for all Z layers, resulting in a center point for each associated height.



Figure 2.6: Principle of the iterative closest point method. The scene (blue) is kept fixed, while a model (red) is transformed (rotation and translation) to best match the input.

RANSAC line fit. Next, the newly calculated center-points of the circles are used to fit a line representing the shank axis correctly. This is done by using the RANSAC approach [61]. In general, the principle of this iterative method is to estimate parameters of a predefined mathematical model, as visualized in figure 2.7 on the following page. Therefore, two points are randomly taken to generate a hypothesis (fitting model), compare with figure 2.7(b). Points are marked as “inlier” if they are within a threshold d , otherwise (they are marked) as “outlier”. This step is repeated, until the obtained hypothesis exceeds a certain ratio. After that, only inlier-points are used for the calculation of the final fit, depicted in figure 2.7(c). This makes it a robust estimate even if there is a significant number of outliers in the data.

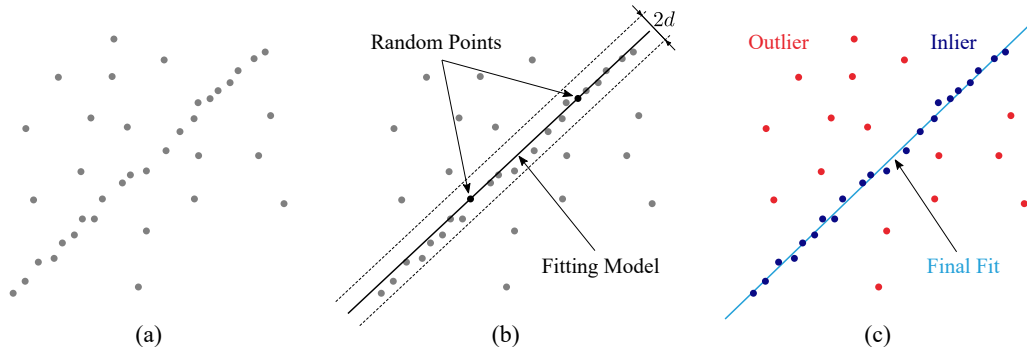


Figure 2.7: Principle of the random sample consensus method. (a) Data points with outliers, (b) randomly selected points with model hypothesis and (c) final fit, in which outliers have no influence on the result.

For the CoLiTrack approach, a threshold d of 30 mm is used. The maximum number of random trials is set to 1000 and the probability to 0.99. The total number of input points is limited by the scene height, approximately between 50 mm and 300 mm, and the Z-slice height, which is set to 30 mm, as depicted in figure 2.5 on page 26. After successfully estimating the axis, this is used to calculate the sagittal plane shank-to-vertical angle α_S , as defined in figure 1.4 on page 6.

2.2.3 Experimental Plan

In order to determine the accuracy and the detection range of the CoLiTrack approach, dynamic, static and real-world experiments were conducted. The system was tested with five healthy volunteers; informed consent was obtained prior to the experiments. The anthropomorphic data of the subjects is given in table 2.1.

ID	Height (m)	Weight (kg)	Age (years)	Sex
S01	1.87	80	25	♂
S02	1.88	78	25	♂
S03	1.67	58	24	♀
S04	1.78	83	23	♂
S05	1.80	76	22	♂

Table 2.1: Basic subjects' information.

Static evaluation. First of all, the static tracking performance of the proposed method was evaluated. Due to the fact that the camera had a very limited field of view (62° horizontal x 45° vertical, taken from the product's datasheet), the sound-side leg is in view only for a small part of the entire gait cycle and out of view for the rest of the time. Therefore, the wearable support, containing the IMU and the depth camera, was mounted on a commercial treadmill facing the subject's shank, as depicted in figure 2.8(a), while the second IMU was still placed on the subject's sound-side shank. This setup allowed to determine the performance over the entire gait cycle. The treadmill's incline was set to 1%, which is considered to correspond to the resistance level of an outdoor surface without incline [62]. In accordance to the walking speed determined for amputees [63], treadmill speed was defined as slow (0.5 km/h), medium (1.0 km/h), and high (1.5 km/h), which is slower than humans' normal walking speed. Since the camera is fixed and did not move within this experiment, the transformation step was not necessary. Instead, a scene crop was applied to limit the view to only the area of the sound-side shank. This experiment was carried out only with one subject (S01), who was asked to walk about 5 minutes at each speed level. The results are presented in the subsequent chapter.

Dynamic evaluation. Next, the dynamic behavior, and thus in particular the maximum trackable range of the entire gait cycle, was explored. Therefore, all five able-bodied subjects from table 2.1 on the facing page were equipped with both, the wearable kit on the ipsilateral leg, and the reference IMU on the sound-side leg. After that, the system was calibrated in an upright standing position without movement. These parameters were stored and used for all subsequent experiments – walking at the slow, medium and high speed level at an incline of 1%, as depicted in figure 2.8(b). Again, each subject was asked to walk for approximately 5 minutes at each speed level. Results are reported in the following chapter.

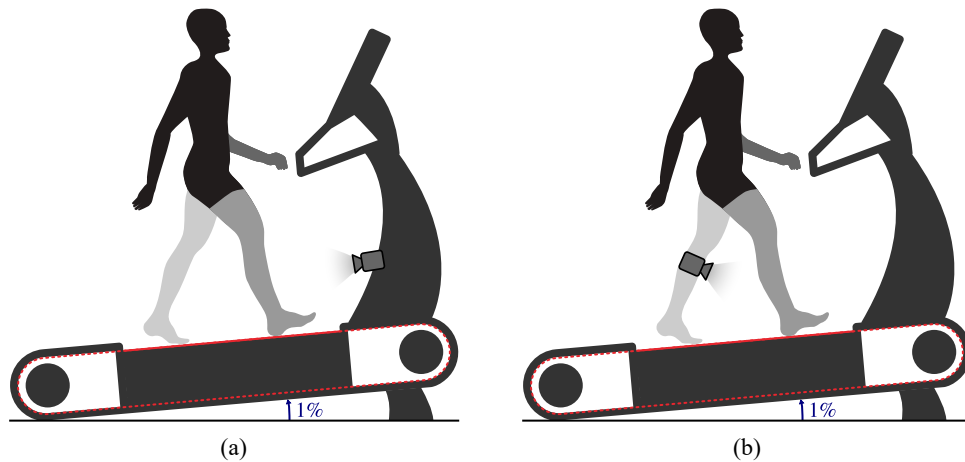


Figure 2.8: Configuration for treadmill experiments. (a) The wearable support, which contains the depth camera and the IMU, was placed stationary on the treadmill. (b) For the dynamic test, the camera was mounted on the subject's shank, as depicted in detail in figure 2.3(a) on page 24.

2. METHODS

Real-world evaluation. Finally, the real-world experiment was conducted to determine the performance of the CoLiTrack approach in other types of terrains (e.g. up/down stairs or ramps), and to analyze the algorithm behavior with unknown objects (e.g. banisters) in the depth camera's field of view. For this, an online walking test with one subject, S01 from table 2.1 on page 28, was conducted. The instrumentation was almost identical to the dynamic experiment described before: on one leg the kit, on the other leg the reference IMU. The laptop for data collection had to be carried in a backpack on the subject's back to be mobile. The subject was asked to begin with walking at a self-selected speed, before moving to a different terrain or varying the speed. The results are presented in the subsequent chapter.

Data analysis. The performance of the CoLiTrack method was analyzed as follows: The recorded gait data was separated into individual steps with the help of the reference signal $\alpha_{S,IMU}$. The IMU was worn on the contralateral leg, as depicted in figure 2.3(a) on page 24. For determining the individual steps, the data was searched for the local positive peaks, which indicate the initial contact, as shown in figure 1.4 on page 6. Next, due to their kinematics differing from steady-state walking, initiation and termination steps were excluded. Then, individual steps were normalized from 0% to 100%. In order to determine the accuracy, the deviation between the reference signal and the depth camera-based estimation $\alpha_{S,TOF}$ was calculated for each percent of the entire gait cycle. This shank angle error e is defined as $|\alpha_{S,IMU} - \alpha_{S,TOF}|$. Whenever possible, mean and standard deviation were calculated and reported over the entire gait cycle.

2.3 Ultrasonic-based Contralateral Limb Ranging

In order to overcome the limitations of the previously described depth camera system, a second ultrasonic-based contralateral limb ranging approach named CoLiRang was designed, developed and validated. Although this system is still limited by the need for an unobstructed field of view, numerous positive results were found. Most importantly, tracking is possible for the entire gait cycle with update rates of almost up to 70 Hz, which is fast enough for real-time evaluations at normal walking speed levels.

2.3.1 System Overview

The basic idea behind the CoLiRang approach is to use a sonar sensor instead of a depth camera for capturing the contralateral leg, as illustrated in figure 2.9. However, these sensors provide only distance measurements to the closest object in their field of view without any direction information. Therefore, multiple sensors were combined into a sensor array, and a triangulation strategy was developed to be able to obtain a directional estimate. In principle, a 2D direction triangulation with known sensor positions requires only two independent distance measurements. However, practice has shown that measurement artifacts or noise as well as the limited field of view of each individual sensor can prevent a successful estimation. Thus, four of these ultrasonic sensors were combined to ensure a robust estimation of the contralateral leg.

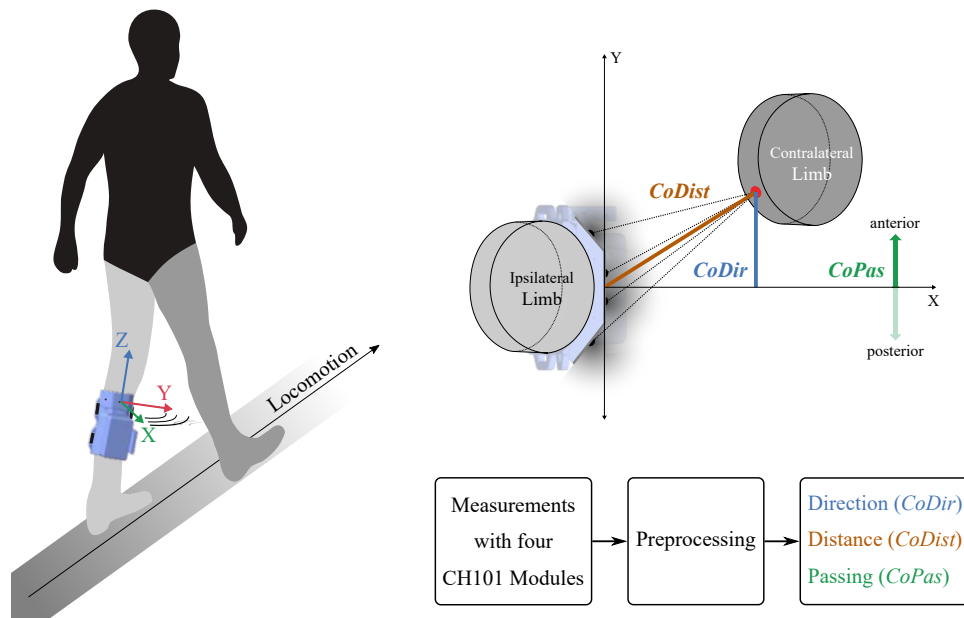


Figure 2.9: Overview of CoLiRang. Four CH 101 ultrasonic sensors are used to determine the direction, distance and passing of the contralateral leg relative to the kit.

2. METHODS

CH 101 ultrasonic sensor. The CH 101 sensor used within this CoLiRang concept is a tiny state-of-the-art product. It combines a micro-electro-mechanical system (MEMS)-based piezoelectric ultrasonic transducer and a power-efficient digital signal processor unit into a small-sized package with only 3.5 x 3.5 x 1.25 mm. Although it was already introduced back in 2015 at the annual Consumer Electronics Show in Las Vegas by Chirp Microsystems, it has only been available since the end of 2019 and is now distributed by TDK InvenSense [64]. Together with a symmetrical horn, it creates a compact module for rapid prototyping with an field of view up to 180°, as depicted in figure 2.10(a). The MEMS structure of the ultrasonic engine shown in figure 2.10(b) is produced in 0.18 μm complementary metal-oxide-semiconductor (CMOS) process technology which is one thousandth compared to the volume of conventional ultrasonic sensors [65].

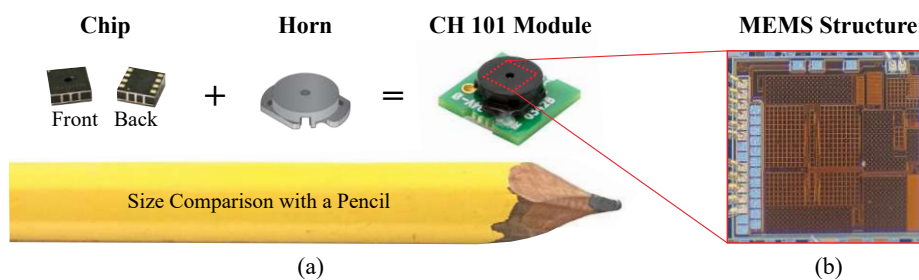


Figure 2.10: Sensor Overview. (a) An ultra-small MEMS-based TOF sensor combined with a symmetrical 180° horn creates the compact omnidirectional CH 101 module for rapid prototyping. (b) Zoomed view of the piezoelectric ultrasonic engine, adapted from [64, 66].

This ultrasonic sensor supports a detection range of 100 mm up to 1.2 m, regardless of the object's color or its optical transparency. Furthermore, this sensor is neither affected by ambient light – it works in complete darkness as well as in full sunlight – nor by unwanted sounds and noise in the environment. Figure 2.11 depicts the block diagram of the CH 101 module and the corresponding development kit. The sensor unit consists of a piezoelectric membrane vibrating at

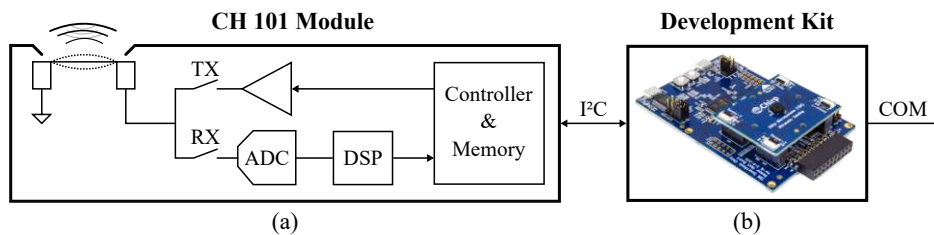


Figure 2.11: Block Diagram of CH 101 module with development kit. (a) Inside the CH 101 module there is a piezoelectric micromachined ultrasonic transceiver and an ultra-low power system on a chip. (b) Range measurements are read out via IIC. The provided development kit supports up to four sensors and offers an easy-to-use COM interface, adapted from [66, 67].

a fixed frequency near 175 kHz. This is interconnected with an application-specific integrated circuit providing a standardized IIC interface. The development kit supports up to four CH 101 sensors and offers an easy-to-use serial interface for rapid prototyping.

Furthermore, the module supports three different operating modes, which are *standby* (recommended to be used if inactive), *free-running* (where the chip runs autonomously) and *hardware-triggered* (most useful for synchronizing several CH 101 ultrasonic sensors). Additionally, it supports either *full range* or *closest detection* read-out configuration. A visualization of the full range mode for two objects is depicted in figure 2.12, with the setup shown in (a) and a snapshot of the amplitude-range diagram taken with the SonicLink graphical user interface provided by the manufacturer in (b). A single measurement cycle consists of 150 (time) samples, with the time directly related to the distance. The chip determines the presence of a target by comparing the amplitude of each sample against a threshold value. Note: This threshold value cannot be modified and varies across the range to compensate for the weaker signals from remote targets. If the amplitude exceeds the corresponding threshold, the presence of an object is detected and the resulting distance can be read out. Moreover, if a real target is closer than the lower range limit, the sensor still reports this minimal value (clipping).

The maximum detection distance is the main limitation for the achievable sampling rate. As already described in section 1.2.2 on page 13, the round trip time of an object at a distance of 1 m is approximately 6 ms. After receiving the signal, the processing time is specified as another 5 ms [67]. The update rate of the CH 101 ultrasonic sensor can, therefore, be as high as almost 100 Hz for the closest detection read-out mode. However, in the full range setting, the additional time required to read out the data via the IIC interface reduces the maximum sampling frequency to as little as 30 Hz.

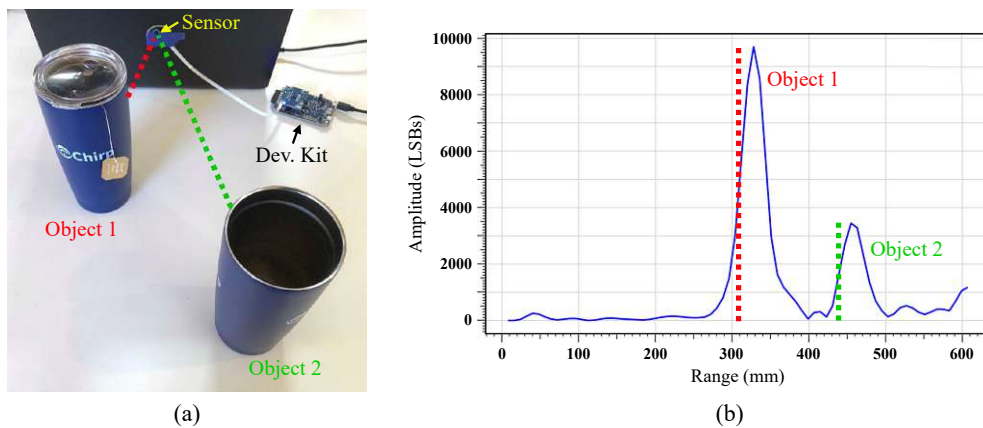


Figure 2.12: Multiple object range measurement. (a) Setup with one CH 101 sensor and two objects in the field of view. (b) Full range read-out via the provided SonicLink graphical user interface showing the received signal peaks for the two objects, adapted from [67].

2.3.2 Signal-Processing Chain

Configuration. The CoLiRang configuration utilized four of these ultrasonic sensors (model CH 101 module manufactured by TDK InvenSense, United States) to determine the distance and the orientation of the sound side. For the evaluation with healthy subjects, a compact kit was designed and tested, as shown in figure 2.9 on page 31. As the kit is worn on the ipsilateral leg directly facing the contralateral leg, this setup allows for an easy integration into a prosthesis system, described in detail in the subsequent chapter *Enhanced Prosthesis Control System*.

As an additional signal for later analysis, an IMU (model BNO055 manufactured by Bosch Sensortec, Germany) was integrated into the sensor kit, too. This information could be used as a control signal or as a reliable basis in order to enhance gait segmentation. However, in contrast to the previously presented CoLiTrack (see section 2.2 on page 22), the estimated orientation and acceleration from the kit was not used to stabilize the ultrasonic input. Instead, all measured and calculated parameters (direction, distance and passing) are reported to the kit itself – the origin is fixed to the center of the sensor casing with a (positive) X-axis going laterally from the kit and a Y-axis in sagittal (locomotion) direction, as shown in figure 2.9 on page 31. Since the kit is universal for wearing on the left and right leg, the direction (Y-value) must be inverted accordingly. A description of the implemented processing approach is given in the following.



Figure 2.13: Block Diagram of the CoLiRang system kit. Ultrasonic sensors measure the distance to the sound-side leg, which is streamed to a laptop via a bluetooth module.

A (hardware) block diagram of the CoLiRang kit is depicted in figure 2.13. The CH 101 modules themselves were powered by the development kit operating in hardware-triggered closest detection mode with an interval of 15 ms between synchronized measurements. Based on the typical step length combined with the average body height and the kit position itself, the system was configured to a working distance from 100 up to 400 mm, which should be sufficient for tracking the entire gait cycle. Both, the IMU and the development kit with the ultrasonic sensors were combined into a custom designed and 3D printed wearable kit, depicted in figure 2.14 on the next page. This setup allowed a quick and easy mounting on the subject's leg. All components were supplied by a commercial 5 V power bank. The captured raw data – distance measurements between the kit and the contralateral leg as well as the ipsilateral shank angle – was streamed to the laptop via a bluetooth module. Finally, processing and analysis was performed using Matlab R2018b running on a laptop with 8 GB memory size and an Intel Core i5-8250U.

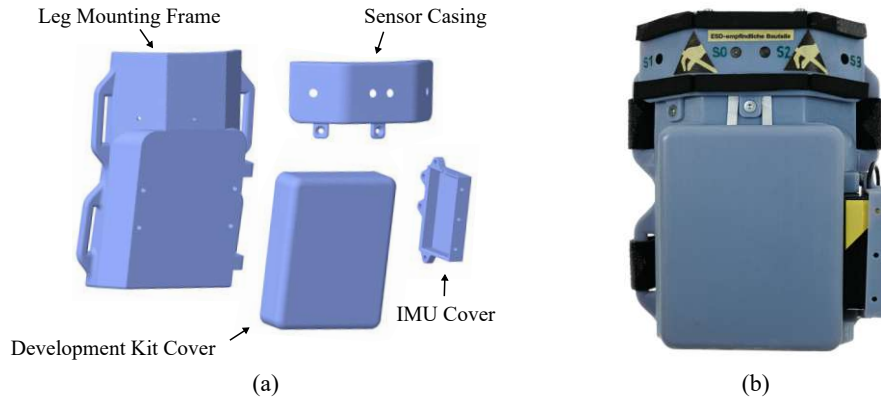


Figure 2.14: CoLiRang casing. (a) Custom 3D printed parts. (b) Assembled system.

Preprocessing. After measuring, the distance raw data is preprocessed, as illustrated in the processing chain in figure 2.9 on page 31. In order to suppress erroneous measurements, an additional spike detection is applied. If the latest sensor value exceeded the previous one by a certain amount, this (potentially wrong) value is discarded and replaced by the previous one (zero-order hold). For the CoLiRang approach, a spike-peak threshold of 180 mm is used, which was derived from typical dynamic gait situations. In addition, spike suppression is performed for a maximum of two cycles (samples) before updating to the actual input value.

Direction triangulation (CoDir). In general, a 2D direction triangulation with known sensor positions requires only two independent distance measurements. However, in order to obtain a robust estimation of the contralateral leg, four sensors were combined into the CoLiRang kit as shown in the illustration 2.15.

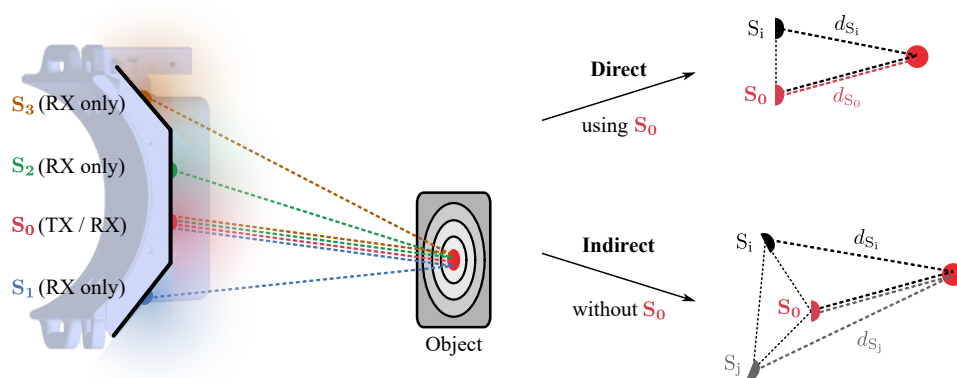


Figure 2.15: Visualization of the triangulation strategy using four CH 101 ultrasonic sensors.

2. METHODS

The sensors were synchronized to start transmitting or recording synchronously, whereby only one sensor, S_0 , was used in transmit and receive mode (TX / RX). The other three sensors, S_1 , S_2 and S_3 , were set to receive mode (RX) only. In this configuration, each sensor reports the distance from sensor S_0 , which is the only one transmitting, to the object where it is reflected and back to the respective detector. Since the sensors operate in the closest detection read-out mode, it is assumed that the reflection point is identical for all four sensors. Different triangulations always between two sensors are calculated to estimate the direction information of the contralateral leg correctly. These can be categorized into two groups: *direct*, using the measured distance d_{S_0} from S_0 , or *indirect*, calculating the object's position without this information.

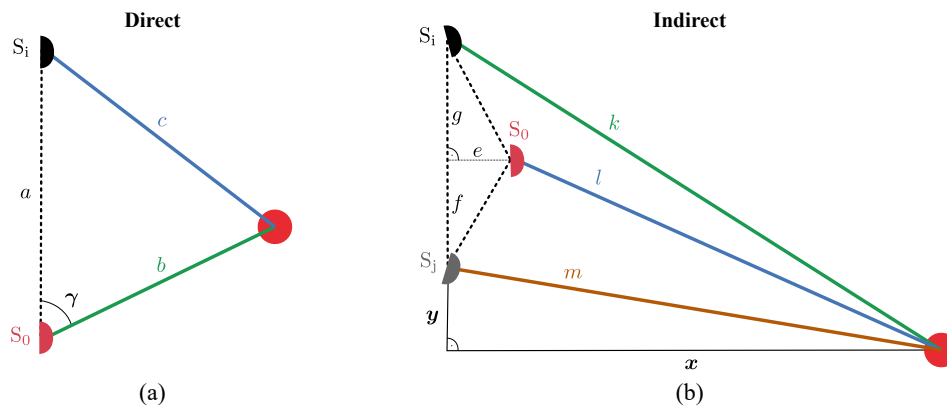


Figure 2.16: Principle of 2D triangulation with known sensor positions. (a) Direct triangulation using the distance d_{S_0} . (b) Indirect triangulation without using the measured distance d_{S_0} .

The *direct* triangulation approach uses the measured distance d_{S_0} from sensor S_0 . As depicted in figure 2.16(a), this creates a triangle with known lengths of the sides, and the law of cosines can be used to calculate the unknown angles. In general, the law states:

$$c^2 = a^2 + b^2 - 2ab \cos(\gamma) \quad (2.1)$$

where γ represents the angle between the sides a and b . If the angle γ is 90° (right triangle), the law of cosines reduces to the Pythagoras's theorem. In this setting, the length of side a is known as the sensor position is known. The length of side b corresponds directly to the half distance d_{S_0} measurement with sensor S_0 , and the length of side c is given by the difference of the distances $d_{S_i} - d_{S_0}/2$. Therefore, equation 2.1 can be rewritten to calculate the unknown angle γ , which can then be used to determine the direction information of the target. Note: For the sensor S_0 running in TX / RX mode, the development board already divides the distance d_{S_0} by the factor of 2 (distance from/to the object).

In contrast to this, the information of sensor S_0 is not used in the *indirect* approach. As illustrated in figure 2.16(b), the direction information of the object is estimated based on geometric constraints. With the help of the known sensor positions, the lengths of e , f and g can be determined.

According to the schematic, the measured distance d_{S_i} of sensor S_i is given by $l + k$, and the measured distance d_{S_j} of sensor S_j is represented by $l + m$. Now, each of these sides (k , l and m) creates a right triangle, rewritten based on the Pythagoras's theorem, as follows:

$$\begin{aligned} k &= \sqrt{(g + f + y)^2 + x^2}, \\ l &= \sqrt{(f + y)^2 + (x - e)^2}, \\ m &= \sqrt{y^2 + x^2}. \end{aligned} \tag{2.2}$$

These equations can then be put into the relations for the measured distances d_{S_i} and d_{S_j} and be solved for x and y . According to the design of the system depicted in figure 2.9 on page 31, this represents the direction information of the target relative to the kit.

For developing and optimizing the different triangulation configurations, the ‘‘leg test bench’’, shown in figure 2.4 on page 25, was used again. However, since the reflection signal was strongly attenuated by the loose trousers, the jeans cover was removed. Overall, six different triangulations, half belonging to the direct and half to the indirect approach, are calculated to estimate the direction information of the contralateral leg correctly. Beside latest individual measurements (t_{new}), also values from the previous sampling cycle (t_{old}) were used to detect and exclude erroneous ones. A summary of all combinations of triangulations is given in table 2.2.

In order to get an accurate and noise-free direction signal, the information about all 18 combinations listed in table 2.2 was postprocessed. To begin with, impossible triangulations were excluded; for example, cases with values reported by the sensor that are too high or too low, which prevent (geometric) triangulation. Next, only results within a certain range around the old (last known) position are selected to calculate the new position by averaging the remaining values. Finally, the signal is enhanced by first-order low-pass filtering with 5 Hz cut off frequency, which is commonly used for movement analysis in biomechanics [33, 68]. In the following, the sagittal component of this final triangulation output is referred to as *contralateral direction* signal and abbreviated as *CoDir*.

Approach	Combinations of Triangulations		
Direct	$d_{S_0,t_{\text{new}}} / d_{S_1,t_{\text{new}}}$	$d_{S_0,t_{\text{new}}} / d_{S_1,t_{\text{old}}}$	$d_{S_0,t_{\text{old}}} / d_{S_1,t_{\text{new}}}$
Direct	$d_{S_0,t_{\text{new}}} / d_{S_2,t_{\text{new}}}$	$d_{S_0,t_{\text{new}}} / d_{S_2,t_{\text{old}}}$	$d_{S_0,t_{\text{old}}} / d_{S_2,t_{\text{new}}}$
Direct	$d_{S_0,t_{\text{new}}} / d_{S_3,t_{\text{new}}}$	$d_{S_0,t_{\text{new}}} / d_{S_3,t_{\text{old}}}$	$d_{S_0,t_{\text{old}}} / d_{S_3,t_{\text{new}}}$
Indirect	$d_{S_1,t_{\text{new}}} / d_{S_2,t_{\text{new}}}$	$d_{S_1,t_{\text{new}}} / d_{S_2,t_{\text{old}}}$	$d_{S_1,t_{\text{old}}} / d_{S_2,t_{\text{new}}}$
Indirect	$d_{S_1,t_{\text{new}}} / d_{S_3,t_{\text{new}}}$	$d_{S_1,t_{\text{new}}} / d_{S_3,t_{\text{old}}}$	$d_{S_1,t_{\text{old}}} / d_{S_3,t_{\text{new}}}$
Indirect	$d_{S_2,t_{\text{new}}} / d_{S_3,t_{\text{new}}}$	$d_{S_2,t_{\text{new}}} / d_{S_3,t_{\text{old}}}$	$d_{S_2,t_{\text{old}}} / d_{S_3,t_{\text{new}}}$

Table 2.2: Triangulation overview.

2. METHODS

Passing point (*CoPas*). Another very interesting gait event is the moment when the contralateral side passes the ipsilateral leg. Although this information is already available within the *CoDir* signal – searching for the change of sign – it could be helpful to calculate it directly. This was done by comparing the distances measured by S_1 and S_3 . For example, assuming the situation when the kit is worn on the left shank. As long as the right leg is behind: $d_{S_1} < d_{S_3}$; however, if the leg is in front: $d_{S_1} > d_{S_3}$. In the following, this swing-by detection is referred to as *contralateral passing* signal and abbreviated as *CoPas*. It is defined to be -1 if the contralateral is posterior and to be 1 if it is anterior. If one or even both of the distances used to calculate it are invalid, the *CoPas* signal is set to 0 for this measurement cycle.

Raw distance (*CoDist*). In addition to the direction, the distance to the nearest object is also evaluated. For this, the range values from all four CH 101 sensors are averaged and filtered. Again, a first-order 5 Hz cut off low pass filter is used to enhance the signal quality. In the following, this (raw) range information is referred to as *contralateral distance* signal and abbreviated as *CoDist*. This signal is always positive (from 100 up to 400 mm), regardless of whether the contralateral leg is forward or backward, with a (local) minimum at the moment of passing by.

2.3.3 Experimental Plan

In order to determine the performance of the CoLiRang approach, static, behavior-simulation and dynamic experiments were carried out. Static experiments were conducted to determine the sensor's distance performance as well as the accuracy of the triangulation approach. Next, the robustness of the triangulation methodology against noise and the performance of correctly detecting a sound-side passing was evaluated. Furthermore, the level-ground walking behavior was simulated using a 4-link biped walking model. Finally, the CoLiRang system was tested with two healthy volunteers; informed consent was obtained prior to the experiments. The anthropomorphic data of the participants as well as the related segment lengths are given in table 2.3.

ID	Height (m)	Age (years)	Sex	Simulation Parameters (mm)
P01	1.87	26	♂	$h_{KIT} = 375 \mid l_P = 220 \mid l_T = 410 \mid l_S = 545$
P02	1.67	25	♀	$h_{KIT} = 360 \mid l_P = 220 \mid l_T = 385 \mid l_S = 465$

Table 2.3: Basic participant's information.

Static evaluation. To begin with, distance accuracy of the sensors as well as triangulation accuracy of the CoLiRang method were evaluated. For the (*sensor*) *distance accuracy* experiment, four CH 101 modules were mounted in a flat plate parallel to a normal wall or pin board, respectively, as shown in figure 2.17 on the next page. The distance was increased in 50 mm steps from 100 up to 400 mm. 1,000 measurements were performed at each level ($n=1,000$), whereby sensor S_0 was configured in TX/RX mode, while the other three sensors, S_1 , S_2 and S_3 , were set to RX only. The provided SonicLink graphical user interface was used to record the amplitude as well as the distance for each configuration.

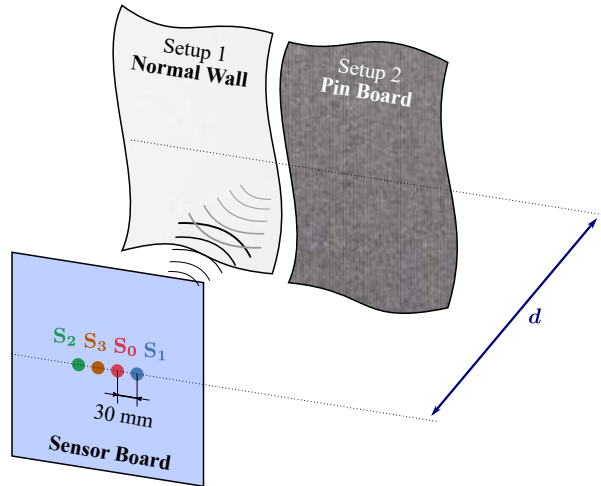


Figure 2.17: Configuration for the (sensor) distance accuracy evaluation. Four CH 101 modules: S₀ (red), S₁ (blue), S₂ (green) and S₃ (orange) are mounted 30 mm apart on a flat plate. The distance between the *Sensor Board* and the *Setup 1: Normal Wall* as well as against *Setup 2: Pin Board* is varied, while amplitude and distance are measured.

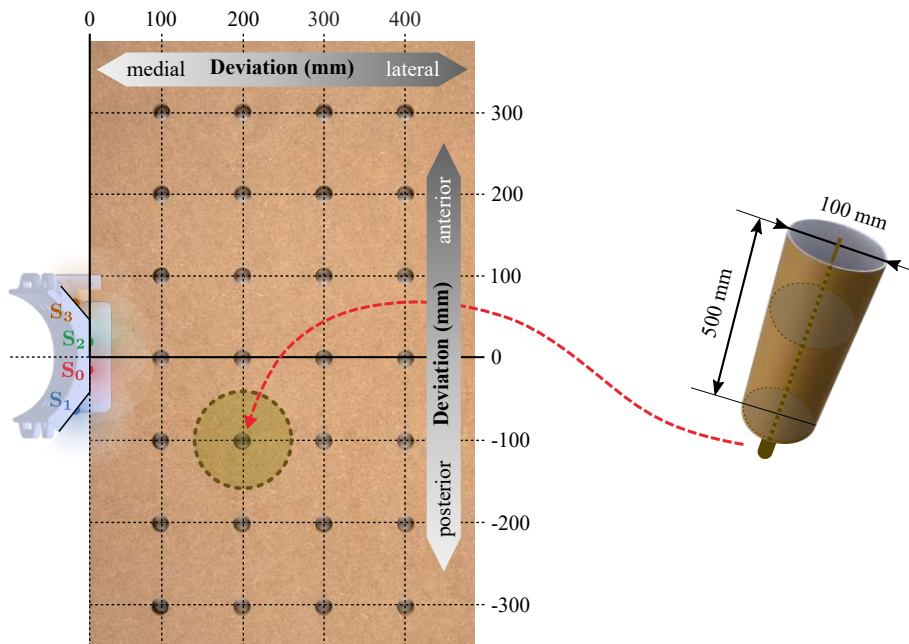


Figure 2.18: Configuration for triangulation accuracy evaluation of the CoLiRang system. The kit is placed on a hole pattern plate with 100 mm grid size. A cardboard cylinder with a bench hook adapter simulates the “human shank”.

2. METHODS

For the *triangulation accuracy* experiment, the kit was placed on the side of a 100 mm grid hole-pattern plate. A 0.5 m high cardboard cylinder served to simulate the human shank. As depicted in figure 2.18 on the preceding page, the position was varied in the range from -300 mm posterior to 300 mm anterior and from 100 mm medial to 300 mm lateral. This test was done for the left and for the right configuration of the kit, averaging 1,000 samples in each position ($n=1,000$). The results of these static experiments are presented in the subsequent chapter.

Behavior simulation. Next, the robustness of the algorithm against noise and the performance of detecting a sound-side passing correctly were explored. Furthermore, the level-ground walking behavior was simulated. The methodology for the *triangulation robustness* experiment was as follows: First, the correct distance values were generated out of the known positions of the CH 101 modules within the kit and the simulation target position. Next, an additional *noise*-factor was added. This was done by generating a uniformly distributed random number in the interval $(-e/2, e/2)$, which was used to introduce noise to each simulated distance. Based on the results from the distance accuracy testing, the standard (distance) deviation was below 8 mm, as shown in figure 3.6 on page 68. Therefore, the error level e used for this experiment was set to 5, 10 and 15 mm, respectively. Finally, all four generated noise-corrupted values were used to calculate the triangulations and the final *CoDir* signal. Within this experiment, the position of the sound side was varied in 100 mm steps from -400 mm posterior to 400 mm anterior and from 100 mm medial to 300 mm, averaging 1,000 samples at each position and each noise level ($n=1,000$).

For the *passing performance* experiment, the kit was placed in front of the “leg test bench” pendulum, as shown in figure 2.19 on the following page. Next, the pendulum was deflected manually by approximately 15° in both directions with about half an oscillation per second. The distance was increased in 100 mm steps from 100 up to 300 mm. 100 repetitions were performed at each (distance) level ($n=100$), to analyze the (reference) pendulum angle at the moment of the sign change of *CoPas*, which represents the passing detection by the kit.

For the *walking behavior* experiment, a 4-link biped model was generated. As shown in figure 2.20 on the facing page, the lower extremities (shank and thigh) are modeled by links, and the joints (hip and knee) are reduced to hinges – motion is therefore only possible in a sagittal (Y/Z) plane. The segment proportions for both healthy participants are summarized in table 2.3 on page 38. The contralateral shank is approximated by the shape of a cylinder with 100 mm in diameter. The basic idea of this simulation approach is as follows: The (norm) gait data from Perry et al. [32], visualized in figure 1.4 on page 6, is taken as input, with the sound-side leg input data generated by 50% gait-cycle shift. Next, this is used to calculate the minimum distance d_{SIM} between the kit worn by the participant on the ipsilateral leg and the contralateral shank for each percent of the gait cycle. In the following, this simulated distance signal d_{SIM} serves as a reference for the *CoDist* behavior at level-ground walking. The results for the behavior simulation experiments are given in the subsequent chapter.

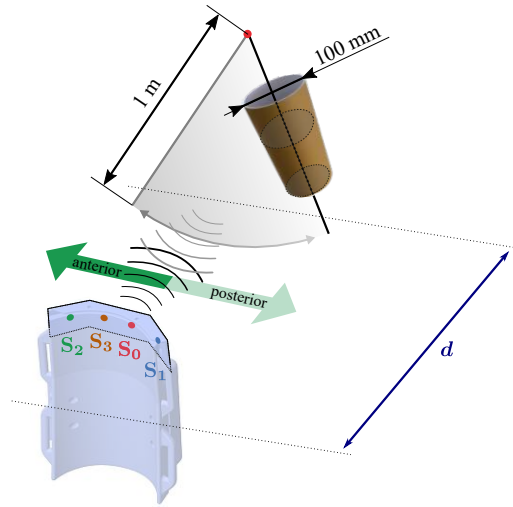


Figure 2.19: Configuration for passing performance evaluation of the CoLiRang system. The kit is placed in front of the cardboard cylinder pendulum simulating the “human leg”. The distance is varied, while the moment of passing and the pendulum angle are measured.

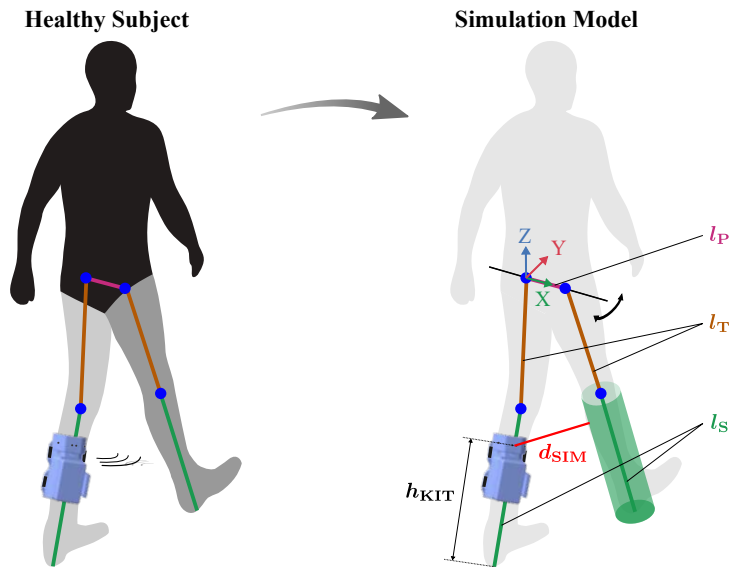


Figure 2.20: 4-link simulation model. The lower extremity of a healthy subject is transferred into a 4-link biped walking model. Motion is simulated only in sagittal (Y/Z) plane. The segment length of pelvis (l_P), thigh (l_T) and shank (l_S) as well as the height of the sensor-kit (h_{KIT}) are given in table 2.3 on page 38. The sound-side shank is approximated by the primitive shape of a cylinder. The minimum distance (d_{SIM}) between the kit and the sound-side leg for each percent of the gait cycle is determined by using the joint angle data from [32].

2. METHODS

Dynamic evaluation. Finally, the dynamic testing was done to analyze the performance of the CoLiRang approach in real-world terrains. For this, an online walking test was conducted with both participants from table 2.3 on page 38. The instrumentation is shown in figure 2.14 on page 35 – the participant wore the kit on the ipsilateral shank, measuring the state of the contralateral side. Next, the participant was asked to start level-ground walking at a self-selected speed, before moving to different terrains, as shown in figure 2.21. Data was recorded individually for the settings of walking at level ground, going down the ramp and descending the stairs. In order to analyze the algorithm behavior with respect to external influences (e.g. sunlight or wind), participant P01 also conducted a short “outdoor walk”, however, this data was only evaluated qualitatively.

The performance of the CoLiRang approach was analyzed as follows: With the help of the IMU, which was embedded into the kit, as depicted in figure 2.14 on page 35, recorded gait data was separated into individual steps. This was done by detecting the local positive peak in the shank data as indicator for the initial contact. Next, due to their kinematics differing from steady-state walking, initiation and termination steps were excluded for all types of terrains (level ground and a ramp and stairs, both downward). Then, individual steps were normalized from 0% to 100%. This was done for the ipsilateral shank angle signal $\alpha_{S,IMU}$ recorded with the IMU as well as for the *CoDist*, *CoDir* and *CoPas* signal captured with the CH 101 modules. The results of the two participants wearing the kit on the left side and on the right side, respectively, are presented in the following chapter.

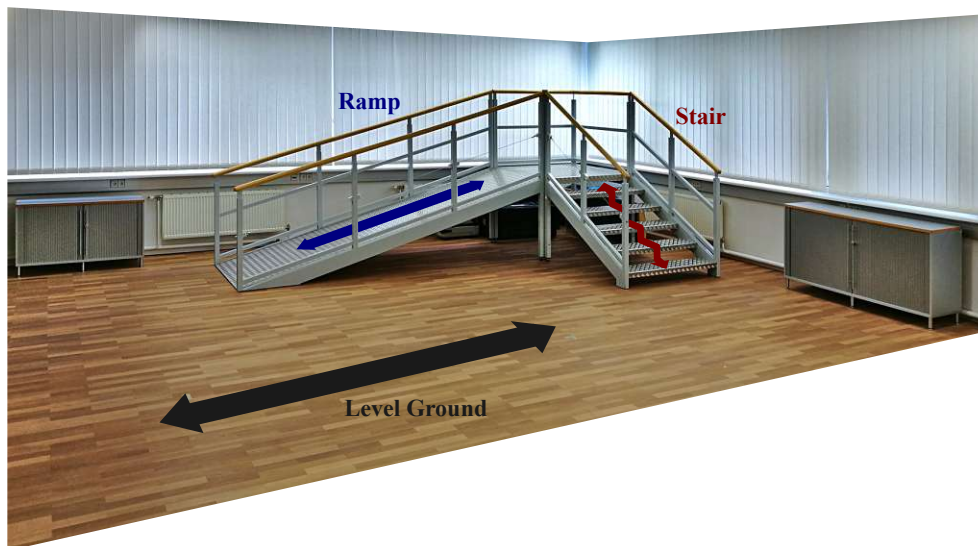


Figure 2.21: Ottobock’s in-house gait laboratory with a 3.5 m / 15° ramp and a 6-steps staircase.

2.4 Enhanced Prosthesis Control System

From this novel perspective, the ultrasonic-based CoLiRang approach was integrated into a prosthesis system, which is referred to as SEP. A prospective clinical pilot study was designed, approved and conducted with the aim to enhance the device control by incorporating information about the amputee's healthy contralateral leg.

2.4.1 System Integration

The CoLiRang approach described previously was extended in order to be integrated into a prosthetic system. Instead of processing sensor data offline, Matlab code was converted and executed directly on an embedded hardware (Arduino Due). This was done by using the support package for Arduino provided with the Matlab Simulink Toolbox. The (hardware) block diagram of this approach is shown in figure 2.22, the complete system in figure 2.23 on the next page.

First, identical to the prior CoLiRang kit (see section 2.3), four ultrasonic CH 101 modules in combination with the development board are used to measure the distances to the contralateral leg. Next, these measurement results are sent to the Arduino for processing. However, additionally, this raw data can also be streamed directly to a laptop via a wireless serial bluetooth module (BT-Raw). In the embedded hardware, the signals (*CoDir*, *CoPas* and *CoDist*) are calculated and sent to a prosthesis – a C-Leg – which is modified so that external data can be read in. Finally, within the high-level layer of the prosthesis, this (healthy leg) information can be used to improve control – the concrete modification is described subsequently in this chapter on page 45. Two additional (safety) signals are generated and sent to the prosthesis: one reporting the status of the “Ultrasonic System” and another to monitor the status of the “Embedded Control” itself. Moreover, a synchronization signal is generated, which can be used for wireless synchronization with external systems (RF-Sync). The power supply of all additional components is provided by a battery pack which is certified for medical applications.

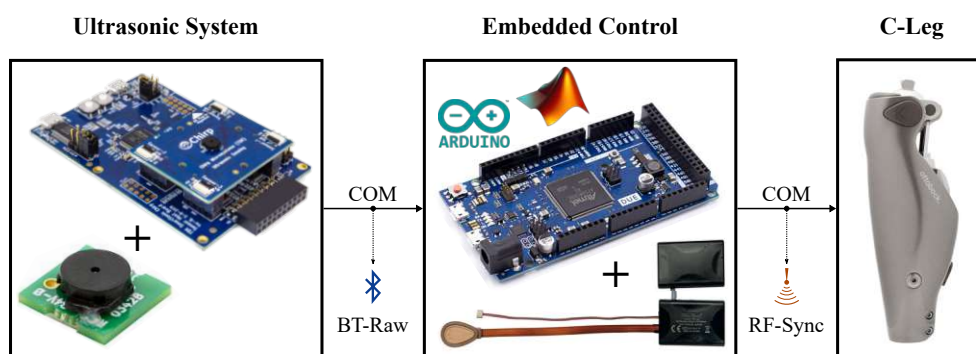


Figure 2.22: Block Diagram of the enhanced prosthesis control system. Ultrasonic sensors measure the distance to the contralateral leg, which is processed in real time directly on an Arduino Due before being sent to a C-Leg prosthesis.

2. METHODS

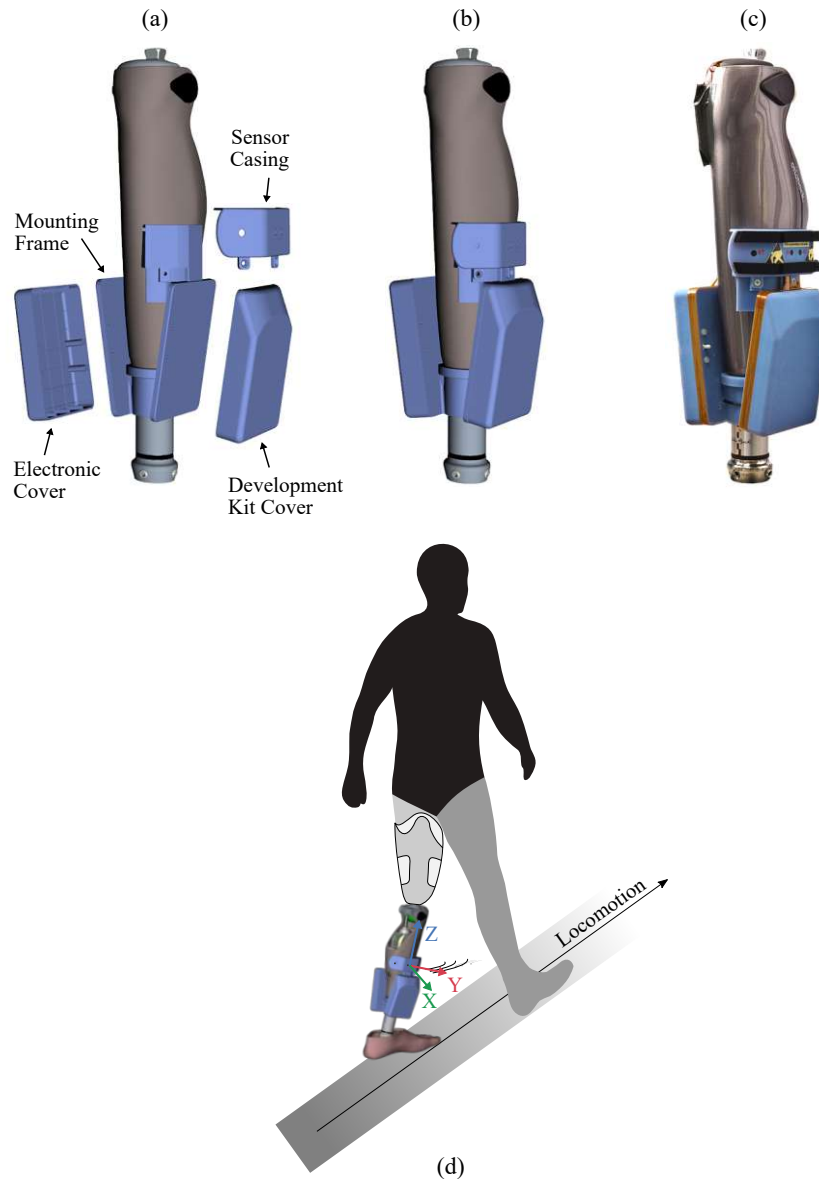


Figure 2.23: Enhanced Prosthesis Control System using four CH 101 ultrasonic sensors to determine the distance and orientation of the sound-side leg. (a,b) Custom designed and manufactured parts; 3D printed. (c) Assembled SEP system. (c) Visualization of the entire concept: An amputee wears the system on the ipsilateral (prosthetic) leg, which determines the state of the contralateral (healthy residual) leg.

Control modification. One of the most important aims of the SEP system is the imitation of the natural gait pattern. However, the currently available C-Leg only provides a constant damping behavior for yielding activities, such as going down ramps or staircases. This is not optimal: First, for the initial contact the damping is too high, later on the support is too low. Therefore, based on the experience gathered from the Ottobock flagship pMPK Genium® [69] as well as from the analysis of able-bodied and disabled lower limbs' kinematic parameters, three novel control enhancements were proposed, implemented and tested. Figure 2.24 depicts these improvements, which are described in the following:

- I** In order to provide an effective absorption of the initial impact, the knee is not fully stretched during the swing phase. This *PreFlex*-feature is set to 2° and can be activated or deactivated individually.
- II** For improving the performance further, the damping factor is reduced to DF_{\min} below the original value and linearly increased to DF_{\max} above the reference, with the maximum to be reached at a configurable knee angle KA_{\max} . These three parameters for this advanced *RampUp*-dampening can be adjusted depending on the subject's personal preferences.
- III** Finally, in order to support a smooth weight transition, the heightened flexion damping is again linearly reduced, until the original damping factor is reached. This is controlled via the contralateral leg information *CoPas*.

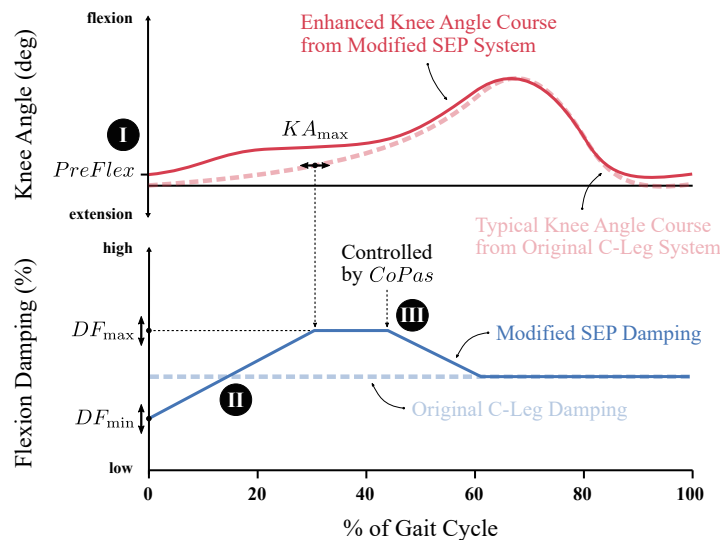


Figure 2.24: Schematic of the high-level control modification for yielding activities.

2.4.2 Clinical Pilot Study

One of the main goals of this thesis was to validate the developed SEP system. For this purpose, a clinical pilot study for testing the system on amputees was designed, and approved by the ethics commission of the city of Vienna (EK 20-296-1220). This section describes the main points from the clinical investigation plan for this study.

General design. The aim of this study is to assess the safety and efficacy of SEP in activities of daily living. The study should help to understand the effect of SEP on the ability to walk, especially down ramps and downstairs. Therefore, the SEP's effect on safety, level walking, stairs and ramps mobility, and patients' satisfaction with the system will be assessed.

The study was conducted at two different study sites: One is the in-house gait laboratory and the orthopaedic workshop at Ottobock and the other one the Orthopädisches Spital Speising, referred to as OSS, both located in Vienna, Austria. As shown in Figure 2.25, this study consists of the four phases *Enrollment*, *Fitting*, *Optimization* and *Evaluation*. A detailed description for each of them is given subsequently in the section 2.4.3 of this chapter.

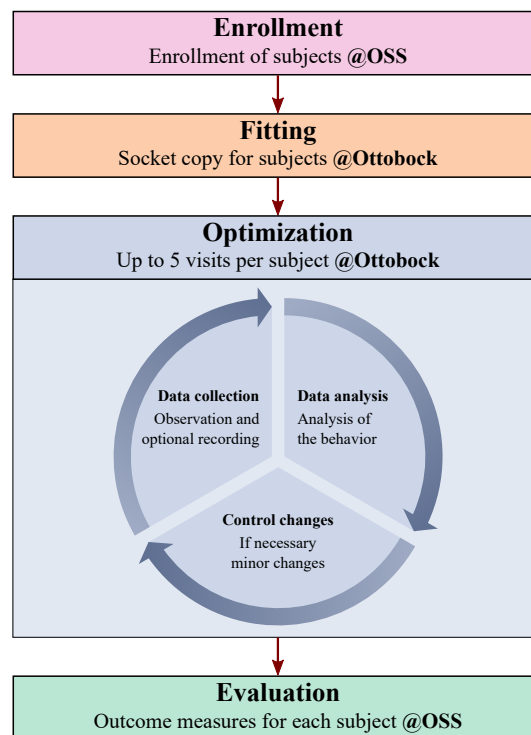


Figure 2.25: Clinical pilot study outline.

Recruitment process. Potential participants for this clinical pilot study were selected according to the following criteria:

Indications:

- + Person is between ≥ 18 and ≤ 60 years old.
- + Person is willing and able to independently provide informed consent.
- + Person is willing and able to comply with study procedures.
- + Person is a unilateral knee-exarticulation or transfemoral amputee with a completely healed amputation wound.
- + Person is a Level 3 or Level 4 ambulator based on the K levels.
- + Person is currently fitted with an pMPK (preferably Genium or C-Leg).
- + Person's weight is ≤ 125 kg (without prosthesis).
- + Person is able to negotiate stairs.
- + Person is able to walk at different speed levels.
- + Person is able to ascend and descend ramps with different inclinations.

Contraindications:

- Pregnant women.
- Person after bilateral lower limb amputation.
- Person has serious problems with current socket (not well fitting socket).
- Person has an unhealed amputation wound, a wound dehiscence or a history of chronic skin breakdown on the residual limb.
- Person falls at least once a week for reasons that are not related to prosthetic use (e.g. problems with vestibular system).
- Person has conditions that would prevent participation and pose increased risk (e.g. terminal cancer, unstable cardiovascular conditions, neurological disorder).
- Person is unwilling/unable to follow instructions.
- Person cannot personally provide their consent.
- Person is using underarm auxillary crutches or a walker.
- Person is currently using an implanted or not implanted medical electrical device (e.g. pace maker or oxygen supply). The abovementioned medical electrical device may be influenced by the electromagnetic emissions from the SEP (exception: the patient's knee and foot prostheses, hearing aids or cochlea implants).
- Person after osseointegration surgery.

2. METHODS

Regulatory requirements. Concerning the regulatory considerations, the Guidelines of the World Medical Association Declaration of Helsinki, the Guidelines of Good Clinical Practice, ISO 14155 as well as the demands of national drug and data protection laws were strictly followed. According to EN ISO 14971, a risk analysis was carried out for the SEP system (depicted in figure 2.23 on page 44) and its technical clearance has been verified. In accordance with the Regulation (EU) 2017/745 regarding the clinical investigation and sale of medical devices for human use, SEP meets the applicable requirements for the clinical study.

COVID-19 pandemic. As this study was done during the COVID-19 pandemic, special precautions had to be taken in order to minimize the risk of an infection: First, participants were enrolled considering patients' medical history and following the recommendations of local authorities at the given time. Second, whenever possible, the number of visits at the study site was kept as low as possible. Moreover, during patient visits, every effort was taken to minimize any potential infection risk by limiting the number of staff to a minimum, providing sufficient protection material to the patients as well as to the staff (e.g. gloves, coats and face masks). Finally, in case of increasing health risk or for any other reason, subjects were able to withdraw from the study at any time. Therefore, it can be concluded that the risks associated with a study visit during the COVID-19 pandemic minimized by the mitigation measures described above are acceptable, when weighed against the benefit that this research can generate for the individual and the population in general.

2.4.3 Experimental Plan

Enrollment. Potential participants were invited to attend an information meeting. If the subject was eligible to participate in the study, they were fully informed about the setting, given an opportunity to ask questions and ample time to consider. Subjects who wished to enter signed the consent form and were subsequently enrolled. In total, five amputees participated in this study. The anthropomorphic data of the subjects is given in table 2.4. Note: The color assignment is only for easier identification and will be reused in the subsequent results chapter.

ID	A01	A02	A03	A04	A05
Sex	♂	♂	♂	♂	♂
Height (m)	1.78	1.78	1.85	1.88	1.73
Weight (kg)	98.3	80.9	91.1	100.7	94.3
Year of Birth	1964	1988	1969	1963	1973
Amputation Side	right	right	right	left	left
Amputation Time	2005	2015	1986	1980	1981

Table 2.4: Basic amputees' information.

Fitting. After the patient enrollment, a certified prosthetist evaluated the participant's socket and foot. Copies of the patient's current socket were manufactured, and the subject was fitted with the SEP system and a suitable prosthetic foot, compare with 2.23 on page 44. As shown in figure 2.26, prosthetic alignment was optimized using the 3D L.A.S.A.R. Posture [70], a live orthopaedic device to improve the subject's static body posture. Acclimatization time was offered after the fitting process and before testing. While an established minimum acclimatization time has not been defined, up to 2 hours accommodation time was recommended [71].

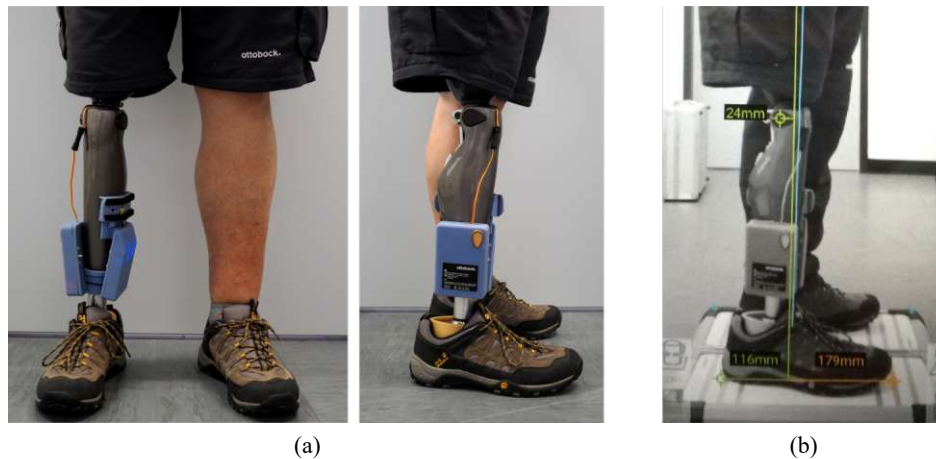


Figure 2.26: SEP setup on an amputee. (a) Frontal and sagittal view taken with a color camera. (b) Sagittal view from the 3D L.A.S.A.R. Posture system used for posture optimization.

Optimization. The aim of the optimization phase was to determine the ideal control parameters DF_{\min} , DF_{\max} and KA_{\max} for each participant, as shown in figure 2.24 on page 45. The initial parameters were defined systematically, however, the final settings varied from patient to patient according to numerous factors, such as the (subjective) sense of safety and the dynamic of the fitting itself or through variations in the (trained) gait pattern. In order to ensure a safe operation of the device, a functional testing of the SEP system was done before each optimization session. This included checking the battery charge, manually testing the stand- and swing-phase, visual inspection of the hardware to eliminate loose components (e.g. loose screws), and monitoring the sensor's signals according to predefined conditions (e.g. movements or loading). Moreover, it is important to mention that there was no home-use phase; patients tested the novel SEP only under supervision and were not allowed to take the test system home. After every single session, the patients were refitted with their own prosthesis, before they left the study site.

As depicted in figure 2.25 on page 46, the cycle for optimization included the three steps of *data collection*, *data analysis* and *control changes*. First, the participants performed the activities of level-ground walking, walking on ramps as well as walking on stairs without any control improvements at the in-house laboratory at Ottobock shown in figure 2.21 on page 42. This status

2. METHODS

is referred to as “OFF (C-Leg)”. During this phase, data was collected and video recordings were made. Next, the obtained data was analyzed. Finally, the enhanced controlling was activated: “ON (SEP)” and the activities were repeated. Based on the participant’s feedback, (minor) changes were made to the control, which were then re-evaluated; the cycle required to optimize the control was repeated. According to the study protocol, up to five (optimization) visits per subject were possible. Note: Walking on stairs and ramps was approached gradually by first doing one stair or just a shallow incline, and then increasing the demands step-by-step.

Evaluation. The SEP system with optimized parameters was evaluated in the gait laboratory at OSS, as shown in figure 2.27. The goal was to provide an objective and comprehensive assessment of walking on level ground (a,b) as well as going down the ramps (c) or stairs (d). According to the Cleveland clinic marker set, 54-markers were placed on the patient’s body, which were subsequently captured by a 17-camera VICON® motion analysis system [72, 73].

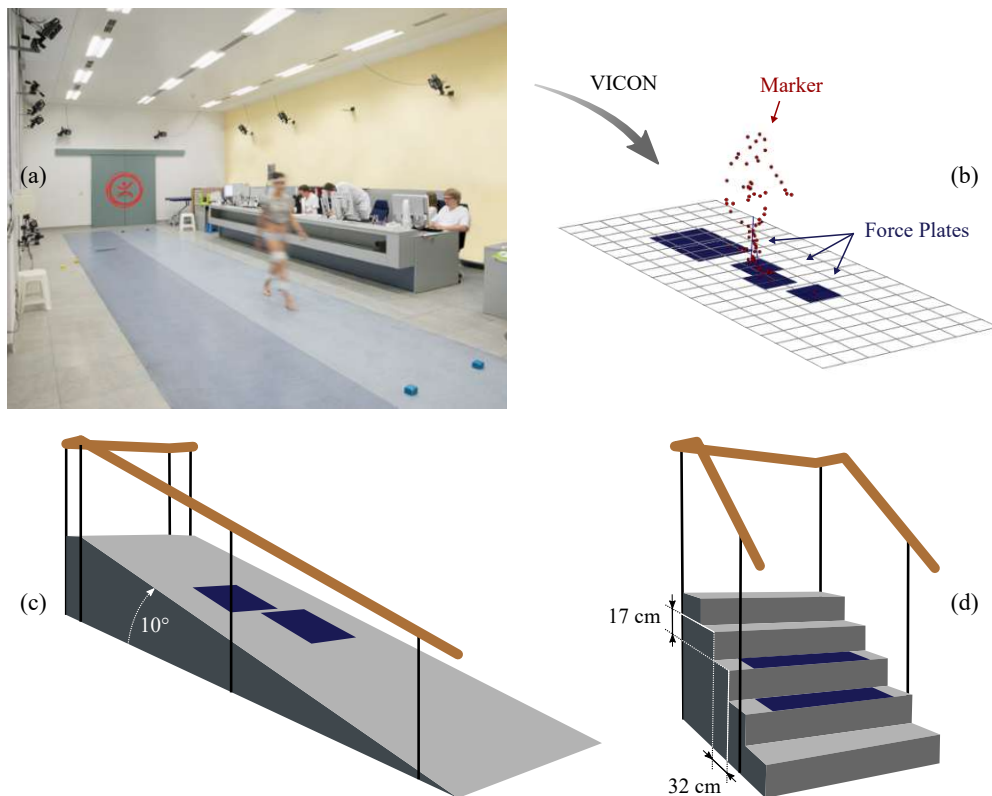


Figure 2.27: Biomechanical analysis system. (a) Laboratory at the Orthopädisches Spital Speising using a 17-camera clinical gait analysis system. (b) Visualization of the 54-markers captured to calculate kinematics as well as the force plates to determine kinetics at level-ground walking. Schematic of the 5 m ramp (c) and 5-steps staircase (d) with embedded force plates.

The following parameters were examined in detail for the activities of walking on level ground as well as going down the ramps or staircases:

- Spatiotemporal gait parameters describe the spatial (distance) and temporal (time) parameters of walking. Within this study, *stance phase* and *step length* are expressed as “gait symmetries” – differences between the ipsilateral (prosthesis) side and the contralateral (healthy) leg. Instead, the *velocity*, *cadence* and *step width* are given as “absolute values”.
- Body center of mass motion describes the displacement of the body during human walking. Within this study, only the vertical displacement was analyzed, because gravity acts as a downward force and, therefore, lifting the body up requires work. In general, minimizing vertical displacement results in a more energy-efficient gait.
- Ground reaction forces describe the force exerted by the ground on a body in contact with it. Within this study, only the vertical component was analyzed, which is responsible for the acceleration of the body’s center of mass in the vertical direction while walking.
- Kinematic and kinetic gait data describe the joint angles and mechanical moments and powers. The kinematic data is acquired directly with such a VICON system, while the kinetic values are calculated based on the measured ground reaction forces and a 3D body model. Within this study, the sagittal components of the hip, knee, and ankle joints of the human body were analyzed.

In this clinical pilot study neither randomization nor blinding was possible – the test sequence was identical for all five subjects. Moreover, the number of trials per activity was relatively low too, somewhere between five to ten, depending on the number of successful hits on the force plates. However, it was not possible to do more repetitions (than that) for two reasons: First, the procedure already took about 3 hours per session and, second, the testing in its current form was exhausting for the amputees. Nevertheless, to be consistent with literature and academia, results were calculated and reported in form of mean and standard deviation.

Finally, in order to assess the end users’ perception of use, safety, performance and satisfaction of the novel SEP system, a self-report test was done. Figure 2.28 on the following page depicts the self-designed questionnaire in German language, which was developed for the case report form *Evaluation* used in this clinical pilot study. All results are reported in the subsequent chapter.

2. METHODS

Case Report Form – Evaluation		ottobock.
Patienten ID: _ _		Datum: _ _ _ _ 2 0 2 _
SELF DESIGNED QUESTIONNAIRE		
Frage	Bitte markieren Sie eine Antwort pro Frage	Bitte optional Kommentare ergänzen
Wie empfinden Sie das Gehen Rampe abwärts?	<input type="checkbox"/> Sehr komfortabel <input type="checkbox"/> Komfortabel <input type="checkbox"/> Unkomfortabel <input type="checkbox"/> Sehr unkomfortabel	
Wie empfinden Sie das Gehen Treppe abwärts?	<input type="checkbox"/> Sehr komfortabel <input type="checkbox"/> Komfortabel <input type="checkbox"/> Unkomfortabel <input type="checkbox"/> Sehr unkomfortabel	
Gewicht: Wie empfinden Sie das Gewicht Ihrer Testprothese?	<input type="checkbox"/> Sehr leicht <input type="checkbox"/> Leicht <input type="checkbox"/> Schwer <input type="checkbox"/> Zu schwer	
Sicherheit: Wie sicher fühlen Sie sich mit Ihrer Testprothese?	<input type="checkbox"/> Sehr sicher <input type="checkbox"/> Sicher <input type="checkbox"/> Unsicher <input type="checkbox"/> Sehr unsicher	
Körperliche Anstrengung: Wie anstrengend empfinden Sie das Gehen mit Ihrer Testprothese?	<input type="checkbox"/> Nicht anstrengend <input type="checkbox"/> Mäßig anstrengend <input type="checkbox"/> Anstrengend <input type="checkbox"/> Sehr anstrengend	
Mentale Anstrengung: Wie stark müssen Sie sich auf das Gehen mit Ihrer Testprothese konzentrieren?	<input type="checkbox"/> Nicht anstrengend <input type="checkbox"/> Mäßig anstrengend <input type="checkbox"/> Anstrengend <input type="checkbox"/> Sehr anstrengend	
Zufriedenheit: Wie zufrieden sind Sie mit Ihrer Testprothese?	<input type="checkbox"/> Sehr zufrieden <input type="checkbox"/> Zufrieden <input type="checkbox"/> Unzufrieden <input type="checkbox"/> Sehr unzufrieden	
Präferenz: Welches System würden Sie im Alltag bevorzugen?	<input type="checkbox"/> Alltagsprothese (C-Leg 4) <input type="checkbox"/> Testprothese (SEP)	

Figure 2.28: Excerpt of the self-designed questionnaire from the case report form *Evaluation*.

CHAPTER 3

Results

The presentation of the results starts with the findings from the current state of research in section 3.1. In the following, the results from the performed experiments are given: the CoLiTrack approach in section 3.2 and the CoLiRang system in section 3.3. The outcomes from the closed-loop prosthesis system testing are presented in section 3.4. A detailed evaluation is given in the following chapter *Discussion*.

3.1 Current State of Research

The search process resulted in 32 publications of interest, as depicted in the flowchart in figure 2.1 on page 21. 24 articles were identified using the database and the snowballing strategy, another 8 were added through the author cross-check.

According to the classification described in section 1.1.3 on page 7 – implicit and explicit environmental sensing – each retrieved publication was assigned to one category. 18 of the publications were found to be related to EES, the remaining 14 to IES. A summary of all included records is given in table 3.1 on the next page. Note: The *Group* field shows the assigned control strategy category; a detailed explanation is given in the discussion chapter.

3.1.1 Implicit Environmental Sensing

Vallery et al. [74] used a linear mapping function to control the missing limb (prosthesis) in dependence of the healthy contralateral leg. Therefore, angle and angular velocity sensors were attached to the residual sound-side hip and knee. The use of this complementary limb motion estimation strategy enabled a transfemoral amputee to achieve an almost physiological gait pattern. However, no further (detailed) technical information was given.

3. RESULTS

Study	Type / Group	Sensor selection	Sensor placement	Concept description
Vallery et al. (P, 2011) [74]	IES / 1	2 x angle & angular velocity sensors	C: hip & knee	Mapping function for control of knee prototype with estimated contralateral limb motion data.
Bernal-Torres et al. (H, 2018) [75, 76]	IES / 1	1 x IMU	C: thigh	Active biomimic polycentric knee prototype with contralateral echo-control strategy.
Su et al. (P, 2019) [77]	IES / 1	3 x IMUs	C: thigh, shank & ankle	Intent recognition system based on convolutional neural network classification.
CYBERLEGs project series ¹ (P, 2017) [78–81]	IES / 1	2 x pressure insoles 7 x IMUs	B: shoe inlays B: thighs, shanks, feet & 1 x trunk	Finite-state control of a powered ankle-knee coupled prototype using whole-body aware noninvasive, distributed wireless sensor control.
Hu et al. (P, 2018) [82–84] Extended by: Krausz et al. (H, 2019) [85]	IES / 2 EES / 2	4 x IMUs 4 x GONIOs 14 x EMGs 1 x IMU 1 x depth camera	B: thighs & shank B: knee & ankle B: leg muscles On the waist in a belt construction	Classification error reduction through fusion of bilateral lower-limb neuromechanical signals, providing feasibility & benchmark datasets. Adding vision features to the prior concept improving the classification.
Hu et al. (H, 2018) [52]	IES / 3	1 x IMU 1 x depth camera	I: thigh	Bilateral gait segmentation from ipsilateral depth sensor with the contralateral leg in field of view.
Zhang et al. (H, 2018) [86]	IES / 3	1 x depth camera	On the waist with tilt angle	Depth signal from legs as input to an oscillator-based gait phase estimator.
Scandaroli et al. (T, 2010) [87]	EES / 4	2 x gyroscopes 4 x infrared sensors	Built into a foot prototype	Infrared distance sensor setup for estimation of foot orientation with respect to ground.
Ishikawa et al. (H, 2018) [88]	EES / 4	2 x infrared sensors 1 x IMU	Left & right on one normal shoe	Infrared distance sensor setup for estimation of foot clearance with respect to ground.
Kleiner et al. (T, 2011) [89]	EES / 5	1 x motion tracking 1 x laser scanner	I: between artificial ankle & knee joint	Concept and prototype of a foresighted control system using a 2D laser scanner.
Huang's group ² (P, 2016) [90–93]	EES / 5	1 x IMU 1 x laser sensor	I: lateral side of the trunk	Terrain recognition based on laser distance, motion estimation and geometric constraints.
Carvalho et al. (H, 2019) [94]	EES / 5	1 x laser sensor	On the waist with 45° tilt angle	Terrain recognition based on laser distance information and geometric constraints.
Sahoo et al. (H, 2019) [95]	EES / 5	3/4 x range sensors 1 x force resistor	I: On the shank & on the heel of the foot	Array of distance sensors for geometry-based obstacle recognition in front of the user.
Varol et al. and Massalin et al. (H, 2018) [96, 97]	EES / 5	1 x depth camera	I: shank	Intent recognition framework using a single depth camera and a cubic kernel support vector machine for real-time classification.
Laschowski et al. (H, 2019) [98]	EES / 5	1 x color camera	Wearable chest-mounting	Terrain identification based on color images and deep convolutional network classification.
Yan et al. (H, 2018) [99]	EES / 5	1 x depth camera	On the trunk in 1.06m height	Locomotion mode estimation based on depth feature extraction and finite-state classification.
Diaz et al. (H, 2018) [100]	EES / 5	1 x IMU 1 x color camera	I: foot & shin	Terrain context identification and inclination estimation based on color image classification.
Krausz et al. (H, 2015) [101]	EES / 5	1 x depth camera 1 x accelerometer	Fixed in 1.5m height with -50° tilt angle	Stair segmentation strategy from depth sensing information of the environment.
Kleiner et al. (P, 2018) [102]	EES / 5	1 x IMU 1 x radar sensor	I: thigh	Stair detection algorithm through fusion of motion trajectory and radar distance data.
Zhang et al. (P, 2019) [103, 104]	EES / 5	1 x IMU 1 x depth camera	I: knee lateral	Environmental feature extraction based on neural network depth scene classification.

P / H / T ... Tested on: (P)atient / (H)ealthy subjects / (T)heoretical; I / C / B ... Mounted on: (I)psilateral / (C)ontralateral / (B)ilateral side;

¹Publications through CYBERLEG: Ambrozic et al. [78, 79], Gorsic et al. [80] and through CYBERLEG++: Parri et al. [81].

²Research group from Huang: F. Zhang et al. [90], X. Zhang et al. [91], Wang et al. [92] and Liu et al. [93].

Table 3.1: Overview of records reviewed, adapted from [MT2].

Bernal-Torres et al. [75, 76] proposed a concept using the echo-control schema. To estimate the trajectory of the unimpaired knee, an inertial measurement unit was mounted on the sound-side thigh. So far, only results from a workbench setting were presented, showing an average tilt angle error between the active polycentric knee prototype and the lower limb of a healthy subject of about 2° .

Su et al. [77] used three IMUs for intent recognition. Sensor data from the contralateral thigh, shank and ankle were processed in a convolutional neural network. These computational processing systems, which are strongly inspired by biological neural networks, “learn” how to perform tasks by optimizing weights and biases during training (example-based learning). Especially through the use of filters, hierarchical patterns can be easily recognized, which makes them very interesting for image recognition systems [105]. Ten healthy subjects and one transfemoral amputee participated in this study. Its aim was to analyze different strategies for user-independent as well as for user-dependent classification approaches. The highest accuracy was achieved in the classification of five terrain types and eight transitions between them, with 89.2% for the amputee and 94.2% for the non-disabled, respectively.

Ambrozić et al. [78, 79] and **Gorsic et al.** [80] implemented a “whole-body aware” control approach for the α -prototype of the *CYBERLEG* project. Seven IMUs – one on the trunk and two each on the feet, the shanks and the thighs – were used to capture user intent. In addition, the ground reaction forces were measured with two pressure inserts on both sides. Control decisions were made with a state machine with unified states and transitions, which were obtained by analyzing the gait of healthy subjects. 85.2% intent recognition accuracy was reported for level-ground walking, tested with three unilateral transfemoral amputees. Within the subsequent *CYBERLEG Plus Plus* project, **Parri et al.** [81] implemented this wearable sensory control approach also in the β -prototype. In contrast to the previous study, more activities than just level-ground walking were analyzed here. The overall accuracy of intention recognition in four unilateral transfemoral amputees was reported to be 100% when walking on a treadmill, even at a low walking speed. With 94.8%, the lowest score was obtained for the sit-to-stand task.

Hu et al. [82–84] were the first to analyze the positive effect of contralateral signals for intention prediction systematically. First, in this study, a (publicly available) benchmark dataset of lower limb electromyography (EMG) and joint kinematics data was collected from ten healthy subjects. Kinematic signals were recorded with electrogoniometers (GONIO) on the knee and on the ankles of both legs, and with IMUs on the subject’s upper and lower leg. Simultaneously, EMG data was recorded by using bipolar surface electrodes on seven muscles in each leg. Second, different combinations of sensors and algorithms were analyzed, with the result that even a single additional sound-side sensor could reduce the error rate in intention detection significantly. Third, data from a transfemoral amputee walking with a (powered) prosthesis was analyzed offline. Compared to ipsilateral sensor placement as baseline (on one side only), two additional IMUs on the patient’s contralateral upper and lower leg reduced overall, steady-state and transitional error rates by more than 60%. **Krausz et al.** [85] extended the system by a single depth camera and an IMU worn on a belt-like construction. Three types of vision-based features were extracted from

3. RESULTS

the environment in front of the subject, namely motion information, distance and orientation as well as the shape of the terrain. Again, the benefits of such a sensor modality were analyzed, and it was concluded that “vision information” reduces variability across activities and subjects, while the repeatability increases.

Hu et al. [52] used the results of their own previous research and presented a novel method for bilateral gait segmentation only from unilaterally worn sensors. In this study, bilateral gait events were detected using a single depth camera and an IMU on the patient’s thigh. Within the depth scene, the RANSAC method [106], an iterative approach for estimating a model in a set of data containing outliers, was applied to detect the ground plane (floor). Next, filtering and grouping methods were used to correctly estimate the shank angle of the sound-side leg. Finally, the ipsilateral IMU data and the contralateral features were fused for improved intention recognition. So far, the system has only been tested with one healthy subject. However, the results showed that it is possible to detect bilateral gait events from sensors worn on only one side .

Zhang et al. [86] also used a depth camera within their study. Both legs were in the camera’s field of view, which was fixed to the waist. The tilt angle was such that the toes were just not captured when standing still. However, walking resulted in a periodic detection that was captured as a variation in the depth values. This data was fed into an adaptive oscillator gait phase detector [107], a concept the author had published earlier. The main idea was to extract “gait features” triggered by the periodic signal. In this study, four healthy subjects participated in a level-ground walking experiment. The maximum estimation error between the (reference) gait phase calculated out of two consecutive steps and the estimated gait phase with the proposed approach was about 0.3 rad.

3.1.2 Explicit Environmental Sensing

Scandaroli et al. [87] proposed a concept to estimate foot clearance, which is an important indicator of gait quality and safety. In this study, two gyroscopes and four infrared distance sensors were mounted on a prosthetic foot prototype. Results from a test bench experiment were presented showing the height and inclination of the foot in relation to the ground. However, detailed technical information was not given.

Ishikawa and Murakami [88] mounted an IMU and two infrared distance measuring elements on a normal shoe. The system was tested with a healthy subject in five different locomotion activities. The analysis of the recorded data revealed a characteristic waveform of the measurement signal for the different modes of locomotion. For example, within leveled walking, a dominant double peak was reported. There was no further information presented.

Kleiner et al. [89] proposed an approach of a foresighted control for a lower limb prosthesis. The idea behind their study was to use an optical measurement system to detect objects such as stairs or ramps in front of the user. For this purpose, an inertial navigation system and a laser scanner were attached between the foot and knee of a prosthetic fitting. It was planned to combine the

motion information gathered from the inertial navigation system with the depth data captured from the laser scanner to create a full 3D representation of the environment. However, so far only “images” from a single indoor experiment without any technical details have been presented.

F. Zhang et al. [90], **X. Zhang et al.** [91], **Wang et al.** [92] and **Liu et al.** [93], as part of Huang’s research group, extended the mode recognition approach. It was based only on mechanical load information on the device and neuromuscular EMG measurements of the residual muscles [108, 109] by adding a single IMU and a laser distance sensor. Six healthy subjects and one transfemoral amputee took part in this study, wearing the additional sensors on the trunk facing forward. Based on geometric constraints and thresholds, the decision tree approach was used to classify the environment in front of the user into five different categories. With an accuracy of 98%, new terrains were identified already 500 ms before executing the locomotion mode transition.

Carvalho et al. [94] used only a waist-mounted laser sensor for terrain recognition. The data collected from ten healthy subjects was classified using a three-layer decision tree with heuristic rules. The proposed approach achieved an overall accuracy of over 80% classifying eight types of locomotion mode transitions. The transition from stair descent or ramp descent into level ground was even recognized correctly to 100%.

Sahoo et al. [95] used an array of distance sensors to classify four terrain types in front of the user. Three laser sensors or four distance sensors were mounted on the subject’s shank. In order to obtain reliable data, a force resistor attached to the heel of the foot was used to trigger the measurement during every stance phase. Two classification approaches were explored on the data gathered from two healthy subjects: a rule-based system and a quadratic discriminant analysis approach. An accuracy above 97% was achieved with the ultrasonic distance sensors, however, the detection range was reported to be less than 50 cm. Therefore, using the ultrasonic sensors could lead to the risk of “missing” a transition if the user’s step length exceeded the detection range. By using the laser distance sensors, this maximum range could be increased to up to 100 cm. Within a single step, the proposed system was able to identify the new terrain with an accuracy of over 98% already 650 ms before executing the locomotion mode transition.

Varol et al. [96] and **Massalin et al.** [97] proposed a system to differentiate between five different locomotion modes. A depth camera was worn on the shank oriented to the front of the user with an angle of inclination relative to the ground of 45°. By subtracting the previous and a current image, a certain motion information was generated. These “depth difference images” were then classified by a support vector machine, a trained algorithm that sorts data into predefined groups. A total of twelve healthy subjects participated in the study. The data from eight subjects was used to train the system, which was then tested by the remaining four. The cubic kernel classifier achieved the highest accuracy of 94.1%, with an averaged computation time of 14 ms.

Laschowski et al. [98] used a color camera mounted on the subject’s chest with the environment ahead in its field of view. A 10-layer deep convolutional neural network was used to classify between three types of terrains. In this study, one healthy subject wore the camera and walked

3. RESULTS

around while capturing over two million images. Around 34,000 of them were labeled manually to train the classifier. The final overall accuracy of the system was reported to be about 94.85%.

Yan et al. [99] proposed a strategy for locomotion recognition without the need of classifier pre-training. In this study, a depth camera was mounted on the user's waist in approximately 1 m height with such a tilt angle that the toes were just slightly captured. Next, the depth images were segmented into twelve blocks and averaged within each segment. The use of a finite-state machine with predefined thresholds made it possible to distinguish between four modes of locomotion. In addition, staircase edges were detected using the Hough Line Transform [110]. This is a feature extraction and voting technique for finding a specific class of shapes, here in this study "lines" representing the stair edges. In total, data from nine able-bodied subjects' trials were analyzed, resulting in 100% accuracy for steady state locomotion and 82.4% for locomotion mode transitions, respectively. Although the calculation time was given as only 5 ms, no online (real-time) evaluation was carried out in this study.

Diaz et al. [100] published an approach for estimating the surface inclination as well as classifying the soil material in front of a subject. An IMU was worn on the foot and a color camera slightly higher up the shin of one healthy participant. In order to capture comparable images, IMU sensor information was used to trigger the camera within the gait cycle's stance phase. Next, the Bag of Words method [111] was applied to distinguish between six types of terrains (cobblestone, grass, carpet, asphalt, tile and mulch). In general, this method classifies the input image according to a predefined bag of local scene features. In this study, an averaged accuracy of 86% was determined for the correct detection of soil properties. Furthermore, the deviation of the inclination prediction compared to a reference was given to be only 0.76°.

Krausz et al. [101] proposed a strategy for estimating stair parameters. Data recorded from a healthy subject holding a depth camera at a height of 1.5 m with a tilt angle relative to the ground of 50° was analyzed. The classification of depth images was done by searching for basic stair structure elements such as edges and planes. The results from the online experiment, in which the participant walked through a hallway and entered a stairwell, achieved an accuracy of 98.8% for distinguishing whether the person was approaching a staircase or not.

Kleiner et al. [102], who were one of the first to publish a foresighted control approach, see above, were also the first group to use radar technology in prosthetic applications in 2018. In this study, a transtibial prosthetic fitting was equipped with an IMU and a radar distance sensor for stair detection. By combining the orientation and depth information, a 2D sagittal plane image of the terrain in front of the subject was generated. Results from an experiment were presented, indicating a mean distance accuracy of 1.5 ± 0.8 cm for objects in a range up to 5 m and a height accuracy of 0.34 ± 0.67 cm.

Zhang et al. [103] published the most advanced environmental feature recognition system to be mentioned in this current state of research evaluation. In this study, an IMU and a depth camera were combined to classify five types of environments. First, the camera scene was transformed into a world coordinate system. Next, 3D input was projected into a sagittal 2D binary image.

Finally, the type of scene was classified using a deep convolutional neural network. In addition, basic computer vision methods were applied to estimate terrain features such as the height and width of stairs or the incline of a ramp. Data from simulations, indoor and outdoor experiments conducted with six healthy subjects and three transfemoral amputees were used to evaluate the proposed approach. The network training was accomplished with simulation results and data from a healthy subject, while the rest was used to test the proposed system performance. The achieved accuracy for amputees was 98.5% for the outdoor experiment. For the indoor experiment, where the terrain change was identified at least 600 ms before the locomotion mode transition was executed, 99.3% accuracy were reached. The most recent article fulfilling the inclusion criteria is also by **Zhang et al.** [104]. In order to improve the classification further, they extended their own approach and included an appreciation of the relationship between states and the credibility of decisions.

3.2 Open-Loop Depth Camera Tracking

This section contains the results of the *static*, *dynamic* and *real-world* experiments carried out with the depth camera-based CoLiTrack approach.

3.2.1 Static Evaluation

The static evaluation experiment shows the potential of this depth camera-based contralateral shank estimation methodology. The gait data from one subject ($N=1$) walking 30 steps ($n=30$) at each speed level on a treadmill was statistically analyzed. In this setup, the camera was mounted on the treadmill itself, facing the subject's shank, as shown in figure 2.8(a) on page 29. Therefore, tracking was possible for the entire gait cycle at all three walking speed levels, as depicted in figure 3.1 on the facing page. Further, camera estimations $\alpha_{S,TOF}$ closely correspond to the IMU reference $\alpha_{S,IMU}$. The shank angle error was calculated for each percent of the gait cycle and summarized in table 3.2. For the medium walking speed, the error e is also depicted as individual box plots (median, lower and upper quartile, as well as the minimum to maximum range), in figure 3.1(b) on page 61. Although higher errors were found in the range between 85% to 95% of the gait cycle, these can be explained by imperfectly synchronized data read-in procedures rather than by estimation errors. Instead, the slightly higher errors at the beginning of the gait cycle, from 5% to about 30%, can be attributed to relative movement of the pants with respect to the leg. Overall, the lowest mean error of $1.4 \pm 1.2^\circ$ was measured at the slow walking speed, while the highest mean error of $3.4 \pm 1.9^\circ$ occurred at the high speed level.

N=1 / n=30	% of Gait Cycle		Shank Angle Error (deg)		
	Speed	Min / Max	\bar{x} / σ	Min / Max	\bar{x} / σ
	slow	100 / 100	100 / 0	$1.4e^{-4} / 09.3$	1.4 / 1.2
	medium	100 / 100	100 / 0	$4.4e^{-4} / 11.3$	1.8 / 1.4
	high	100 / 100	100 / 0	$3.2e^{-5} / 14.1$	3.4 / 1.9

Table 3.2: Static performance of CoLiTrack, adapted from [MT4].

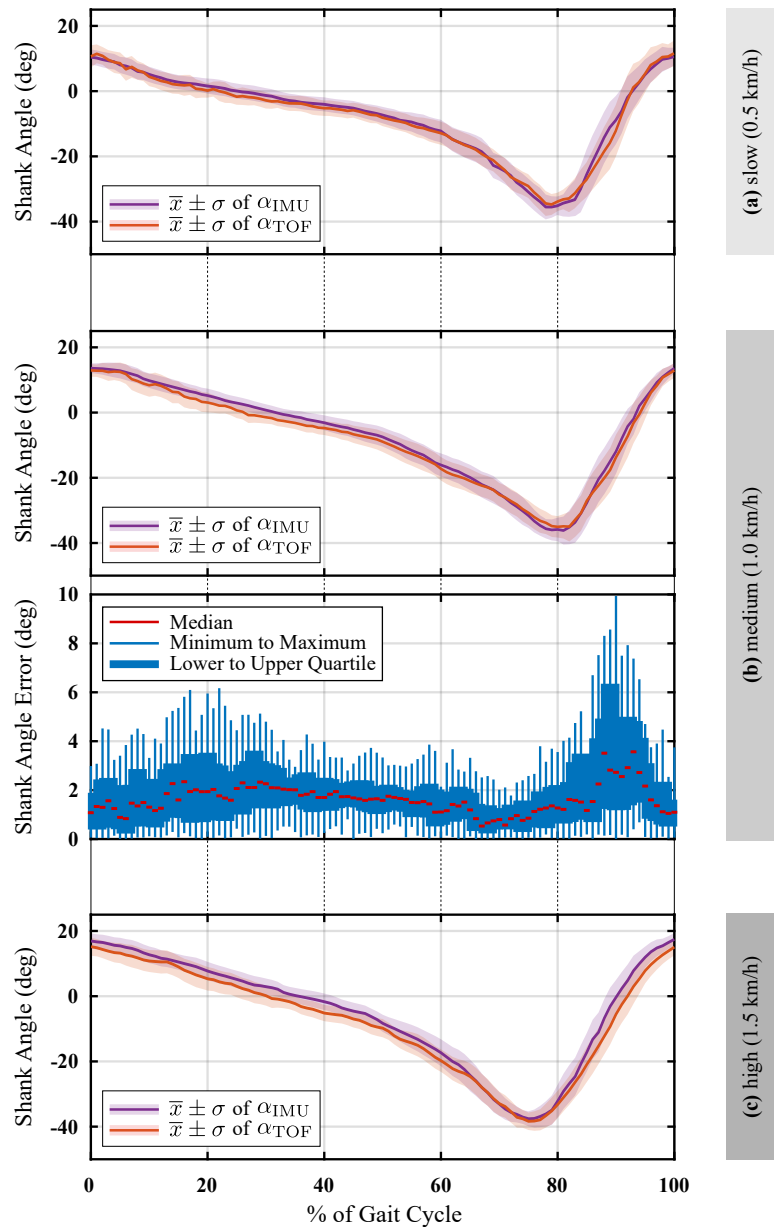


Figure 3.1: Static performance visualization of CoLiTrack at (a) slow, (b) medium and (c) high walking speed. Diagrams depict the statistical analysis of α_{REF} and α_{IMU} for subject S01 ($N=1$) walking 30 steps ($n=30$) at each speed level. The bottom diagram at (b) shows the corresponding shank angle error e as box plots depicting the *minimum to maximum*, the *lower to upper quartile* and the *median* error for each percent of the gait cycle, adapted from [MT4].

3.2.2 Dynamic Evaluation

In order to prove the claim that the CoLiTrack approach does not have a subject-related bias and works independently of the gait speed, it was important to carry out a dynamic test. As depicted in figure 3.2 on the facing page, tracking is possible for about one sixth of the entire gait cycle at all three walking speed levels. The trackable range corresponds thereby with the end of the swing phase, where the heel strike initiates the next step, compare with figure 1.4 on page 6. For some steps, tracking was even possible for longer periods – up to 28% of the total cycle at medium walking speed, as shown in the magnified area in figure 3.2(b) on page 63. With the help of statistical evaluation of 150 steps, plots were generated. For this, 30 steps from each walking speed level ($n=30$) for all subjects ($N=5$) were taken, as listed in table 2.1 on page 28. Through the combination of the depth camera and the IMU into the wearable kit, depicted in figure 2.3(a), instrumentation and calibration of the system on the subjects shank took less than 10 minutes. Although the error for individual steps was higher, the mean error for all three walking speed levels was below 3° . The results of the dynamic testing can be found summarized in table 3.3.

Throughout this testing procedure, the processing time was also analyzed in detail. Overall, the averaged computation time was 50 ms, with the first 10 ms needed to read in the data from both IMUs and the camera itself. The next 25 ms are taken up by preprocessing, since the raw camera data consists of more than 38,000 depth points. The remaining 15 ms are almost entirely needed for fitting the circular models with ICP, whereas the processing time of RANSAC is negligible. Therefore, an online evaluation with up to 20 frames/s is possible.

N=5 / n=30	% of Gait Cycle		Shank Angle Error (deg)	
	Min / Max	\bar{x} / σ	Min / Max	\bar{x} / σ
Speed				
slow	7 / 29	16.7 / 4.6	$4.7e^{-3} / 16.9$	2.8 / 2.1
medium	6 / 28	17.5 / 4.4	$1.6e^{-3} / 13.7$	2.4 / 2.0
high	9 / 26	18.4 / 3.8	$1.0e^{-3} / 14.1$	2.4 / 1.9

Table 3.3: Dynamic performance of CoLiTrack, adapted from [MT4].

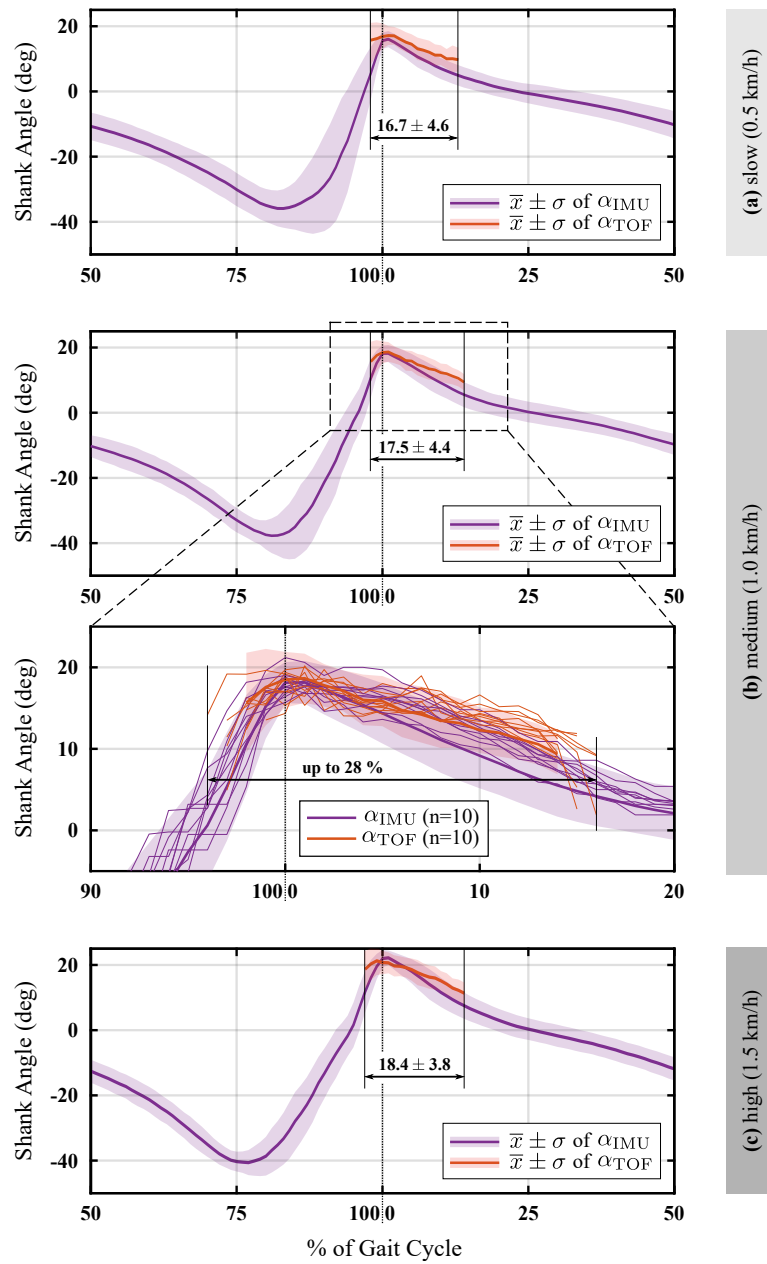


Figure 3.2: Dynamic performance visualization of CoLiTrack at (a) slow, (b) medium and (c) high walking speed. Diagrams depict the statistical analysis of α_{REF} and α_{IMU} for all five subjects (N=5) from table 2.1 on page 28 walking 30 steps (n=30) at each speed level. The x-axis was shifted for a better visualization. The bottom diagram in (b) magnifies the total tracking area and shows ten randomly taken curves out of all 150 steps, adapted from [MT4].

3. RESULTS

3.2.3 Real-World Evaluation

The final test revealed the suitability of the proposed method under real conditions. The one subject (N=1) participating in this experiment was first equipped and then asked to walk normally, before varying gait-speed or moving to different terrains, as depicted in figure 3.3.

Walking on level ground yielded an almost similar result to the dynamic treadmill experiment, whereby initiation and termination steps were successfully tracked as well. However, if the subject walked too fast, a meaningful (real-time) evaluation failed. This was due to the limited sampling and processing rate of a maximum of 20 frames/s, as previously analyzed in detail.

As assumed during preprocessing, the closest point in the depth camera's field of view belongs to the contralateral leg. In this case, other unknown objects (e.g. banisters or even another person standing in front of the subject) were effectively eliminated. However, if the contralateral shank was out of sight, such close obstacles occasionally led to misclassifications. By contrast, ground reflection or clutter did not have any negative impact on the tracking performance.

Since the camera positioning was optimized for walking at ground level, going into other terrains affected the performance negatively. While going from level ground up a ramp had almost no influence on the trackability, depicted in figure 3.3(a), transitioning down a ramp reduced it, as shown in (b). Nevertheless, the tracking of the contralateral leg worked better on ramps than on stairs, where it mostly failed, both up and down. Despite the fact that the contralateral leg was still in the view, as depicted in figure 3.3(c) for up the stairs and (d) for down the stairs, folds in the shoe area often prevented a successful evaluation. In contrast, during level-ground walking, the camera captured a more proximal part of the shank, where the trousers are usually less wrinkled, as shown in figure 2.2 on page 23.

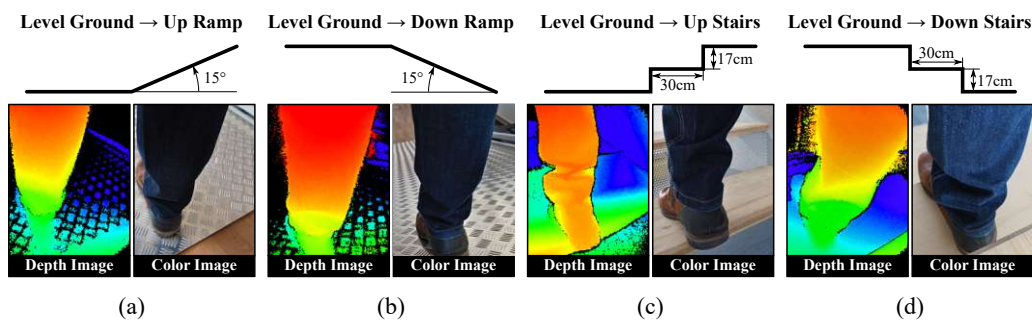


Figure 3.3: Visualization of terrain changes from level ground into (a) up a ramp, (b) down a ramp, (c) up the stairs and (d) down the stairs. *Depth Images* were taken straight out of the depth camera without any preprocessing. *Color Images* were taken with a mobile phone and are for comparison only, adapted from [MT4].

3.3 Open-Loop Ultrasonic Ranging

This section contains the results of the *static evaluation*, the *behavior simulation* and the *dynamic evaluation* carried out with the ultrasonic based CoLiRang approach.

3.3.1 Static Evaluation

Two experiments were conducted in a static setup – one to determine the *distance accuracy* of the sensors and another to identify the *triangulation accuracy* used in the CoLiRang approach.

(Sensor) distance accuracy. The first experiment showed that CH 101 sensors can be seen as both, reliable and valid. This is especially important as the subsequent triangulation strategy requires precise distance values. Range measurements were possible for the full range from 100 up to 400 mm. For each configuration, 1,000 measurements ($n=1,000$) were analyzed statistically and plotted in figure 3.4 on the next page. The colors used correspond to the different sensors, as described in figure 2.17 on page 39. Note: The increased path due to the spacing between the sensors is ignored, as this distance is relatively small compared to the range of interest. Overall, the standard deviation in range is below 8 mm for all measurements and for most of them even below 1 mm, which is in line with the specifications given in the manufacturer’s datasheet [66]. Moreover, the measured range and the true distance fall within 5 mm.

Although the actual amplitude is less important for the final application, it is crucial for the correct distance determination by the development board. As shown in the graph, the amplitude decreases with increasing distance. Moreover, the amplitude is lower for the pin board than it is for the normal wall. This is consistent with theory, as the pin board’s surface structure is more absorbent and less reflective than a normal wall. It is notable that at the minimal measurable range of 100 mm, the amplitude of sensor S_0 is lower than for all the other (longer) distances. As this sensor is the only one operating in transmit and receive mode, the listening (receiving) period could therefore be negatively effected by the previous sending (transmitting) cycle. Instead the other sensors are not effected, as they are operate permanently in receive mode. Nevertheless, this had no effects on the overall (distance) measurement performance as the range was still correctly determined.

Triangulation accuracy. The second experiment proved that the implemented triangulation procedure is sound. Although a single ultrasonic distance measurement does not provide directional information, the CoLiRang method was able to determine the correct position. For each setup, 1,000 measurements ($n=1,000$) were analyzed statistically and plotted in figure 3.5 on page 67; the top diagram for the left-side configuration and the bottom diagram for the right-side configuration. Overall, the mean deviation error lies around 30 mm with an standard deviation for this triangulation approach even below 10 mm. Moreover, an increased lateral deviation had almost no effect on either of them. Therefore, the accuracy of this novel CoLiRang triangulation approach can be deemed sufficient.

3. RESULTS

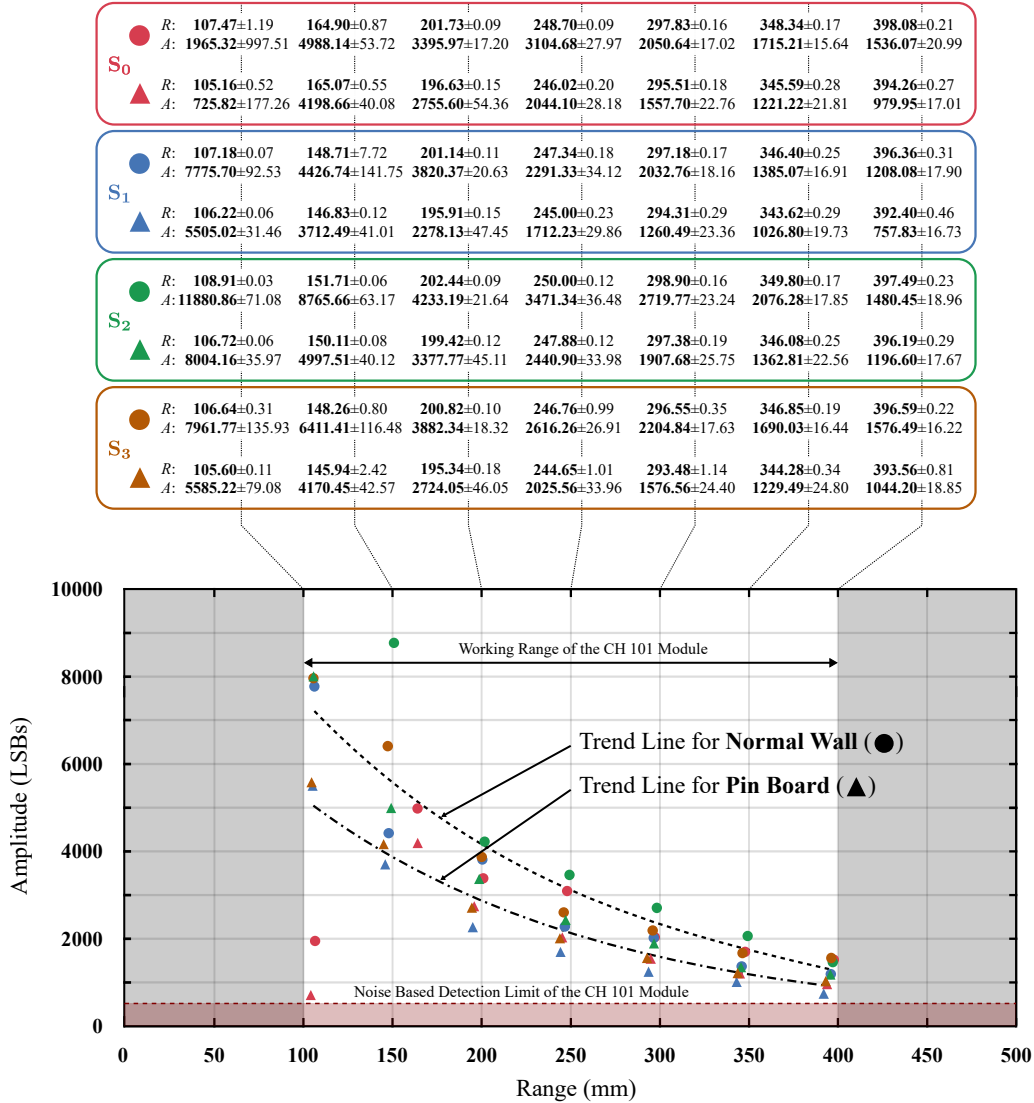


Figure 3.4: Distance accuracy of four CH 101 modules. The diagram clearly shows the decrease in amplitude with increasing distance. Important for the subsequent CoLiRang triangulation strategy is the range deviation, which lies below 8 mm for all measurements and for most of them even below 1 mm. The pin board (\blacktriangle) has a weaker reflection than the normal wall (\bullet). In the table above the diagram, the values for each sensor are given as **mean value** \pm standard deviation ($n=1,000$). The first line refers to the *range* (R), the second line to the *amplitude* (A). In the graphic, the sensors are each shown in the corresponding colors.

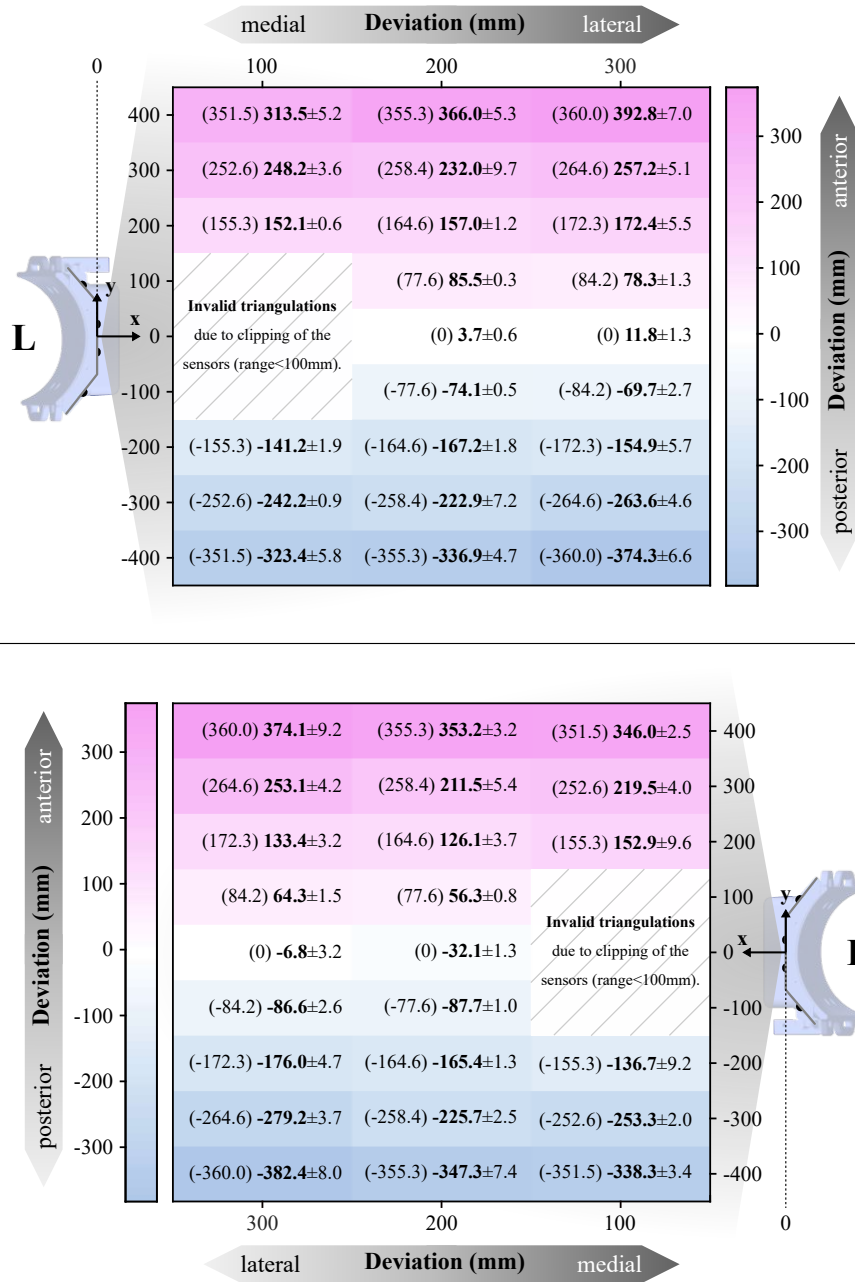


Figure 3.5: Triangulation accuracy achieved by the CoLiRang kit. The top diagram visualizes the results for the left-side configuration, the bottom diagram for the right-side setup. The notation within the fields is as follows: (reference value) **mean value** ± standard deviation of the *CoDir* signal (n=1,000) at each position defined in figure 2.18 on page 39.

3. RESULTS

3.3.2 Behavior Simulation

In order to develop a sense for the CoLiRang system, three behavior simulations were carried out. The first one determined the *triangulation robustness*. Next, the *passing performance* was evaluated and finally the *walking behavior* was explored.

Triangulation robustness. The (triangulation) algorithm developed proved robust against artificially added noise. The statistical analysis of 1,000 calculations ($n=1,000$) for three different noise levels is shown in figure 3.6. For completeness, it should be noted that when the noise level was set to zero, the simulated output matched the input perfectly. Therefore, it is not depicted.

In general, more noise caused more deviation. For example, at the simulation position 100 mm medial / 100 mm anterior: At the lowest noise level, shown in figure 3.6(a), the mean deviation error is only 1.3 mm, while at the highest level (c) the mean deviation error increased up to 7.5 mm. In summary, at the medium noise level (b) which corresponds with the previously determined standard deviation of the distance accuracy, the mean deviation between the known target position and the calculated algorithm output is less than 30 mm for all examined positions.

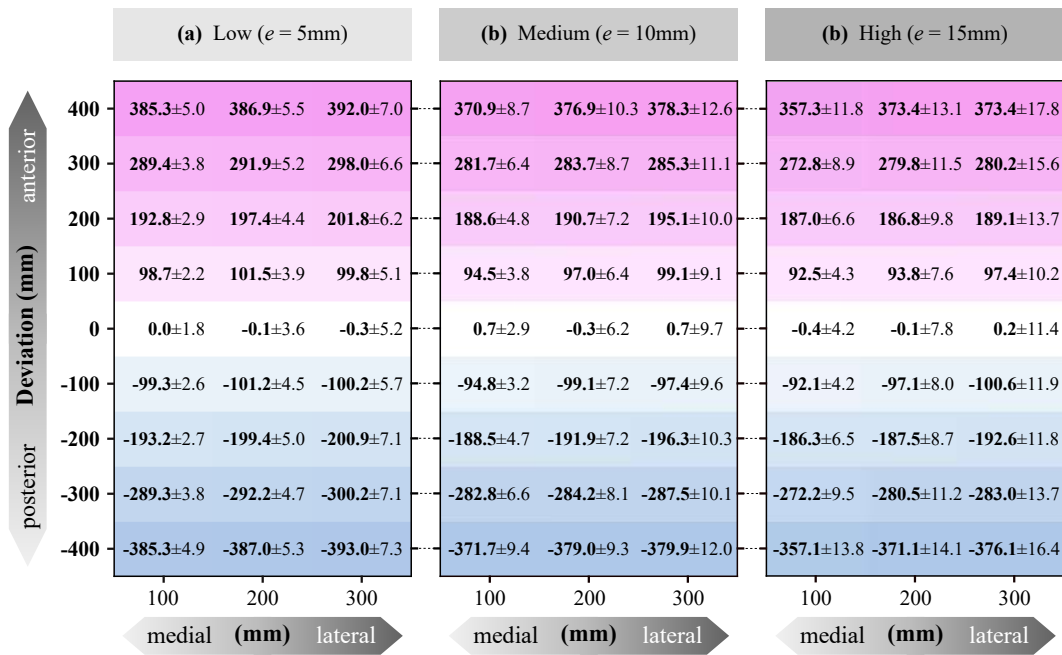


Figure 3.6: Simulation of triangulation deviation caused by (a) low, (b) medium and (c) high uniformly distributed *noise*. The notation is as follows: **mean value** ± standard deviation of the simulated *CoDir* signal ($n=1,000$), with the reference value given by the posterior-anterior deviation in **bold**.

Passing performance. The experiment proved that the CoLiTrack kit can correctly identify the moment of passing (sign change of *CoPas*) independently of the distance between the kit and an object. The pendulum (reference) angle and the *CoPas* signal itself are plotted in figure 3.7. In the scatter plot (b) it can be seen that the maximum deviation lies within $\pm 4^\circ$. For each (distance) configuration, 100 measurements ($n=100$) were analyzed statistically and summarized in table 3.4. Overall, the mean deviation lies below 1° for all distances between the kit and the pendulum. Therefore, the passing performance of this novel approach can be deemed sufficient.

Distance (mm)	Pendulum Angle at the sign change of <i>CoPas</i>			
	min (deg)	\bar{x} (deg)	σ (deg)	max (deg)
100	-3.3	0.16	1.48	3.5
200	-4.1	0.50	1.59	3.8
300	-4.2	-0.29	1.71	4.2

Table 3.4: Passing performance of CoLiRang.

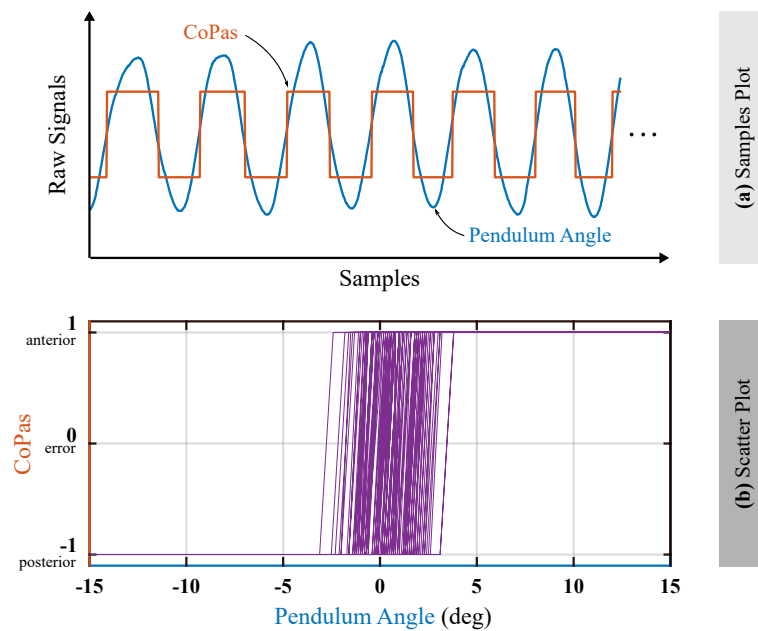


Figure 3.7: Visualization of the passing performance achieved by the CoLiRang kit at a distance of 200 mm. The diagram (a) visualizes the pendulum angle as well as the *CoPas* signal over some samples. (b) Depicts the scatter plot of those signals for 100 (pendulum) swings. The purple area corresponds to the pendulum angle range at the moment of passing, sign change of *CoPas*.

3. RESULTS

Walking behavior. This test simulated the potential *CoDist* behavior for level-ground walking situations. The only input parameter is the nominal joint angle data taken from [32]. Nevertheless, the simulation represents the actual result quite well, compared with the results of the dynamic evaluation in figure 3.9 on page 72 for participant P01 and in figure 3.10 on page 73 for participant P02, respectively. The simulation itself is depicted in figure 3.8.

The local d_{SIM} minimum, for both participants at approximately 30% and 75%, corresponds to the passing of the legs. However, since the minimum range of the CH 101 modules is limited to 100 mm, this limitation was also taken into account for the simulation. As expected, the shape is relatively smooth. Nevertheless, the almost linear increase from about 45% up to 55% was surprising. A detailed analysis revealed that this corresponds closely to the double support phase starting with the contralateral initial contact and ending with ipsilateral toe off.

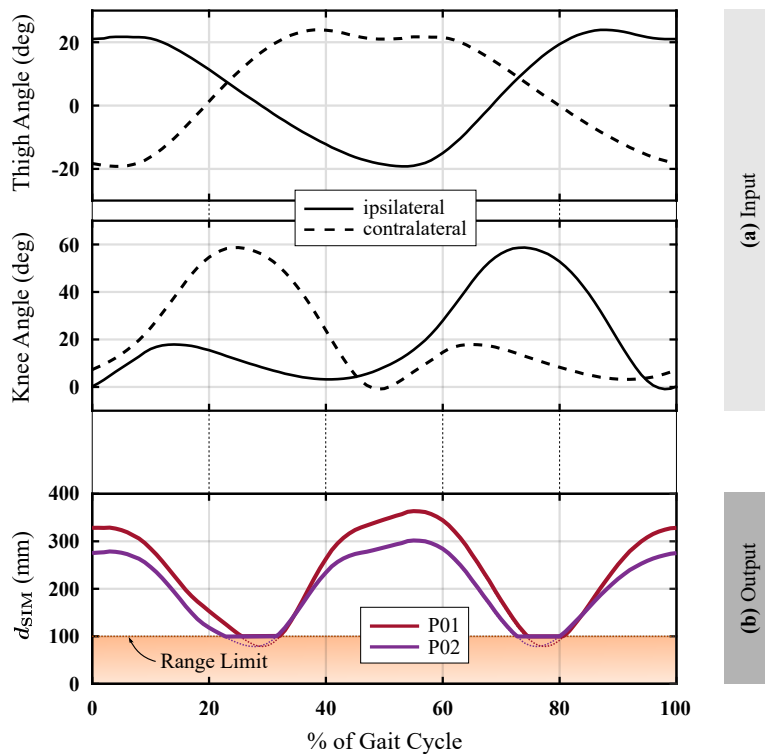


Figure 3.8: Simulation of the *CoDist* behavior at level-ground walking for both participants from table 2.3 on page 38. Joint angle data from [32] are used as input (a) to calculate the output (b): minimum distance d_{SIM} between the kit worn on the ipsilateral leg and the contralateral shank for each percent of the gait cycle.

3.3.3 Dynamic Evaluation

Finally, a dynamic evaluation of different activities was done. The experiment started with the equipping of the participants listed in table 2.3 on page 38 with the CoLiRang kit, first on the left side, and then repeating the procedure on the right side. The instrumentation took less than five minutes. Next, the participants started with level-ground walking, before going into the ramp and staircase, as shown in figure 2.21 on page 42. With the help of the additional IMU integrated into the kit, gait segmentation became possible. Normalized data of the ipsilateral shank angle $\alpha_{S,IMU}$ as well as the corresponding contralateral *CoDist*, *CoDir* and *CoPas* signal measured with the CoLiRang kit are depicted in figure 3.9 on the following page for participant P01 and in figure 3.10 on page 73 for participant P02.

The distance information *CoDist* for walking on level ground showed an almost similar result to the simulation experiment, with body height directly influencing step length and, thus, the maximum values. The two almost identical peaks at around 10% and 60% indicate a symmetric behavior – the leg is as far away in the back as it is in the front. Especially during passing at about 35% and 85%, respectively, the distance would actually be lower. However, since the kit is worn medially on the shank, this remains undetected due to clipping of the sensors – all sensor values are limited to the minimum range. Overall, the step length and thus, the maximum *CoDist* values are lower for the ramp and even lower for the stairs. However, for both terrains, there exists also the distinct second peak at around 60% for the ramp and approximately at 40% for the stairs, which indicates that the sound side is considerably in front.

The direction information *CoDir* provides reliable information about the direction of the sound-side, i.e. whether the leg is behind or in front of the kit. However, the results also revealed that the triangulations itself were less consistent in determining the moment when the contralateral side passes the ipsilateral leg accurately. This is due to the fact that sensor clipping truncates this (close) situations. Strictly speaking, the input for the calculations at these moments is invalid.

In contrast, the direct passing determination *CoPas* proved to be more reliable. The analysis for both subjects in each terrain concluded as follows: For each cycle, an explicit switching from “posterior” to “anterior” and vice versa can be observed. For the ramp this is at around 35% and for the stairs slightly earlier at approximately 30%. The same exists for walking on level ground. However, in this situation, the (contralateral) leg moves forward or backward so far that *CoPas* becomes zero, as one of the underlying distances becomes invalid – the leg is out of range/view for one of the utilized sensors. Note: For better identifiability, the *CoPas* signal is visualized in the plots 3.9 and 3.10 only by a gray band for the complete switching range. Additionally, one random taken curve indicates the typical change from posterior to anterior and vice versa.

Throughout this test, the processing time was analyzed as well. As the approach was already optimized for timing, preprocessing, triangulation and filtering took on average only 1 ms. However, so far, calculation was done only offline in Matlab running on a normal laptop. Furthermore, the short outdoor walk proved the robustness of the sensor modality – a inspection of the signals revealed that external influences such as sunlight or wind did not have any effects at all.

3. RESULTS

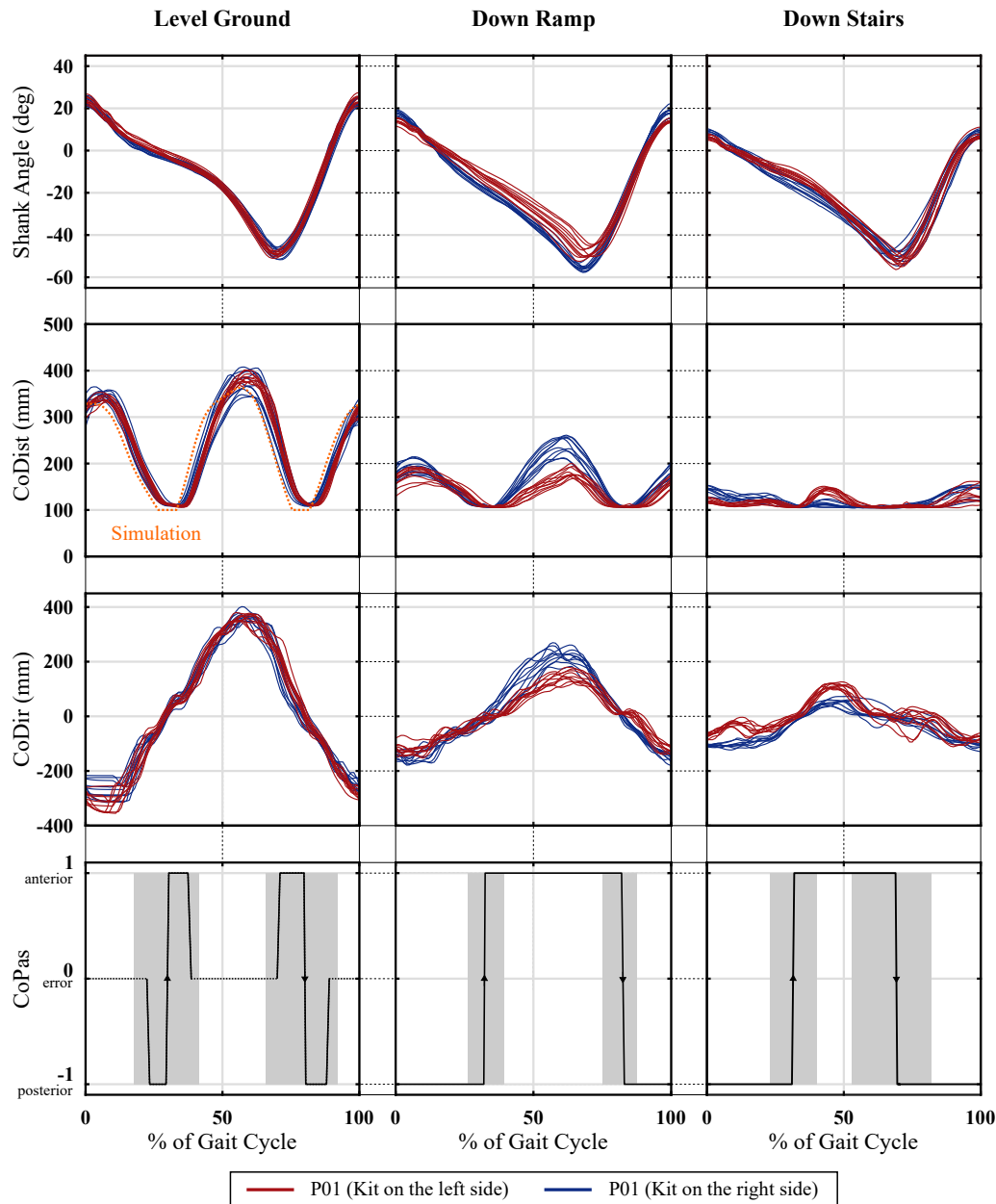


Figure 3.9: Dynamic performance visualization of CoLiRang. Participant P01 wears the kit on the left side (red) and the right side (blue), respectively. The diagrams depict ten randomly taken curves for the ipsilateral shank angle $\alpha_{S,IMU}$ as well as the corresponding contralateral *CoDist*, *CoDir* signal walking at level ground, going down the ramp and going down the stairs. For better recognizability, only one *CoPas* curve is plotted showing the change from posterior to anterior and vice versa with a gray band for the complete switching range. Note: At *Level Ground* the leg comes so far forward or backward that *CoPas* becomes zero, as one of the underlying raw distances used for the calculation of this parameter becomes invalid.

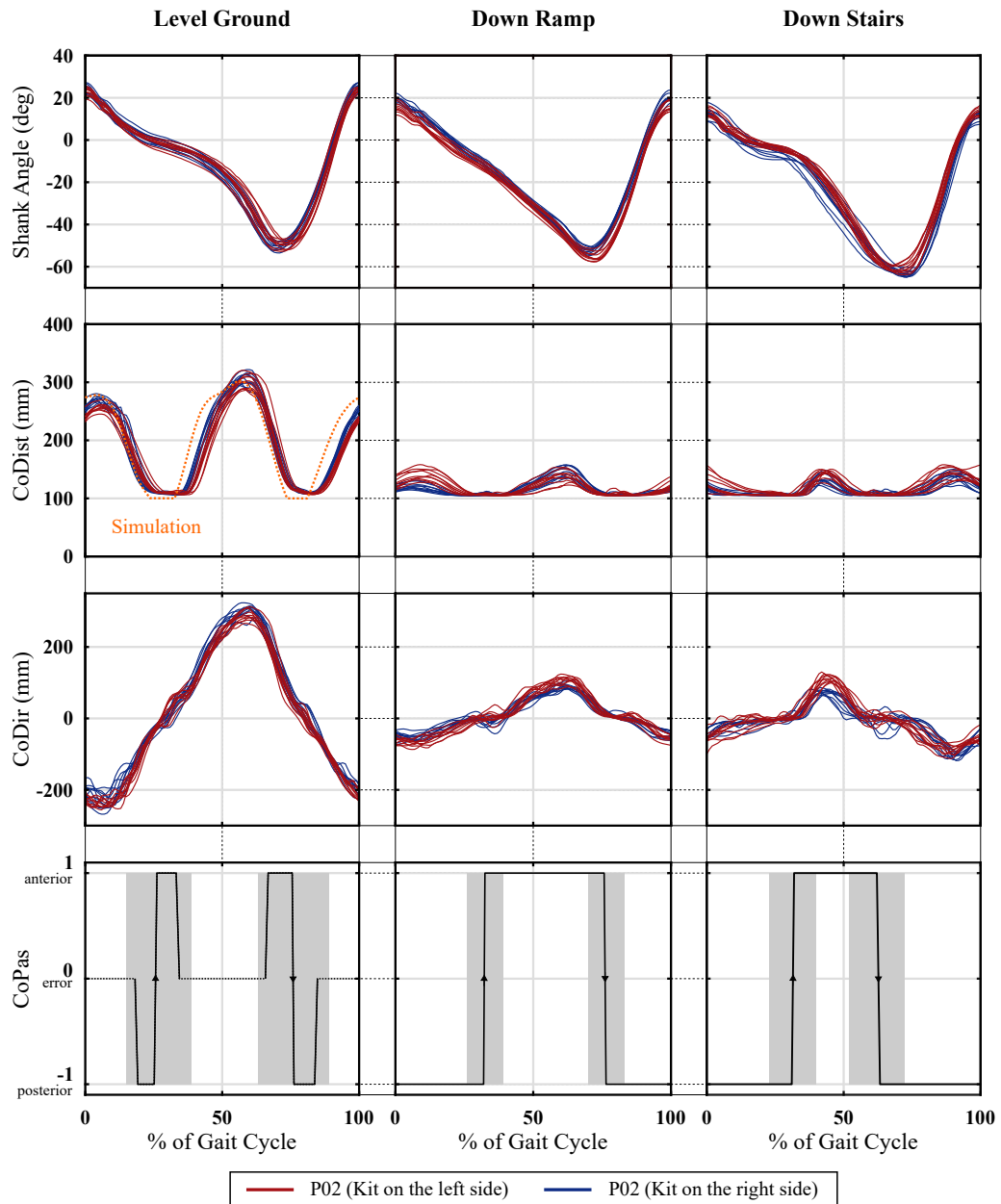


Figure 3.10: Dynamic performance visualization of CoLiRang. Participant P02 wears the kit on the left side (red) and the right side (blue), respectively. The diagrams depict ten randomly taken curves for the ipsilateral shank angle $\alpha_{S,IMU}$ as well as the corresponding contralateral $CoDist$, $CoDir$ signal walking at level ground, going down the ramp and going down the stairs. For better recognizability, only one $CoPas$ curve is plotted showing the change from posterior to anterior and vice versa with a gray band for the complete switching range. Note: At *Level Ground* the leg comes so far forward or backward that $CoPas$ becomes zero, as one of the underlying raw distances used for the calculation of this parameter becomes invalid.

3.4 Closed-Loop Prosthesis System

This section contains the results of the ultrasonic enhanced prosthesis system SEP, which were obtained during the clinical pilot study. First, the *optimized parameters* are summarized. Next, the outcomes from the *biomechanical analysis* are presented, and finally the *satisfaction questionnaires* are evaluated.

3.4.1 Optimized Parameters

According to the clinical investigation plan for this study, patients completed up to five (optimization) visits at the study site Ottobock. In every single session, the patients were fitted with the SEP system, which took about an hour on average. Next, the participants were given an acclimatization time with the deactivated system OFF (C-Leg). The individual C-Leg damping factors for all subjects are summarized in table 3.5. The aim of the optimization was to determine the enhanced parameters for each subject. Therefore, the system was activated ON (SEP), and the activities of level walking, walking on ramps and walking on stairs were repeated.

Overall, the high-level control modifications shown in figure 2.24 on page 45 proved to be effective and convenient. With the help of the recorded gait data footage and all the detailed feedback from the participants, the ideal control parameters were derived. It is important to note that there were neither sudden nor large damping changes, which was perceived as pleasant, or as one amputee said: “*The smoother, the better!*” Table 3.5 summarizes DF_{\min} , DF_{\max} , $PreFlex$, KA_{\max} and $CoDist_{\text{limit}}$ for all subjects. As already suggested in the discussion section of the previous CoLiRang system (see section 2.3 on page 31), the distance signal $CoDist$ and the passing signal $CoPas$ were combined. This means that detecting a passing is only possible, when the $CoDist$ value is below the $CoDist_{\text{limit}}$ threshold. Moreover, due to the narrower kit design, as seen in figure 2.23 on page 44, the medial spacing between the legs increased. This eliminated the sensor clipping, which occurred in the prior CoLiRang work (see section 3.3 on page 65). Finally, after testing, the patients were refitted with their own devices.

Parameter \ ID	A01	A02	A03	A04	A05
C-Leg DF^*	82.5	79	81	82.5	82.5
SEP DF_{\min}^*	80	75	78.5	80	75
SEP DF_{\max}^*	90	89	90	90	92.5
SEP $PreFlex$ [deg]	2	2	2	2	2
SEP KA_{\max} [deg]	30	25	25	25	25
SEP $CoDist_{\text{limit}}$ [mm]	140	150	140	155	150

*Damping factor in % from 0 (nil damping) to 100 (infinity damping).

Table 3.5: Optimized amputees’ parameters.

3.4.2 Biomechanical Analysis

This final measurement was crucial in order to objectively determine the “better behavior” subjectively perceived by the amputees during the optimization sessions of this study. Therefore, all of them had to undergo a full biomechanical gait analysis. According to the clinical investigation plan shown in figure 2.25 on page 46, this was the final visit at the clinical partner study site OSS. Again, each patient was fitted with the SEP system and 54-markers were placed on the participant’s body necessary for the biomechanical (VICON) analysis, compare with figure 2.27 on page 50. Enhanced control parameters were taken from table 3.5 on the facing page. The test procedure was as follows:

In order to prove that the novel SEP system is sound, three different activities were analyzed. First, the subject started *level-ground walking* with the deactivated system OFF (C-Leg). Then, only the *PreFlex*-feature was activated ON (SEP) and the activity was repeated. Therefore, the damping itself was not modified for the level ground task. Second, the system was again deactivated OFF (C-Leg) and the participant was asked to *walk on the ramp*. Now, the complete enhanced control approach with the damping modification was activated ON (SEP) and the subject repeated this activity. Third, the system was deactivated OFF (C-Leg) one more time and the amputee started to *walk on the stairs*. Finally, after that, the system was reactivated ON (SEP), before repeating the staircase activity. Between each configuration, acclimatization time was given and after all conditions the patient was refitted with their own system.

Gait pathology. The observation that was first made during the optimization sessions was confirmed in the biomechanical analysis: All the participants in this study have very individual gait patterns, even despite the fact that the prosthetic fitting is virtually identical for everyone of them. Figure 3.11 on the next page depicts the pelvis and ankle joint angle of all five amputees walking on level ground with the deactivated system OFF (C-Leg). As seen within this group, the gait strategy is (fundamentally) different, as they have to compensate for the prosthesis system itself and probably also for muscle tension or weakness. Therefore, the gait patterns are heterogeneous. For example, A01 and A05 try to compensate with their pelvis. Instead, A02 and A04 use their pelvis less, but compensate with the contralateral (healthy) ankle by vaulting. In this case, the sound foot is on the tip of the toe lifting the body’s center of mass to support the ipsilateral (prosthesis) side with the necessary clearance in the swing phase. The participant A03 is the only one using a foot with a “shock absorber unit” [112], which helps to reduce vertical and torsional forces in the extremities during walking.

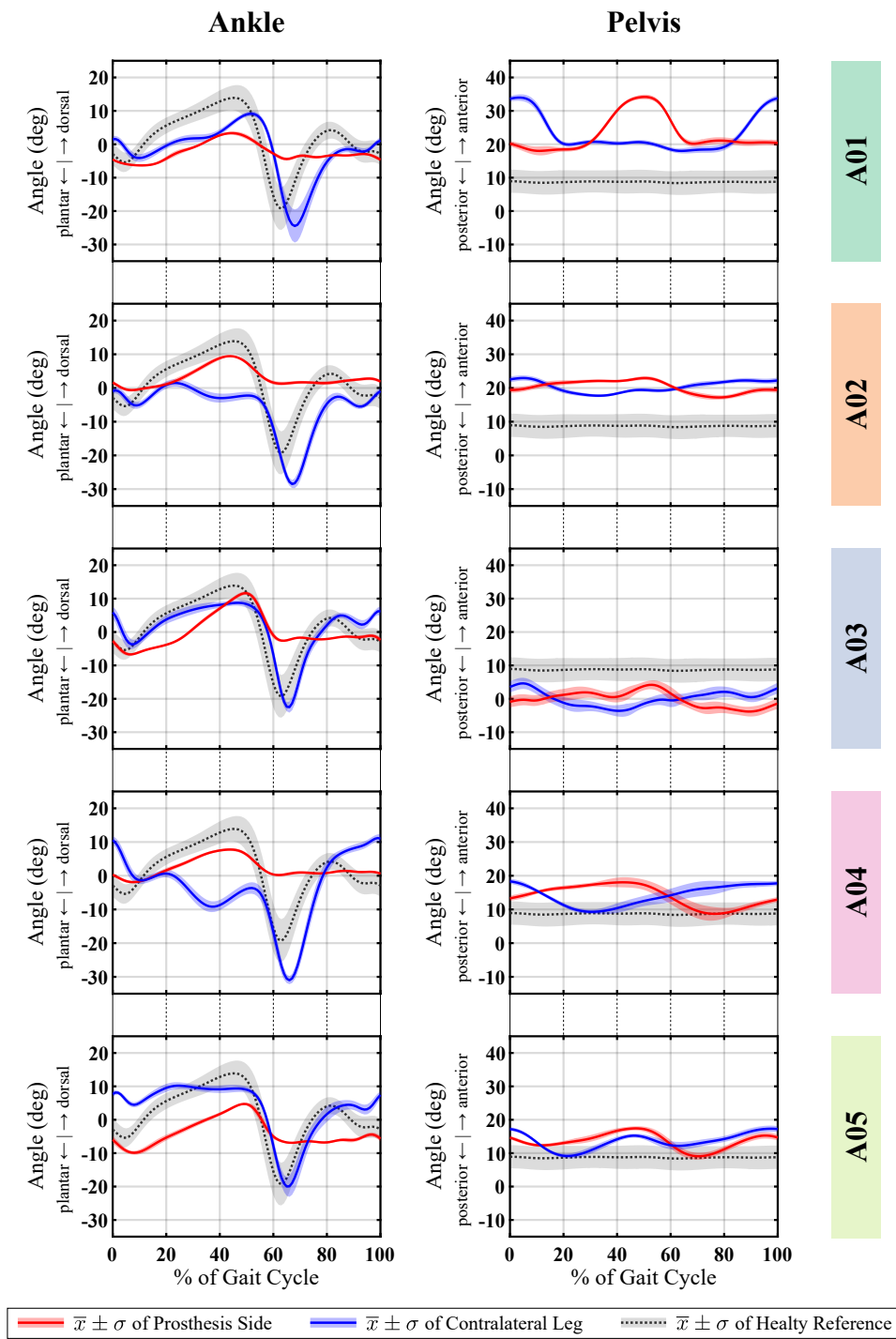


Figure 3.11: Gait pattern deviations of all five amputees walking on level ground.

Level-ground walking. Following the test procedure, level-ground walking was the first activity within the final evaluation session done in this pilot study. The subjects started with the deactivated OFF C-Leg, before repeating it again with the activated *PreFlex*-feature. Note: The damping factor of the prosthesis was not modified for the level ground task. Based on subjective feedback from amputees, no noticeable difference could be perceived between these two conditions.

The mean spatiotemporal gait parameters are depicted in figure 3.12 on the following page. Again, gait pattern differences are clearly noticeable, however the difference with or without the *PreFlex*-feature is less prominent. For three (A01, A02 and A04) out of five participants the gait symmetry improved, while for the remaining two (A03 and A05) the symmetry even decreased. What is not discernible from the graphs but applicable for all subjects: the *stand phase* on the healthy leg is larger than on the prosthesis side. Instead, again for all, the *step length* of the contralateral leg is lower than for the ipsilateral side. In terms of *velocity*, *cadence* or *step width*, there were no considerable differences between the deactivated (C-Leg) or activated (SEP) system.

The mean body center of mass motion is shown in figure 3.13 on page 79. The total *center of mass range* and the *contralateral leg landing* do not show a homogeneous alteration. Instead, the *prosthesis side lifting* is slightly reduced for all five subjects, which is presumably caused by the preflexed prosthesis. However, overall, the changes are very small.

The ground reaction force is plotted in figure 3.14 on page 80, however, no clear variations can be distinguished between the two conditions (with or without the *PreFlex*-feature).

The individual kinematic and kinetic gait data are shown in figures 3.15 to 3.19 on pages 81 to 85. Although the *PreFlex*-feature would support a higher knee stance-phase flexion on the prosthesis side, only three (A01, A04 and A05) out of five actually did do so. For the remaining two (A02 and A03), the preflexed prosthetic joint had almost no influence on the (knee) gait pattern. Again, gait pattern differences are clearly noticeable. For example, patient A01, who is very active with his pelvis, as described in the gait pathology section, has also a very high hip moment and power. The higher standard deviation of hip angle seen with subject A03 could indicate that, despite the acclimatization time provided, he is still not yet completely familiarized with the SEP system. Patient A05 is doing an extreme stance-phase flexion on the contralateral knee, resulting also in very high contralateral knee moment and power, irrespective of the system enhancement.

In summary, the additional *PreFlex*-feature of 2° was only a minor modification to the (commercially available) C-Leg system, and led to hardly any measurable changes. Therefore, both the (subjective) perception of all five patients and the (objective) biomechanical measurements are in agreement for the task of level-ground walking.

3. RESULTS

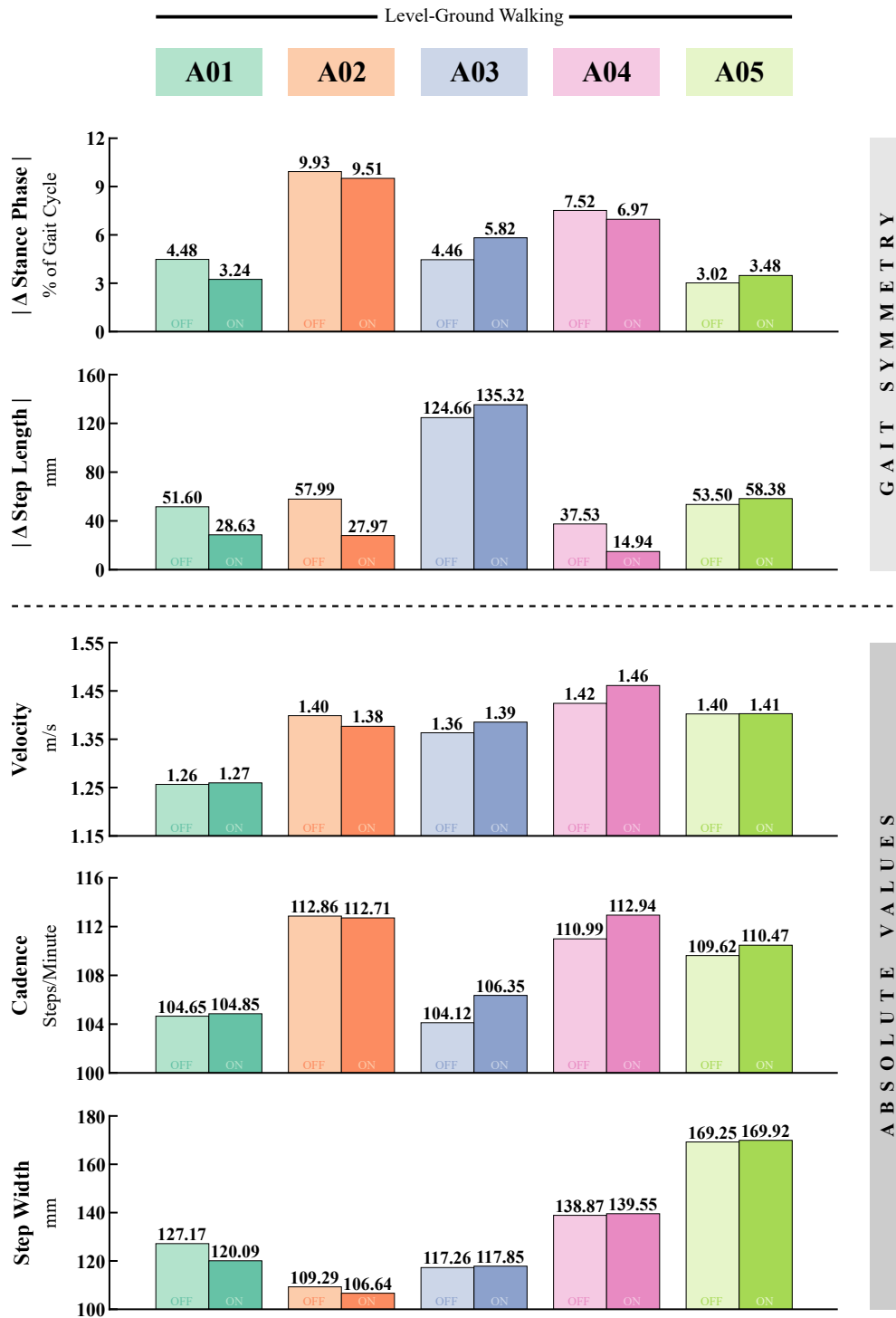


Figure 3.12: Spatiotemporal gait parameters of all five amputees walking on level ground.

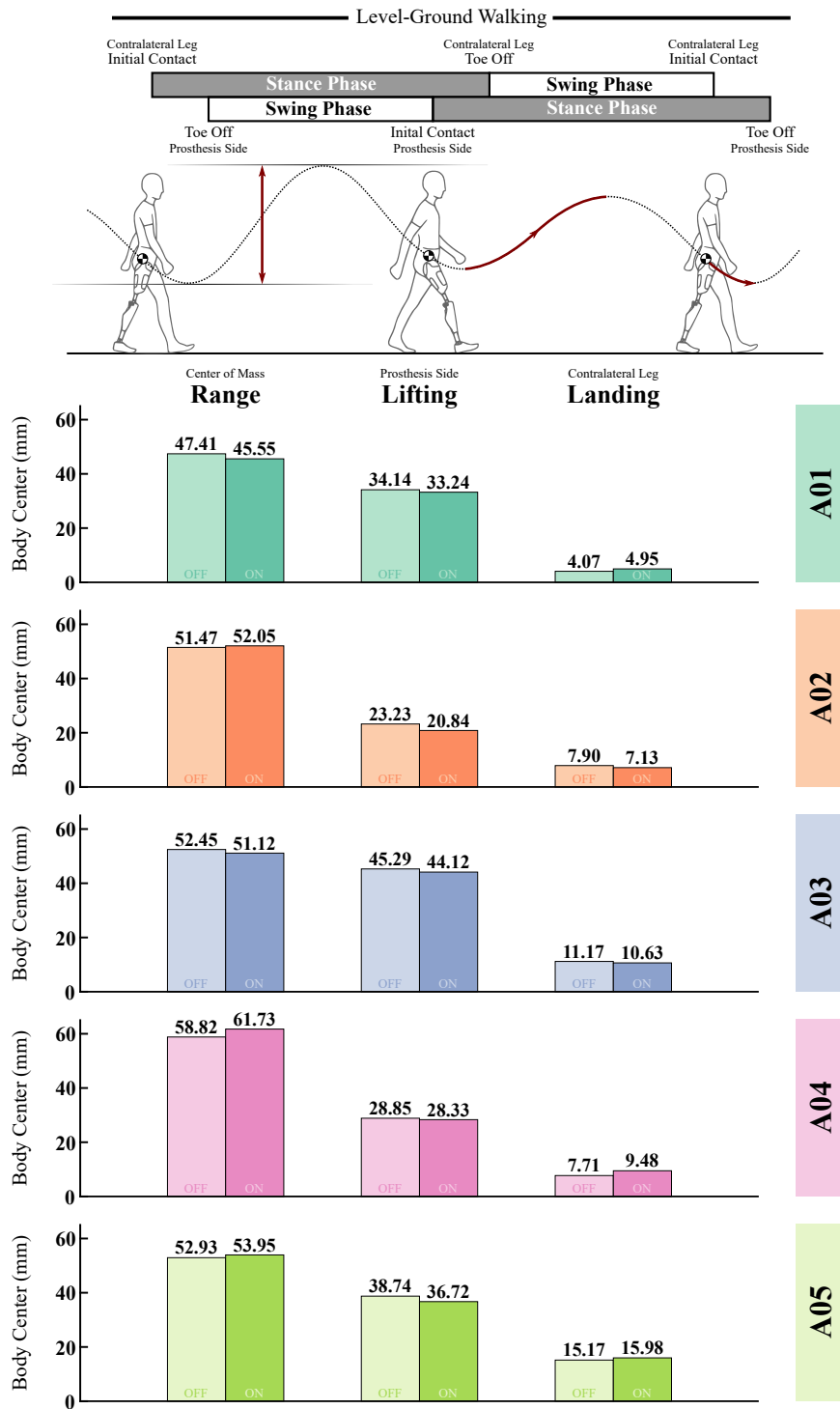


Figure 3.13: Body center of mass motion of all five amputees walking on level ground.

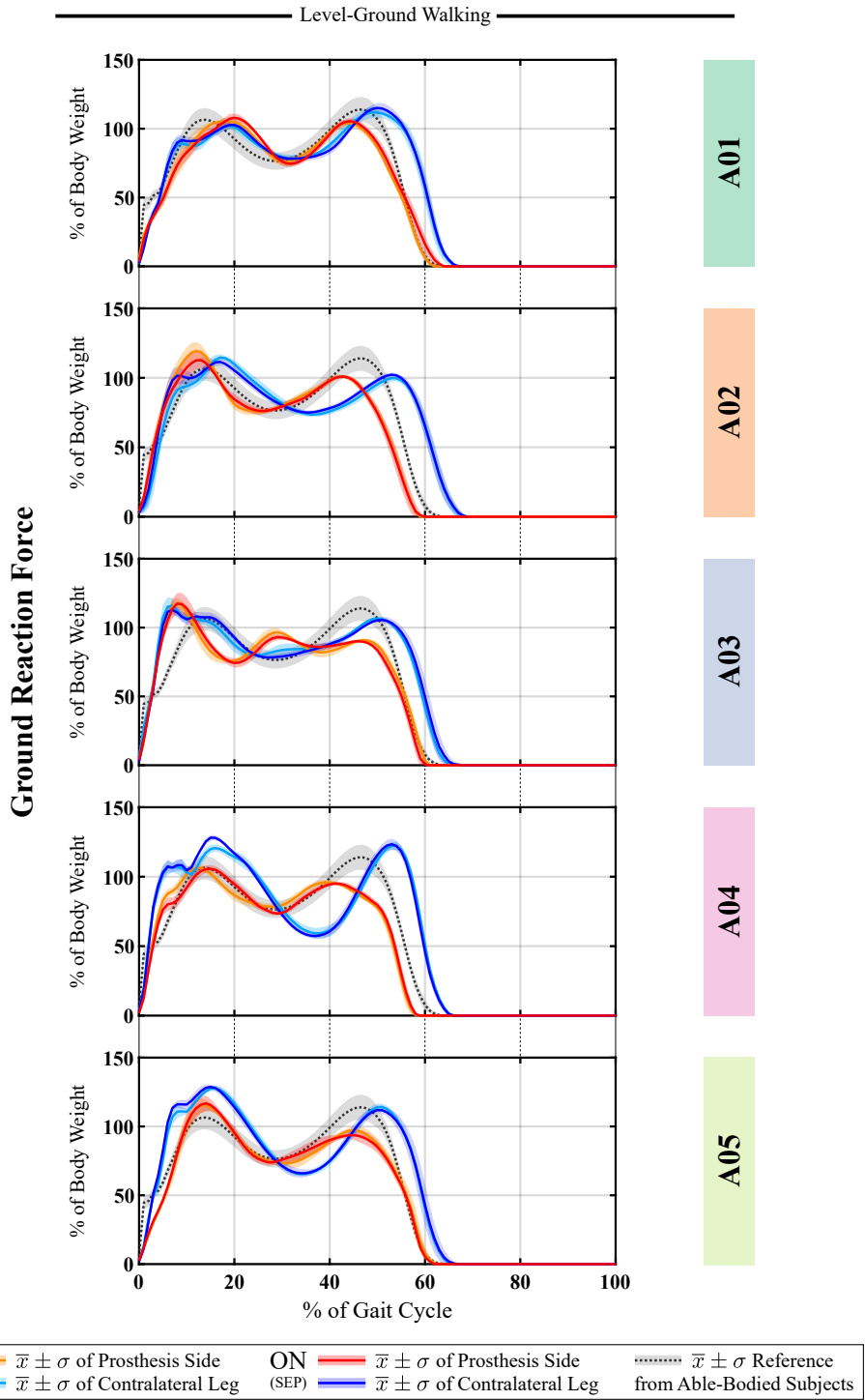


Figure 3.14: Ground reaction force of all five amputees walking on level ground.

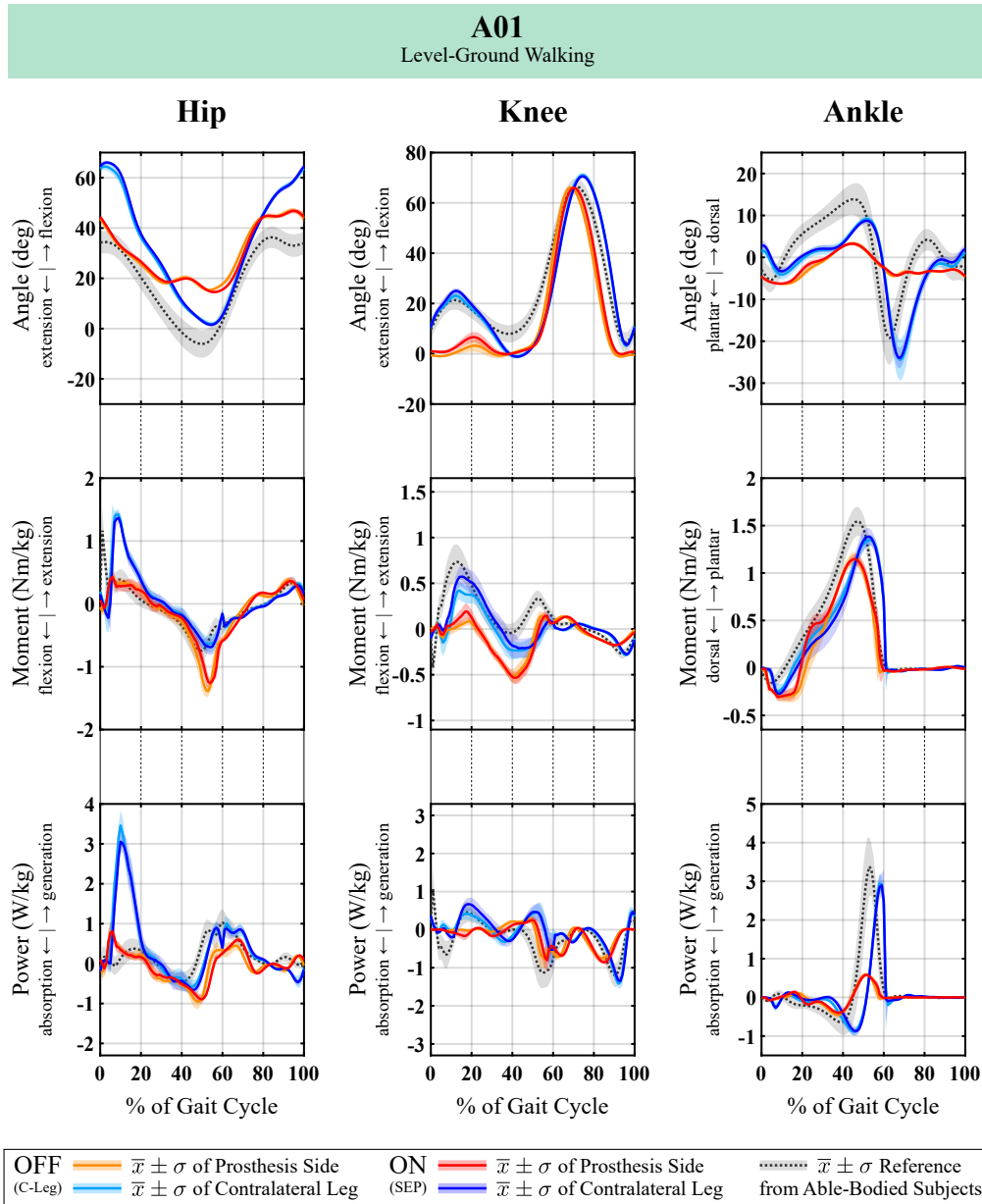


Figure 3.15: Kinematic and kinetic gait data of amputee A01 walking on level ground.

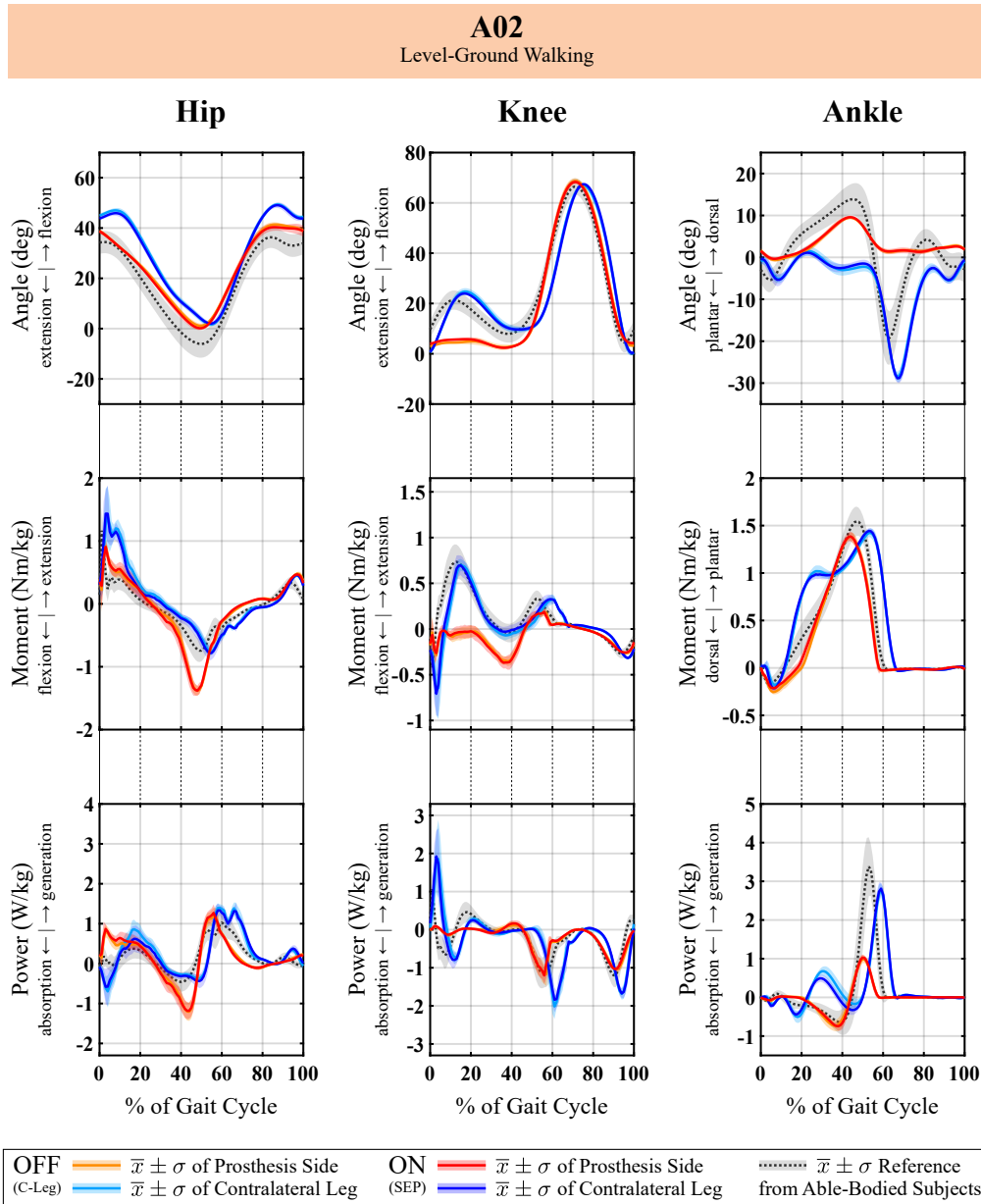


Figure 3.16: Kinematic and kinetic gait data of amputee A02 walking on level ground.

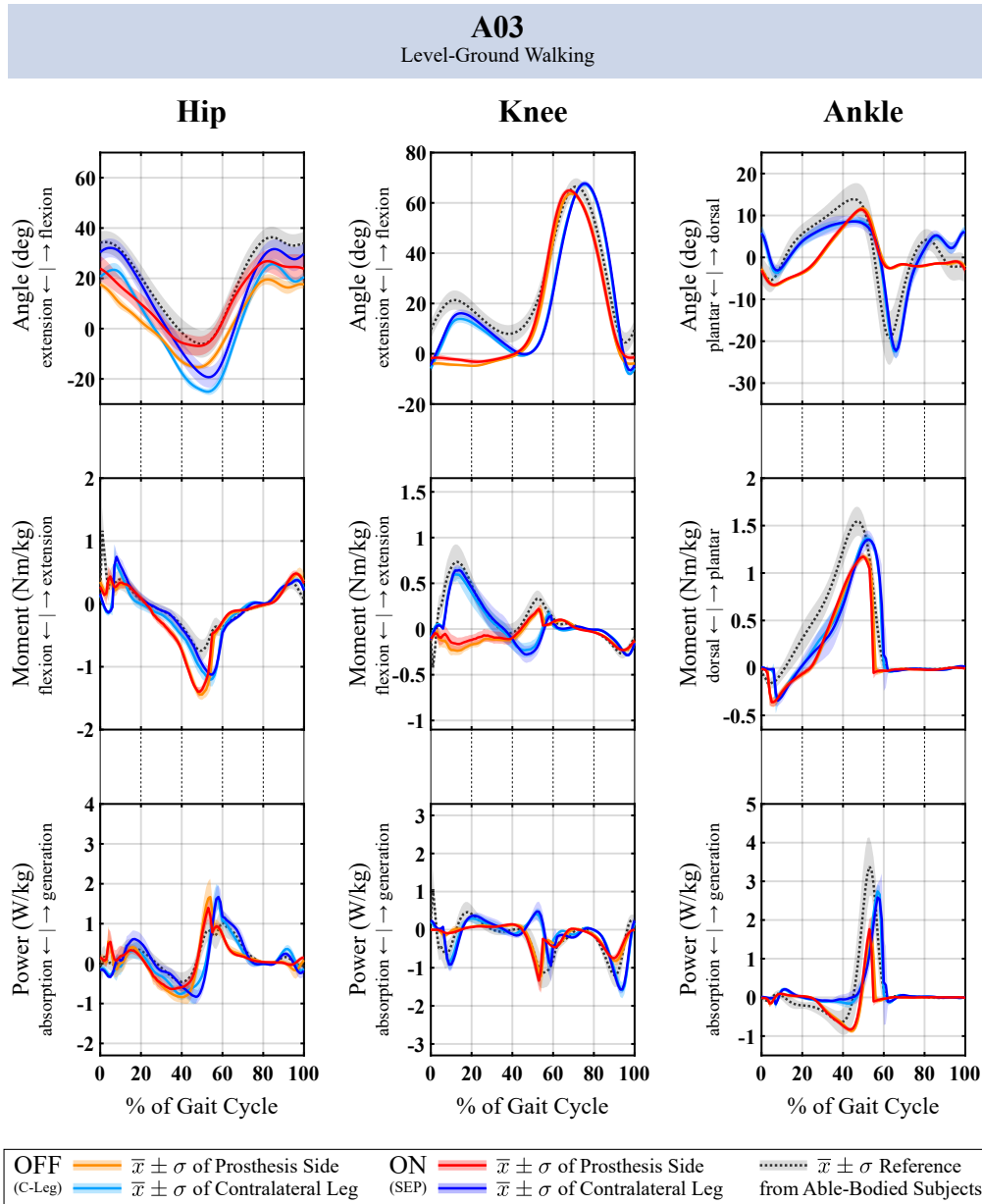


Figure 3.17: Kinematic and kinetic gait data of amputee A03 walking on level ground.

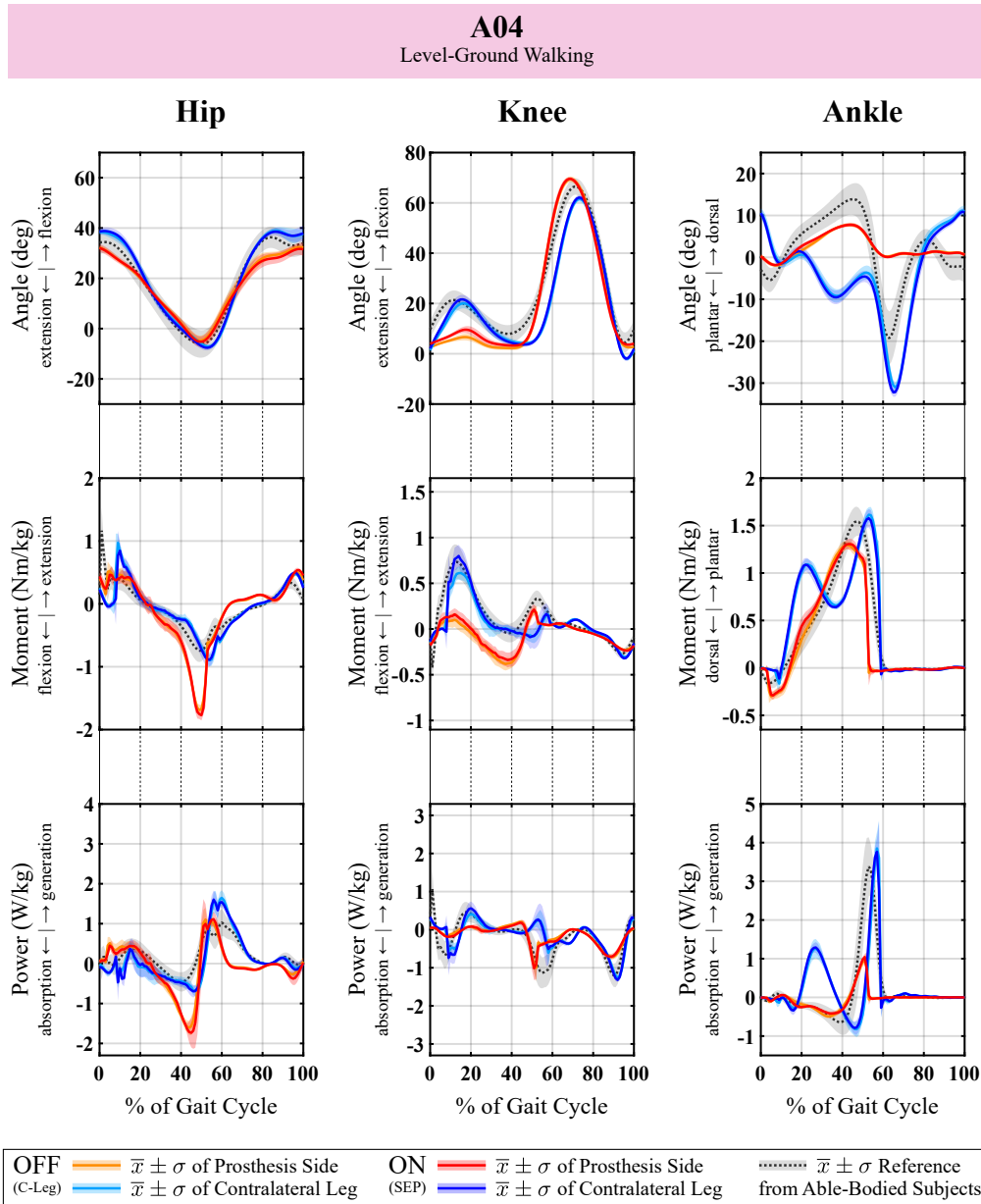


Figure 3.18: Kinematic and kinetic gait data of amputee A04 walking on level ground.

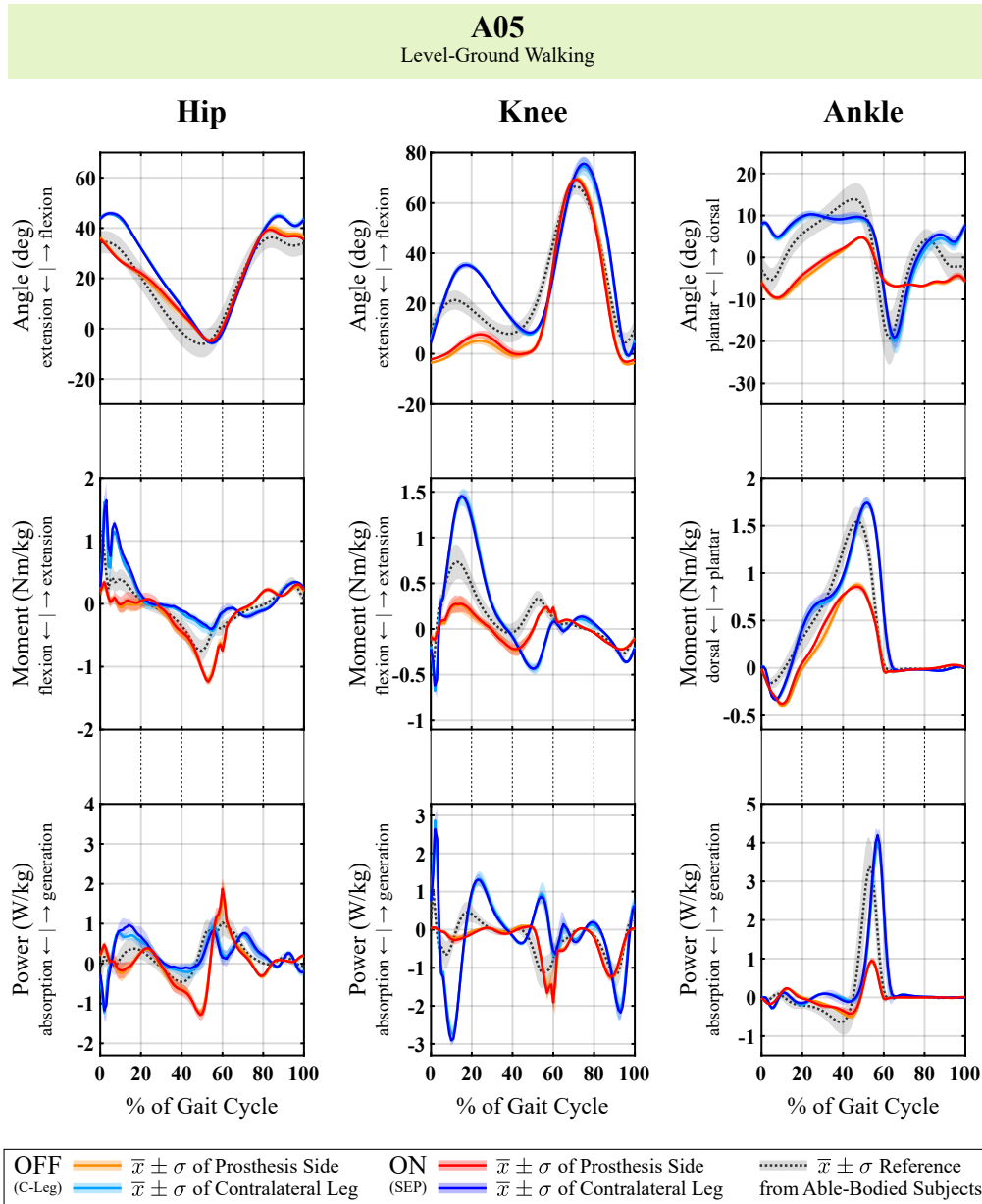


Figure 3.19: Kinematic and kinetic gait data of amputee A05 walking on level ground.

3. RESULTS

Down the ramp. Following the test procedure, walking down the ramp was the second task in the final evaluation session. The subjects started again with the deactivated OFF (C-Leg) system, before the modification was activated ON (SEP). For the ramp task, the damping factor of the prosthesis was modified too, using the individual parameters summarized in table 3.5 on page 74. According to the participants' subjective perception, this modification reduced the load on the contralateral side and allowed them to walk in a more controlled manner than without it.

The mean spatiotemporal gait parameters are depicted in figure 3.20 on the facing page. Again, gait pattern differences are clearly noticeable. For example, while patient A01 has the lowest stance phase asymmetry of only 4%, A03 has almost 20% deviation. For subject A04, the SEP system improved both symmetry measurements, while for participants A02, A03 and A04 this was only the case for the stand phase, which is also evident in the ground reaction force graphs. For all subjects, the *stand phase* on the healthy leg is larger than on the prosthesis side. In contrast, the *step length* with the contralateral leg is lower than on the ipsilateral side, again for all participants. More important, however, are the changes that have shown up in the absolute values: The *cadence* was reduced for all subjects, and the *velocity* and *step width* for four out of five, with the exception of patient A05. This indicates a more stable and controlled gait.

The mean body center of mass motion is shown in figure 3.21 on page 88. For going down the ramp, the vertical displacement was reduced for all measurements, partly at very high percentages. The total *center of mass range* was reduced by almost 10%, resulting in a more energy-efficient gait. Due to the *PreFlex*-feature of 2°, *prosthesis side lifting* was reduced too. Most important, however, was the distinct reduction of the *contralateral leg landing*, by about 25% on average for all of the subjects and almost up to 40% for participant A05.

The ground reaction force is plotted in figure 3.22 on page 89. The graphs show a reduction of the maximum weight acceptance on the contralateral (healthy) leg. On average, this reduction is about 18% for all subjects and even up to 30% for participant A05. The extended stand phase on the ipsilateral (prosthesis) side is also identifiable.

The individual kinematic and kinetic gait data are shown in figures 3.23 to 3.27 on pages 90 to 94. With the activated SEP system, the prosthesis allowed more knee flexion (lower damping) at loading response and provided then more support (higher damping) during stance phase. However, an explicit extension, as seen in the reference from able-bodied individuals, is not possible, as the used pMPK is unable to provide net positive work. Nevertheless, the maximum knee angle during the swing phase was also reduced. At the same time, it led to a relief of the contralateral (healthy) side, with knee progressions more toward the reference – knee flexion and, thus, knee moment and power, are reduced. These effects were seen for all five patients.

In summary, the enhanced SEP system allowed the patient to walk down the ramp in a more controlled manner. This resulted in a slower and more stable gait and, more importantly, reduced the load on the healthy leg. Therefore, both the (subjective) perception of all amputees and the (objective) biomechanical measurements are in consensus for the task of walking down the ramp.

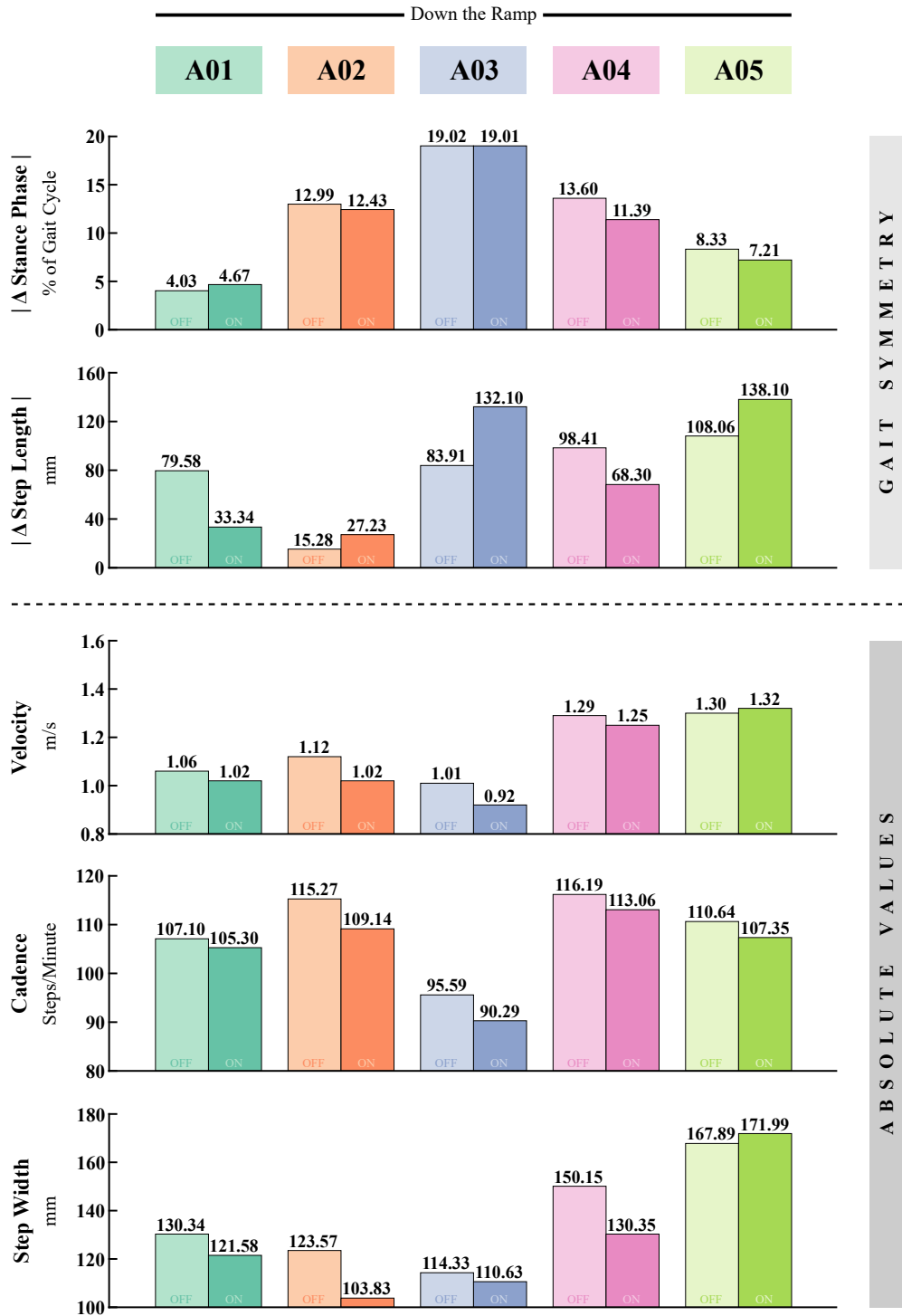


Figure 3.20: Spatiotemporal gait parameters of all five amputees walking down the ramp.

3. RESULTS

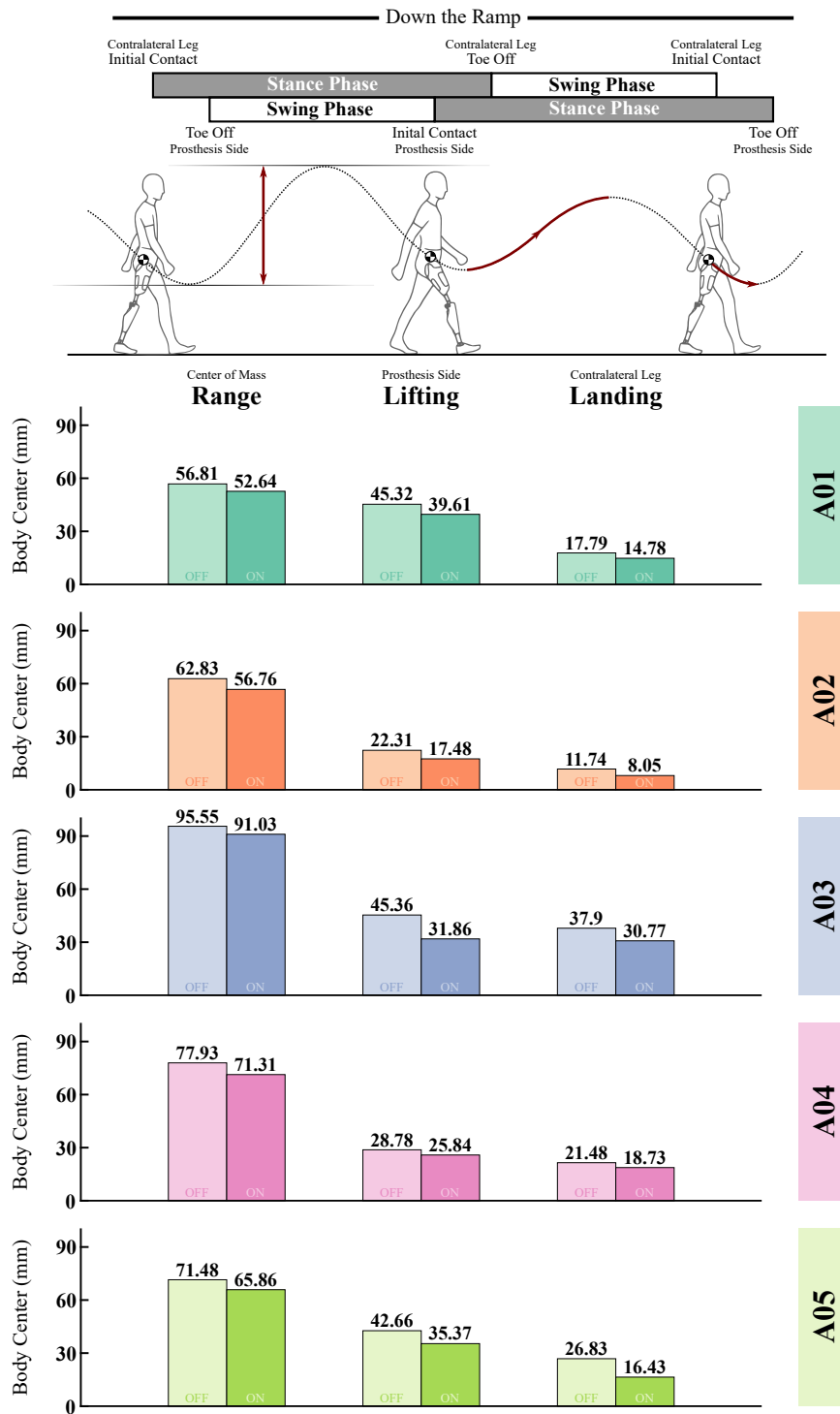


Figure 3.21: Body center of mass motion of all five amputees walking down the ramp.

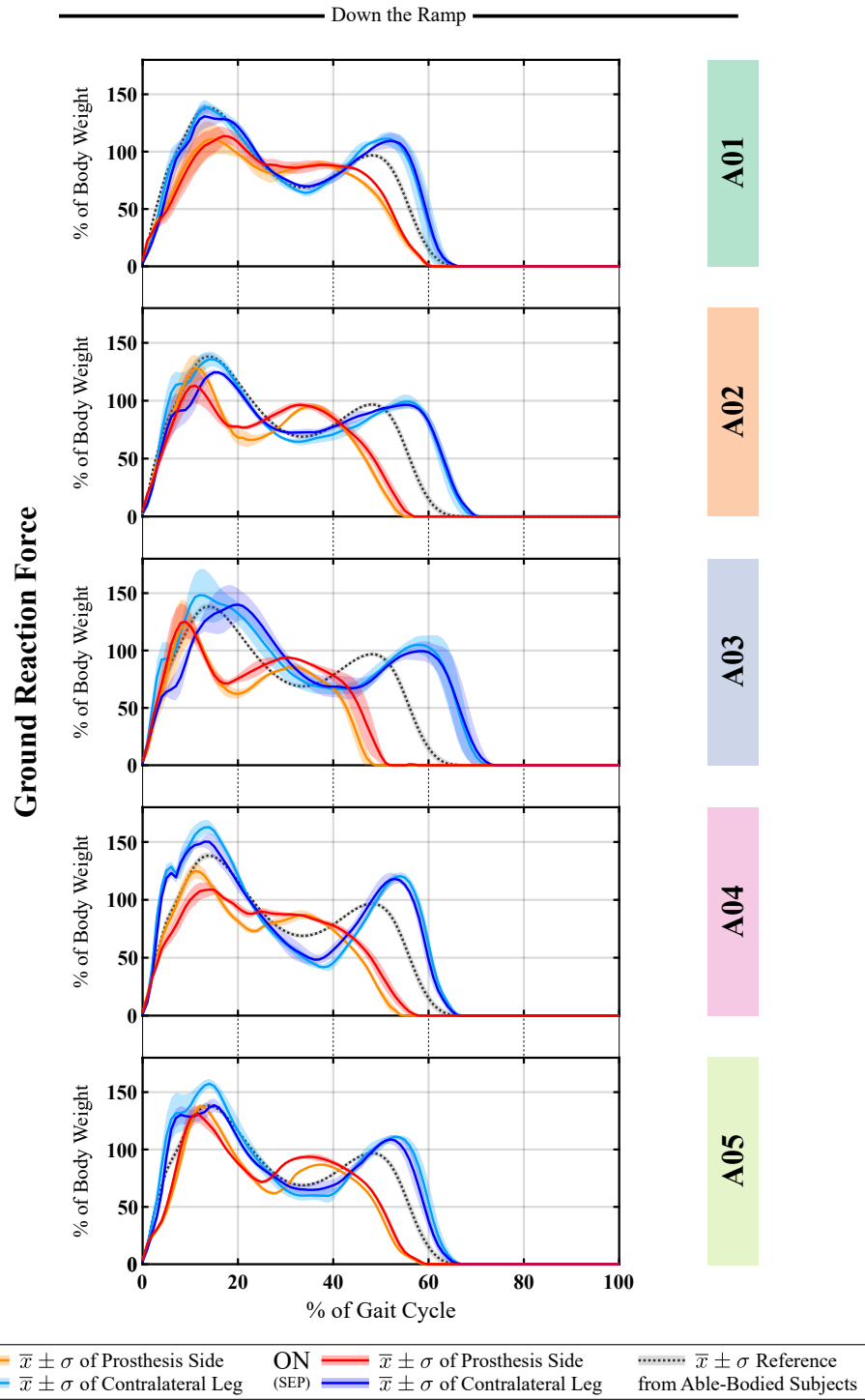


Figure 3.22: Ground reaction force of all five amputees walking down the ramp.

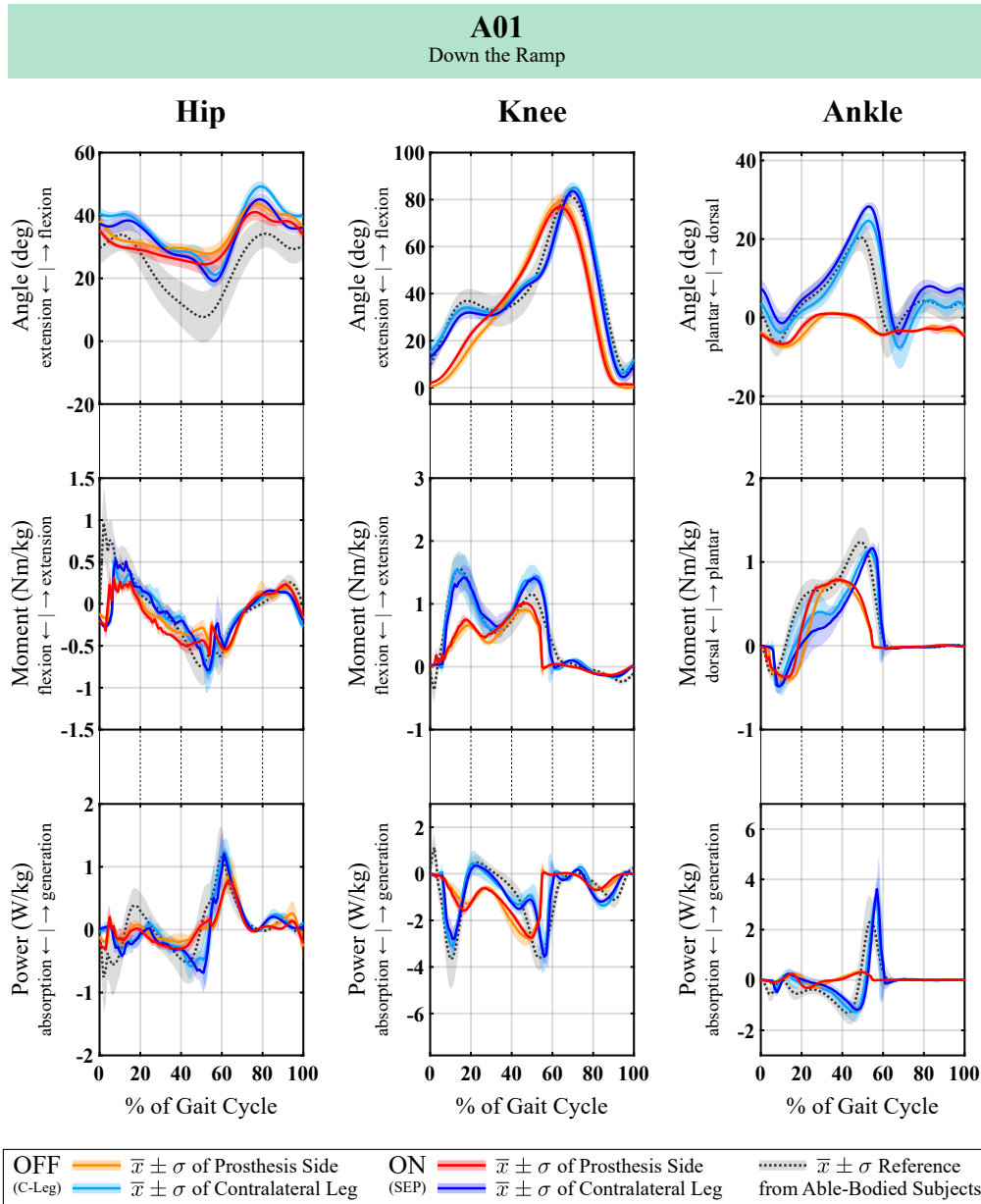


Figure 3.23: Kinematic and kinetic gait data of amputee A01 walking down the ramp.

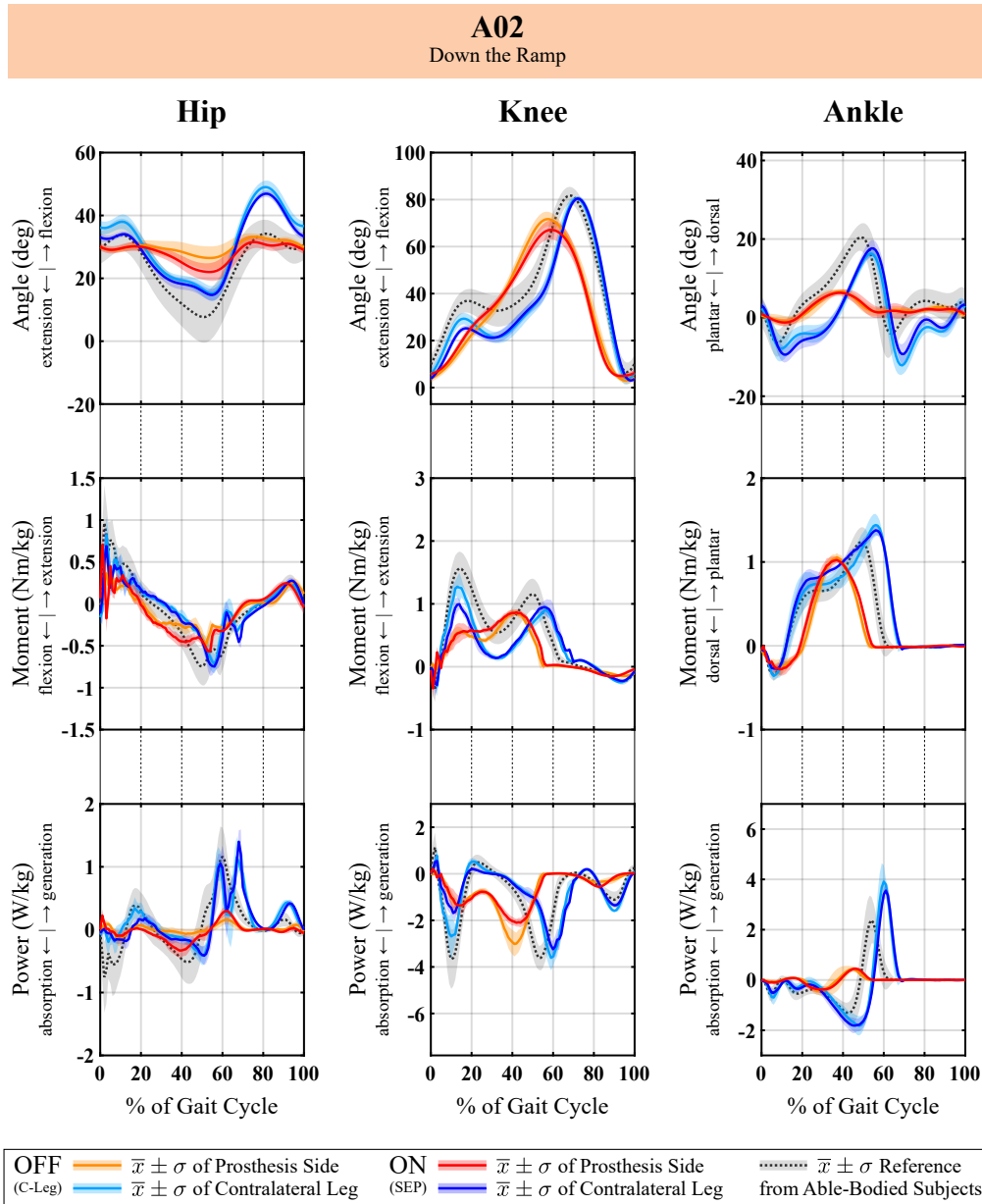


Figure 3.24: Kinematic and kinetic gait data of amputee A02 walking down the ramp.

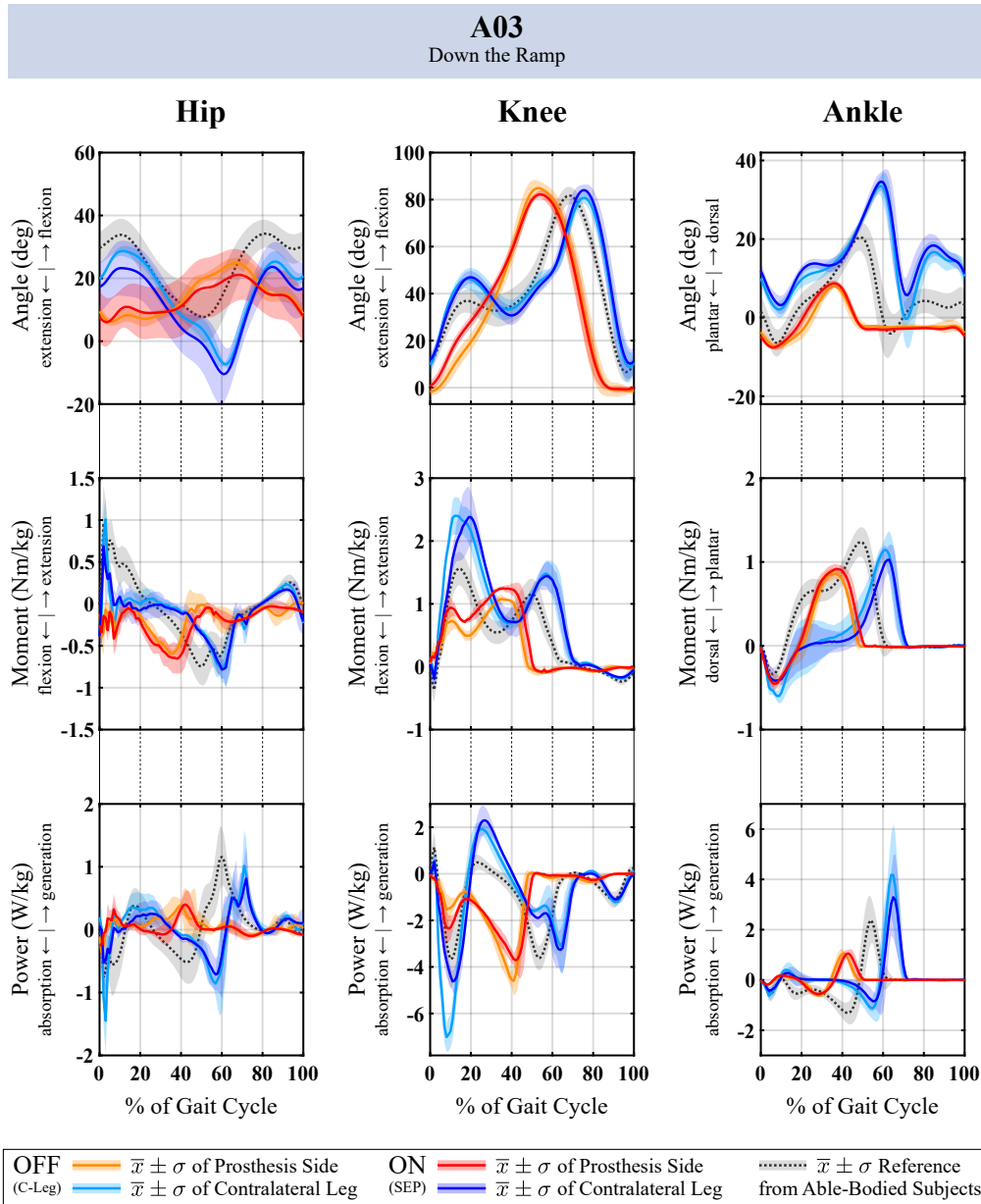


Figure 3.25: Kinematic and kinetic gait data of amputee A03 walking down the ramp.

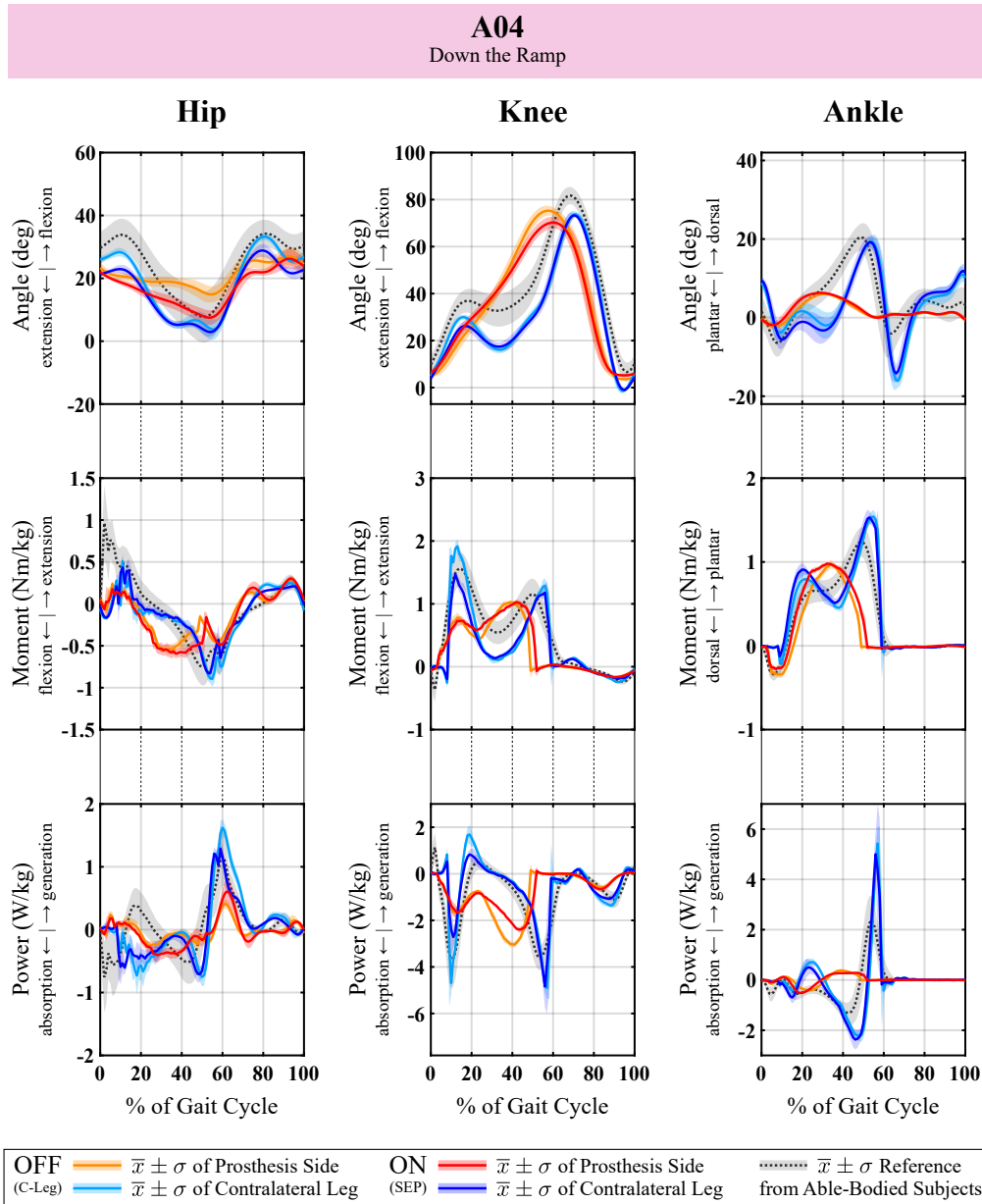


Figure 3.26: Kinematic and kinetic gait data of amputee A04 walking down the ramp.

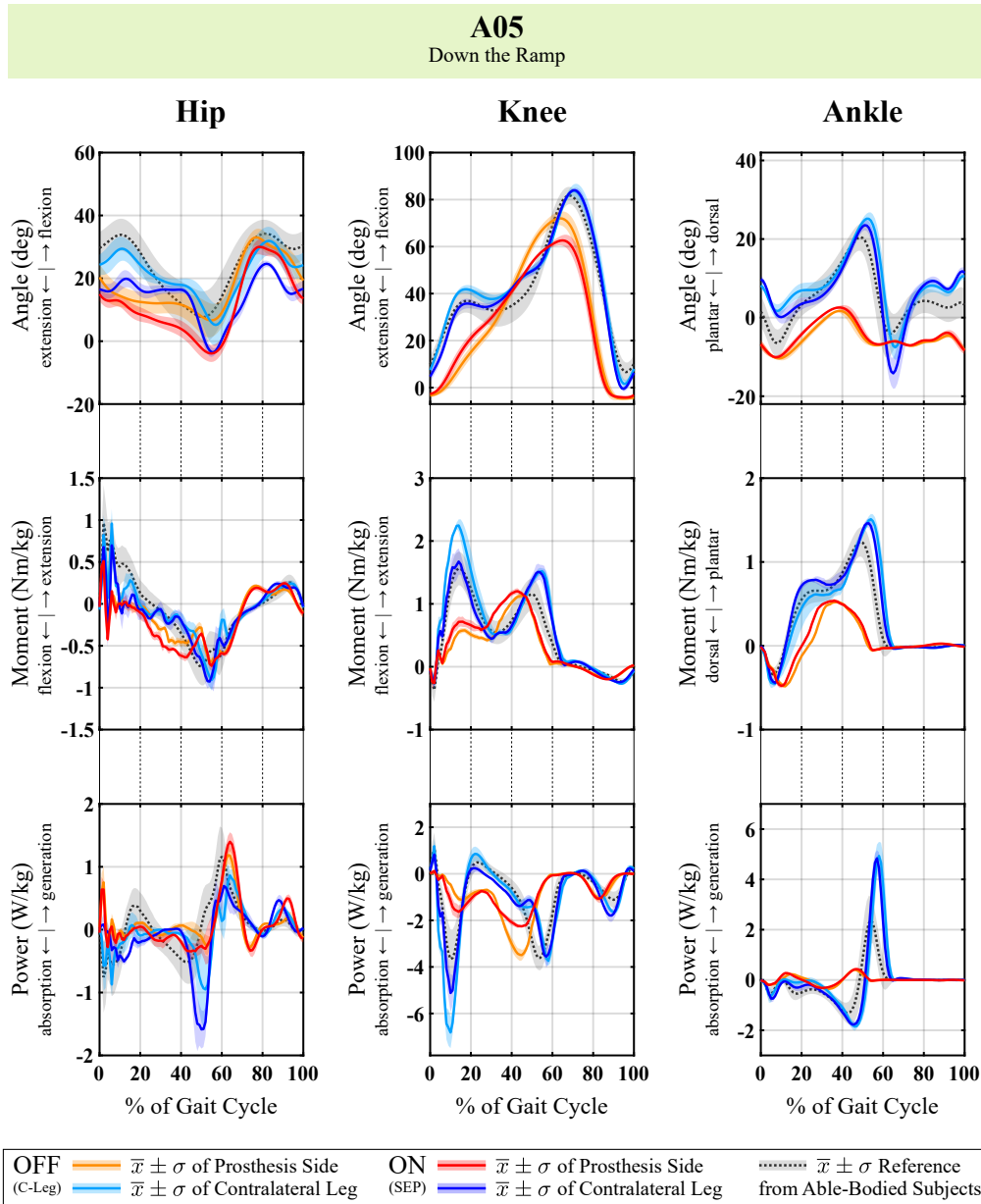


Figure 3.27: Kinematic and kinetic gait data of amputee A05 walking down the ramp.

Down the stairs. Finally, walking down the stairs was the third and last task within the evaluation session of this study. The subjects started again with the deactivated OFF (C-Leg) system, before the damping modification was activated ON (SEP). Again, the subjective perception of the patients was that the novel SEP system reduced the load on the contralateral leg, resulting in a more stable and controlled gait.

The mean spatiotemporal gait parameters are depicted in figure 3.28 on the next page. It is remarkable that the activated SEP system improved the symmetry for all five subjects, with *stand phases* on the contralateral side larger than on the prosthesis leg. For the staircases, neither *step length* nor *velocity* were evaluated. The *step width* was reduced for four out of five participants, with the exception of patient A03, indicating more stability and less sidelong movements.

The mean body center of mass motion is shown in figure 3.29 on page 97. The total *center of mass range* and the *prosthesis side lifting* do not show a homogeneous alteration. The distinct reductions that have shown up in the *contralateral leg landing*, however, are more important: 40% on average for all five patients and even up to 65% for A02. This is a strong sign that amputees need to intercept less with the healthy leg.

The ground reaction force is plotted in figure 3.30 on page 98. The graphs show a reduction of the maximum weight acceptance on the contralateral side for all five patients: 20% on average and up to 30% for patient A02 and A03. It is worth mentioning that the novel SEP system reduces the load on the healthy leg for four out of five subjects to such an extent that it is more or less perfectly within the reference range of the able-bodied individuals. Moreover, the extended stand phase on the ipsilateral (prosthesis) side is identifiable yet again.

The individual kinematic and kinetic data are shown in figures 3.31 to 3.35 on pages 99 to 103. Again, similar to the previous ramp task with the activated SEP system, the patients can be observed doing more stand phase flexion. Simultaneously, the contralateral knee was relieved and compensatory movements were reduced. Note: The kinematic (angle) data of the hip, knee and ankle are both evaluated from the steady-state range of the stairs [113]. Therefore, these progressions can be compared directly. Due to the relatively short staircase, see figure 2.27 on page 50, not all force plates are within the steady-state range, meaning that the (calculated) moments and powers could deviate. However, our clinical partner OSS reported that kinetic gait data should not be interpreted anyway, as there are still unsolved problems, which could either originate from the construction itself or from the evaluation routine. Nevertheless, for the sake of completeness, they are still plotted (within one graph) but not interpreted any further. It must also be mentioned that patient A05 used the handrail lightly, thus influencing the measurements.

In summary, the novel SEP system improved the staircase performance. Gait asymmetry as well as weight bearing on the healthy, unimpaired leg were reduced for all amputees participating in this study. Therefore, both the (subjective) perception of all amputees and the (objective) biomechanical measurements are in accordance for the task of walking down the stairs.

3. RESULTS

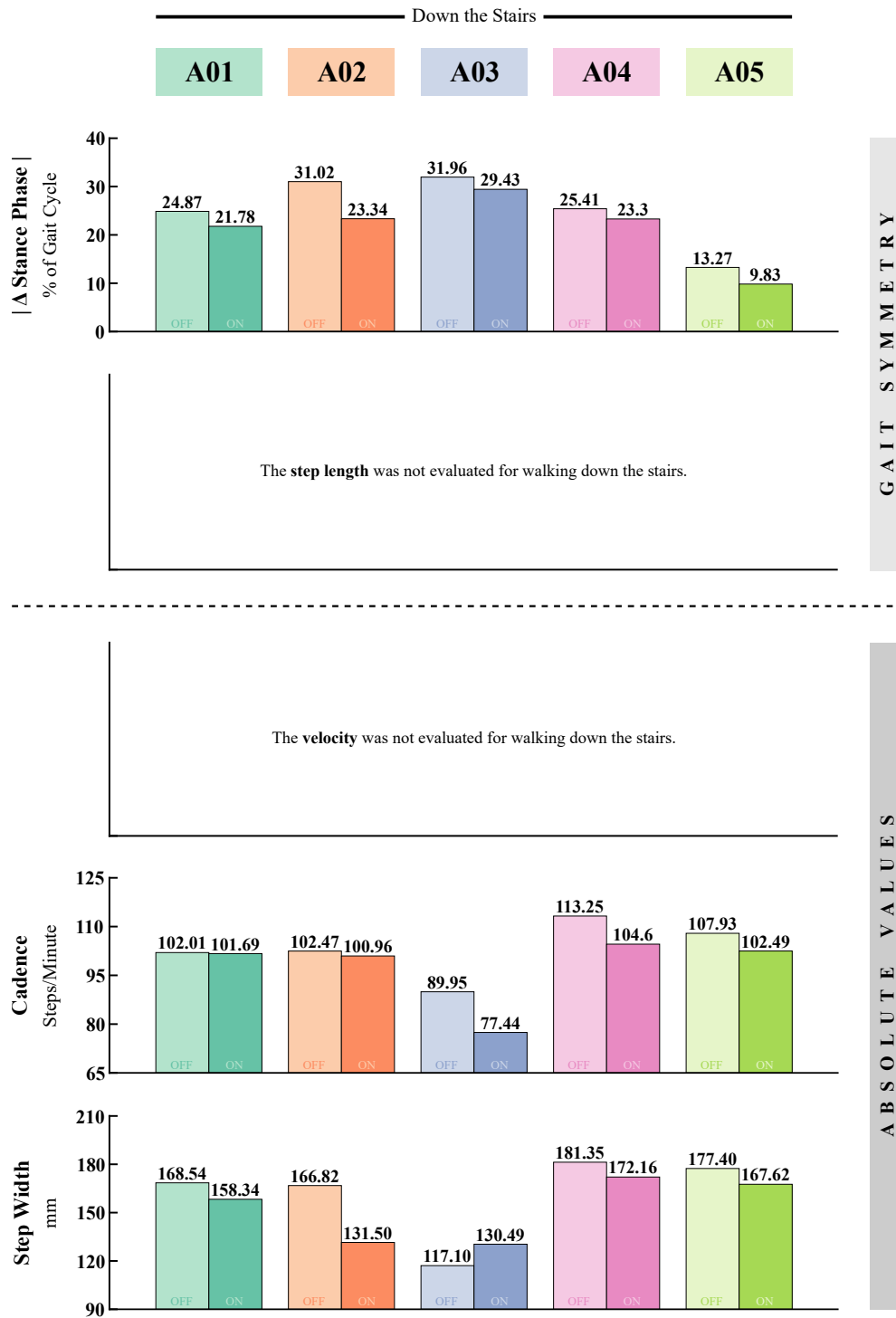


Figure 3.28: Spatiotemporal gait parameters of all five amputees walking down the stairs.

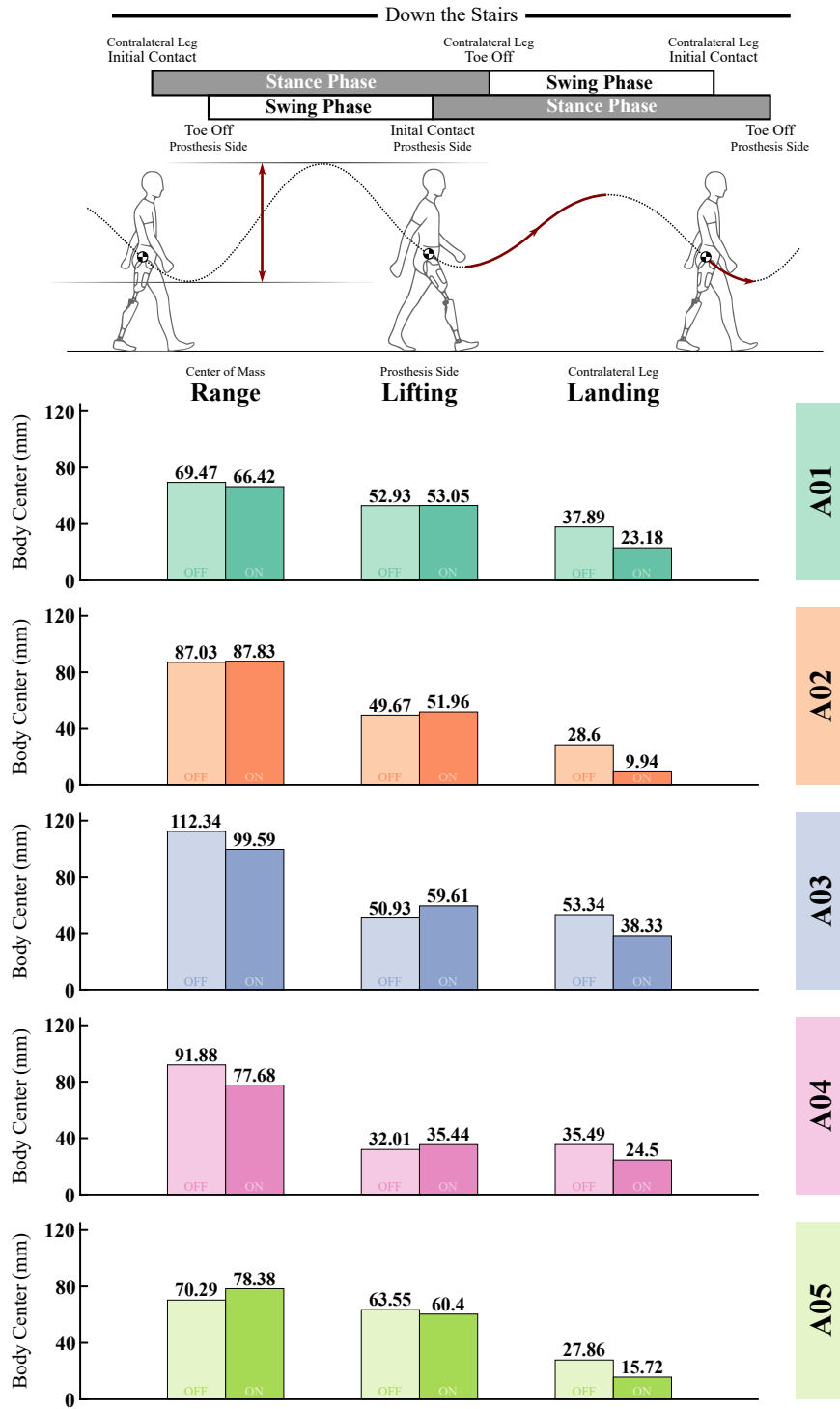


Figure 3.29: Body center of mass motion of all five amputees walking down the stairs.

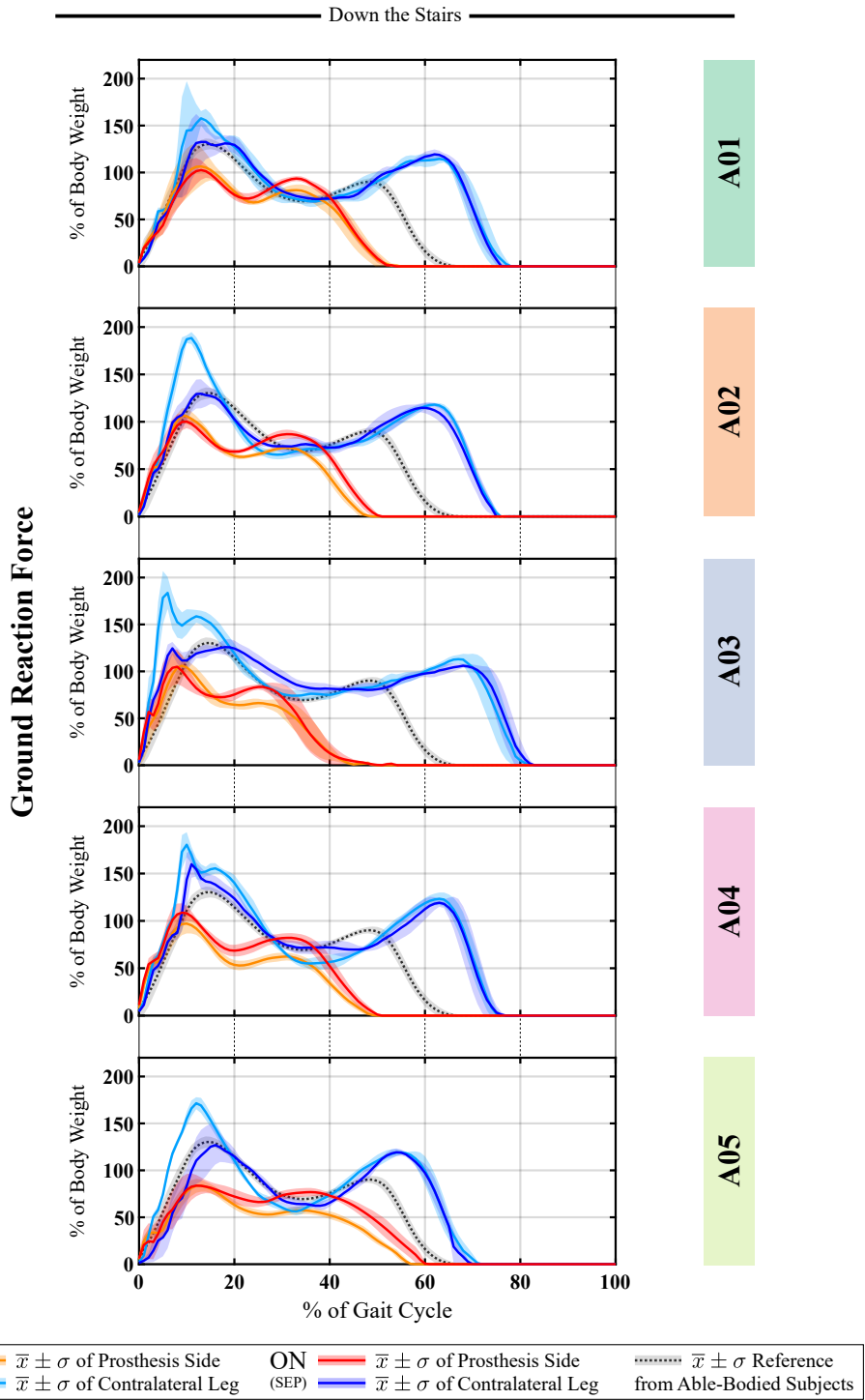


Figure 3.30: Ground reaction force of all five amputees walking down the stairs.

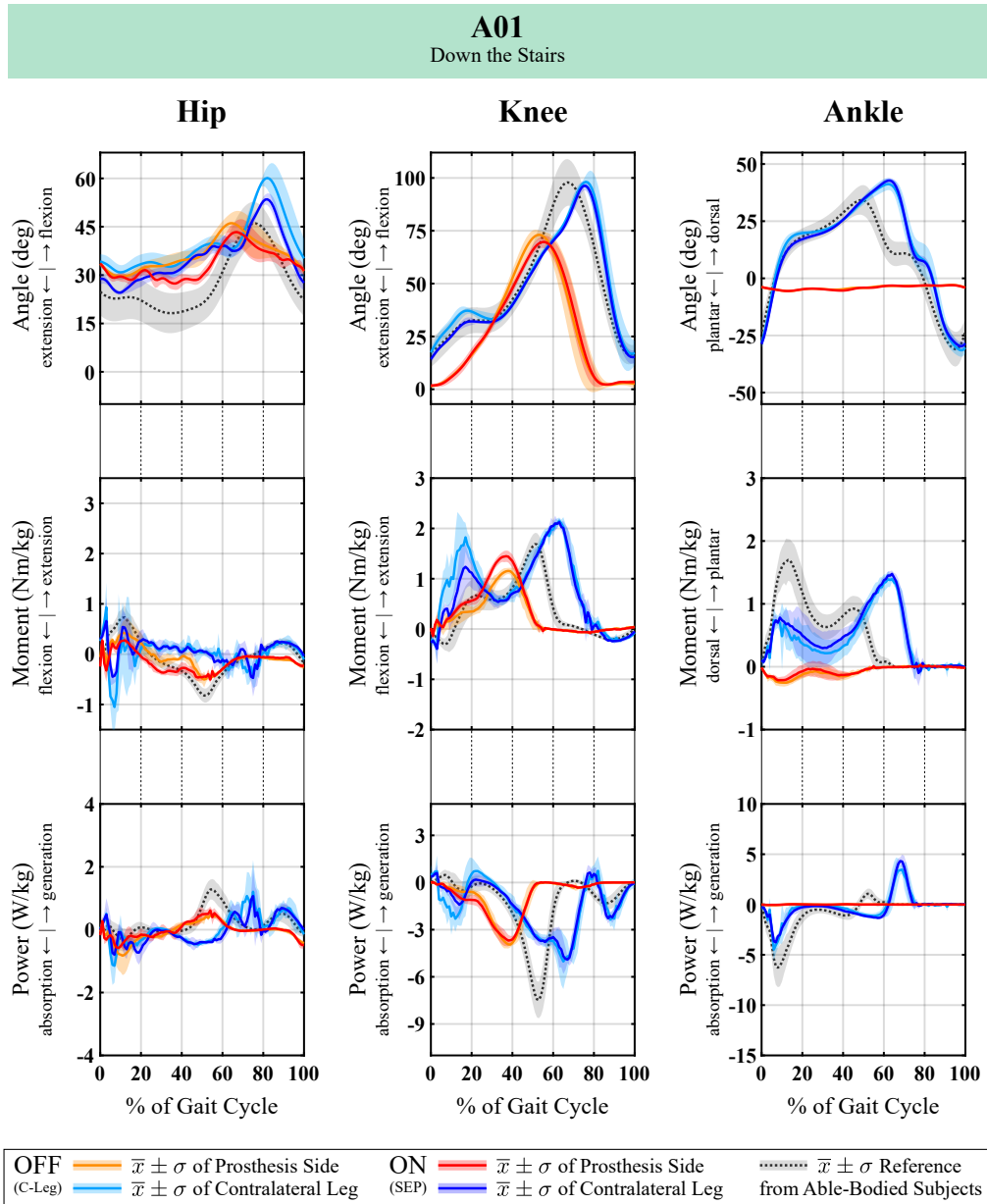


Figure 3.31: Kinematic and kinetic gait data of amputee A01 walking down the stairs.

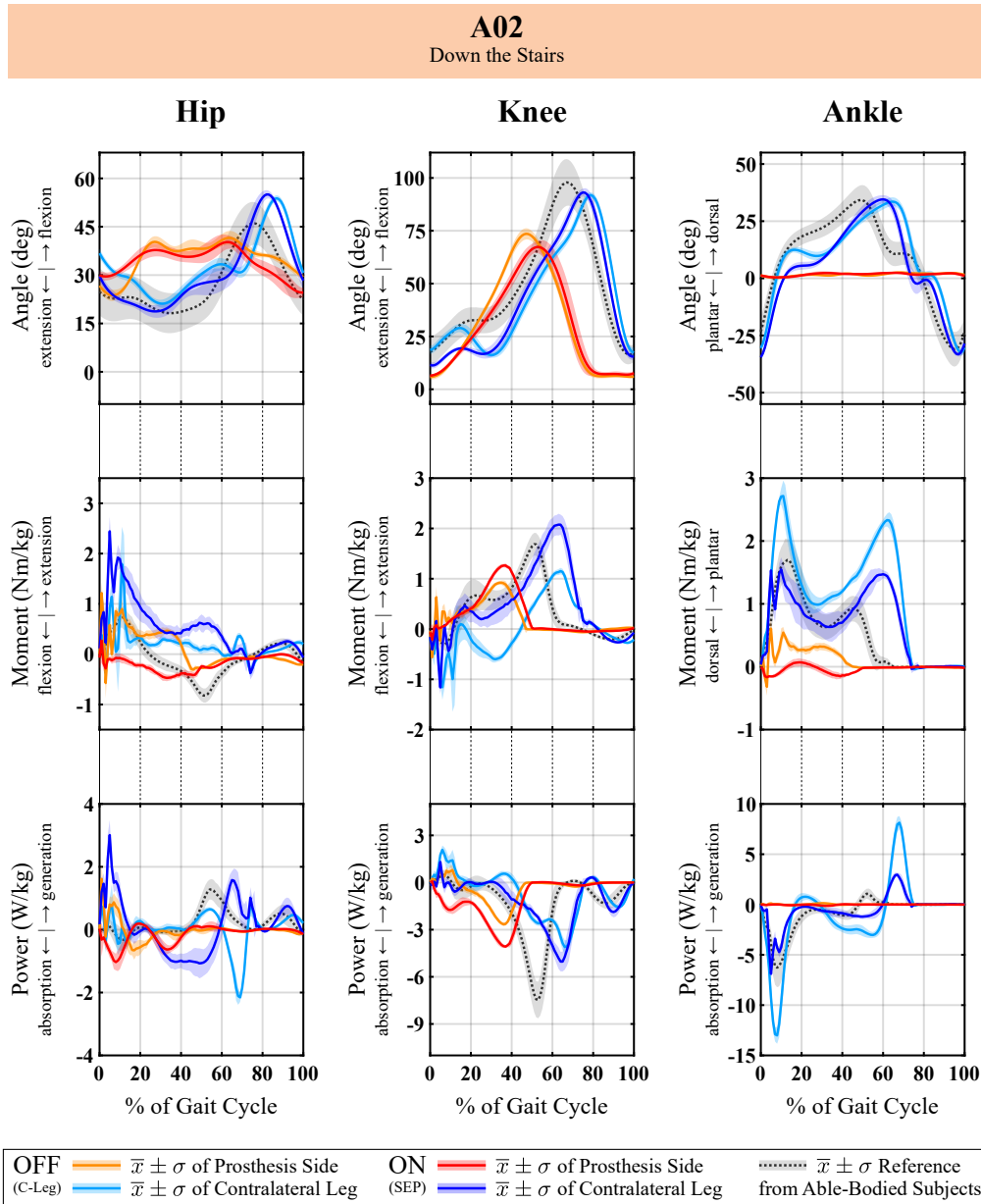


Figure 3.32: Kinematic and kinetic gait data of amputee A02 walking down the stairs.

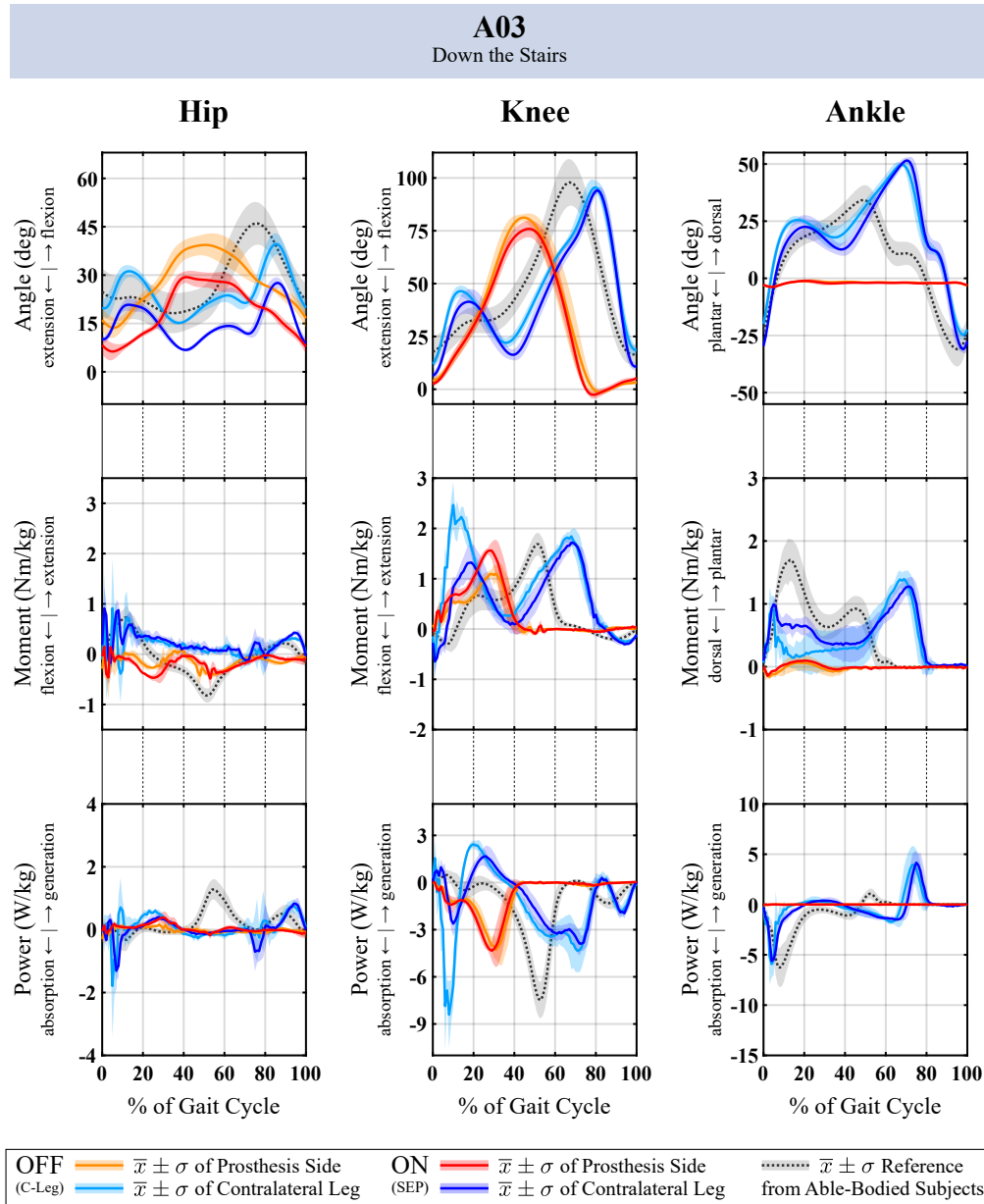


Figure 3.33: Kinematic and kinetic gait data of amputee A03 walking down the stairs.

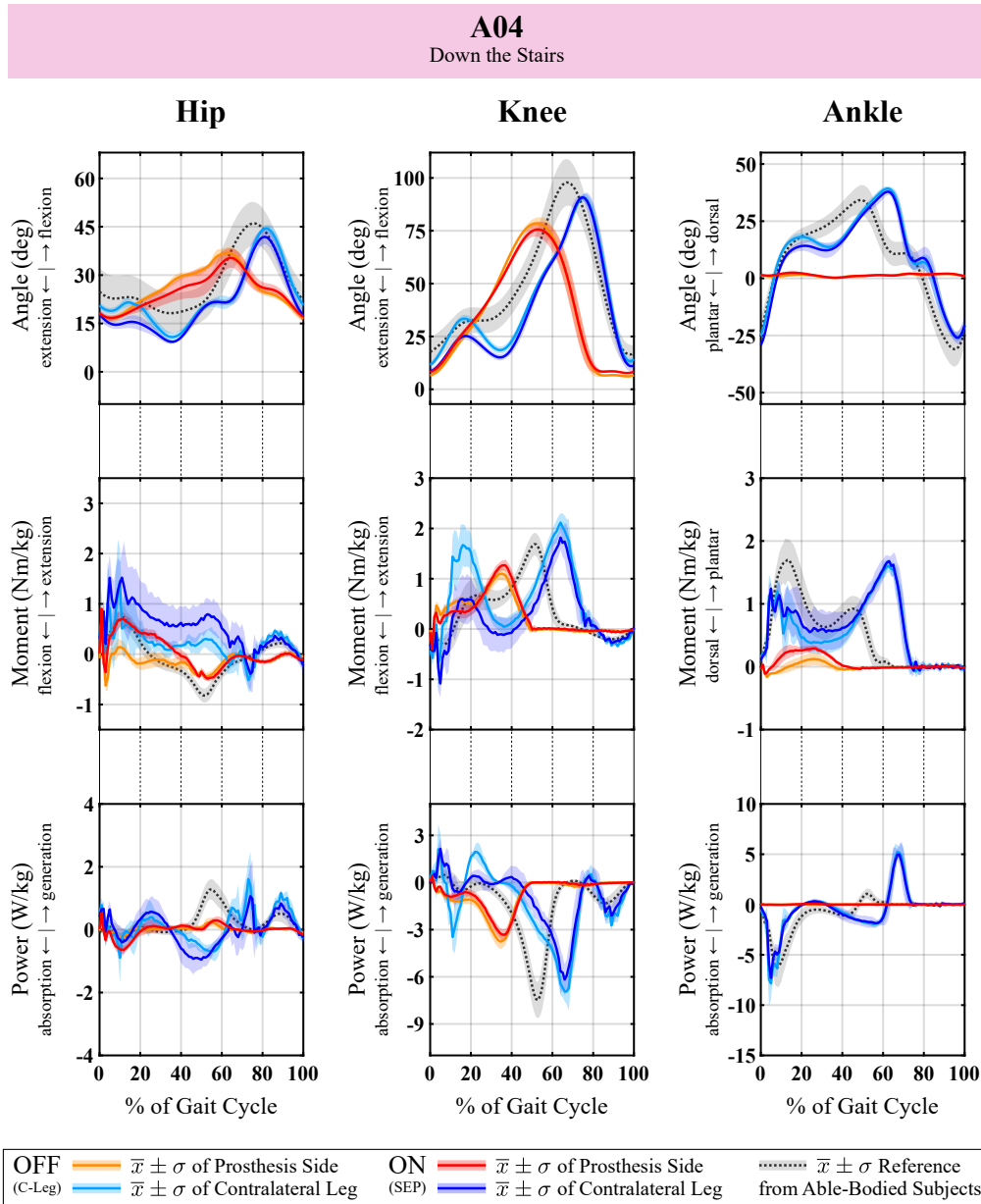


Figure 3.34: Kinematic and kinetic gait data of amputee A04 walking down the stairs.

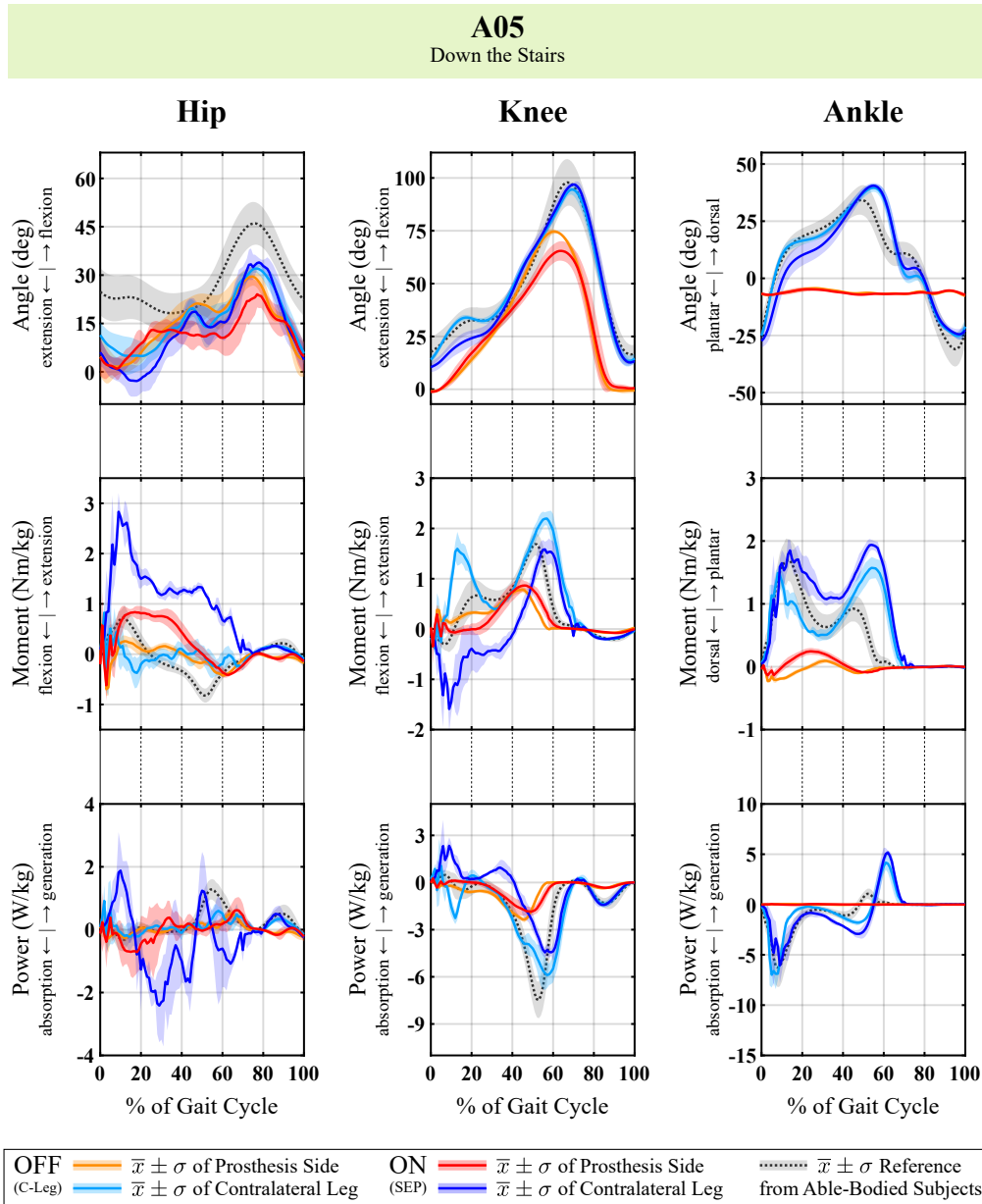


Figure 3.35: Kinematic and kinetic gait data of amputee A05 walking down the stairs.

3. RESULTS

3.4.3 Satisfaction Questionnaire

All five patients finished the study by filling out the questionnaire shown in figure 2.28 on page 52, with the aim to assess their subjective perception of this novel SEP system. Most importantly, none of the amputees experienced pain; stumbles, trips or falls did not occur at any time. In order to properly estimate a prospective user's possibly gained surplus, the (individual) answers were grouped and evaluated. Figure 3.36 on the facing page displays the distribution of the users' answers.

The activity of walking down the ramp as well as walking down the stairs were described as "very convenient" for four of the participants and at least "convenient" by one. A patient commented in the allocated field that the SEP system allows a *super easy initiation of the knee flexion with a pleasant initial damping*.

Three out of five subjects rated the weight of the system as "light". One even said "very light", whereas the system felt "heavy" for the remaining subject. Although the majority stated that the *weight difference is not really dominant*, the one participant who rated the system as heavy argued that feeling *the more distal mass* (comment: sensor kit) *made the system more inert*.

Regarding the perception of safety the subjects felt "very secure" (three out of five) or at least "secure" (two participants). This emphasizes the reliability of the fundamental concept.

When being asked to assess the perception of physical effort and the perception of mental effort, three out of the five participants described it as "not strenuous" and the remaining two only as "medium strenuous". One patient stated in the comment field that the *SEP system is better, but not yet the familiar daily device*.

In terms of the satisfaction with SEP, three amputees responded that they were at least "satisfied", while the other two were even "very satisfied". In the corresponding comment field, it was stated that the SEP system *relieves the contralateral leg, facilitates downward tasks and reduces tilting effects within the socket*. However, one patient also pointed out that *the increased damping could result in a faster heating, thus leading to a shortened uptime* (comment: if the prosthesis becomes too hot, it switches to a safety mode).

Finally, all five patients answered that they would prefer the novel SEP system for day-to-day use, instead of the commercially available C-Leg, at least for the yielding tasks. Note: According to the clinical investigating plan, there was no home-use phase – patients were not allowed to take the device home at any point of time. Nevertheless, the feedback showed that although it is only a research prototype, there was already a lot of interest in using it.

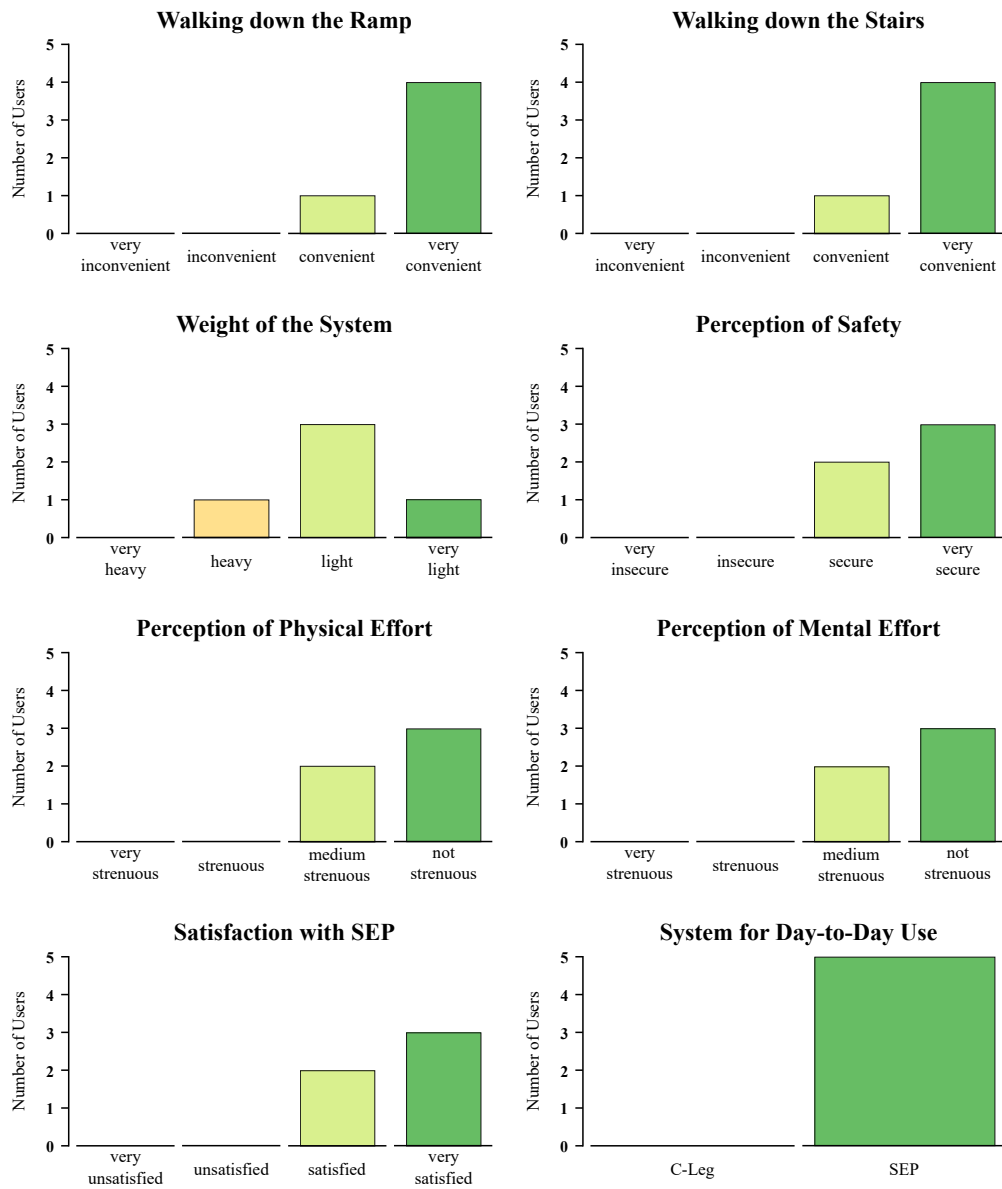


Figure 3.36: Distribution of the amputees' responses in the satisfaction questionnaire.



Die approbierte gedruckte Originalversion dieser Dissertation ist an der TU Wien Bibliothek verfügbar.
The approved original version of this doctoral thesis is available in print at TU Wien Bibliothek.

Discussion

The discussion begins in section 4.1 by outlining the possibilities of novel environmental perception sensors to improve control of lower limb prostheses and the constraints that need to be considered for further development. With the idea of an improved patient-prosthesis interaction in mind, completely new contralateral limb estimation strategies were designed, integrated and tested. In the following, the *advantages* as well as the concept-inherent *limitations* of the different systems are presented: first, for the open-loop CoLiTrack system in section 4.2; next, for the open-loop CoLiRang approach in section 4.3; finally, for the closed-loop prosthesis system in section 4.4. Necessary adaptations for producing a marketable product are summarized in the *future work* paragraph of each concept.

4.1 Current State of Research

4.1.1 Control Strategy Landscape

The detailed analysis of the current state of research made it possible to clarify how environmental sensing can improve the control of next-generation prostheses. The approaches can be grouped into five clusters: (1) continuous control, (2) motion classification, (3) event detection, (4) safety functions, and (5) upcoming object or terrain prediction, as shown in figure 4.1. An important decision factor for assigning the approaches into these groups is the required resolution and update rate of the underlying sensor modalities. In the column labeled “Group” in table 3.1 on page 54, each retrieved publication was classified into one of these main categories.

Approaches belonging to the field of *continuous control* measure, process and, finally, control in real time. This requires sensor modalities with high resolutions and high update rates. Based on Tucker’s three-level controller hierarchy, which is described in detail in section 1.1.3 on page 7, input processing for continuous control strategies is done on mid-level layer of the controller. Within the retrieved papers, mostly kinematic sensors such as GONIOs or IMUs were investigated

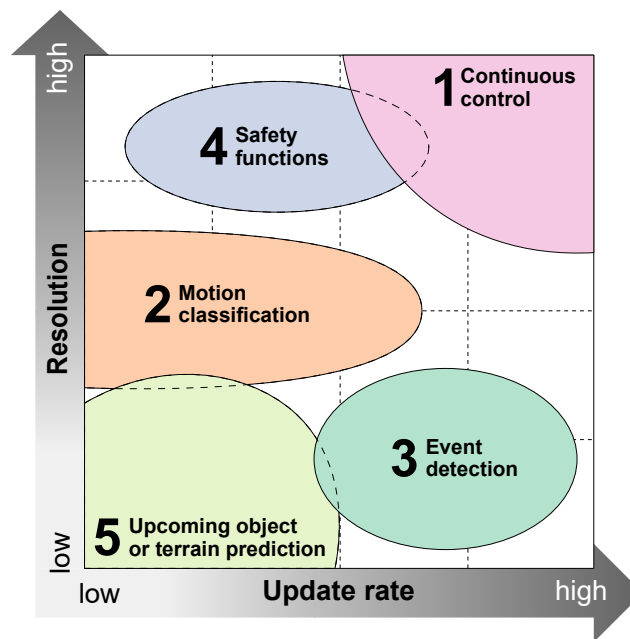


Figure 4.1: Control strategy landscape overview based on required resolution and update rate of the underlying sensor modality, adapted from [MT2].

in this category, estimating the state of the (residual) user’s body. Using information about the sound-side leg was found to be a promising approach [74–77]. Although primitive “echo-control” strategies have been studied for more than 40 years [114], errors often occur at the end of an activity, when the leg should stop but echoes again. The extended measurement of the entire (lower) body, referred to as “whole-body awareness”, made it possible to distinguish between different types of locomotion and transitions [78–81]. However, all of these concepts require to wear numerous additional sensors, which compromises usability and practicality for amputees.

Motion classification systems process the sensory input at the high-level layer of the controller to classify the user’s intent correctly. The sensor requirements in terms of resolutions and update rates are typically lower than for the continuous control class. As systematically proven [82–85], the fusion of various whole-body signals increased the intent recognition rates. Although this was not unexpected, the finding that already a single sound-side leg parameter could significantly reduce misclassification rates was remarkable. This means that instead of attaching and calibrating a number of sensors to the user’s body, a single contralateral sensor is enough to improve device control. The group of motion classification also overlaps with the category of upcoming object or terrain prediction. This is due to the fact that obstacles and terrain features are the “boundary conditions” for all types of movement. Nevertheless, this group is mainly concerned with correctly identifying the user’s intention, rather than predicting upcoming objects or terrains.

The category *event detection* summarizes all approaches that attempt to identify certain “events” from locomotion. Important factors for level-ground walking are the heel strike and the toe off, as shown in figure 1.4 on page 6. According to Tucker’s framework, movement-dependent actions are triggered by this information in the mid-level layer of the controller. Therefore, timing is crucial. Sensors used within this group should have high update rates, but the resolution may be lower. As an example, pressure inserts are often used to determine the exact moment of ground contact. However, the resolution of sensors like these is not relevant, since the distinction whether the foot does or does not touch the ground is often sufficient. For a continuous estimation of the gait phase, a gait-related depth signal combined with an adaptive oscillator detector was used [86]. Instead, the concept proposed by Hu et al. [52], which predicts bilateral gait events from unilaterally worn sensors only, seems to be more promising. Nevertheless, as the implementation was not optimized for processing time, the high computation time of more than 1.16 ± 0.56 s prevented any real-time evaluation.

Approaches that increase the safety of a lower limb prosthesis belong to the *safety function* group, interacting at the low-level layer of the controller. In general, a high resolution is mandatory, for being able to detect small barriers correctly. Although the update rate could be lower, a high update rate would enable a “(re)action” in real time. In terms of device control, reliable stumbling prevention in unexpected terrain is still an open (research) question. A study conducted with healthy individuals found that an unrecognized object with a height of only 1 cm can already lead to stumbling. Therefore, it concluded that foot clearance is an important gait parameter for safety [115]. Within this survey, there were two publications in which the foot clearance was estimated [87, 88], but none of them were investigated in a prosthetic setup. Although few concepts have been found for this category, some are obvious: By taking a single (color or depth) image during the stance phase when the leg is vertical, path planning could reduce the risk of falling during the next step. Furthermore, it would be beneficial to correctly estimate the ground inclination. This could be done via an IMU in combination with two distance sensors, one more heel-related and the other more toe-related.

Upcoming object or terrain prediction approaches are the biggest research trend, across all five categories, depicted in figure 4.1. Half of all the publications reviewed attempt to observe the amputee’s environment, classify the input and, finally, provide a probability for changing the locomotion mode. Based on the controller framework by Tucker, input is processed at the high-level of the controller. For a smooth transition between different terrains, humans link visual information with proprioception, whereas, for prosthetic devices, the correct recognition of these transitions is very challenging. Currently available lower limb prostheses require the patient to perform a predefined “special movement”, which is not very intuitive. This is detected by the built-in sensors and triggers the transition between modes of locomotion with distinctly different properties [116]. For the smooth and safe switching between terrains without losing balance or interrupting the transition, the term “critical timing” was coined by Huang et al. [109]. Approaches combining distance information with geometric constraints [90–95] to predict upcoming terrain features proved to be fast and accurate enough. However, all of these concepts require an unobstructed field of view, and the research group studying the radar sensor [102] did not evaluate the the feature of “look-through” cosmetics (cover of a prosthesis to appear lifelike) or clothes.

4. DISCUSSION

A fundamentally different approach is the explicit recognition of upcoming objects. The aim of systems like these is to recognize and identify object parameters directly, which is a crucial capability for autonomous systems in particular. Especially the development of low-cost and high-resolution depth cameras opened up a wide range of applications in many areas [117]. In terms of smart vehicles, the first fully autonomous wheelchair already successfully navigated the hospital's corridors in 2016 [118]. However, in terms of lower limb prostheses, the amputee voluntarily decides what to do or where to go. Based on this fact, the sensor input is usually processed to obtain a probability for the change of locomotion mode. With this in mind, depth cameras were used to detect if the user was approaching a staircase [101] or to distinguish between various locomotion modes [96,97,99,103,104]. Instead, a color camera was used to determine the soil material [100]. All these image-based concepts, however, required an unobstructed field of view and were (very) computationally intensive, as will be discussed in the next paragraph. Although concepts with pre-trained classifiers [96–98,100,101,103,104] achieved higher accuracies compared to finite-state machines without learning [90–95,99], the performance of the former strongly depends on the quality and size of the training data. In addition, training with predefined step sequences led to unintended biases, which then occasionally led to misclassifications in unpredictable real-world situations.

4.1.2 Development Considerations

Sensor modalities. Out of the retrieved 32 publications, eleven different types of sensors were used to enhance the control of prosthetic devices. Most of these are various distance-based and depth-based sensors for environmental scanning, which were already described in detail section 1.2 on page 9. Furthermore, kinematic sensors, typically IMUs, are used in 24 out of 32 publications. In fact, all commercially available MPKs from Fluit's review [14] employed an IMU for motion estimation. Although widely utilised, IMUs have a fundamental problem: Integrating sensor information – for example, calculating a position from acceleration data – can lead to cumulative errors that may cause drifts. Instead of IMUs, some of the papers use GONIOs to measure kinematic parameters. Although sensors like these are very reliable and highly precise, they usually restrict the natural freedom of movement of the complex human joints. Some studies also use force resistive insoles or surface EMG electrodes, both of which require direct contact with the body – insoles need to be in contact with the foot to detect ground contact and electrodes with the skin to register muscle activity, respectively. Although they are not really “environmental sensors”, they can provide valuable input for (gait) event detection or conscious device control. In general, each type of sensor modality has their own pros and cons. Especially for distance-based and depth-based sensors, the main limitation seems to be the need for an unobstructed view.

Computing power. The publications analyzed within this state of research survey used powerful computers with memory sizes of up to 32 GB and clock rates of 3 GHz or more to evaluate and process the (image) inputs. The computing power available in commercial prostheses, however, is very limited. As described in detail in section 1.1.3 on page 7, finite-state machines running on low-power microprocessors are typically used for intention recognition and prosthetic control. It is obvious that limited processing power also affects processing time. Nevertheless, to ensure re-

liable and user-friendly functioning, the extraction and classification of interpretable information from the complex input should be as fast as possible. For real-time (prosthetic) applications, the update rate is typically in the range of 100 Hz [14]. This leads to the conclusion that the system architecture of prostheses must be modified significantly to support on-board vision processing in real time. One solution would be to integrate Intel's Myriad 2, a vision processor developed for mobile phones with less than 0.5 W power consumption [119], into prostheses.

Energy consumption. In addition to the limitation presented by computing power and processing time, energy consumption is also a critical factor. The CamBoard pico flexx from pmdtechnologies, which was used in [52, 85, 103], has the lowest power consumption of 300 mW [120]. The depth camera DS 325 from SoftKinetic used in [96, 97] needs more energy, but is still under 2.5 W [121]. With nearly the same geometrical dimensions as the depth sensors, the radar module used in [102] has a rated power consumption of 5 W [122]. For comparison, actuators with a power consumption of up to 200 W are integrated into advanced aMPKs [14]. Regardless of this, the energy consumption of processors and sensors can still be reduced through further developments and is, therefore, probably not the main factor for the exclusion of a particular technology.

Freedom to operate. As this is an industrial-related thesis, it was also important to know whether patents of others oppose potentially commercial plans. In order to find such patents, a freedom-to-operate search was carried out, which led to one relevant finding: Already in 2009, the Fraunhofer-Gesellschaft, Europe's largest application-oriented research organization, patented a concept of a foresighted control of a prosthetic device [123]. The claims describe a system of a foot or leg prosthesis with at least a socket (for coupling to the patient's leg), a treading body (which is in contact with the ground), a joint with a controllable actuator (in between the socket and the treading body replacing the missing body part) and one sensor to detect the "conditions of the ground". In theory, EES approaches are still highly interesting, but because of this relatively broad patent, they are no longer commercially viable. Although licensing this technology would be an option, possible alternative concepts were investigated in detail.

IES concepts are not protected by any patents and have two further positive side aspects: First, the object of interest is already known, since parameters of the patient's residual body have been estimated (e.g. contralateral shank). For EES systems this is not the case – everything can be in front of the amputee. Second, the physical inter-joint coordination that exists between human limbs is very strong [124]. As systematically proven by Hu et al. [82–84], even a sound-leg estimate can significantly reduce the error rate in intention recognition.

From this novel perspective, the author has filed a patent related to the IES area [MT3]. This covers the idea of controlling a prosthetic or orthopedic device which has (at least) one controllable actuator, by measuring with (at least) one sensor (at least) one parameter of a second body part of the user, as depicted in figure 4.2 on the following page.

(12) NACH DEM VERTRAG ÜBER DIE INTERNATIONALE ZUSAMMENARBEIT AUF DEM GEBIET DES PATENTWESENS (PCT) VERÖFFENTLICHTE INTERNATIONALE ANMELDUNG

(19) Weltorganisation für geistiges Eigentum
Internationales Büro

(43) Internationales Veröffentlichungsdatum
10. Dezember 2020 (10.12.2020)

(10) Internationale Veröffentlichungsnummer
WO 2020/245400 A1

WIPO | PCT

- (51) Internationale Patentklassifikation:
A61F 2/68 (2006.01) A61F 2/70 (2006.01)
A61B 5/11 (2006.01)
- (21) Internationales Aktenzeichen: PCT/EP2020/065690
- (22) Internationales Anmeldedatum:
05. Juni 2020 (05.06.2020)
- (25) Einreichungssprache: Deutsch
- (26) Veröffentlichungssprache: Deutsch
- (30) Angaben zur Priorität:
10 2019 115 096.5
05. Juni 2019 (05.06.2019) DE
- (71) Anmelder: OTTO BOCK HEALTHCARE PRODUKTS GMBH [AT/AT]; Brehmstraße 16, 1110 Wien (AT).
- (72) Erfinder: SEIFERT, Dirk; Kaiserstraße 43/2, 1070 Wien (AT). TSCHIEDEL, Michael; Zippererstraße 18/15/19, 1110 Wien (AT). HOFFMANN, Robert; Heigerleinstraße 60/4/424, 1160 Wien (AT).
- (74) Anwalt: GRAMM, LINS & PARTNER PATENT- UND RECHTSANWÄLTE PARTGMBB; Theodor-Heuss-Straße 1, 38122 Braunschweig (DE).
- (81) Bestimmungsstaaten (soweit nicht anders angegeben, für jede verfügbare nationale Schutzrechtsart): AE, AG, AL, AM, AO, AT, AU, AZ, BA, BB, BG, BH, BN, BR, BW, BY, BZ, CA, CH, CL, CN, CO, CR, CU, CZ, DE, DJ, DK, DM, DO, DZ, EC, EE, EG, ES, FI, GB, GD, GE, GH, GM, GT, HN, HR, HU, ID, IL, IN, IR, IS, JO, JP, KE, KG, KH, KN, KP, KR, KW, KZ, LA, LC, LK, LR, LS, LU, LY, MA, MD, ME, MG, MK, MN, MW, MX, MY, MZ, NA, NG, NI, NO, NZ, OM, PA, PE, PG, PH, PL, PT, QA, RO, RS, RU, RW,

(54) Title: METHOD FOR OPERATING AN ORTHOPEDIC DEVICE AND CORRESPONDING ORTHOPEDIC DEVICE

(54) Bezeichnung: VERFAHREN ZUM BETREIBEN EINER ORTHOPÄDIETECHNISCHEN EINRICHTUNG UND ENTSPRECHENDE EINRICHTUNG

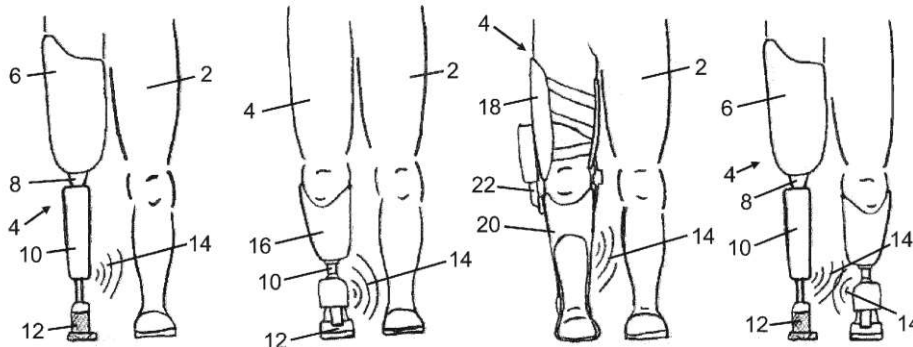


Fig. 1

(57) Abstract: The invention relates to a method for operating an orthopedic device, which supports or replaces a first body part of a wearer and has at least one controllable actuator, wherein the method comprises the following steps: a) determining a chronological profile of at least one parameter, which allows for a conclusion to be made regarding a movement status of the wearer, from measurement values of at least one sensor; b) detecting the movement status from the at least one determined chronological profile; and c) controlling the at least one controllable actuator depending on the identified movement status, wherein at least the chronological profile of at least one parameter of a second body part of the wearer is also used to identify the movement status.

(57) Zusammenfassung: Die Erfindung betrifft ein Verfahren zum Betreiben einer orthopädietechnischen Einrichtung, die ein erstes Körperteil eines Trägers unterstützt oder ersetzt und wenigstens einen steuerbaren Aktuator aufweist, wobei das Verfahren die folgenden Schritte aufweist: a) Bestimmen eines zeitlichen Verlaufes wenigstens eines Parameters, der eine Aussage über einen Bewegungszustand des Trägers erlaubt, aus Messwerten wenigstens eines Sensors, b) Erkennen des Bewegungszustandes aus dem wenigstens einen bestimmten zeitlichen Verlauf und c) Steuern des wenigstens einen steuerbaren Aktuators in Abhängigkeit des erkannten Bewegungszustandes, wobei zum Erkennen des Bewegungszustandes zumindest auch der zeitliche Verlauf wenigstens eines Parameters eines zweiten Körperteiles des Trägers verwendet wird.

Figure 4.2: First page of the author's own patent application [MT3].

4.2 Open-Loop Depth Camera Tracking

This section discusses the *advantages* as well as the *limitations* of the novel CoLiTrack approach. Finally, necessary adjustments for a possible product are resumed in *future work*.

4.2.1 Advantages

This depth camera-based solution is the first concept capable of estimating sound-side leg information from unilaterally worn sensors only and in real time. Although it was developed with prostheses in mind, the novel approach could be applied to a wide variety of applications in many areas. Several qualities underline the effectiveness of this proposed CoLiTrack system:

- + First, the most important achievement to be mentioned is the low processing time of only 50 ms, which is fast enough for a real-time evaluation with up to 20 frames/s. In contrast to the work by Hu et al. [52], this presents a decrease by a factor of 23. Moreover, the proposed algorithm is based only on a direct computation strategy. There is no prior network training required, in contrast to machine learning approaches. This guarantees user independence, which was also confirmed by the experiments.
- + Additionally, the estimation accuracy was also high. Throughout the static experiment, the proposed approach successfully estimated the contralateral shank angle over the entire gait cycle and for all three speed levels, as depicted in figure 3.1 on page 61. As the predefined speed levels on the treadmill were slower than humans' normal walking speed, the global minimum of the shank angle is shifted from about 70% towards 80%, compare with figure 1.4 on page 6. Nevertheless, the estimation $\alpha_{S,IMU}$ closely corresponds to the reference $\alpha_{S,TOF}$. The highest mean error of $3.4 \pm 1.9^\circ$ was measured at high speed level, while the lowest mean error of $1.4 \pm 1.2^\circ$ occurred at the slow walking speed.
- + The dynamic experiment yielded a trackable range for about one sixth of the entire gait cycle: $16.7 \pm 4.6\%$ at slow speed, $17.5 \pm 4.4\%$ at medium speed and $18.4 \pm 3.8\%$ at high walking speed. However, as shown in the magnified area in figure 3.2(b) on page 63, for some steps, tracking was even possible for longer periods (up to 28%). Beside the trackable range, the estimation error was also low. Overall, the lowest mean error of $2.4 \pm 1.9^\circ$ was measured at the high walking speed, while the highest mean error of $2.8 \pm 2.1^\circ$ occurred at the low speed level.
- + In terms of gait analysis, a deviation of more than 5° is regarded as a clinically significant difference [125]. Therefore, the accuracy of the novel CoLiTrack approach can be claimed to be sufficient. In contrast, results from a walker [126] as well as from crutches [127], both equipped with a depth camera for estimating the shank angle, showed deviations of up to 10° .
- + Finally, the real-world experiment proved that neither clutter nor ground reflection had a negative impact on the tracking performance. Furthermore, as long as the sound-side shank was in the camera's field of view, unknown other obstacles were successfully suppressed, which underlines the efficiency of the preprocessing strategy. Thanks to the integration of the IMU

4. DISCUSSION

and the depth camera into a compact kit, depicted in figure 2.3(a) on page 24, the fitting and calibration of the system on the subject's shank took less than 10 minutes. As the camera was already worn on the ipsilateral (prosthesis-side) shank, this design would also allow for easy integration into a future product.

4.2.2 Limitations

Besides the numerous advantages of the novel CoLiTrack approach, there are also some limitations that need to be considered:

- Firstly, although the concept was optimized for timing and is real-time capable with an update rate of up to 20 frames/s, the real-world experiment has shown that higher velocity levels can lead to misclassification.
- Additionally, the trackable range is also very limited. So far, the proposed system is able to estimate the sound-side shank axis only in the range of about one sixth of the total gait cycle, as determined by the dynamic experiments.
- Finally, (invisible) light-based depth cameras, as used within this approach, are limited by needing an unobstructed field of view. Therefore, no garments or prosthetic covers can be worn over them, as they would restrict the view.

4.2.3 Future Work

The proposed CoLiTrack method can accurately estimate the contralateral shank axis with only a short time delay. Nevertheless, all of the above-mentioned constraints should be appropriately considered in product design, whereupon the following thoughts can serve as a guide for further research in this area.

Update rate. Assuming a step length of 1 m and a walking speed of 3.6 km/h for active amputees [63] resulted in one gait cycle per second. Now, considering that the CoLiTrack approach in its current form tracks about one sixth of the entire gait cycle and processes at 20 frames/s, no more than three to four shank-angle calculations can be done per gait cycle. However, according to the author's experience, at least ten images would be required for use in real life. Therefore, the 20 frames/s achieved are not bad at all for lower walking speeds, but an increase to at least 60 Hz would be needed for more normal speed levels. In comparison, typical update rates for prosthetic applications are in the range of 100 Hz [14]. Nevertheless, the maximum sampling rate is inherently limited by the supported frame rate of the camera. For reference, the camera used in this study provides a maximum of 45 (depth) frames/s, according to the manufacturer's data sheet. This shows clear that the read-in and computing time must also be reduced even further. For example, instead of running Matlab code on a consumer laptop, it could be converted to C++ programs and executed on dedicated vision processors.

Tracking range. In addition to the update rate, the trackable gait cycle range also needs to be extended. In its current form, the system can estimate the sound-side leg axis in the range of one sixth of the entire gait cycle, as it is out of view for the rest of time, compare with the results of the dynamic experiment in figure 3.2 on page 63. A solution would be to combine multiple depth cameras to increase the field of view and, thus, the trackable range. Moreover, the camera position and orientation within the wearable support kit must be adjusted for other activities. In particular, it must be optimized for stairs or ramps to capture the areas of the pants that are less wrinkled.

Unobstructed view. Although the sensor positioning within this study would allow a direct implementation into a prosthesis, the camera is restricted by the requirement of having an unobstructed view. This means that no prosthetic covers or clothing can be worn over them, drastically limiting usability for amputees. As already described in chapter 1.2 on page 9, the only sensor modality not limited by this factor is a radar solution. Thanks to the high-frequency, plastics or fabrics typically appear transparent for such sensors allowing them to “look through” these materials. Therefore, the deployment of these sensors should be considered.

Enhanced processing. During the phases of design, integration and testing of this innovative CoLiTrack approach, some ideas for possible further developments have emerged, but they have not yet been implemented: To begin with, the preprocessing of the raw input could be enhanced. For example, depth regions below a minimum size could automatically be removed. Furthermore, the “region of interest” (contralateral shank) could be selected based on the last valid position. These minor modifications could make the algorithm more robust against unknown obstacles without the need to implement more computationally intensive approaches, such as background subtraction or transformation strategies. Next, it seems possible to determine the heel strike by using the method presented in [128]. It is assumed that the swing phase is indicated by a positive angular velocity of a shank, while a negative velocity indicates the stance phase. Based on this information, the timing of the heel strike could be obtained. Finally, the depth camera directly provides the distance information between the sound-side leg and the sensor itself. However, this parameter has not been used so far, but (in future) it could help to estimate spatial parameters (e.g. step length).

4.3 Open-Loop Ultrasonic Ranging

This section outlines the *advantages* as well as the *limitations* of the novel CoLiRang approach. Finally, necessary adjustments for the integration into an enhanced prosthesis system are resumed in the section *future work*.

4.3.1 Advantages

This ultrasonic-based solution is the first approach, which is capable of estimating sound-side leg information over the entire gait cycle. Several qualities underline the effectiveness of this proposed CoLiRang system:

- + First, the used CH 101 ultrasonic (distance) sensors itself can be seen as reliable and valid. Based on that, the implemented triangulation strategy is able to determine the sound-side leg position correctly. The triangulation (*CoDir*) accuracy is below 30 mm, as depicted in figure 3.5 on page 67, and robust against noise, as shown in figure 3.6 on page 68. Moreover, the mean passing (*CoPas*) performance lies within 1°, as summarized in table 3.4 on page 69.
- + Furthermore, the walking simulation corresponded closely to the actual measurements, depicted in figure 3.9 on page 72 for participant P01 and in figure 3.10 on page 73 for participant P02. And, although limited by the minimal range (clipping) of the sensors, the *CoPas* signal indicated the sound-side passing correctly for all three terrains. Nevertheless, the most important achievement to be mentioned is the traceability of the contralateral leg over the entire gait cycle. In contrast, the prior CoLiTrack work (see section 4.2 on page 113) was only able to track one sixth of the gait cycle.
- + Additionally, the processing time is also low. Although the calculation was done only offline in Matlab running on a normal business laptop, the optimization for timing reduced the processing time to only 1 ms on average. Overall, the sampling interval time of the CH 101 module of 15 ms limits the maximal update rate, which would allow a potential online evaluation with up to 67 Hz. In contrast, the maximal update rate of the prior CoLiTrack approach was only 20 frames/s. Moreover, the processing steps needed within this ultrasonic system are “easier to implement” on a traditional microprocessor than the previous image processing tasks.
- + Furthermore, this novel CoLiRang system is based only on a (conventional) triangulation strategy. Therefore, compared to readily used machine learning approaches, prior network training is not required. Moreover, neither sunlight nor wind had any negative impact on the system performance.
- + Finally, thanks to the compact design of the kit, depicted in figure 2.14 on page 35, the fitting of the system on the subject’s shank takes less than five minutes. Furthermore, this compact integration also allows for easy integration into a future product, as the kit was already worn on the ipsilateral (prosthesis side) shank.

4.3.2 Limitations

Besides all the advantages of the novel CoLiRang approach, there are also some limitations that need to be addressed:

- Firstly, although the concept was already optimized for timing, no online (real-time) evaluation was done.
- Additionally, the minimum detectable range is (too) limited. Due to the medial positioning of the kit on the subject's shank, clipping of the sensors occurs.
- Finally, ultrasonic sensors, as used within this approach, are limited by their need for an unobstructed field of view. Therefore, no garments or prosthetic covers can be worn over them, as these would restrict the view.

4.3.3 Future Work

The proposed CoLiRang method can accurately estimate sound-side leg parameters with only a short time delay. Nevertheless, all of the above-mentioned constraints should be considered in product design. The following thoughts can serve as a guide for further research in this area.

Online evaluation. Although the approach was already optimized for timing – time needed for triangulation and filtering was below 1 ms – so far, processing was done only offline. Therefore, the Matlab code should be converted to C++ programs and ideally executed directly on the embedded device hardware. – the processing steps needed within this ultrasonic system are comparatively “easy to implement” on a traditional microprocessor. Overall, the sampling interval of 15 ms for the CH 101 modules seems to be the only major limitation. Nevertheless, according to the author's experience, an online evaluation with up to 67 Hz should be sufficient for a real-time (prosthetic) implementation.

Range limitation. In addition to the need for an online implementation, it is also important to avoid sensor clipping during passing. In its current form, the system can estimate the sound-side parameters correctly in the range from 100 up to 400 mm, compare with the results of the dynamic experiment for both subjects. However, if the sound side is closer than this minimum sensor distance, this remains undetected. As a possible solution, the width of the kit could be reduced, thus increasing the medial spacing to the other leg. Another option would be to move the kit further caudally (more towards the feet). This would increase the distance even more, as the lower limbs are normally thinner in this area. Furthermore, the kit could be placed more towards the midline of the leg. Although this is obviously not possible for healthy subjects, the general design of a transfemoral prosthesis system as presented in figure 1.2 on page 3 would allow for such a placement – the tube adapter is a very thin part compared to a sound shank.

4. DISCUSSION

Unobstructed view. Although the sensor positioning within this study would allow for a direct implementation into a prosthesis, the ultrasonic sensors are limited by requiring an unobstructed view. This means that neither prosthetic covers nor clothing can be worn over them, thus drastically limiting usability. As already described in chapter 1.2 on page 9, the only sensor modality not limited by this factor is a radar. Thanks to the high frequency, plastics or fabrics appear transparent to sensors like these allowing them to “look through” those materials.

Signal usage. During the phases of design, integration and testing of this innovative CoLiRang approach, some ideas of how to use the derived signals for enhanced prosthesis control have emerged, but they have not yet been explored: The *CoDist* signal provides a reliable distance information of the contralateral leg relative to the kit, however, this does not give any directional statement. Instead, as a result of the triangulation approach, the *CoDir* signal allows a detailed prediction about the direction of the sound side. The interesting moment when the contralateral side passes the ipsilateral one is provided in the *CoPas* signal. Besides the possibility of using these signals individually, it would also be conceivable to deduce them. For example, if the contralateral leg is very far in front or behind, passing feature calculation is invalid and therefore zero, as seen in figure 3.9 on page 72 for participant P01 and in figure 3.10 on page 73 for participant P02, respectively. One solution would be to combine the distance and the passing signal. This would mean that the *CoPas* information is only used when the *CoDist* is below a certain threshold. Overall, the different experiments have proven that all derived signals (*CoDist*, *CoDir*, and *CoPas*) are accurate and precise. There is definitely a high potential in those parameters for improving device control, as investigated in the following chapter *Enhanced Prosthesis Control System*.

4.4 Closed-Loop Prosthesis System

This section discusses the *advantages* as well as the *limitations* of the novel SEP system approach. Finally, necessary adjustments for a possible (commercially) product are resumed in *future work*.

4.4.1 Advantages

This enhanced prosthesis system is the first concept capable of adapting the damping behavior based on the state of the unimpaired residual contralateral leg. Several qualities underline the effectiveness of this proposed SEP system:

- + First, from a technical point of view, the CH 101 ultrasonic distance sensors as well as the embedded control hardware were successfully integrated into a compact prosthesis-mounted kit, as depicted in figure 2.23 on page 44. This allowed a stand-alone processing and a utilization within the prosthesis on a perceived real-time base of about 67 Hz, only limited by the sampling interval time of the ultrasonic sensor. Moreover, thanks to the narrower design, the medial spacing between the legs increased, eliminating thereby the sensor clipping. In contrast, the prior CoLiRang work (see section 4.3 on page 116) was limited by this effect.
- + Next, a prospective clinical pilot study was successfully designed, approved and conducted. In total, five amputees participated in the evaluation of the enhanced high-level control strategy, as shown in figure 2.24 on page 45. The optimal control parameters for each subject, summarized in table 3.5 on page 74, were retrieved within the optimization sessions of this study.
- + Subsequently, in order to prove that the novel SEP system objectively improved the subjects' situation, all of them conducted a clinical biomechanical gait analysis. As presented in detail in section 3.4.2 on page 75, this resulted in smoother gait patterns for yielding activities. Further, compensatory mechanisms within the entire remaining musculoskeletal system (e.g. maximum knee flexion at loading response and during swing phase or pelvis and hip movements) were reduced. For example, for going down the ramp, body center of mass motion was reduced by almost 10%, leading to a more energy-efficient gait, as depicted in figure 3.21 on page 88. Moreover, using the novel SEP system on stairs reduced the load on the contralateral (healthy) leg by about 20% on average to be within the typical reference range of the able-bodied individuals, as plotted in figure 3.30 on page 98.
- + Finally, a self-report questionnaire, evaluated in section 3.4.3 on page 104, assessed the patients' perception of use, safety and performance of the novel SEP system as well as their satisfaction with it. In summary, all five participants within this study described that the modifications facilitate the unimpaired residual contralateral side, allowing them to walk in a more controlled manner than without. Not at any time did the amputees experience pain, nor did any stumbles, trips or falls occur. Subjects felt secure using the prototype, while physical and mental effort were also low. When asked to decide which system they would rather use, all of the participants preferred the novel SEP system over the commercially available C-Leg for daily use.

4. DISCUSSION

4.4.2 Limitations

Besides all the advantages of the novel SEP approach, there are also some limitations that need to be considered:

- Firstly, although this concept was evaluated within a prospective clinical pilot study, no home-use experiences were gathered. Therefore, it is not possible to judge how the used sensor technology on the one hand, and the system behavior on the other hand, behave in real-life situations.
- Additionally, the study was limited to a relatively low number of patients per design. Neither randomization nor blinding was, therefore, possible. The number of trials per activity was also relatively low.
- Moreover, the increased damping provided by the system could result in a faster heating of the device. This would, however, shorten the operating time, as the prosthesis switches into a locked safety mode, when it becomes too hot.
- Finally, ultrasonic sensors, as used again within this approach, are limited by their need for an unobstructed field of view. Therefore, no garments or prosthetic covers can be worn over them, as these would restrict the view.

4.4.3 Future Work

The proposed SEP method successfully used the information of the contralateral healthy leg to enhance the commercially available C-Leg. Nevertheless, all of the above-mentioned constraints should be considered in further product design. The following thoughts can serve as a guide for further research in this area.

Tracking range. In the current approach, the system is able to determine the position of the unimpaired residual contralateral leg over the entire gait cycle. However, in its current form, only the moment of passing is used to reduce the damping again. Therefore, it would make sense to modify the sensor placing or even downsize the total number of sensors, thus reducing the (sensor) costs and, at the same time, the system complexity.

Sensor selection. Although the CH 101 ultrasonic sensors used in this system worked reliably and validly, they are restricted by the requirement of having an unobstructed view. This means that no prosthetic covers or clothing can be worn over them, which drastically limits the practicability for amputees. However, if this (ultrasonic) technology should be used in the future as well, the recently introduced ICU-10201 successor sensor version with improved performance [129] would be preferable. The only sensor modality not limited by this factor is a radar: Due to the high frequency of radar sensors, plastics or fabrics appear transparent. Thus, they are able to “look through” those materials and should, therefore, be considered for future (SEP) systems.

Sensor-less approach. Furthermore, the question arises whether the additional sensors, either ultrasonic or radar, could not be eliminated entirely. However, if the modified damping behavior as shown in figure 2.24 on page 45 is to be maintained, the control strategy must be adapted. So far, the increased flexion damping was reduced using the contralateral leg information *CoPas*, which would no longer be available (without a sensor). Alternatively, the damping could be controlled as a function of time. However, this would inevitably lead to the problem that the (ideal) walking speed is predefined. Thus, the patient has to adapt to the system again, instead of the system reacting to the user's needs. Instead, damping control could also be accomplished using only the internally available sensors, such as knee angle or IMU data. However, the optimal signal (combinations) were not investigated during this work and should be investigated first.

Real-life testing. Until now, this novel SEP system was tested only under well-controlled laboratory conditions. However, it is unclear how the system will perform in a real-world environment. For example, the more rapid heating of the device did not lead to any restrictions in the execution of this study. Nevertheless, it could become a problem in more extreme situations, such as hiking. Therefore, after the approval of the fundamental concept itself, an extended investigation with more users in a home-use setting would make sense.

New opportunities. Finally, also the potential of new applications should be pointed out. For example, the information whether the contralateral side is posterior or anterior was eventually not used. However, this could help in deciding whether the patient is doing a forward or a backward step. Possibly, this could also simplify the transition between forms of locomotion. In contrast, currently available lower limb prostheses require the patient to perform a predefined "special movement", which is not very intuitive. Lastly, especially when combined with aMPKs, which can provide net positive work, enhanced control capabilities are more important than ever.



Die approbierte gedruckte Originalversion dieser Dissertation ist an der TU Wien Bibliothek verfügbar.
The approved original version of this doctoral thesis is available in print at TU Wien Bibliothek.

CHAPTER 5

Conclusion

Can information about the unimpaired contralateral leg enhance the control of a prosthetic device? This thesis presents a scientific investigation into this question, following the aim of achieving an improved patient-prosthesis interaction. Environmental sensing is not a completely new technology, but the limited sensor resolution as well as the computing power required meant that in the past sensors like these were less practical for low-power, battery-operated medical devices.

In recent years, the robotic and automotive industry have driven innovation and development of environmental sensor systems. This reduced the computing power, increased the resolution and, at once, improved the overall efficiency of these sensors. Therefore, a detailed investigation became interesting. The analysis of the state of research showed that despite the many different research activities in academia, not a single environmentally improved prosthesis system is yet commercially available. In total, five major control categories were identified using all types of depth-based sensors. Half of all the studies reviewed presented upcoming object or terrain prediction approaches that provided switching probabilities between different locomotion modes with accuracies ranging from 82% to 99% in well-controlled laboratory environments. However, it is unclear how these systems will perform in real-world scenarios, both indoors and outdoors. Nevertheless, the finding that implicit environmental sensing strategies which incorporate the state of the patient's residual body can significantly improve motion-dependent control applications was highly relevant to this work. Understanding that even one contralateral leg measurement can significantly reduce the error rate in intention recognition guided further development.

From this novel perspective, a depth camera-based leg tracking method named CoLiTrack was proposed. This system consists of an IMU and a depth camera worn on the ipsilateral (prosthetic) side, capable of estimating the axis of the contralateral (healthy) shank in real time. Three open-loop experiments were conducted to validate the proposed algorithm. First, a static evaluation was performed on a treadmill with one subject at three different walking speed levels. Results showed trackability with a mean error of less than 4° degrees over the entire gait cycle, with an overall processing time of 50 ms. Therefore, the estimation of the shank axis can be up to 20 frames/s.

5. CONCLUSION

Next, the evaluation of the dynamic testing, in which five subjects wore the sensor kit, while walking on a treadmill at three different speeds, demonstrated a trackability of the sound-side leg of one sixth of the entire gait cycle with a mean error of less than 3° . Finally, the real-world experiment conducted with one subject confirmed the robustness of the proposed system against clutter or ground reflectance. Despite the promising results of this novel CoLiTrack method, several limitations were noted. To begin with, although the system in its current form was real-time capable, higher velocity levels can lead to misclassifications. In addition, the field of view also needs to be increased. Currently, only one sixth of the entire gait cycle can be captured because the leg is out of view for the rest of the period. Furthermore, the camera position needs to be adjusted especially for stair or ramp activities in order to capture less wrinkled parts of the clothes. Finally, the depth camera is inherently limited by the need for an unobstructed field of view, making it less promising for a commercial application.

Based on these learnings, a second ultrasonic-based system was derived. This system called CoLiRang consists of four novel ultrasonic time-of-flight sensors on the ipsilateral (prosthetic) leg. It is capable of estimating the relative distance and position of the contralateral (healthy) leg over the entire gait cycle. Several open-loop experiments were conducted to validate the sensor modality itself as well as the proposed algorithmic. First, a (sensor) distance accuracy and a triangulation accuracy evaluation were performed. The results revealed a mean triangulation deviation of below 30 mm and even less than only 5 mm for the distance deviation. Furthermore, the simulation experiment confirmed the robustness against noise. Next, an experiment proved that the CoLiTrack kit can identify the moment of passing correctly. Finally, a dynamic testing done with two participants wearing the kit demonstrated a reliable performance for all three different terrains (level ground and a ramp and stairs, both downward) over the entire gait cycle. In addition, the results of level-ground walking were consistent with those of the simulation. Moreover, an outdoor test done with one participant proved that external influences, such as sunlight or wind, did not have any negative effects on the proposed approach. Despite the new CoLiRang method's promising results, some limitations need to be mentioned. To begin with, although the processing time was low, 1 ms on average, no online (real-time) evaluation was carried out. Furthermore, the sensor caused clipping, when the sound-side leg was below the minimum range limit. Finally, ultrasonic sensors, such as the camera from the previous approach, are inherently limited by their need for an unobstructed field of view.

Finally, the previously derived ultrasonic-based time-of-flight approach was integrated into a prosthesis system. This concept called SEP consists of a commercial C-Leg extended by the ability to utilize information about the patient's unimpaired residual contralateral leg, with the aim to improve the damping behavior of the prosthesis. In order to obtain a working prototype for stand-alone operations, processing was transferred into an embedded hardware, running on a perceived real-time basis of about 67 Hz. To evaluate the developed system, a prospective clinical pilot study was designed, approved and conducted. In total, five transfemoral amputees were eligible to participate in testing this novel SEP system. First, several optimization sessions were conducted to derive the ideal closed-loop control parameters. Next, clinical biomechanical gait analyses were performed to determine improvements objectively. The results revealed a more physiological gait pattern with a distinct relief of the remaining musculoskeletal system for all

of them. In particular, intercepting on the contralateral (healthy) leg was on average reduced by about 25% for going down the ramp and even by about 40% for the staircase task, respectively. Finally, a self-report questionnaire was used to assess the amputees' perception and satisfaction with this innovative approach. All patients perceived the system as advantage, as it allowed them to walk in a more controlled manner. Moreover, they felt safe using the prototype. When asked to choose a system for everyday use, all of them preferred the novel SEP system over the commercial C-Leg. Despite the promising results of this enhanced control strategy, the following constraints should be considered. To begin with, although the approach was evaluated within a clinical study, so far, no home-use (real-world) experiences were gained. Next, due to the modified damping, the operating time might be shorter, which could in turn affect the acceptance of such a product negatively. Lastly, the ultrasonic sensors used in this approach again are still inherently limited by their need for an unobstructed field of view. This means that neither prosthetic covers nor clothing can be worn over them, limiting the usability even further.

In conclusion, this thesis showed that environmental sensing technologies can improve the patient-prosthesis interaction successfully. From today's perspective, future development could refine the proposed systems using radar technology, and thus eliminate the main limitation. However, before that, research must prove that radar sensors are sufficiently accurate and efficient.



Die approbierte gedruckte Originalversion dieser Dissertation ist an der TU Wien Bibliothek verfügbar.
The approved original version of this doctoral thesis is available in print at TU Wien Bibliothek.

**RELYING ON MORE SENSE FOR ENHANCING
LOWER LIMB PROSTHESES CONTROL: A REVIEW**

by **Michael Tschiedel, Michael Friedrich Russold and Eugenijus Kaniusas**,
published in the *Journal of NeuroEngineering and Rehabilitation*.

Received: 20 December 2019 • Accepted: 6 July 2020 • Published: 17 July 2020

Abstract

Modern lower limb prostheses have the capability to replace missing body parts and improve the patients' quality of life. However, due to the lack of environmental information, a seamless adaptation to transitions between different forms of locomotion is often challenging. Novel sensors for environmental awareness, which have driven innovation in the robotic and automotive industry in recent years, are required. This work presents a detailed review on environmental sensing technologies applicable for enhancing the control of lower limb prostheses. A literature search was conducted on two Internet databases, PubMed and IEEE Xplore. A total of 6739 studies was reviewed based on the criteria for inclusion/exclusion. 32 papers were selected for the review analysis, 18 of those are related to explicit environmental sensing and 14 to implicit environmental sensing. Concept characteristics were discussed with a focus on computing power, computation time and energy consumption. The unobstructed field of view as well as the sensor placement are criteria for an implementation in "next generation prostheses". In summary, the research studies reported accuracies in the range from 82% up to 99% in well-controlled laboratory settings, but it is unclear how the systems will perform in realistic environments, both indoor and outdoor. According to the review analysis, high-frequency RADAR sensors capable to "look through" clothing or cosmetics seem to be the most seminal approach.

REVIEW

Open Access

Relying on more sense for enhancing lower limb prostheses control: a review

Michael Tschiedel^{1,2*} , Michael Friedrich Russold² and Eugenijus Kaniusas¹**Abstract**

Modern lower limb prostheses have the capability to replace missing body parts and improve the patients' quality of life. However, missing environmental information often makes a seamless adaptation to transitions between different forms of locomotion challenging. The aim of this review is to identify the progress made in this area over the last decade, addressing two main questions: which types of novel sensors for environmental awareness are used in lower limb prostheses, and how do they enhance device control towards more comfort and safety. A literature search was conducted on two Internet databases, PubMed and IEEE Xplore. Based on the criteria for inclusion and exclusion, 32 papers were selected for the review analysis, 18 of those are related to explicit environmental sensing and 14 to implicit environmental sensing. Characteristics were discussed with a focus on update rate and resolution as well as on computing power and energy consumption. Our analysis identified numerous state-of-the-art sensors, some of which are able to "look through" clothing or cosmetic covers. Five control categories were identified, how "next generation prostheses" could be extended. There is a clear tendency towards more upcoming object or terrain prediction concepts using all types of distance and depth-based sensors. Other advanced strategies, such as bilateral gait segmentation from unilateral sensors, could also play an important role in movement-dependent control applications. The studies demonstrated promising accuracy in well-controlled laboratory settings, but it is unclear how the systems will perform in real-world environments, both indoors and outdoors. At the moment the main limitation proves to be the necessity of having an unobstructed field of view.

Keywords: Prosthesis control, Artificial limb, Locomotion mode estimation, Terrain, Environment, Contralateral, Systematic review

Background

The amputation of a limb is an irreversible intervention into the physiological integrity of a human being. Limb loss is often caused by cardiovascular complications or diabetes; increasing obesity and aging population are the main contributing factors [1, 2]. Recent projections indicate that the number of major limb amputations will increase substantially [1].

Passive prostheses can replace the missing body parts to a high degree and improve patients' independence

and mobility. However, these devices lack the capability of generating power and therefore result in higher metabolic expenditure, increased stress to other joints and an asymmetric gait [3]. An unphysiological gait, especially reduced toe clearance, increases the risk of falling. Modern active powered prostheses have the capability to overcome this issue by providing net positive work required in daily activities [4]. But the question arises: do we already have the best sensor and control concepts to integrate such devices seamlessly into the patients' lives and autonomously adapt to their needs?

Focusing on lower limb prostheses, many state-of-the-art devices use finite-state controllers, decomposing the gait into a series of distinct phases with a discrete set

*Correspondence: michael@tschiedel.at

¹Research Group Biomedical Sensing, TU Wien, Institute of Electrodynamics, Microwave and Circuit Engineering, 1040 Vienna, Austria

²Global Research, Ottobock Healthcare Products GmbH, 1110 Vienna, Austria



© The Author(s). 2020 **Open Access** This article is licensed under a Creative Commons Attribution 4.0 International License, which permits use, sharing, adaptation, distribution and reproduction in any medium or format, as long as you give appropriate credit to the original author(s) and the source, provide a link to the Creative Commons licence, and indicate if changes were made. The images or other third party material in this article are included in the article's Creative Commons licence, unless indicated otherwise in a credit line to the material. If material is not included in the article's Creative Commons licence and your intended use is not permitted by statutory regulation or exceeds the permitted use, you will need to obtain permission directly from the copyright holder. To view a copy of this licence, visit <http://creativecommons.org/licenses/by/4.0/>. The Creative Commons Public Domain Dedication waiver (<http://creativecommons.org/publicdomain/zero/1.0/>) applies to the data made available in this article, unless otherwise stated in a credit line to the data.

of parameters [5]. In 2015, Tucker et al. [6] conducted a comprehensive review on control strategies for lower extremity prosthetics and orthotics. The ideas by Varol et al. 2010 [7] were extended to a generalized control framework consisting of four major sub-blocks: the Controller, the Device, the User and the Environment, as depicted in Fig. 1. The *Controller* can be represented as a three level hierarchy. At the highest level, the system is responsible for correctly estimating the patient's intent. Different terrains like level ground, stairs or ramps are related to different locomotion modes. The proper identification of transitions between different forms of locomotion is the most challenging task. The mid-level layer maps the estimated locomotion mode to the desired state outputs of the device. Finally, at a low-level, feedforward and feedback controllers minimize the error between the current state and the reference. The *Device* itself contains the mechanical and actuation structure for restoring or assisting the human functional morphology. The *User* and the device should work together in an intuitive and synergistic way, in which the device supports the patient's motion intentions. From the perspective of the device everything else is *Environment*. Tucker categorizes the environment interaction into implicit environmental sensing and explicit environmental sensing. *Implicit Environmental Sensing* (IES) creates an understanding of the locomotion mode by measuring the state of the residual patient's body. *Explicit Environmental Sensing* (EES), on the other hand, tries to directly estimate terrain features.

In order to guarantee a safe and comfortable control, a seamless estimation of IES and EES is required. In recent

years, the automotive and robotic industry have driven innovation and development mainly in the fields of TOF (time of flight) cameras, LIDAR (light detection and ranging) systems or RADAR (radio direction and ranging) solutions. This resulted in reduced prices for evaluation kits with powerful computer vision tools.

For the first time, the progress made in this area over the last ten years will be identified, focusing on the modalities of the sensors used in lower limb prostheses and on the strategies for enhancing device control. From this novel perspective, we conclude by outlining the most promising approaches and improvements that could make "next generation prostheses" more user-friendly, functional and safe.

Methods

The selection process for this review combined three different search strategies.

Firstly, the comprehensive review from Tucker et al. in 2015 [6] was used as starting point for the snowballing approach [8], going backward from Tuckers paper by reviewing the reference list as well as going forward by identifying articles citing this publication.

Secondly, a systematic literature review, based on the PRISMA [9] guidelines was conducted. Therefore, a search string was defined for retrieving publications of interest from two different databases (i.e. IEEE Xplore and PubMed.gov). In order to find relevant articles, the first term was either "prosthesis", "extremity" or "limb". It was connected via a logical AND with either "radar", "lidar", "time-of-flight" or "depth" for focusing on dedicated

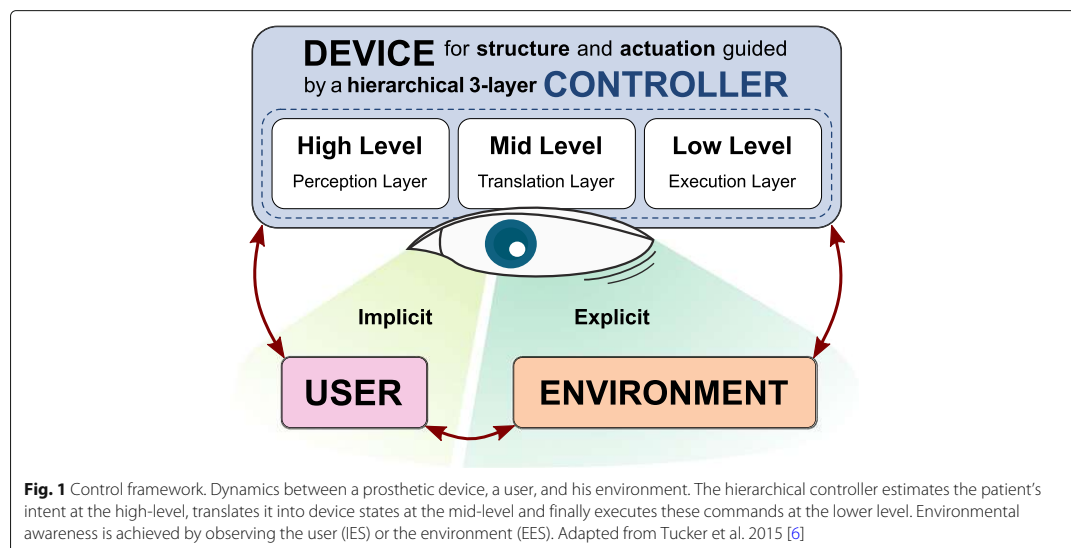


Fig. 1 Control framework. Dynamics between a prosthetic device, a user, and his environment. The hierarchical controller estimates the patient's intent at the high-level, translates it into device states at the mid-level and finally executes these commands at the lower level. Environmental awareness is achieved by observing the user (IES) or the environment (EES). Adapted from Tucker et al. 2015 [6]

sensor expressions as well as with “terrain”, “environment” or “locomotion” for more holistic synonyms. Duplicates were removed, title, abstract and full publication were screened, and the following inclusion and exclusion criteria were applied to select or reject publications:

Criteria for inclusion: Strategies for estimating environmental information to improve existing prosthesis control as well as all types of locomotion modes were included. Only portable prototypes were considered. The application for enhancing “prosthesis control” must be mentioned. Only articles published in “English” during the last 10 years (i.e. 2009 – 2019, final update: 12 November 2019) were included.

Criteria for exclusion: Systematic reviews and literature reviews, any kind of upper extremity solution, exoskeletons or orthotics-related papers were excluded. Systems based on inertial measurement units (IMU), for analyzing human motion (gait) without any link to prosthesis control are not in the focus of this review. Also not included were studies focusing only on neuromuscular or mechanical signals from the device itself or the residual ipsilateral limb. Computer vision publications without association to enhancing prosthesis control were excluded as well.

Finally, the selected publications of the outlined search strategies were used for an author cross-check. The publication lists of all referred authors retrieved from Google Scholar, ORCID or institutional and private websites were rechecked to see if individual publications meet the inclusion criteria. For example, if an earlier conference paper was discovered in the database search, but the same author had also published a journal paper covering the topic of interest, which was not caught by the first two search methods, it was also included in this review.

Results

An overview of the selection process is shown in the flow diagram in Fig. 2. Twenty four out of the 6739 articles identified with the search strategies met the inclusion criteria. Another 8 were added through the final author cross-check, resulting in 32 publications included in this review.

Overview

The retrieved 32 publications were categorized by the two types of environment. The majority (18) of those are related to EES, the remaining (14) to IES. Table 1 provides a summary of all included records. The main characteristics of the publications are structured in the following columns:

Study: In this column, the first author as well as the publication year and the reference are mentioned. If more than one reference is given, the year indicates the most

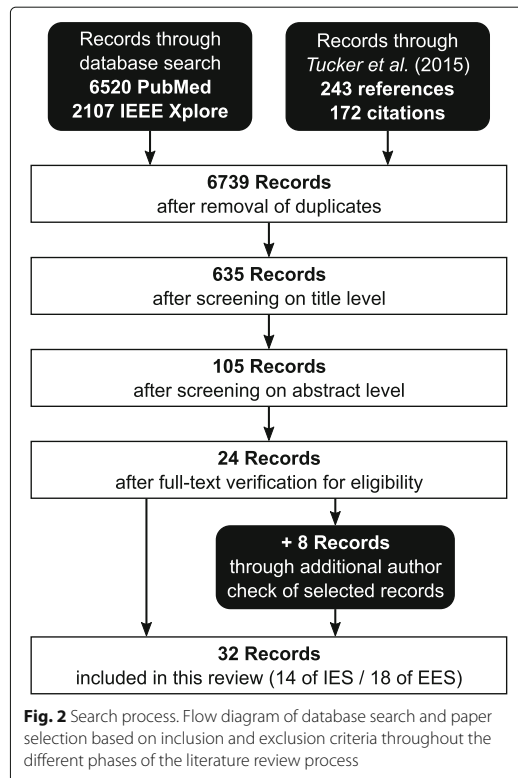


Fig. 2 Search process. Flow diagram of database search and paper selection based on inclusion and exclusion criteria throughout the different phases of the literature review process

recent publication. If research groups have performed tests with amputees, this is indicated by (P). If they have evaluated their system only with healthy subjects, it is marked with (H). (T) implies that it is a theoretical concept, eventually tested in an experimental setup, but not tried in interaction with human beings.

Type / Group: *Type* serves as an indicator, to show if the record is more related to implicit or to explicit environmental sensing. *Group* assigns each publication a particular control strategy out of five main categories retrieved within this review – a detailed explanation is given in “Discussion” section. The overview table is sorted by this column.

Sensor selection: This column describes the type of sensors used in the study.

Sensor placement: This column gives an overview, where the respective sensors are placed on the human body. The lower part of the human body is segmented into foot, shank, thigh and trunk. The connecting joints are ankle, knee and hip. Bilateral (B) means “on both sides of the body”. Ipsilateral (I) means “located on the same side

Table 1 Overview of records reviewed

Study	Type / Group	Sensor selection	Sensor placement	Concept description
Vallery et al. (P, 2011) [10]	IES / 1	2 x angle & angular velocity sensors	C: hip & knee	Mapping function for control of knee prototype with estimated contralateral limb motion data.
Bernal-Torres et al. (H, 2018) [11, 12]	IES / 1	1 x IMU	C: thigh	Active biomimic polycentric knee prototype with contralateral echo-control strategy.
Su et al. (P, 2019)[13]	IES / 1	3 x IMUs	C: thigh, shank & ankle	Intent recognition system based on convolutional neural network classification.
CYBERLEGS project series ¹ (P, 2017) [15–18]	IES / 1	2 x pressure insoles 7 x IMUs	B: shoes inlays B: thighs, shanks, feet & 1 x trunk	Finite-state control of a powered ankle-knee coupled prototype using whole-body aware noninvasive, distributed wireless sensor control.
Hu et al. (P, 2018) [19–21]	IES / 2	4 x IMUs 4 x GONIOs	B: thighs & shank B: knee & ankle	Classification error reduction through fusion of bilateral lower-limb neuromechanical signals, providing feasibility & benchmark datasets.
Extended by: Krausz et al. (H, 2019) [22]	EES / 2	14 x EMGs 1 x IMU 1 x depth camera	B: leg muscles On the waist in a belt construction	Adding vision features to the prior concept improving the classification.
Hu et al. (H, 2018)[23]	IES / 3	1 x IMU 1 x depth camera	I: thigh	Bilateral gait segmentation from ipsilateral depth sensor with the contralateral leg in field of view.
Zhang et al. (H, 2018) [25]	IES / 3	1 x depth camera	On the waist with tilt angle	Depth signal from legs as input to an oscillator-based gait phase estimator.
Scandaroli et al. (T, 2010) [27]	EES / 4	2 x gyroscopes 4 x infrared sensors	Built into a foot prototype	Infrared distance sensor setup for estimation of foot orientation with respect to ground.
Ishikawa et al. (H, 2018) [28]	EES / 4	2 x infrared sensors 1 x IMU	Left & right on one normal shoe	Infrared distance sensor setup for estimation of foot clearance with respect to ground.
Kleiner et al. (T, 2011) [29]	EES / 5	1 x motion tracking 1 x laser scanner	I: between artificial ankle & knee joint	Concept and prototype of a foresighted control system using a 2D laser scanner.
Huang's group ² (P, 2016) [30–33]	EES / 5	1 x IMU 1 x laser sensor	I: lateral side of the trunk	Terrain recognition based on laser distance, motion estimation and geometric constrains.
Carvalho et al. (H, 2019) [36]	EES / 5	1 x laser sensor	On the waist with 45° tilt angle	Terrain recognition based on laser distance information and geometric constrains.
Sahoo et al. (H, 2019) [37]	EES / 5	3/4 x range sensors 1 x force resistor	I: On the shank & on the heel of the foot	Array of distance sensors for geometry-based obstacle recognition in front of the user.
Varol et al. and Massalin et al. (H, 2018) [38, 39]	EES / 5	1 x depth camera	I: shank	Intent recognition framework using a single depth camera and a cubic kernel support vector machine for real-time classification.
Laschowski et al. (H, 2019) [40]	EES / 5	1 x color camera	Wearable chest-mounting	Terrain identification based on color images and deep convolutional network classification.
Yan et al. (H, 2018) [41]	EES / 5	1 x depth camera	On the trunk in 1.06m height	Locomotion mode estimation based on depth feature extraction and finite-state classification.
Diaz et al. (H, 2018) [43]	EES / 5	1 x IMU 1 x color camera	I: foot & shin	Terrain context identification and inclination estimation based on color image classification.
Krausz et al. (H, 2015) [45]	EES / 5	1 x depth camera 1 x accelerometer	Fixed in 1.5m height with -50° tilt angle	Stair segmentation strategy from depth sensing information of the environment.
Kleiner et al. (P, 2018) [46]	EES / 5	1 x IMU 1 x radar sensor	I: thigh	Stair detection algorithm through fusion of motion trajectory and radar distance data.
Zhang et al. (P, 2019) [47, 48]	EES / 5	1 x IMU 1 x depth camera	I: knee lateral	Environmental feature extraction based on neural network depth scene classification.

¹Publications through CYBERLEG: Amrozić et al. [15, 16], Gorsic et al. [17] and through CYBERLEG++: Parri et al. [18]

²Research group from Huang: F. Zhang et al. [30], X. Zhang et al. [31], Wang et al. [32] and Liu et al. [33]

of the body part” or respectively on the same side as the device. The opposite is contralateral (C) which signifies “located on the opposite part”.

Concept description: This field shortly summarizes how environmental information is used for enhancing prosthesis control in each record.

Within the publications, 11 different types of sensors were used. It was possible to divide those sensors into three categories, as shown in Fig. 3. In particular, *Distance & depth* differentiating sensors based on ultrasonic or electromagnetic waves with different frequencies and *Kinematic* grouping sensors for measuring the motion of bodies. EMG electrodes, pressure insoles and color cameras were summarized into *Other*. Information was extracted from the reviewed publications itself and, if missing, completed with the help of the manufacturer’s datasheet. The main characteristics are the sensor update rate, resolution and the need for an unobstructed field of view.

Implicit environmental sensing

Vallery et al. [10] presented a complementary limb motion estimation strategy. In this application, a linear mapping function outputs the state of the missing limb dependent on the state of the residual sound side. The angle and angular velocity is measured by sensors attached to

the contralateral hip and knee. So far, only results from one above-knee amputee were presented. The patient was almost able to achieve a physiological gait pattern. However, detailed technical information was not given.

Instead of using a monocentric knee prototype, Bernal-Torres et al. [11, 12] proposed a concept of an active polycentric knee prosthesis using the echo-control schema. An inertial measurement unit fixated on the contralateral thigh estimates the trajectory of the unimpaired knee. The average tilt angle error between the polycentric knee prototype, mounted in a test workbench, and the anatomical lower limb of one non-impaired subject was about 2°.

Three IMUs on the contralateral thigh, shank and ankle for locomotion intent recognition, were used by Su et al. [13]. The sensor data was taken as input into a convolutional neural network, a class of computational processing systems heavily inspired by biological neural networks. It “learns” to perform tasks using self-optimizing weights and biases throughout example-based learning. Filters are used to extract hierarchical patterns in data, which makes them particularly interesting for (image) recognition systems [14]. Ten able-bodied subjects and one above-knee amputee participated in the study. Different strategies for user-independent and user-dependent classification with varying amount of test and training data were analyzed. The highest accuracy was reported with 94.2% for the

	Update rate	Resolution	Unobstructed field of view
Distance & depth			
- ULTRASONIC (1D)	low	low	yes
- INFRARED (1D)	medium	medium	yes
- LASER (1D)	high	high	yes
- RADAR (1D)	high	low	no
- LIDAR (2D)	medium	high	yes
- DEPTH CAMERA (3D)	medium	medium	yes
Kinematic			
- GONIO	high	high	n/a
- IMU / MOTION	high	medium	n/a
Other			
- EMG	medium	medium	n/a
- INSOLE	high	low	n/a
- COLOR CAMERA	medium	high	yes

Fig. 3 Sensor comparison. Different sensors used within the retrieved publications were divided into the three categories: *Distance & depth*, *Kinematic* and *Other*. *Update rate* describes the number of measurements per second. The rating scale: (low), (medium) and (high) is used instead of absolute values, representing a scale from approximately 10 Hz up to 100 Hz for real-time applications. The smallest change that can still be detected by a sensor is its *Resolution*. The rating scale: (low), (medium) and (high) is used instead of absolute values, representing a scale from several centimeters down to the millimeter range. *Unobstructed field of view* indicates whether the sensor functionality does or does not require an unobstructed field of view: (yes/no). If its not applicable, this is indicated by: (n/a)

able-bodied and 89.2% for the amputees, classifying five types of terrains and eight transitions between them.

As part of the CYBERLEGS project Ambrozic et al. [15, 16] and Gorsic et al. [17] used the α -prototype prosthesis (actuated ankle and a passive knee) with a “whole-body aware” control approach. The user intention was measured through seven wireless IMUs, attached bilaterally to the feet, shanks and thighs and one on the trunk. Additionally, two pressure insoles measured the ground force and the center of pressure. The control scheme combined the intent detection from the body-worn sensors and the prosthesis control into one state machine with unified states and transitions based on the analysis of gait in healthy subjects. The overall intent recognition for three unilateral transfemoral amputees was accurate in 85.2% of the cases for level-ground walking. Parri et al. [18] used a similar wearable sensory concept and the advanced β -prototype throughout the CYBERLEGS Plus project. In this study, four unilateral transfemoral amputees participated in the study with different activities. 100% accuracy was reported in treadmill walking, even at a low walking speed. The lowest score was achieved for the sit-to-stand task at 94.8%.

A systemic analysis of different signals from the contralateral side for predicting the locomotion mode was done by Hu et al. [19–21]. Ten healthy subjects participated in the study generating a public available benchmark dataset of lower limb joint kinematic and electromyography (EMG) data, simultaneously recorded with wearable sensors. Electrogoniometers (GONIO) were used to record joint kinematic signals of knee and ankle of both legs. IMUs were placed bilaterally on the subject’s thigh and shank. Bipolar surface EMG electrodes were placed on seven muscles in each leg. They analyzed different combinations of sensors and algorithms. It was shown that only one additional contralateral sensor could significantly reduce intent recognition error rates. Finally, an offline analysis of one above-knee amputee walking with a powered leg prosthesis was presented. Placing two additional IMUs on the contralateral thigh and shank could reduce overall, steady-state and transitional error rates by more than 60%, compared to ipsilateral sensor placement as baseline. Parallel to this, Krausz et al. [22] extended the system by an IMU and a single depth camera. These sensors were worn on a belt-like construction with the environment in front of the subject in the field of view. The IMU was used to transform the vision information into a global reference system. Each frame was segmented into a grid of regions of interest before extracting three types of vision-based features: distance and orientation, motion information and the projected shape of the terrain on them. The influence of each sensor modality was analyzed, reporting that adding “vision information”

increases the repeatability and, at the same time, reduces the variability across subjects and locomotion modes.

Despite the positive outcomes, the additional instrumentation of the non-prosthetic side is not really practical and comfortable for amputees. Hu et al. [23] extended their ideas and presented a novel method for bilateral gait segmentation using only unilaterally worn sensors. A single IMU and a depth camera were placed on one thigh to detect bilateral gait events. RANSAC [24], an iterative method to estimate a model in a set of data containing outliers, was used to identify the ground plane in the depth points. Vision filtering and grouping methods were applied to correctly estimate the shank angle of the contralateral leg. IMU data and sound side features were fused for intent classification. The system was tested with one healthy subject showing that it is possible to detect bilateral gait events even from unilaterally worn sensors.

Zhang et al. [25] conducted a study, in which both legs were within the sensor’s field of view. A depth camera was mounted on the waist looking forward with such a tilt angle, that the toes are just not captured when the person is standing still. A movement led to a periodic variation of depth values. This signal was then used as input into an earlier published concept of an adaptive oscillator gait phase detector [26], a method for extracting features and synchronizing to periodic signals. Four able-bodied subjects participated in a level ground walking study, reporting a maximum estimation error of 0.3 rad between the estimated gait phase and the reference gait phase calculated out of two consecutive steps.

Explicit environmental sensing

Foot clearance is an important gait parameter and serves as an indicator for gait quality and safety. Scandaroli et al. [27] presented a prototype of a prosthetic foot equipped with two gyroscopes and four infrared distance measuring elements. The concept was to estimate foot orientation with respect to the ground. So far, only test-bench results estimating the inclination and height of the foot above the ground have been presented. Ishikawa and Murakami [28] equipped a normal shoe with two infrared distance sensors and one IMU. The data gathered from one healthy subject walking in five different terrains was analyzed. The waveform of the sensor signal was reported to be unique for different locomotion modes – a dominant double peak was the characteristic of leveled walking, but detailed technical information was not given.

Already in 2011, Kleiner et al. [29] published a concept of a foresighted control for a foot prosthesis. An optical measuring system consisting of a laser scanner and an inertial navigation system was mounted between the ankle and the knee on the side of the prosthesis. The two-dimensional (2D) depth data from the laser scanner was combined with the motion information from the inertial

system to create a three-dimensional (3D) representation of the environment. The idea was to use computer vision methods in order to detect objects like stairs, or ramps in the environment. So far, only “images” from a single indoor experiment were presented without any technical details.

Instead of using a 2D laser scanner, the research group from Huang [30–33] used a single laser distance meter and one IMU for terrain recognition. They extended the concept of a locomotion mode recognition system based on neuromuscular EMG signals from the residual limb and mechanical load information on the device [34, 35]. The additional sensors were mounted laterally on the trunk of the prosthetic side. A decision tree classified the terrain in front of the user into five different categories depending on thresholds and geometric constraints. The system was tested on six able-bodied subjects and one above-knee amputee. It identified the new terrain 500 ms before executing locomotion mode transition with an accuracy of 98%.

A concept without an IMU was introduced by Carvalho et al. [36]. The information from an infrared laser mounted on the user’s waist was classified with a three-layer decision tree with heuristic rules. Tested on 10 able-bodied subjects, the classification accuracy for eight locomotion mode transitions was above 80%, achieving 100% success for identifying the transition from ramp descent or stair descent into level ground.

An array of distance sensors was used by Sahoo et al. [37]. In this study, a prototype with either four ultrasonic distance sensors or three laser distance sensors was mounted on the shank of the participant. Reliable measurements were always taken during the stance phase triggered by a force resistor attached at the heel of the foot. The distance signals were used to classify four types of terrains ahead of the user. Two classification approaches, such as quadratic discriminant analysis and rule-based system, were explored with two able-bodied subjects. The ultrasonic sensors achieved an accuracy above 97%, however the range within obstacles were detected was less than 50 cm leading to the risk to “miss a transition” if the step length of the subject was greater than the detection range. In comparison, the laser distance sensors increased this range up to 100 cm. By taking the most frequent prediction class within a single step, the system identified the new terrain 650 ms before executing locomotion mode transition with an accuracy of above 98%.

Varol et al. [38] and Massalin et al. [39] attempted to detect five different locomotion modes with a depth sensor. In this application, a single depth camera was mounted unilaterally on the shank with a 45° tilt angle to the ground plane. In order to embed motion information, so called “depth difference images” were calculated. This was done through pixelwise subtraction of the preceding

depth frame. Twelve healthy subjects participated in the study. Data of eight subjects was used to train different variations of support vector machine classifiers, a supervised learning algorithm that sorts data into predefined categories. The highest reported accuracy of 94.1% was achieved with a cubic kernel and no dimension reduction classifier on the test-data of the remaining four subjects. The averaged computation time was reported with 14 ms.

Three different types of terrains were classified with an overall accuracy of 94.85% in the study from Laschowski et al. [40]. A chest-mounted color camera with the environment in front of the subject in its field of view was used for data acquisition. One able-bodied subject walked around, collecting over two million sample images. Around 34,000 of them were individually labeled to train the 10-layer deep convolutional neural network used for classification.

Yan et al. [41] presented a depth image-based locomotion recognition approach that does not require any pre-training. A depth camera mounted on the waist in a height of 1.06 m, having the terrain and a small portion of the user’s feet in its field of view, is used in this setup. Depth images were segmented into 12 blocks and locally averaged. A finite-state machine with predefined thresholds is then used to classify between four locomotion modes. Additionally, stair edges were detected by using a Hough Line Transform [42], a feature extraction technique to find a certain class of shapes by a voting procedure. Nine healthy subjects participated in the study. The accuracy for steady state locomotion tasks was reported as 100%. However, correctly detecting the transitions was challenging. Nevertheless, 82.4% of the terrain changes could be detected before executing a locomotion mode transition. In this study, there was no real-time evaluation performed, although the computation time was only 5 ms.

Rather than classifying the locomotion mode of the user, Diaz et al. [43] proposed a concept of estimating the soil properties as well as the surface inclination in front of the user’s leg. In this application, a normal color camera was mounted on the shin and an IMU on the top of the foot of an able-bodied subject. Comparable images were always taken during the stance phase of the gait cycle. The images were classified with the Bag of Words method [44], analyzing the input against a predefined bag of local image features. The classifier was able to identify 6 types of terrains (asphalt, carpet, cobblestone, grass, mulch and tile) with an averaged accuracy of 86%. The prediction of the terrain inclination in front of the leg was accurate to 0.76° compared with a reference.

Krausz et al. [45] presented a method for estimating stair parameters with a depth vision system in 2015. The proposed algorithm used prior knowledge of a basic stair structure and input of a single three-axis accelerometer. One able-bodied subject held the camera in 1.5 m in height with a -50° tilt angle from horizontal and walked

through a hallway entering into a stairwell. This online test resulted in 98.8% accuracy for classification if they were either “approaching” stairs or “not approaching”.

The first and only group using a RADAR sensor for stair detection was Kleiner et al. [46] in 2018. In this application, a radar distance sensor and an IMU were mounted on the thigh of the prosthetic device. Fusing both signals created a 2D image of the sagittal plane in its virtual field of view. For objects in a range up to 5 meters in front of the device, a mean accuracy of 1.5 ± 0.8 cm was reported. The mean accuracy for height estimation lies within 0.34 ± 0.67 cm.

The most advanced environmental feature recognition system was presented from Zhang et al. [47]. In this application, five different environments could be distinguished. A depth camera and an IMU mounted ipsilaterally on the knee joint were combined to transform the captured scene into world coordinates. The 3D scene was reduced to a 2D binary image, which reduced total computing time remarkably to only 23 ms. A deep convolutional neural network was used to classify the type of input scene. Finally, after classifying the type of terrain, basic computer vision methods were used to estimate features such as the slope angle of a ramp or the height and width of stairs. The proposed system was evaluated using data from simulation, indoor and outdoor experiments. Six able-bodied subjects and three above-knee amputees participated in the study. Data from the simulation and one healthy subject was used to train the network, the remaining data was used for validation only. The classification accuracy for amputees was reported with 99.3% for indoor and 98.5% for outdoor experiments, predicting the terrain change at least 0.6 s before switching the locomotion mode. The latest publication from Zhang et al. [48] considered the credibility of decisions and the relationship between states for improving the classification even further.

Discussion

Commercially available lower limb prostheses use mainly device-embedded sensors to “(re)act” to the patient’s intent. However, due to the lack of contextual (environmental) information, misclassifications can result in stumbling or even falling down. The present review describes the progress made over the last decade towards more “foresighted” prosthetic systems. From this novel perspective, a “control strategy landscaping” was derived, how environmental information can enhance “next generation prostheses”.

Control strategy landscape

New concepts for environmental sensing in “next generation prostheses” can be distinguished according to how they improve existing control systems. As depicted in Fig. 4, enhanced control strategies can be separated into

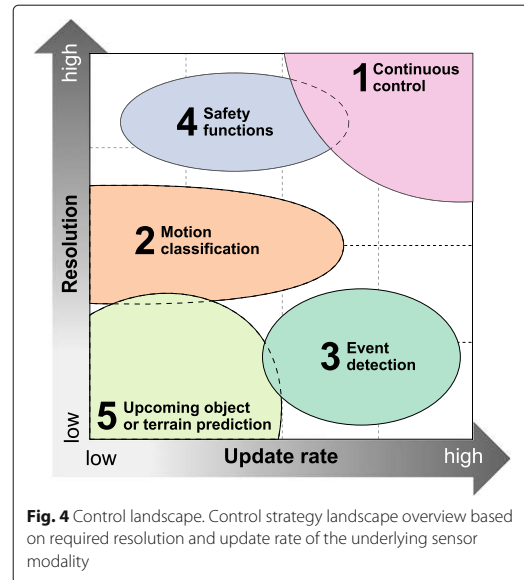


Fig. 4 Control landscape. Control strategy landscape overview based on required resolution and update rate of the underlying sensor modality

five groups, namely continuous control (1), motion classification (2), event detection (3), safety functions (4), and upcoming object or terrain prediction (5). The required update rate and resolution is a criterion to select the best sensor modalities for each of them. All retrieved publications were assigned into one of these main groups, dedicated in column 2 of Table 1.

Continuous control systems measure and adjust in real time. Hence, sensors with high update rates as well as high resolutions are needed. In accordance with three-level controller hierarchy framework from Tucker, input is processed directly at mid-level layer to control the prosthetic device state in real time. In this category, only IES-based residual patient’s body estimation strategies were investigated. Typically, kinematic sensors like IMUs or GONIOS are used. Using contralateral leg information seems to be a common concept [10–13]. However, simple echo-control strategies caused errors, especially at the beginning and the end of an activity, when the limbs are not required to “echo” each other. Placing sensors not only on the contralateral leg, but rather measuring the entire (lower) body, expands the possibilities. These concepts [15–18] can control in real-time throughout numerous locomotion modes and transitions between them. However, for all the presented “body aware” concepts, it was necessary to mount additional sensors on the patient’s body, which reduced usability.

Not controlling, but rather classifying is meant by *motion classification*. Signals measured from distributed sensors are used to perceive the patient’s intent at the

high-level layer of the controller hierarchy framework better. Therefore, sensor update rates as well as resolutions are typically lower. Unsurprisingly, fusing whole body kinematic signals lead to higher intent recognition rates, as was proven systematically [19–22]. Remarkably, however, it could be shown that an additional sensor on the unimpaired sound side can reduce misclassifications. Instead of mounting and calibrating a large number of additional sensors to the patient's body, a single contralateral sensor would be sufficient to enhance device control. As depicted in Fig. 4, motion classification also overlaps with the group of upcoming object or terrain prediction. Although the focus of this section here lies mainly on the correct intent recognition rather than on predicting the upcoming terrain directly, these two are strongly related by nature – obstacles and terrain features are in this sense the “boundary conditions” for all movements.

Strategies extracting specific “events” from the human gait cycle are combined into *event detection*. The most prominent are the “heel strike”, initiating the stance phase, and the “toe off”, responsible for the beginning of the swing phase [49]. Normally, this information is used at the mid-level control layer to trigger movement-dependent actions. Therefore, the required sensor update rate is typically higher than for motion classification, however, the resolution can be lower. For example, pressure insoles are typically used for measuring ground contacts. While timing is very important, it can often be sufficient to differentiate, whether the foot is, or is not, in contact with the ground. A continuous gait phase estimation was carried out on the basis of a gait-related depth signal captured from a waist-worn depth camera [25]. The approach from Hu et al. [23] seems to be more practical, where a unilaterally mounted depth camera detected bilateral gait events. However, the computation time of more than 1 s prevented any real-time (online) application.

Safety functions summarize all concepts which contribute to the safety of a prosthetic device. In terms of environmental sensing, reliable prevention of stumbling and falling in unexpected terrains is still an open question. A study with able-bodied individuals found that an unrecognized object with a height of 1 cm can lead to stumbling, concluding that foot clearance is an important parameter to prevent falling [50]. For measuring this parameter, infrared distance sensors were used in two publications [27, 28], but not evaluated in a prosthetic setup. In general, the resolution of the sensor modality has to be high enough to correctly detect small barriers, ideally with a high update rate to “(re)act” in real time. While high resolution is mandatory, update rates can also be lower. For instance, a leg-mounted depth or color camera, capturing a single image during the mid-stance phase when the leg is almost vertical, could minimize stumbling risks during the next step. It is also conceivable that two distance sensors,

one more toe-related and the other more heel-related, in combination with an IMU, could estimate the correct ground inclination. This could be especially interesting for the further development of active ankle devices, but it was not evaluated in any of the reviewed publications.

Half of all the reviewed studies deal with *upcoming object or terrain prediction* concepts. The underlying principle of all these publications is to observe the front environment of the user, interpret the input and then provide a probability for mode switching. This is mainly, due to the fact that the correct detection of locomotion mode transition between different terrains, e.g. switching from level-ground walking to stair ascent mode, is often challenging and unintuitive. For instance, in commercially available products, the user must switch between locomotion modes with substantially different characteristics by carrying out a predefined “special movement”. This action triggers the transition by using only sensors embedded into the prosthesis [51]. In accordance with the controller framework by Tucker, upcoming object or terrain prediction strategies provide input for the high level of the controller. Earlier listed safety functions on contrast, interact mainly at the low-level layer, increasing patient safety.

Huang et al. [35] coined the term “critical timing” for switching mode, neither interrupting the transition nor disturbing the balance. Concepts using 1D laser distance meter [30–33, 36, 37] combine the sensory input with geometric constraints to estimate upcoming terrain features early enough and accurately. Although one group used a RADAR sensor as an input device [46], the feature of “looking through” materials was not evaluated in this study.

Explicit object recognition is another approach for classifying upcoming barriers directly. The invention of low-cost high-resolution depth and color cameras opened up an entirely new field of vision-based object recognition [52]. Especially for autonomous robots, the capability to detect and classify objects correctly is critical. For example, a self-driving wheel-chair was able to successfully navigate through the hallways of a hospital [53]. However, in terms of lower limb device control, the final decision “where to go” or “what to do” is made by the user anyway. Therefore, the sensor raw data are usually pre-processed to obtain probabilities for possible terrain changes.

Depth cameras [38, 39, 41, 45, 47, 48] were used to differentiate between a limited number of terrains and whether the user is approaching stairs. The approach of soil property estimation based on a color camera [43] was also evaluated, but not in a prosthetic setup. Nevertheless, all vision-based systems are computationally intensive and require an unobstructed field of view. Concepts using pre-trained classifiers [38–40, 43, 45, 47, 48] achieved

higher accuracies compared to finite-state machines without any training [30–33, 36, 37, 41]. However, pre-trained classifier performance depends strongly on the size of training data. Moreover, predefined step sequences during the acquisition of training data can lead to an undesired bias – the system is trained with specific parameters, but in real life step sequence and walking speed are unpredictable.

In general, it is very difficult to compare the different approaches, as they use non-standardized test procedures. In summary, the research studies reported accuracies ranging from 82% to 99%. Assuming 100 locomotion mode changes per day and expecting only every tenth misclassification to cause a fall, there would still be 3 to 54 serious tumbles per month, which does not seem very promising.

Sensor modalities

The 32 publications reviewed use 11 types of sensors, as depicted in Fig. 3. Kinematic sensors are widely used – 24 out of 32 publications, use IMUs for motion estimation. Even all five commercially available microprocessor-controlled prosthetic knees, reviewed by Fluit et al. [5], use a shank IMU as sensory input. However, the integration of IMU information tends to suffer from accumulating errors, which can lead to drifts. Alternatively, GONIOs are accurate and reliable, but they usually limit the degree of freedom of complex human joints.

Distance sensors usually use the principle of time of flight, measuring the round trip time between emitting and receiving back a specific pulse. Ultrasonic sensors are based on mechanical (acoustic) waves. The propagation speed for these sensors is limited by the speed of sound, which results in a round trip time of approximately 6 ms for an object at 1 m distance. Thus, nature limits the update rate of ultrasonic sensors. Nevertheless, they are common for close proximity applications, as they are able to detect even transparent materials like glass. By using electromagnetic waves, the round trip time is usually negligible, because the speed of light is substantially higher. The update rate of these sensors is, therefore, limited only by the processing rate of the internal hardware. Infrared sensors emit light below the visible light range. Instead, laser sensors have operating frequencies in the visible range (red or green light) or above (invisible ultraviolet range). Update rate and resolution are normally lower for ultrasonic sensors than they are for lasers. LIDAR sensors combine laser distance meters with a complex mechanical mirror system to generate high-resolution 2D or even 3D scans. However, shocks or vibrations can disrupt the moving parts in such devices. Historically seen, these sensors used to be very expensive, whereas nowadays industries have shifted to develop low-cost solid-state LIDARs for a broad application.

Depth perception refers to the ability to estimate the surrounding world in 3D – nature (human eyes) has perfected this over millions of years. Historically, color cameras, working on passive light sensors, were combined to stereo vision systems to extract depth information from well-known digital images. Performance depends primarily on the underlying stereo correspondence algorithms (depth calculation process), which tries to match pixels of the two individual images. Today, depth cameras based on the time-of-flight principle have become increasingly more available. Similar to TOF sensors, an artificial light impulse is emitted, while the reflection is simultaneously captured by multiple sensitive elements. This generates a full 3D perception at once with resolutions up to 640 x 480 pixels, small enough to be implemented into a smartphone [54]. The resolution of depth cameras, for time of flight as well as for stereo vision based concepts, is in the range of 1% of distance with update rates varying from 5 to 60 (depth) frames per second. Nevertheless, all concepts based on infrared, visible or even ultraviolet light are limited by their explicit need of an unobstructed field of view. The additional sensors must be worn over any type of prosthetic cosmetic or clothing and can, therefore, not be integrated directly into the device. RADAR technology, however, is not limited by this factor. Although radar technology was already discovered in the late 19th century, only recent developments have made new sensors with operating frequencies up to 100 GHz available. While RADAR sensors have much lower resolutions compared to optical or depth sensors, they can still operate in harsh outdoor conditions. To which degree an object is detectable, is expressed in its cross-section, a property of the target's reflectivity [55]. Due to the high-frequency range, certain materials, such as fabrics or plastics, typically appear transparent. On one hand, this is a good feature of RADAR sensors, as it allows an implementation directly into the prosthetic device making it possible to “look-through” clothes or cosmetics (cover of an artificial limb to appear lifelike). However, on the other hand, objects or barriers made out of these materials remain undetected. Nowadays, there is a shift towards the development of super near-field RADAR sensors which are able to detect human extremities and gestures for a broad application. For example, Google's radar-based gesture sensing technology (Project Soli) is implemented in their Pixel 4 smartphone allowing a touchless interaction [56].

For the sake of completeness, surface EMG electrodes as well as force resistive insoles are mentioned, although they are not really “environmental sensors”. Conceptually, both type of sensors require a direct contact with the body. Surface EMG electrodes with the skin to register muscle activity and insoles with the foot to detect ground contact. The unobstructed field of view, mandatory for all types of cameras, has no influence on the application

here. Nevertheless, especially for event detection, insoles can provide valuable information, but the sensors need to be worn either ipsilaterally, contralaterally or bilaterally in the user's shoe. EMG information is commonly used for real-time hand prosthesis control [57], but barely in lower limb devices, since movement artifact and baseline noise contamination is more prominent there.

Computing power & energy consumption

Nowadays, commercial prostheses have very limited *computing power*. Typically, finite-state machines with heuristic rule-based approaches are used for intent recognition and device control. In contrast, most of the reviewed studies, carried out data acquisition and analysis on powerful computers with clock rates of 3 GHz or above and memory sizes up to 32 GB. The available computing power also influences the calculation time for interpreting or extracting usable information from the complex sensory input. The delay from measuring until adapting needs to be short enough to guarantee a safe and comfortable device operation. Typically, update rates for real-time prosthetic device applications are in the range of 100 Hz [5]. Therefore, the embedded system architecture of prosthetic devices needs to be modified significantly if real-time on-board processing should be enabled. For example, Intel's Myriad 2 is optimized for vision processing in mobile applications within 0.5 W of power envelope [58] and could also be used in lower limb prostheses.

The *energy consumption* of advanced sensors also needs to be considered, when designing and developing new systems. The power consumption of Softkinetic's DS 325 depth camera used in [38, 39] is below 2.5 W [59]. The pmdtechnologies's CamBoard pico flexx used in [22, 23, 47] is below 0.3 W [60]. The radar module used in [46] has a total power consumption of 5 W [61], with almost identical geometric dimensions to those of depth sensors. Ongoing development will thus reduce energy consumption of sensors and processors even further. In contrast, research and commercial active (powered) knee prostheses use actuators consuming up to 200 W [4]. Therefore, the energy consumption of additional sensors cannot be regarded as the main reasons for exclusion.

Conclusions

In this review, we summarized both implicit and explicit approaches of environmental sensing. For this purpose, a systematic literature review as well as a snowballing analysis of the survey from Tucker et al. [6] was performed. From our novel perspective, five broad control strategies were identified, how environmental information can make "next generation prostheses" more user-friendly, functional and safe.

There is a clear trend towards more upcoming object or terrain prediction concepts, providing switching probabilities between different locomotion modes. In summary, the research studies reported accuracies ranging from 82% to 99% in well-controlled laboratory settings, but it is unclear how the systems will perform in realistic environments, both indoor and outdoor. It was also shown that implicit environmental sensing strategies in particular can significantly improve control. Furthermore, information about the contralateral leg can play a crucial role in movement-dependent control applications.

Throughout the 32 reviewed publications, 11 types of sensors were used. Technology differences were discussed, and aspects of computing power and energy consumption mentioned. The update rate and resolution were found to be essential criteria to determine a suitable control category. Distance sensors and depth cameras are widely used, but they are limited by an unobstructed field of view. Moreover, the latter also requires higher computing power for calculating interpretable features from the (complex) raw inputs. In almost all studies, kinematic sensors are used, either to estimate movements directly or to stabilize other inputs. However, the additional instrumentation of residual body parts seems less practical.

Together with the derived "control strategy landscaping"; our in-depth evaluation of the novel sensors for environmental awareness can serve as decision guidance for future research in this field. New high-frequency RADAR sensors may be the best choice for upcoming object or terrain prediction approaches, perhaps even for event detection strategies. Thanks to their ability to "look through" clothing or cosmetic covers, these sensors could be embedded directly into a prosthetic device, resulting in numerous new possibilities. Before that, however, research must prove that they are sufficiently accurate and efficient.

Abbreviations

2D: Two-dimensional; 3D: Three-dimensional; IES: Implicit environmental sensing; EES: Explicit environmental sensing; TOF: Time of flight; LIDAR: Light detection and ranging; RADAR: Radio direction and ranging; IMU: Inertial measurement unit; EMG: Electromyography; GONIO: Electrogoniometer; RANSAC: Random sample consensus; n/a: Not applicable

Acknowledgements

The authors acknowledge TU Wien University Library for financial support through its Open Access Funding Programme.

Authors' contributions

MT designed the study, compiled and analyzed the data and wrote the manuscript. MFR was closely involved for the definition of the paper structure and provided critical feedback on all of the figures and text. EK provided support for the methodical work and supervision. All author(s) read and approved the final manuscript.

Funding

The project was partially funded by the Austrian Research Promotion Agency (FFG) program "Industrienahe Dissertationen".

Availability of data and materials

Not applicable.

Ethics approval and consent to participate

Not applicable.

Consent for publication

Not applicable.

Competing interests

The authors declare that they have no competing interests.

Received: 20 December 2019 Accepted: 6 July 2020

Published online: 17 July 2020

References

- Ziegler-Graham K, Mackenzie EJ, Ephraim PL, Trivison TG, Brookmeyer R. Estimating the Prevalence of Limb Loss in the United States 2005 to 2050. *Arch Phys Med Rehabil.* 2008;89(3):422–9.
- Sinha R, van den Heuvel WJ, Arokiasamy P. Factors affecting quality of life in lower limb amputees. *Prosthetics Orthot Int.* 2011;35(1):90–96. <https://doi.org/10.1177/0309364610397087>.
- Winter DA. The biomechanics and motor control of human gait: normal, elderly and pathological, 2nd ed. Waterloo: Ont: Waterloo Biomechanics; 1991.
- Pieringer DS, Grimmer M, Russold MF, Rieni R. Review of the actuators of active knee prostheses and their target design outputs for activities of daily living. In: *International Conference on Rehabilitation Robotics (ICORR)*. IEEE; 2017. p. 1246–1253. <https://doi.org/10.1109/ICORR.2017.8009420>.
- Fluit R, Prinsen E, Wang S, Kooij HVD. A comparison of control strategies in commercial and research knee prostheses. *IEEE Trans Biomed Eng.* 2019;67(1):277–90. <https://doi.org/10.1109/TBME.2019.2912466>.
- Tucker M, Olivier J, Pagel A, Bleuler H, Bouri M, Lamberty O, et al. Control strategies for active lower extremity prosthetics and orthotics: a review. *J Neuroengineering Rehabil.* 2015;12(1):1.
- Varol HA, Sup F, Goldfarb M. Multiclass Real-Time Intent Recognition of a Powered Lower Limb Prosthesis. *IEEE Trans Biomed Eng.* 2010;57(3):542–51.
- Webster J, Watson RT. Analyzing the Past to Prepare for the Future: Writing a Literature Review. *MIS Q.* 2002;26(2):xiii–xxiii.
- Moher D, Liberati A, Tetzlaff J, Altman DG. Preferred Reporting Items for Systematic Reviews and Meta-Analyses: The PRISMA Statement. *J Clin Epidemiol.* 2009;62(10):1006–12.
- Vallery H, Burgkart R, Hartmann C, Mitternacht J, Rieni R, Buss M. Complementary limb motion estimation for the control of active knee prostheses. *Biomed Tech Biomed Eng.* 2011;56(1):45–51. <https://doi.org/10.1515/BMT.2010.057>.
- Bernal-Torres M, Medellín-Castillo H, González A. Development of an Active Biomimetic-Controlled Transfemoral Knee Prosthesis. 2016. <https://doi.org/10.1115/IMECE2016-67211>.
- Bernal-Torres MG, Medellín-Castillo HI, undefined Juan C Arellano-González. Design and Control of a New Biomimetic Transfemoral Knee Prosthesis Using an Echo-Control Scheme. *J Healthc Eng.* 2018;2018:–. <https://doi.org/10.1155/2018/8783642>.
- Su B, Wang J, Liu S, Sheng M, Jiang J, Xiang K. A CNN-Based Method for Intent Recognition Using Inertial Measurement Units and Intelligent Lower Limb Prosthesis. *IEEE Trans Neural Syst and Rehabil Eng.* 2019;27(5):1032–42. <https://doi.org/10.1109/TNSRE.2019.2909585>.
- Goodfellow I, Bengio Y, Courville A. Deep learning. In: *Adaptive computation and machine learning*. Cambridge, Massachusetts London: The MIT Press; 2016.
- Ambrozic L, Gorsic M, Slajpah S, Kamnik R, Munih M. Wearable sensory system for robotic prosthesis. *Internation J Mech Control JoMaC.* 2014;15(1):53–59.
- Ambrozic L, Gorsic M, Geeroms J, Flynn L, Lova RM, Kamnik R, et al. CYBERLEGS: A User-Oriented Robotic Transfemoral Prosthesis with Whole-Body Awareness Control. *IEEE Robot Autom Mag.* 2014;21(4):82–93.
- Goršič M, Kamnik R, Ambrožič L, Vitiello N, Lefeber D, Pasquini G, et al. Online phase detection using wearable sensors for walking with a robotic prosthesis. *Sensors (Basel).* 2014;14(2):2776–94.
- Parri A, Martini E, Geeroms J, Flynn L, Pasquini G, Crea S, et al. Whole Body Awareness for Controlling a Robotic Transfemoral Prosthesis. *Front Neurobot.* 2017;11(25). <https://doi.org/10.3389/fnbot.2017.00025>.
- Hu B, Rouse E, Hargrove L. Fusion of Bilateral Lower-Limb Neuromechanical Signals Improves Prediction of Locomotor Activities. *Front Robot AI.* 2018;5:78.
- Hu B, Rouse E, Hargrove L. Using bilateral lower limb kinematic and myoelectric signals to predict locomotor activities: A pilot study. In: *2017 8th International IEEE/EMBS Conference on Neural Engineering (NER)*. IEEE; 2017. p. 98–101. <https://doi.org/10.1109/NER.2017.8008301>.
- Hu B, Rouse E, Hargrove L. Benchmark Datasets for Bilateral Lower-Limb Neuromechanical Signals from Wearable Sensors during Unassisted Locomotion in Able-Bodied Individuals. *Front Robot AI.* 2018;5:14.
- Krausz NE, Hu BH, Hargrove LJ. Subject- and Environment-Based Sensor Variability for Wearable Lower-Limb Assistive Devices. *Sensors.* 2019;19:4887.
- Hu B, Krausz NE, Hargrove LJ. A novel method for bilateral gait segmentation using a single thigh-mounted depth sensor and IMU. In: *2018 7th IEEE International Conference on Biomedical Robotics and Biomechatronics (Biorob)*. IEEE; 2018. p. 807–12. <https://doi.org/10.1109/BIOROB.2018.8487806>.
- Fischler MA, Bolles RC. Random Sample Consensus: A Paradigm for Model Fitting with Applications to Image Analysis and Automated Cartography. *Commun ACM.* 1981;24(6):381–95. <https://doi.org/10.1145/358669.358692>.
- Zhang F, Yan T, Meng MQ. Gait Phase Recognition Based on A Wearable Depth Camera*. In: *2018 IEEE International Conference on Information and Automation (ICIA)*. IEEE; 2018. p. 756–60. <https://doi.org/10.1109/ICInFA.2018.8812542>.
- Zheng E, Manca S, Yan T, Parri A, Vitiello N, Wang Q. Gait Phase Estimation Based on Noncontact Capacitive Sensing and Adaptive Oscillators. *IEEE Trans Biomed Eng.* 2017;64(10):2419–30.
- Scandaroli GG, Borges GA, Ishihara JY, Terra MH, Rocha AFD, de Oliveira Nascimento FA. Estimation of foot orientation with respect to ground for an above knee robotic prosthesis. In: *2009 IEEE/RSJ International Conference on Intelligent Robots and Systems*. St. Louis: IEEE; 2009. p. 1112–7. <https://doi.org/10.1109/IROS.2009.5354820>.
- Ishikawa T, Murakami T. Real-time foot clearance and environment estimation based on foot-mounted wearable sensors. In: *IECON 2018-44th Annual Conference of the IEEE Industrial Electronics Society*. IEEE; 2018. p. 5475–5480. <https://doi.org/10.1109/IECON.2018.8592894>.
- Kleiner B, Cesmeci D. D8.4 - Foresighted Control of Active Foot Prostheses. In: *SENSOR+TEST Conferences 2011 Nürnberg*. vol. Proceedings SENSOR 2011 of D8 - Medical III; 2011. p. 669–72. <https://doi.org/10.5162/sensor11/d8.4>.
- Zhang F, Fang Z, Liu M, Huang H. Preliminary design of a terrain recognition system. In: *2011 Annual International Conference of the IEEE Engineering in Medicine and Biology Society*. vol 2011. Boston: IEEE; 2011. p. 5452–5. <https://doi.org/10.1109/IEMBS.2011.6091391>.
- Zhang X, Wang D, Yang Q, Huang H. An automatic and user-driven training method for locomotion mode recognition for artificial leg control. In: *2012 Annual International Conference of the IEEE Engineering in Medicine and Biology Society*. vol 2012. San Diego: IEEE; 2012. p. 6116–9. <https://doi.org/10.1109/EMBC.2012.6347389>.
- Wang D, Du L, Huang H. Terrain recognition improves the performance of neural-machine interface for locomotion mode recognition. In: *2013 International Conference on Computing, Networking and Communications (ICNC)*. San Diego: IEEE; 2013. p. 87–91. <https://doi.org/10.1109/ICNC.2013.6504059>.
- Liu M, Wang D, Huang H. Development of an Environment-Aware Locomotion Mode Recognition System for Powered Lower Limb Prostheses. *IEEE Trans Neural Syst Rehabil Eng.* 2016;24(4):434–43.
- Zhang F, Liu M, Harper S, Lee M, Huang H. Engineering platform and experimental protocol for design and evaluation of a neurally-controlled powered transfemoral prosthesis. *J Vis Exp.* 2014;89(e51059). <https://doi.org/10.3791/51059>.
- Huang H, Zhang F, Hargrove LJ, Dou Z, Rogers DR, Englehart KB. Continuous Locomotion-Mode Identification for Prosthetic Legs Based on Neuromuscular-Mechanical Fusion. *IEEE Trans Biomed Eng.* 2011;58(10):2867–75.

36. Carvalho S, Figueiredo J, Santos CP. Environment-aware locomotion mode transition prediction system. In: 2019 IEEE International Conference on Autonomous Robot Systems and Competitions (ICARSC). IEEE; 2019. p. 1–6. <https://doi.org/10.1109/ICARSC.2019.8733658>.
37. Sahoo S, Maheshwari M, Pratihari DK, Mukhopadhyay S. A Geometry Recognition-Based Strategy for Locomotion Transitions' Early Prediction of Prosthetic Devices. *IEEE Trans Instrum Meas*. 2019;69(4):1259–1267. <https://doi.org/10.1109/TIM.2019.2909246>.
38. Varol HA, Massalin Y. A feasibility study of depth image based intent recognition for lower limb prostheses. In: 2016 38th Annual International Conference of the IEEE Engineering in Medicine and Biology Society (EMBC). Orlando: IEEE; 2016. p. 5055–8. <https://doi.org/10.1109/EMBC.2016.7591863>.
39. Massalin Y, Abdrakhmanova M, Varol HA. User-Independent Intent Recognition for Lower Limb Prostheses Using Depth Sensing. *IEEE Trans Biomed Eng*. 2018;65(8):1759–70.
40. Laschowski B, McNally W, Wong A, McPhee J. Preliminary design of an environment recognition system for controlling robotic lower-limb prostheses and exoskeletons. In: 2019 IEEE 16th International Conference on Rehabilitation Robotics (ICORR). IEEE; 2019. p. 868–73. <https://doi.org/doi:10.1109/ICORR.2019.8779540>.
41. Yan T, Sun Y, Liu T, Cheung C, Meng MQ. A locomotion recognition system using depth images. In: 2018 IEEE International Conference on Robotics and Automation (ICRA). IEEE; 2018. p. 6766–6772. <https://doi.org/10.1109/ICRA.2018.8460514>.
42. Duda R, Hart P. Use of the Hough transformation to detect lines and curves in pictures. *Commun ACM*. 1972;15(1):11–15.
43. Diaz JP, da Silva RL, Zhong B, Huang HH, Lobaton E. Visual terrain identification and surface inclination estimation for improving human locomotion with a lower-limb prosthetic. In: 2018 40th Annual International Conference of the IEEE Engineering in Medicine and Biology Society (EMBC). Honolulu: IEEE; 2018. p. 1817–20. <https://doi.org/10.1109/EMBC.2018.8512614>.
44. Csurka G, Dance CR, Fan L, Willamowski J, Bray C. Visual categorization with bags of keypoints. In: In Workshop on Statistical Learning in Computer Vision, ECCV. Prague: CTU Prague; 2004. p. 1–22.
45. Krausz NE, Lenzi T, Hargrove LJ. Depth Sensing for Improved Control of Lower Limb Prostheses. *IEEE Trans Biomed Eng*. 2015;62(11):2576–87.
46. Kleiner B, Ziegenspeck N, Stolyarov R, Herr H, Schneider U, Verl A. A radar-based terrain mapping approach for stair detection towards enhanced prosthetic foot control. In: 2018 7th IEEE International Conference on Biomedical Robotics and Biomechatronics (Biorob). Enschede: IEEE; 2018. p. 105–10. <https://doi.org/10.1109/BIOROB.2018.8487722>.
47. Zhang K, Xiong C, Zhang W, Liu H, Lai D, Rong Y, et al. Environmental Features Recognition for Lower Limb Prostheses Toward Predictive Walking. *IEEE Trans Neural Syst Rehabil Eng*. 2019;27(3):465–76.
48. Zhang K, Zhang W, Xiao W, Liu H, Silva CWD, Fu C. Sequential Decision Fusion for Environmental Classification in Assistive Walking. *IEEE Neural Syst Rehabil Eng*. 2019;27(9):1780–90. <https://doi.org/10.1109/TNSRE.2019.2935765>.
49. Perry J, Burnfield J. *Gait Analysis: Normal and Pathological Function*, 2nd ed. NJ, USA: Slack Incorporated: Thorofare; 2010.
50. Dadashi F, Mariani B, Rochat S, Büla CJ, Santos-Eggimann B, Aminian K. Gait and foot clearance parameters obtained using shoe-worn inertial sensors in a large-population sample of older adults. *Sensors (Basel)*. 2013;14(1):443–57.
51. Genium. Set-up Guide. <https://shop.ottobock.us/media/pdf/647G868-EN-02-1210w.pdf>. Accessed 9 Sept 2019.
52. Han J, Shao L, Xu D, Shotton J. Enhanced Computer Vision With Microsoft Kinect Sensor: A Review. *IEEE Trans Cybern*. 2013;43(5):1318–34.
53. Scudellari M. Self-driving wheelchairs debut in hospitals and airports [News]. *IEEE Spectrum*. 2017;54(10):14–14. <https://doi.org/10.1109/MSPEC.2017.8048827>.
54. CES 2020 Press Release: new pmd 3D VGA ToF modul. https://www.pmdtec.com/html/pdf/press_release/PR20200107_CES_VGA_module.pdf. Accessed 18 Mar 2020.
55. Richards MA. *Principles of Modern Radar: 1 Basic Principles*. Edison, NJ: Scitech Publ; 2010.
56. Lien J, Gillian N, Karagozler ME, Amihoud P, Schwesig C, Olson E, et al. Soli: ubiquitous gesture sensing with millimeter wave Radar. *ACM Trans Graph*. 2016;35(4):1–19. <https://doi.org/10.1145/2897824.2925953>.
57. Parajuli N, Sreenivasan N, Bifulco P, Cesarelli M, Savino S, Niola V, et al. Real-time EMG based pattern recognition control for hand prostheses: a review on existing methods, challenges and future implementation. *Sensors*. 2019;19(20):4596.
58. Moloney D, Barry B, Richmond R, Connor F, Brick C, Donohoe D, Myriad 2: Eye of the computational vision storm. In: 2014 IEEE Hot Chips 26 Symposium (HCS). Cupertino: IEEE; 2014. p. 1–18. <https://doi.org/10.1109/HOTCHIPS.2014.7478823>.
59. SoftKinetic. DS325 Datasheet. https://www.sony-depthsensing.com/Portals/0/Download/WEB_20120907_SK_DS325_Datasheet_V2.1.pdf. Accessed 26 Sept 2019.
60. CamBoard pico flexx Datasheet. https://pmdtec.com/picofamily/assets/datasheet/Data-sheet-PMD_RD_Brief_CB_pico_flexx_V0201.pdf. Accessed 26 Sept 2019.
61. Zech C, Hulsmann A, Schlechtweg M, Reinold S, Giers C, Kleiner B, et al. A compact W-band LFM CW radar module with high accuracy and integrated signal processing. In: 2015 European Microwave Conference (EuMC), Paris: IEEE; 2015. p. 554–7. <https://doi.org/10.1109/EuMC.2015.7345823>.

Publisher's Note

Springer Nature remains neutral with regard to jurisdictional claims in published maps and institutional affiliations.

Ready to submit your research? Choose BMC and benefit from:

- fast, convenient online submission
- thorough peer review by experienced researchers in your field
- rapid publication on acceptance
- support for research data, including large and complex data types
- gold Open Access which fosters wider collaboration and increased citations
- maximum visibility for your research: over 100M website views per year

At BMC, research is always in progress.

Learn more biomedcentral.com/submissions



**REAL-TIME LIMB TRACKING IN SINGLE DEPTH IMAGES
BASED ON CIRCLE MATCHING AND LINE FITTING**

by **Michael Tschiedel, Michael Friedrich Russold, Eugenijus Kaniasas and Markus Vincze**,
published in the *Journal The Visual Computer*.

Received: 2 December 2020 • Accepted: 9 April 2021 • Published: 25 April 2021

Abstract

Modern lower limb prostheses neither measure nor incorporate healthy residual leg information for intent recognition or device control. In order to increase robustness and reduce misclassification of devices like these, we propose a vision-based solution for real-time 3D human contralateral limb tracking (CoLiTrack). An inertial measurement unit and a depth camera are placed on the side of the prosthesis. The system is capable of estimating the shank axis of the healthy leg. Initially, the 3D input is transformed into a stabilized coordinate system. By splitting the subsequent shank-estimation problem into two less computationally intensive steps, the computation time is significantly reduced: First, an iterative closest point algorithm is applied to fit circular models against 2D projections. Second, the random sample consensus method is used to determine the final shank axis. In our study, three experiments were conducted to validate the static, the dynamic and the real-world performance of our CoLiTrack approach. The shank angle can be tracked at 20 Hz for one sixth of the entire human gait cycle with an angle estimation error below $2.8 \pm 2.1^\circ$. Our promising results demonstrate the robustness of the novel CoLiTrack approach to make “next-generation prostheses” more user-friendly, functional and safe.



Real-time limb tracking in single depth images based on circle matching and line fitting

Michael Tschiedel^{1,2} · Michael Friedrich Russold¹ · Eugenijus Kaniusas² · Markus Vincze³Accepted: 9 April 2021
© The Author(s) 2021

Abstract

Modern lower limb prostheses neither measure nor incorporate healthy residual leg information for intent recognition or device control. In order to increase robustness and reduce misclassification of devices like these, we propose a vision-based solution for real-time 3D human contralateral limb tracking (CoLiTrack). An inertial measurement unit and a depth camera are placed on the side of the prosthesis. The system is capable of estimating the shank axis of the healthy leg. Initially, the 3D input is transformed into a stabilized coordinate system. By splitting the subsequent shank estimation problem into two less computationally intensive steps, the computation time is significantly reduced: First, an iterative closest point algorithm is applied to fit circular models against 2D projections. Second, the random sample consensus method is used to determine the final shank axis. In our study, three experiments were conducted to validate the static, the dynamic and the real-world performance of our CoLiTrack approach. The shank angle can be tracked at 20 Hz for one sixth of the entire human gait cycle with an angle estimation error below $2.8 \pm 2.1^\circ$. Our promising results demonstrate the robustness of the novel CoLiTrack approach to make “next-generation prostheses” more user-friendly, functional and safe.

Keywords Shank modeling · Body tracking · Depth image · Gait analysis

1 Introduction

Extraction of 3D human limb parameters from depth images is a research topic that has recently attracted the attention of the scientific community. Driven by the availability of low-cost depth cameras, human pose estimation strategies [1–3], telerehabilitation concepts [4,5] and patient interaction monitoring approaches [6,7] are evolving continuously. For lower limb prostheses control, it can be advantageous to gather information about the healthy residual leg. Humans combine proprioception with visual information to navigate different terrains smoothly. In contrast, state-of-the-art commercial prosthetic devices only use device-embedded sensors and finite-state controllers to adapt to the patient’s intent [8]. They do not collect information about the state of the other

leg, which could improve overall system performance. A systematic analysis of different bilateral lower limb signals for predicting locomotion activities was performed by Hu et al. [9,10] in 2018. It came to the conclusion that only one additional contralateral leg parameter could reduce error rates of intent recognition significantly. However, the additional effort of instrumenting the contralateral shank can be inconvenient and impractical for amputees.

In this paper, we propose a novel contralateral limb tracking approach named CoLiTrack, which utilizes unilaterally worn depth cameras. Placing the camera on the ipsilateral (prosthetic) side eliminates the need for an additional sensor on the contralateral shank and allows an easier integration into future products. The key to our method is that it separates the complex modeling problem into two less computationally intensive parts, in order to perform real-time shank axis estimation. Initially, layers from the point cloud input (depicting the residual leg) are projected in 2D, before fitting predefined circular models. Next, a projected line using the center points of the circles is used to estimate the shank axis. This reduces computing time considerably, allowing for accurate estimation of the shank axis fast enough for real-time applications. Furthermore, in comparison with traditional methods,

✉ Michael Tschiedel
michael@tschiedel.at¹ Department of Global Research, Ottobock Healthcare Products GmbH, Vienna, Austria² Institute of Electrodynamics, Microwave and Circuit Engineering, TU Wien, Vienna, Austria³ Automation and Control Institute, TU Wien, Vienna, Austria

Published online: 25 April 2021

Springer

CoLiTrack is unsupervised and has no training-related bias. Experimental results produced by CoLiTrack demonstrate a robust and accurate solution to improve human–device interaction in real time. Although our method was developed with lower limb prostheses in mind, the proposed system could be applied to a wide variety of applications in many areas, including health care, gaming and human–device interaction.

The remainder of the paper is organized as follows: Sect. 2 presents the related work most relevant to the context of this paper. Details of the proposed method for real-time contralateral limb tracking are given in Sect. 3. Section 4 provides the experimental results, which are then discussed in Sect. 5. The conclusion of this paper is presented in Sect. 6.

2 Related work

In this section, we focus primarily on existing work on environment recognition as a means for improving prosthetic control. We present relevant principles of human gait and known approaches to modeling the leg.

2.1 Principles of human gait

Humans use upright gait on two legs for efficient locomotion. Biomechanics of gait have been studied in detail [11]; however, spinal and brain control of human walking cannot yet be fully explained. Walking is described as a repetitive sequence to move forward; a single sequence is called a gait cycle, which begins with the heel strike (the heel touching the ground) and continues until the heel strike of the same foot. For approximately 60% of the gait cycle the foot stays on the ground (stance phase), before the foot is lifted off the ground at toe off and swings freely in the air (swing phase) for the rest of the gait cycle. Numerous papers have been published on markerless motion capture [12–15] in the past, and it is beyond the scope of this paper to provide a complete overview of this literature. For our approach, it is important to mention that the shank kinematics are generally independent of the ankle kinematics. The ankle adjusts automatically to different heel heights, for example, as a result of wearing different types of shoes. The shank kinematics, however, remain the same [16,17]. The shank angle α is therefore a very informative parameter representing the status of the contralateral shank and can play a crucial role in movement-dependent control applications. A typical sagittal plane shank motion during free walking for one entire gait cycle is shown in Fig. 1. The sagittal plane passes across the body, defined by the Y/Z plane in the world coordinate system, as indicated in Fig. 2. The shank angle is defined to be zero, when it is perpendicular to the ground, and positive in the case of a counterclockwise direction around the reference axis.

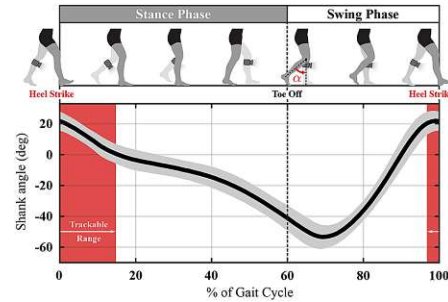


Fig. 1 Sagittal plane shank motion. Heel strike is the first inertial contact, when the foot touches the ground. At about 60% of the full gait cycle, toe off is the end of the stance phase initiating the swing phase. Then, the leg swings freely in the air until the next heel strike, before repeating the cycle. The plot shows nominal shank angle α relative to vertical during free walking with standard deviation in a light gray band, data from [11]. The trackable range of our CoLiTrack approach determined during the dynamic experiment is shown in red

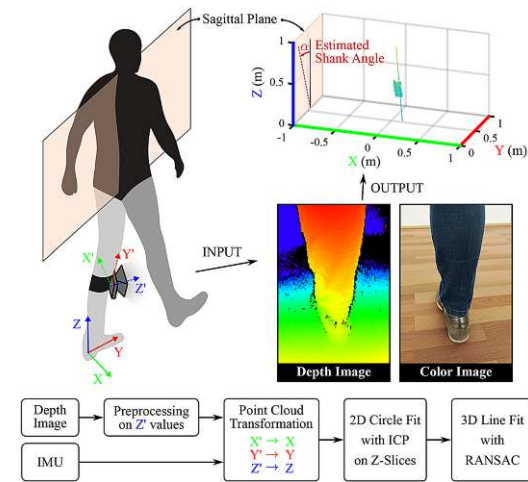


Fig. 2 Sensor configuration and overall process of CoLiTrack. An IMU and a depth camera were fused to estimate the axis of the uninstrumented contralateral shank. (X', Y', Z') represents the camera coordinate system and (X, Y, Z) the stabilized world coordinate system. Mounting is depicted in detail in Fig. 3. The color of the *Depth Image* corresponds to the distance between an object and the camera: red parts are close to the sensor, blue parts are further away. The *Color Image* was taken with a mobile phone and is for demonstration purpose

2.2 Environment detection for prostheses

One of the most important aims of lower limb prosthetic systems is the imitation of the physiological gait pattern [8]. Modern prosthetic systems can replace missing body parts to a high degree and improve patients' independence and mobility [18]. Numerous studies have been carried out to determine the best strategies to control locomotion in pros-

thetic devices. Most of these studies used neuromuscular or mechanical signals of the prosthetic leg, either individually or in combination [19–21]. Inertial measurement units (IMU) are also commonly used to estimate the position and orientation of the prosthetic leg in a world reference system [8]. In contrast, environmental sensor technologies are not yet commercially used in prosthetic devices, although we have identified a clear research tendency toward the recognition of surrounding objects and terrains, as shown in our survey [22]. The work found was divided into two categories: explicit environmental sensing—direct estimation of terrain features—and implicit environmental sensing—creating an understanding of the locomotion mode by measuring the state of the patient’s residual body. Within the first group, distance and depth-based sensors were used to estimate the mode of locomotion. Sensors were placed on different body segments, such as the shank, thigh, trunk or even the upper body, scanning the environment in front of the patient. Intent recognition was performed by means of geometry-based decision trees [23], finite-state or support vector machines [24,25] and neural networks [26,27]. One group investigated whether the patient was approaching stairs [28], and another estimated soil properties with a color camera mounted on the foot [29]. Toe clearance, which is an important parameter to prevent stumbling or falling, was estimated as well [30], but not evaluated in a prosthetic setup.

The second category, implicit environmental sensing, incorporates the state of the amputee’s body, which we consider to be more promising. This is based on the fact that the amputee voluntarily decides where to go or what to do. The strong physical inter-joint coordination between human limbs [31] could be used to improve prosthesis control. Concepts of primitive “echo-control” strategies, which try to estimate the state of the missing limb depending on the state of the residual sound side, have been investigated for more than 40 years [32–35]. For example, stepping over unknown obstacles becomes possible without explicit classification of the environment [36]. However, errors occur especially at the beginning and at the end of an activity, when the limbs do not necessarily “echo” each other. As an improvement, “whole-body” approaches [37–39] with distributed IMUs and pressure insoles can distinguish between a limited number of modes of locomotion in real time, but need numerous additional sensors worn by the user.

For our work, the concept proposed by Hu et al. [40] is the most relevant one: It predicts bilateral gait events from unilaterally worn sensors. A thigh-mounted depth sensor and an IMU are fused to extract the angle between the ground and the shank of the contralateral leg in its field of view. Then, classifiers are used to predict ipsilateral toe off and contralateral heel contact, representing the beginning and end of the human gait double support phase. Although their methodology was sound, and the results suggested that depth

vision could improve device control, several limitations were mentioned. To begin with, the evaluation was carried out with only a single participant. Moreover, initiation and termination steps were excluded due to different kinematics compared to steady-state steps. No tests were performed regarding the influence of different environments, neither to investigate the robustness against reflectance and clutter, nor to analyze the effect of unknown objects in the field of view. Additionally, the implementation was not optimized for timing, resulting in a high computation time of 1.16 ± 0.56 s, which prevented any online (real-time) evaluation.

2.3 Approximation of shank axis

The shank of a human can be modeled relatively well by the primitive shape of a cylinder. The challenge is, however, to fit such a model to the incomplete and deformed point cloud captured with a depth camera. On the one hand, simple least square methods [41] fail due to outliers, and methods using surface normals [42] cannot be applied due to noise from pleats on the clothes. On the other hand, complex object fitting approaches [43] are unsuitable, since the high processing time prevents any real-time evaluation. To address these challenges, we separate the complex shank estimation problem into two less computationally intensive steps: First, predefined circular models are matched in 2D. Second, a projected line using the center points of the circles is used to estimate the shank axis, as shown in Fig. 4. In general, detecting circles and lines is a fundamental task in computer vision and has been widely studied and developed in a variety of ways. Well-known techniques, such as the Hough transform or neural network approaches, are used to detect circle-like foreign objects in chest X-ray images [44–46] or line-like lanes for autonomous driving systems [47,48], to name recent applications.

3 Proposed method

Our contralateral limb tracking method named CoLiTrack consists of four main functions for estimating the axis and, therefore, the angle of the shank. The overall process is illustrated in Fig. 2: In a first step, the depth values were preprocessed in the camera coordinate system. Next, the information from the IMU was used to transform the filtered point cloud data into a ground coordinate system. The transformed points were projected onto 2D planes for fitting circle models with the iterative closest point (ICP) algorithm. Based on these results, the axis was estimated with a 3D line fit using the random sample consensus (RANSAC) method.

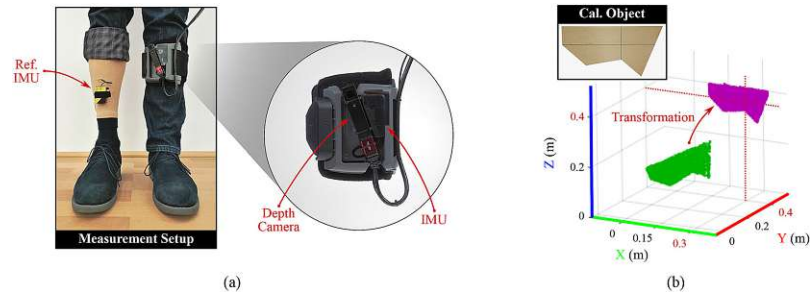


Fig. 3 Measurement setup **a** worn by a participant and the calibration step **b** of the depth camera. IMU and depth camera were fixed on a wearable support, attached to the shank of the participant. The second IMU, mounted within a modified support stocking on the contralateral side, served as reference; trousers were rolled up only for the photo.

For calibration, the camera was placed in the origin of the world coordinate system. The true (pink) position of the calibration object was known. The transformation matrix could be calculated out of the captured (green) image

3.1 Configuration of CoLiTrack

In this study, a 3D time-of-flight depth camera (CamBoard pico flexx, Pmd Tech, Germany) and an IMU (BNO055, Bosch Sensortec, Germany) were used to estimate parameters of the contralateral leg. In addition, a second IMU was mounted on the contralateral shank to serve as reference signal. The sensor configuration is depicted in Fig. 3a. The IMU and the depth camera were fixed together on a wearable support for two reasons: firstly, to combine camera orientation information with vision information. Secondly, this wearable support allowed for fast and easy positioning on the participant's shank. With a resolution of 171×224 pixels, the depth camera could measure the 3D position of object points (point cloud) relative to the camera origin. The IMU was able to estimate the orientation and acceleration of the wearable support relative to the world reference system. By fusing orientation information and point cloud data, scene information could be stabilized. However, after the camera was mounted, its initial rotation needed to be corrected. For this, the wearable support carrying the IMU and the depth camera was placed in an upright position with the known calibration object in its field of view. The object was mounted in a predefined position, as shown in Fig. 3b in pink. The required rigid transformation can be calculated from a scene capture, which is depicted in green. The calculation was done by using the coherent point drift algorithm [49] to assign correspondences between two sets of points, provided within the MATLAB Computer Vision Toolbox. The determined transformation parameters were stored and applied every time before continuing with the evaluation algorithm. The experimental data acquisition and analysis were conducted using MATLAB R2018b and a wrapper library provided by the camera manufacturer, running on a laptop with an Intel Core i5-8250U and 8 GB memory size.

3.2 Preprocessing of depth data

The captured depth information was preprocessed in the camera coordinate system. Pixels without any depth information were removed and then blurred with a Gaussian blur to reduce depth noise. If the contralateral leg was in the camera's field of view, the nearest detected point relative to the camera belonged to the sound leg and was, therefore, selected as "point of interest" (POI). Next, the confidence map, which was also retrieved from the depth sensor, was used to identify all points belonging to the contralateral leg. This parameter represented the confidence of a measured distance (Z') for every pixel (X' , Y') of the input—the closer a point, the higher the corresponding confidence. The confidence of the POI was taken as reference, points above a certain threshold were selected as belonging to the contralateral leg. Finally, the selected point cloud was downsampled using a 1 cm grid filter for computational efficiency.

3.3 Point cloud transformation

As the shank of the human was swinging within a gait cycle, the roll angle (rotation around the X -axis) and the pitch angle (rotation around the Y -axis) were estimated with the help of the ipsilateral IMU. By applying the Euler angle rotation matrix, the retrieved point cloud in camera coordinates was transformed into a stabilized world coordinate system (ipsilateral IMU reference frame). The origin was fixed on the foot calibrated to the sagittal plane, as shown in Fig. 2. Due to the instability of the yaw angle, this parameter was not used, and a rotation around the Z -axis remained unaccounted for.

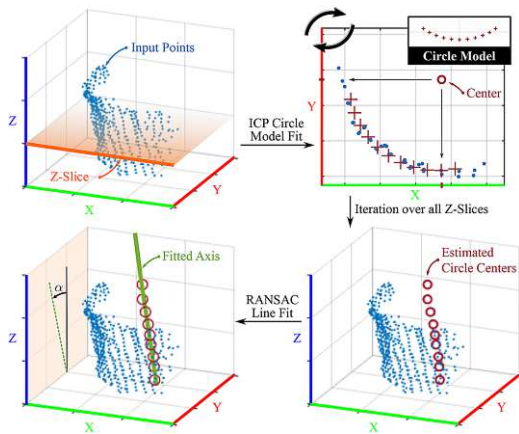


Fig. 4 Visualization of the CoLiTrack algorithm. The point cloud after preprocessing and transforming was taken as input. Z-slices were extracted, and a 10-point circle model was fitted iteratively by using the ICP algorithm in 2D (X/Y plane). All model circle center points were then used to estimate the shank axis correctly by using the RANSAC method in 3D. Finally, the contralateral shank angle α was calculated with respect to the sagittal plane (YZ plane)

3.4 Circle fit with ICP

After transforming the point cloud input, Z-layers were projected in 2D. Then, a predefined circle model of 10 points evenly distributed over 90° in a radius of 5 cm was fitted, as shown in Fig. 4. The Z-layer height was set to 3 cm with 1 cm overlapping on both sides. The model fit itself was realized with the ICP algorithm [50,51]. The basic concept of this algorithm was as follows: The Z-layer projection was kept fixed, while the circle model was rigidly transformed to match the input in the best way possible. By doing this, shape and size were preserved. The algorithm iteratively revised the transformation to minimize the sum of squared differences between the coordinates of the matched pairs. If the error metric fell below a certain threshold, this was a criterion for stopping the iterations. This was done for all Z-layers, which resulted in center points with their associated heights. Figure 4 depicts this ICP and the subsequent RANSAC fitting process.

3.5 Line fit with RANSAC

By using the RANSAC method [52], the newly calculated center points served to estimate the shank axis correctly. The principle of this iterative approach was to estimate parameters of a predefined mathematical model—in our case, a line representing the shank axis—from the input data. Therefore, two circle-center points were randomly taken to generate a hypothesis, which was then verified against all the other

points. If the distance between a point and the current hypothesis lay below a certain threshold, the point was marked as “inlier.” Otherwise it was marked as “outlier.” The algorithm was repeated, until the obtained hypothesis exceeded a certain ratio. Finally, only the points marked as inliers were used to calculate the optimal line, whereas outliers had no further influence on the result. For our specific application, we used a threshold of 3 cm, a probability of 0.99 and 1000 as maximum number of random trials. As shown in Fig. 4, the number of input points was limited by the previous Z-slice height and the total object height, which varied between 5 cm and 30 cm. Finally, the estimated axis was used to calculate the contralateral shank-to-vertical angle α with respect to the sagittal plane. The relative position information between the depth camera and the contralateral leg was not used in our application.

4 Experiments and results

We conducted three experiments to examine the *static performance*, the *dynamic performance* and the *real-world performance* of our novel approach. Generally, we analyzed the performance of our CoLiTrack method as follows: For each step, recorded gait data were separated, based on the local positive peak of the shank angle captured with the (second) reference IMU (α_{REF}). As depicted in Fig. 1, this corresponds with the beginning or, respectively, the ending of one entire gait cycle. Individual steps were then interpolated from 0 to 100%. Furthermore, gait initiation and termination steps were excluded, due to their kinematics differing from steady-state walking. The deviation between the depth camera-based estimation (α_{CLT}) and the reference IMU was calculated as shank angle error $|\alpha_{REF} - \alpha_{CLT}|$ for each percent of the gait cycle. Where possible, mean and standard deviation over the entire gait cycle were calculated and reported.

4.1 Static performance

The goal of the static performance experiment was to evaluate the performance of the proposed algorithm over the entire gait cycle. As the depth camera had a very narrow field of view (62° horizontal x 45° vertical, taken from the product’s datasheet), parameters of the contralateral leg were “trackable” only for a small part of the total gait cycle, as it was out of view for the rest of the time. In order to evaluate our approach over the entire gait cycle, the wearable support, containing the depth camera and the IMU, was placed in front of a commercial treadmill, so that the participant’s contralateral shank was constantly in view. The incline of the treadmill was set to 1% for all experiments, which is considered to be the same resistance level as an outdoor surface without incline [53]. Walking speed was defined as slow (0.5 km/h),

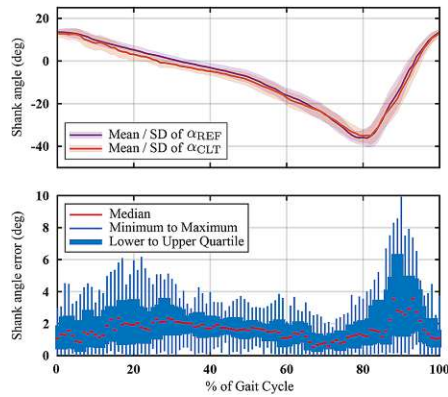


Fig. 5 Static performance visualization of CoLiTrack at medium walking speed. Top diagram depicts the mean and the standard deviation of the α_{CLT} and α_{REF} for one participant ($N=1$) and 30 steps ($n=30$). Bottom diagram shows the corresponding shank angle error $|\alpha_{REF} - \alpha_{CLT}|$ as box-plots depicting the *minimum to maximum*, the *lower to upper quartile* and the *median* error for each percent of the gait cycle. The mean error at medium walking speed was calculated to be $1.8 \pm 1.4^\circ$

Table 1 Static performance of CoLiTrack

Speed	% of Gait cycle		Shank angle error (deg)	
	Min/max	\bar{x} / σ	Min/max	\bar{x} / σ
Slow	100/100	100/0	$1.4e^{-4}/09.3$	1.4/1.2
Medium	100/100	100/0	$4.4e^{-4}/11.3$	1.8/1.4
High	100/100	100/0	$3.2e^{-5}/14.1$	3.4/1.9

medium (1.0 km/h) and high (1.5 km/h), corresponding to the gait speed determined for amputees with a low mobility grade [54], which is slower than healthy subjects' walking speed. The second (reference) IMU was mounted in a modified support stocking on the participant's contralateral (right) shank, as shown in Fig. 3a. In this experiment, the point cloud transformation step was not necessary because the camera did not move. However, the input scene was cropped to the area of the (contralateral) leg of interest.

This experiment was carried out with one participant ($N=1$) at all three walking speeds (slow, medium and high). A total of 30 steps ($n=30$) was extracted from each walking speed level. As shown in Fig. 5, the CoLiTrack estimations corresponded closely to the reference measurements. The individual box-plots—median, lower and upper quartile, as well as the minimum to maximum range—depict the corresponding tracking error for each percent of the gait cycle. The mean error for medium walking speed was about $1.8 \pm 1.4^\circ$. Results for the other walking speeds were summarized in Table 1. The highest mean error of $3.4 \pm 1.9^\circ$ was measured at high walking speed.

4.2 Dynamic performance

The goal of the *dynamic performance* experiment was to determine how the accuracy and the tracking range of our CoLiTrack method might vary across different walking speeds. Therefore, our system was tested by five participants on a treadmill. Parameters were set as previously in the static test—walking speed levels of slow, medium and high at an incline of 1%. The wearable support (depth camera and IMU combination) was mounted on the ipsilateral (left) shank of the participant, and a second (reference) IMU was installed in a modified support stocking on the contralateral (right) shank, as shown in Fig. 3a. To begin, offset calibration was done for each participant in an upright standing position without movement. These parameters were stored and used for all subsequent experiments.

This experiment was carried out with five participants ($N=5$) at all three walking speeds (slow, medium and high). Instrumentation and calibration took less than 10 minutes for all of them. For the statistical evaluation, a total of 150 steps were combined, 30 steps per speed level ($n=30$) from each participant ($N=5$). The dynamic test revealed a trackable range of about one sixth of the total gait cycle, coinciding with the end of the swing phase, when the heel strike initiates the next step, as indicated in Fig. 1. The results from the dynamic test at medium walking speed are shown in Fig. 6. With our CoLiTrack method, it was possible to estimate the contralateral shank angle from about 97–14% of the gait cycle. For some steps, tracking was even possible for longer periods—up to 28% of the entire cycle, as shown in the magnified area of the plot. Although the maximum estimation error for all individual steps at medium walking speed was 13.7° , the mean estimation error was only $2.4 \pm 2.0^\circ$. The highest mean error of $2.8 \pm 2.1^\circ$ was measured at slow walking speed. Table 2 reports the results for the other walking speeds, showing similar values for all three speed levels. Our claim that the proposed method works independently from the walking speed was thus confirmed.

The averaged computation time for the overall process of CoLiTrack was 50 ms: Data read-in from depth camera and IMUs took about 10 ms, preprocessing about 25 ms and fitting, finally, the remaining 15 ms. The processing time of RANSAC, however, was almost negligible. Therefore, processing speed can be as high as 20 frames/s.

4.3 Real-world performance

Finally, the goal of the third experiment was to validate the real-world performance of our CoLiTrack approach, as this is a crucial factor for a successful implementation in a future product. Therefore, an online walking test was administered to evaluate the algorithm behavior with unknown objects in the camera's field of view and to qualify the estimation per-

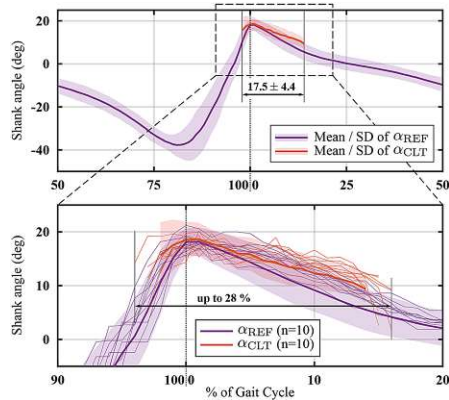


Fig. 6 Dynamic performance visualization of CoLiTrack at medium walking speed. Top diagram depicts the mean and the standard deviation of the α_{CLT} and α_{REF} for all five participants ($N=5$) and 30 steps ($n=30$) each. The x-axis was shifted for a better visualization. Bottom diagram magnifies the total tracking area and shows 10 randomly taken curves out of all 150 steps. The mean error at medium walking speed was calculated to be 2.4°

Table 2 Dynamic performance of CoLiTrack

Speed	% of Gait cycle		Shank angle error (deg)	
	Min/max	\bar{x} / σ	Min/max	\bar{x} / σ
Slow	7/29	16.7/4.6	$4.7e^{-3}/16.9$	2.8/2.1
Medium	6/28	17.5/4.4	$1.6e^{-3}/13.7$	2.4/2.0
High	9/26	18.4/3.8	$1.0e^{-3}/14.1$	2.4/1.9

formance in other types of terrains, such as up/down ramps or stairs. The instrumentation for the real-world test was identical to the dynamic experiment (wearable support on the left leg and reference IMU on the right leg), apart from the laptop for data acquisition, which was carried in a backpack on the participant's back.

This experiment was carried out with one participant ($N=1$) at a self-selected walking speed, starting with normal walking on level ground, before going into other terrains, as shown in Fig. 7. Level-ground walking led mostly to results similar to the treadmill evaluation. Gait initiation and termination steps were successfully tracked, too. However, due to the variability of the walking speed, there was no statistical evaluation carried out. If the participant walked too fast, tracking failed due to the limited update rate of a maximum of 20 frames/s.

As long as the contralateral leg was the closest object in the depth camera's field of view, unknown other obstacles were successfully suppressed. If the leg was out of view, nearby objects such as banisters or even another person standing in front of the participant occasionally led to misclassifications.

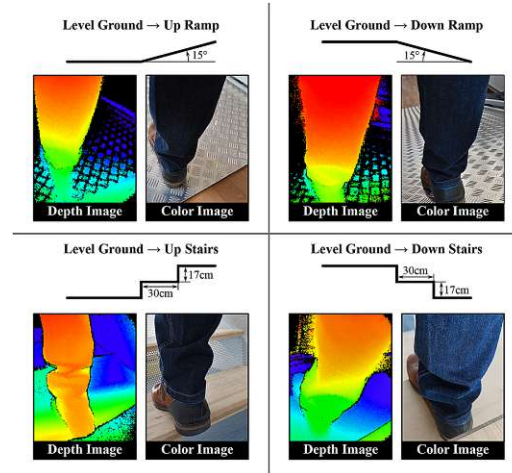


Fig. 7 Visualization of terrain changes from level ground into up/down ramp and stairs. *Depth Images* were taken straight out of the depth camera without any preprocessing. *Color Images* were taken with a mobile phone and are for comparison only

Ground reflectance or clutter, however, had no influence on the estimation performance.

As the camera positioning was optimized for level-ground walking, going into other terrains increased the error. Transitioning from level ground to inclines had almost no influence on the estimation performance, while going from level ground down a ramp reduced it. Still, trackability for ramps worked better than for stairs: In the case of stairs, estimation mostly failed, both upwards and downwards. Although the contralateral leg was still in the camera's field of view, as shown in Fig. 7, wrinkles in the shoe area of the trousers were the main cause for preventing a successful evaluation. In comparison, when walking on level ground, more of the proximal part of the shank was in view, where clothing was normally less wrinkled, as depicted in Fig. 2.

5 Discussion

5.1 Advantages of the proposed method

This paper introduced a robust contralateral limb tracking strategy for enhancing lower limb device control. To the best of the authors' knowledge, this is the first concept capable of detecting contralateral shank parameters only from unilaterally worn sensors and in real time. Several qualities of our proposed CoLiTrack might underline its effectiveness for enhancing "next-generation prostheses."

Firstly, the low computing time of only 50 ms is the most important achievement of our concept to be mentioned. This

allows an online evaluation up to 20 frames/s—fast enough to be implemented in a prosthetic device. Compared to the previous research by Hu et al. [40], this is a decrease by a factor of 23. Furthermore, we do not need any prior network training, as we use direct estimation strategies, guaranteeing that the presented CoLiTrack system is user-independent.

In addition to high processing speed, the estimation accuracy was also high. During the static experiment, the presented algorithm successfully tracked the leg over the entire gait cycle with a maximum mean error of $3.4 \pm 1.9^\circ$. Higher errors were found in the area between 85 and 95% of the duration of the gait cycle (Fig. 5). They are not caused by estimation errors, but can rather be explained by imperfectly synchronized data read-in procedures. The slight increase in errors at the beginning of the gait cycle between 5 to 30%, however, might be explained by a relative movement of the trousers with respect to the shank. In the dynamic experiment, tracking was possible for about one sixth of the full gait cycle with a mean estimation error below $2.8 \pm 2.1^\circ$. Given that a joint angle difference of more than 5° is considered a clinically significant difference for gait analysis [55], we claim the accuracy of our CoLiTrack approach to be sufficient. In comparison, results from instrumented crutches [56] as well as from a smart walker (rollator + depth camera) [57] using principal component analysis to estimate the shank angle showed deviations of up to 10° . Moreover, our real-world experiment demonstrated that neither ground reflectance nor clutter has an influence on CoLiTrack performance. As long as the contralateral leg is in the field of view of the camera, other (unknown) objects are eliminated, which underlines the efficiency of our preprocessing approach.

Finally, through the integration of depth camera and IMU into a compact wearable support frame, instrumentation and calibration of the system on the participants leg take less than 10 minutes. Since the kit is worn on the ipsilateral (prosthesis side) leg, the additional sensors could be embedded directly into a lower limb prosthetic device in the future.

5.2 Limitation and future work

Although the proposed method can estimate the contralateral shank axis accurately and with only a short time delay, there are some limitations, which need to be addressed.

Firstly, the trackable gait cycle range needs to be increased. So far, our system successfully estimates the contralateral shank axis in the range of one sixth of the full gait cycle, limited by the field of view of the camera. Several depth cameras can be combined into a camera array, increasing the field of view and, thus, the trackable range. Furthermore, the optimal position and orientation of the system for other terrains, such as stairs or ramps, need to be defined, in order to capture those trouser areas that are less wrinkled. In addition,

the preprocessing step of the depth data could be extended to make it more robust against unknown objects. Simple solutions, for example, could be to remove depth areas below a minimum size or to select the region of interest based on the last valid position of the shank. In this case, it would not be necessary to implement more computationally intensive approaches of background subtraction, in order to increase the robustness of the algorithm. Nevertheless, in its current form, the system is capable of tracking the contralateral shank angle within its area of coverage. This information can be used for the control of the next step. Additionally, it seems possible to determine the heel strike with the help of the shank's angular velocity, as suggested in [58]. A positive velocity indicates the swing phase, a negative velocity indicates the stance phase. This would allow to derive the timing of the heel strike, representing the beginning of the human gait double support phase, as depicted in Fig. 1. Furthermore, the distance between the contralateral shank and the ipsilateral sensor—inherently detected by a depth camera, but not utilized here—can be used to calculate spatial parameters, such as step length [11].

Additionally, even though the system in its current form is real time capable with an update rate of up to 20 frames/s, practice has shown that higher walking speeds can lead to misclassifications. Considering a walking speed of 3.6 km/h for very active amputees [54] and assuming a step length (heel strike to heel strike of the same leg) of 1 m, we can expect one gait cycle per second. If we further resume that CoLiTrack covers approximately one sixth of the gait cycle and is sampling with an update rate of 20 frames/s, we may calculate that no more than 3–4 images can be captured per gait cycle. Although our approach does not rely on time history, we estimate that a minimum of 10 images is required for use in real life in order to derive heel strike timing as mentioned above. This can be achieved by increasing the update rate to at least 60 Hz. On the one hand, this is naturally constrained by the frame rate of the camera. For example, the one used in our study is limited to 45 frames/s according to the manufacturer's data sheet. On the other hand, calculation time needs to be reduced even further. This can be done by converting MATLAB code into C++ programs and running it on dedicated vision processors.

Finally, the depth camera used in our work is also restricted by the requirement of having an unobstructed field of view. Although sensor positioning would allow an implementation directly into a prosthetic device, clothing or prosthetic covers cannot be worn above it. Instead, high-frequency super near-field radar sensors are able to “look through” them. For example, Google's radar-based gesture-sensing technology (Project Soli) allows a touchless interaction with their new smartphone Pixel 4 [59]. Therefore, the use of these sensors should be considered in future work.

6 Conclusion

In this work, we present a robust real-time leg tracking method called CoLiTrack for improved lower limb prosthetic device control. A depth camera and an IMU are placed on the ipsilateral (prosthetic) leg, capable of estimating the axis of the contralateral (healthy residual) leg. We conducted three experiments to validate our proposed CoLiTrack algorithm. The evaluation of *static performance* demonstrated a trackability of the shank axis throughout the entire gait cycle with a mean error of less than $3.4 \pm 1.9^\circ$ for one participant. *Dynamic performance* was evaluated with five participants wearing the sensor kit while walking on a treadmill at three different speeds. This resulted in a mean trackable range of one sixth of the entire gait cycle, since the leg is out of the camera's field of view for the remaining time. The overall processing time of the presented CoLiTrack system took less than 50 ms, and the mean estimation errors for all walking speed levels were below $2.8 \pm 2.1^\circ$. Finally, the *real-world performance* testing with one participant demonstrated robustness against ground reflectance or clutter, but showed the limitations of the approach in terms of walking speed and terrain variations. Our immediate plan is to enlarge the trackable range by increasing the field of view, as well as to reduce the processing time even further, in order to use the residual healthy leg information in movement-dependent control applications of "next-generation prostheses."

Acknowledgements The authors acknowledge TU Wien University Library for financial support through its Open Access Funding Programme.

Funding Open access funding provided by TU Wien (TUW).

Declarations

Conflict of interest The authors declare that they have no conflict of interest.

Funding The project was partially funded by the Austrian Research Promotion Agency (FFG) program "Industriennahe Dissertationen."

Informed consent All five participants are healthy volunteers (1 female and 4 males) aged between 22 and 25 years, and informed consent was obtained prior to the experiments.

Open Access This article is licensed under a Creative Commons Attribution 4.0 International License, which permits use, sharing, adaptation, distribution and reproduction in any medium or format, as long as you give appropriate credit to the original author(s) and the source, provide a link to the Creative Commons licence, and indicate if changes were made. The images or other third party material in this article are included in the article's Creative Commons licence, unless indicated otherwise in a credit line to the material. If material is not included in the article's Creative Commons licence and your intended use is not permitted by statutory regulation or exceeds the

permitted use, you will need to obtain permission directly from the copyright holder. To view a copy of this licence, visit <http://creativecommons.org/licenses/by/4.0/>.

References

1. Wu, J., Hu, D., Xiang, F., Yuan, X., Su, J.: 3D human pose estimation by depth map. *Vis. Comput.* (2020). <https://doi.org/10.1007/s00371-019-01740-4>
2. Zhang, Y., Tan, F., Wang, S., Yin, B.: 3D human body skeleton extraction from consecutive surfaces using a spatial-temporal consistency model. *Vis. Comput.* (2020). <https://doi.org/10.1007/s00371-020-01851-3>
3. Liu, Z., Zhu, J., Bu, J., Chen, C.: A survey of human pose estimation: the body parts parsing based methods. *J. Vis. Commun. Image Represent.* **32**, 10–19 (2015)
4. Antón, D., Goñi, A., Illarramendi, A., Torres-Unda, J.J., Seco, J.: KiReS: A Kinect-based telerehabilitation system. In 2013 IEEE 15th International Conference on e-Health Networking, Applications and Services (2013). <https://doi.org/10.1109/HealthCom.2013.6720717>
5. Naeemabadi, M., Dinesen, B., Andersen, O., Najafi, S., Hansen, J.: Evaluating accuracy and usability of microsoft kinect sensors and wearable sensor for tele knee rehabilitation after knee operation. In Proceedings of the 11th International Joint Conference on Biomedical Engineering Systems and Technologies (2018). <https://doi.org/10.5220/0006578201280135>
6. Gavrilova, M.L., Wang, Y., Ahmed, F., Paul, P.P.: Kinect sensor gesture and activity recognition: new applications for consumer cognitive systems. *IEEE Consum. Electr. Mag.* (2018). <https://doi.org/10.1109/MCE.2017.2755498>
7. Saini, R., Kumar, P., Kaur, B., Roy, P.P., Dogra, D.P., Santosh, K.C.: Kinect sensor-based interaction monitoring system using the BLSTM neural network in healthcare. *Int. J. Mach. Learn. Cybern.* (2019). <https://doi.org/10.1007/s13042-018-0887-5>
8. Fluit, R., Prinsen, E.C., Wang, S., van der Kooij, H.: A comparison of control strategies in commercial and research knee prostheses. *IEEE Trans. Biomed. Eng.* (2020). <https://doi.org/10.1109/TBME.2019.2912466>
9. Hu, B., Rouse, E., Hargrove, L.: Benchmark datasets for bilateral lower-limb neuromechanical signals from wearable sensors during unassisted locomotion in able-bodied individuals. *Front. Robot. AI* (2018). <https://doi.org/10.3389/frobt.2018.00014>
10. Hu, B., Rouse, E., Hargrove, L.: Fusion of bilateral lower-limb neuromechanical signals improves prediction of locomotor activities. *Front. Robot. AI* (2018). <https://doi.org/10.3389/frobt.2018.00078>
11. Perry, J., Burnfield, J.: *Gait Analysis: Normal and Pathological Function*, 2nd edn. Slack Incorporated, Thorofare, NJ, USA (2010)
12. Li, Q., Wang, Y., Sharf, A., Cao, Y., Tu, C., Chen, B., Yu, S.: Classification of gait anomalies from kinect. *Vis. Comput.* (2018). <https://doi.org/10.1007/s00371-016-1330-0>
13. Wang, K., Zhang, G., Yang, J., Bao, H.: Dynamic human body reconstruction and motion tracking with low-cost depth cameras. *Vis. Comput.* (2020). <https://doi.org/10.1007/s00371-020-01826-4>
14. Colyer, S.L., Evans, M., Cosker, D.P., Salo, A.I.T.: A review of the evolution of vision-based motion analysis and the integration of advanced computer vision methods towards developing a markerless system. *Sports Med. Open* (2018). <https://doi.org/10.1186/s40798-018-0139-y>
15. Latorre, J., Colomer, C., Alcañiz, M., Llorens, R.: Gait analysis with the Kinect v2: normative study with healthy individuals and comprehensive study of its sensitivity, validity, and reliability in

- individuals with stroke. *J. NeuroEng. Rehab.* (2019). <https://doi.org/10.1186/s12984-019-0568-y>
16. Murray, M.P.: Gait as a total pattern of movement. *Am. J. Phys. Med.* **46**, 290–333 (1967)
 17. Elaine, O.: The importance of being earnest about shank and thigh kinematics especially when using ankle-foot orthoses. *Prosthet. Orthot. Int.* (2010). <https://doi.org/10.3109/03093646.2010.485597>
 18. Ballit, A., Mougharbel, I., Ghaziri, H., Dao, T.T.: Computer-aided parametric prosthetic socket design based on real-time soft tissue deformation and an inverse approach. *Vis. Comput.* (2021). <https://doi.org/10.1007/s00371-021-02059-9>
 19. Hargrove, L.J., Huang, H., Schultz, A.E., Look, B.A., Lipschutz, R., Kuiken, T.A.: Toward the development of a neural interface for lower limb prosthesis control. In 2009 Annual International Conference of the IEEE Engineering in Medicine and Biology Society (2009). <https://doi.org/10.1109/IEMBS.2009.5334303>
 20. Varol, H.A., Sup, F., Goldfarb, M.: Multiclass real-time intent recognition of a powered lower limb prosthesis. *IEEE Trans. Biomed. Eng.* (2010). <https://doi.org/10.1109/TBME.2009.2034734>
 21. Young, A.J., Kuiken, T.A., Hargrove, L.J.: Analysis of using EMG and mechanical sensors to enhance intent recognition in powered lower limb prostheses. *J. Neural Eng.* (2014). <https://doi.org/10.1088/1741-2560/11/5/056021>
 22. Tschiedel, M., Russold, M.F., Kaniusas, E.: Relying on more sense for enhancing lower limb prostheses control: a review. *J. NeuroEng. Rehab.* (2020). <https://doi.org/10.1186/s12984-020-00726-x>
 23. Liu, M., Wang, D., Helen, H.: Development of an environment-aware locomotion mode recognition system for powered lower limb prostheses. *IEEE Trans. Neural Syst. Rehab. Eng.* (2016). <https://doi.org/10.1109/TNSRE.2015.2420539>
 24. Yan, T., Sun, Y., Liu, T., Cheung, C.H., Meng, M.Q.H.: A locomotion recognition system using depth images. In 2018 IEEE International Conference on Robotics and Automation (ICRA) (2018). <https://doi.org/10.1109/ICRA.2018.8460514>
 25. Massalin, Y., Abdrakmanova, M., Varol, H.A.: User-independent intent recognition for lower limb prostheses using depth sensing. *IEEE Trans. Biomed. Eng.* **65**, 1759–1770 (2018)
 26. Zhang, K., Xiong, C., Zhang, W., Liu, H., Lai, D., Rong, Y., Fu, C.: Environmental features recognition for lower limb prostheses toward predictive walking. *IEEE Trans. Neural Syst. Rehab. Eng.* (2019). <https://doi.org/10.1109/TNSRE.2019.2895221>
 27. Laschowski, B., McNally, W., Wong, A., McPhee, J.: Preliminary design of an environment recognition system for controlling robotic lower-limb prostheses and exoskeletons. In 2019 IEEE 16th International Conference on Rehabilitation Robotics (ICORR) (2019). <https://doi.org/10.1109/ICORR.2019.8779540>
 28. Krausz, N.E., Lenzi, T., Hargrove, L.J.: Depth sensing for improved control of lower limb prostheses. *IEEE Trans. Biomed. Eng.* **62**, 2576–2587 (2015)
 29. Diaz, J.P., da Silva, R.L., Zhong, B., Huang, H., Lobaton, E.: Visual terrain identification and surface inclination estimation for improving human locomotion with a lower-limb prosthetic. In Annual International Conference of the IEEE Engineering in Medicine and Biology Society (2018). <https://doi.org/10.1109/embc.2018.8512614>
 30. Ishikawa, T., Murakami, T.: Real-time foot clearance and environment estimation based on foot-mounted wearable sensors. In IECON 2018 - 44th Annual Conference of the IEEE Industrial Electronics Society (2018). <https://doi.org/10.1109/IECON.2018.8592894>
 31. St-Onge, N., Feldman, A.G.: Interjoint coordination in lower limbs during different movements in humans. *Exp. Brain Res.* **148**, 139–149 (2003)
 32. Grimes, D.L., Flowers, W.C., Donath, M.: Feasibility of an active control scheme for above knee prostheses. *J. Biomech. Eng.* **99**, 215–221 (1977)
 33. Borjian, R., Khamesee, M., Melek, W.: Feasibility study on echo control of a prosthetic knee: sensors and wireless communication. *Microsyst. Technol.* **16**, 257–265 (2010)
 34. Vallery, H., Ekkelenkamp, R., Buss, M., van der Kooij, H.: Complementary limb motion estimation based on interjoint coordination: experimental evaluation. In 2007 IEEE 10th International Conference on Rehabilitation Robotics (2007). <https://doi.org/10.1109/ICORR.2007.4428516>
 35. Bernal-Torres, M.G., Medellín-Castillo, H.I., Arellano-González, J.C.: Design and control of a new biomimetic transfemoral knee prosthesis using an echo-control scheme. *J. Healthc. Eng.* (2018). <https://doi.org/10.1155/2018/8783642>
 36. Mendez, J., Hood, S., Gunnel, A., Lenzi, T.: Powered knee and ankle prosthesis with indirect volitional swing control enables level-ground walking and crossing over obstacles. *Sci. Robot.* (2020). <https://doi.org/10.1126/scirobotics.aba6635>
 37. Ambrozic, L., Gorsic, M., Geeroms, J., Flynn, L., Molino Lova, R., Kamnik, R., Muni, M., Vitiello, N.: CYBERLEGS: a user-oriented robotic transfemoral prosthesis with whole-body awareness control. *IEEE Robot. Autom. Mag.* **21**, 82–93 (2014)
 38. Goršič, M., Kamnik, R., Ambrožič, L., Vitiello, N., Lefeber, D., Pasquini, G., Muni, M.: Online phase detection using wearable sensors for walking with a robotic prosthesis. *Sensors (Basel)* (2014). <https://doi.org/10.3390/s140202776>
 39. Parri, A., Martini, E., Geeroms, J., Flynn, L., Pasquini, G., Crea, S., Molino Lova, R., Lefeber, D., Kamnik, R., Muni, M., Vitiello, N.: Whole body awareness for controlling a robotic transfemoral prosthesis. *Front. Neurobot.* (2017). <https://doi.org/10.3389/fnbot.2017.00025>
 40. Hu, B.H., Krausz, N.E., Hargrove, L.J.: A novel method for bilateral gait segmentation using a single thigh-mounted depth sensor and IMU. In 2018 7th IEEE International Conference on Biomedical Robotics and Biomechanics (Biorob) (2018). <https://doi.org/10.1109/BIOROB.2018.8487806>
 41. Stigler, S.M.: Gauss and the invention of least squares. *Ann. Stat.* (1981). <https://doi.org/10.1214/aos/1176345451>
 42. Harms, H., Beck, J., Ziegler, J., Stiller, C.: Accuracy analysis of surface normal reconstruction in stereo vision. In 2014 IEEE Intelligent Vehicles Symposium Proceedings (2014). <https://doi.org/10.1109/IVS.2014.6856436>
 43. Balaji, S.R., Karthikeyan, S.: A survey on moving object tracking using image processing. In 2017 11th International Conference on Intelligent Systems and Control (ISCO) (2017). <https://doi.org/10.1109/ISCO.2017.7856037>
 44. Zohora F.T., Santosh, K.C.: Circular Foreign Object Detection in Chest X-ray Images. In: Santosh, K., Hangarge, M., Bevilacqua, V., Negi, A. (eds) Recent Trends in Image Processing and Pattern Recognition. RTIP2R 2016. Communications in Computer and Information Science, vol. 709. Springer, Singapore (2017)
 45. Zohora, F.T., Antani, S., Santosh, K.C.: Circle-like foreign element detection in chest x-rays using normalized cross-correlation and unsupervised clustering. In Proceedings of the SPIE 10574, Medical Imaging 2018: Image Processing (2018). <https://doi.org/10.1117/12.2293739>
 46. Santosh, K.C., Dhar, M.K., Rajbhandari, R., Neupane, A.: Deep neural network for foreign object detection in chest x-rays. In 2020 IEEE 33rd International Symposium on Computer-Based Medical Systems (CBMS) (2020). <https://doi.org/10.1109/CBMS49503.2020.00107>
 47. Yi, S.C., Chen, Y.C., Chang, C.H.: A lane detection approach based on intelligent vision. *Comput. Electr. Eng.* (2015). <https://doi.org/10.1016/j.compeleceng.2015.01.002>

48. Liang, D., Guo, Y.C., Zhang, S.K., Mu, T.J., Huang, X.: Lane detection: a survey with new results. *J. Comput. Sci. Technol.* (2020). <https://doi.org/10.1007/s11390-020-0476-4>
49. Myronenko, A., Song, X.: Point set registration: coherent point drift. *IEEE Trans. Pattern Anal. Mach. Intell.* (2010). <https://doi.org/10.1109/TPAMI.2010.46>
50. Bergström, P., Edlund, O.: Robust registration of point sets using iteratively reweighted least squares. *Comput. Optim. Appl.* **58**, 543–561 (2014)
51. Chang, W.C., Wu, C.H.: Candidate-based matching of 3-D point clouds with axially switching pose estimation. *Vis. Comput.* **36**, 593–607 (2020)
52. Fischler, M.A., Bolles, R.C.: Random sample consensus: a paradigm for model fitting with applications to image analysis and automated cartography. *Commun. ACM* (1981). <https://doi.org/10.1145/358669.358692>
53. Jones, A., Doust, J.: A 1% treadmill grade most accurately reflects the energetic cost of outdoor running. *J. Sports Sci.* (1996). <https://doi.org/10.1080/02640419608727717>
54. Batten, H.R., McPhail, S.M., Mandrusiak, A.M., Varghese, P.N., Kuys, S.S.: Gait speed as an indicator of prosthetic walking potential following lower limb amputation. *Prosthet. Orthot. Int.* (2019). <https://doi.org/10.1177/0309364618792723>
55. McGinley, J.L., Baker, R., Wolfe, R., Morris, M.E.: The reliability of three-dimensional kinematic gait measurements: a systematic review. *Gait Posture* (2009). <https://doi.org/10.1016/j.gaitpost.2008.09.003>
56. Pasinetti, S., Hassan, M.M., Eberhardt, J., Lancini, M., Docchio, F., Sansoni, G.: Performance analysis of the PMD camboard picoflex time-of-flight camera for markerless motion capture applications. *IEEE Trans. Instrum. Meas.* **68**, 4456–4471 (2019)
57. Page, S., Martins, M.M., Saint-Bauzel, L., Santos, C.P., Pasqui, V.: Fast embedded feet pose estimation based on a depth camera for smart walker. In 2015 IEEE International Conference on Robotics and Automation (ICRA) (2015). <https://doi.org/10.1109/ICRA.2015.7139781>
58. Grimmer, M., Schmidt, K., Duarte, J.E., Neuner, L., Koginov, G., Riener, R.: Stance and swing detection based on the angular velocity of lower limb segments during walking. *Front. Neurobot.* (2019). <https://doi.org/10.3389/fnbot.2019.00057>
59. Lien, J., Gillian, N., Karagozler, M.E., Amihoud, P., Schwesig, C., Olson, E., Raja, H., Poupyrev, I.: Soli: ubiquitous gesture sensing with millimeter wave radar. *ACM Trans. Graph.* (2016). <https://doi.org/10.1145/2897824.2925953>

Publisher's Note Springer Nature remains neutral with regard to jurisdictional claims in published maps and institutional affiliations.



Michael Tschiedel was born in Vienna, Austria, in 1994. He received his B.Sc. degree in Electrical Engineering and his diploma (Dipl.-Ing.) in Biomedical Engineering from TU Wien in 2016 and 2018, respectively. He is currently an industry-related doctoral candidate at TU Wien and Ottobock. His research interests include computer vision and environmental sensing for prosthetic devices.



Michael Friedrich Russold was born in Vienna, Austria, in 1974. He obtained a masters degree (Dipl.-Ing.) from TU Wien. He then received a PhD degree from the University of Liverpool, UK. Afterwards, he worked as a post-doc at the University of Sydney, Australia, under a Marie Curie individual outgoing Fellowship. Michael Russold is author and co-author of more than 20 publications. Since 2008, Michael Russold works for Ottobock Healthcare Products GmbH, where he worked in product development and research. In the latter role, he has been involved in several international research projects, based around national and international funding.



Eugenijus Kanius is a professor in the field of biomedical theranostics and heads the research group Biomedical Sensing at TU Wien. His interests include auricular vagus nerve stimulation, prosthetics, perioperative monitoring, and wearable hardware/software concepts for diagnostic/therapeutic/theranostic devices. He gives numerous mandatory lectures at TU Wien, including Biophysics, Biomedical Sensors and Signals, Biomedical Instrumentation. Currently, he is the dean of academic affairs Biomedical Engineering at TU Wien.



Markus Vincze received his diploma in mechanical engineering from TU Wien in 1988 and a M.Sc. from Rensselaer Polytechnic Institute, USA, in 1990. He finished his PhD at TU Wien in 1993. With a grant from the Austrian Academy of Sciences, he worked at HelpMate Robotics Inc. and at the Vision Laboratory of Gregory Hager at Yale University. In 2004, he obtained his habilitation in robotics. Presently, he leads the "Vision for Robotics" team at TU Wien with the vision to make robots see. Markus' special interests are cognitive computer vision techniques for robotics solutions situated in real-world environments.

Author's Publications

- [MT1] M. Tschiedel, *Study of Piezo Motors for Valve Control of Lower Limb Prosthesis*, Diploma Thesis. Institute of Electrodynamics, Microwave and Circuit Engineering of the Vienna University of Technology, 2018.
- [MT2] M. Tschiedel, M. F. Russold, and E. Kaniusas, "Relying on more sense for enhancing lower limb prostheses control: a review," *Journal of NeuroEngineering and Rehabilitation*, vol. 17, no. 1, p. 99, Jul 2020. [Online]. Available: <https://doi.org/10.1186/s12984-020-00726-x>
- [MT3] S. Dirk, M. Tschiedel, and R. Hoffmann, "Method for Operating an Orthopedic Device and Corresponding Orthopedic Device," WO2020245400A1, Dec 10, 2020.
- [MT4] M. Tschiedel, M. F. Russold, E. Kaniusas, and M. Vincze, "Real-time limb tracking in single depth images based on circle matching and line fitting," *The Visual Computer*, Apr 2021. [Online]. Available: <https://doi.org/10.1007/s00371-021-02138-x>



Die approbierte gedruckte Originalversion dieser Dissertation ist an der TU Wien Bibliothek verfügbar.
The approved original version of this doctoral thesis is available in print at TU Wien Bibliothek.

List of References

- [1] C. A. Behrendt, B. Sigvant, Z. Szeberin, B. Beiles, N. Eldrup, I. A. Thomson, M. Venermo, M. Altreuther, G. Menyhei, J. Nordanstig, M. Clarke, H. C. Rieß, M. Björck, and E. S. Debus, “International Variations in Amputation Practice: A VASCUNET Report,” *Eur J Vasc Endovasc Surg*, vol. 56, no. 3, pp. 391–399, 09 2018.
- [2] J. C. Thorud, D. C. Jupiter, J. Lorenzana, T. T. Nguyen, and N. Shibuya, “Reoperation and Reamputation After Transmetatarsal Amputation: A Systematic Review and Meta-Analysis,” *The Journal of Foot and Ankle Surgery*, vol. 55, no. 5, pp. 1007–1012, Sep. 2016.
- [3] M. Ghous, S. Gul, F. Siddiqui, S. Pervaiz, and S. Bano, “DEPRESSION: Prevalence Among Amputees,” *Professional Medical Journal*, vol. 22, no. 2, pp. 263–266, 2015.
- [4] K. Ziegler-Graham, E. J. Mackenzie, P. L. Ephraim, T. G. Trivison, and R. Brookmeyer, “Estimating the Prevalence of Limb Loss in the United States: 2005 to 2050,” *Archives of Physical Medicine and Rehabilitation*, vol. 89, no. 3, pp. 422–429, 2008.
- [5] M. F. Owings and L. J. Kozak, “Ambulatory and inpatient procedures in the United States, 1996,” *Vital Health Stat 13*, no. 139, pp. 1–119, Nov 1998.
- [6] M. Spoden, U. Nimptsch, and T. Mansky, “Amputation rates of the lower limb by amputation level – observational study using German national hospital discharge data from 2005 to 2015,” *BMC Health Services Research*, vol. 19, no. 1, p. 8, Jan 2019.
- [7] J. Parvizi and G. K. Kim, “Chapter 9 - Amputation of the Lower Limb,” in *High Yield Orthopaedics*, J. Parvizi and G. K. Kim, Eds. Philadelphia: W.B. Saunders, 2010, pp. 17–19.
- [8] M. Narres, T. Kvitkina, H. Claessen, S. Droste, B. Schuster, S. Morbach, G. Rümenapf, K. Van Acker, and A. Icks, “Incidence of lower extremity amputations in the diabetic compared with the non-diabetic population: A systematic review,” *PLoS ONE*, vol. 12, no. 8, pp. 1–28, 08 2017.
- [9] K. Heyer, E. S. Debus, L. Mayerhoff, and M. Augustin, “Prevalence and Regional Distribution of Lower Limb Amputations from 2006 to 2012 in Germany: A Population based Study,” *Eur J Vasc Endovasc Surg*, vol. 50, no. 6, pp. 761–766, Dec 2015.

LIST OF REFERENCES

- [10] B. Greitemann, L. Brückner, M. Schäfer, and R. Baumgartner, Eds., *Amputation und Prothesenversorgung*. Georg Thieme Verlag, 2016.
- [11] S. Hussain, S. Shams, and S. J. Khan, “Impact of Medical Advancement: Prostheses,” in *Computer Architecture in Industrial, Biomechanical and Biomedical Engineering*, L. Wang and L. Yu, Eds. Rijeka: IntechOpen, 2019, ch. 2.
- [12] R. F. Baumgartner, “Knee disarticulation versus above-knee amputation,” *Prosthet Orthot Int*, vol. 3, no. 1, pp. 15–19, Apr 1979.
- [13] I. Matthes, M. Beirau, A. Ekkernkamp, and G. Matthes, “Amputation und Prothesenversorgung der unteren Extremität,” *Der Unfallchirurg*, vol. 118, no. 6, pp. 535–548, Jun 2015.
- [14] R. Fluit, E. C. Prinsen, S. Wang, and H. van der Kooij, “A Comparison of Control Strategies in Commercial and Research Knee Prostheses,” *IEEE Trans Biomed Eng*, vol. 67, no. 1, pp. 277–290, 01 2020.
- [15] E. Schaffalitzky, S. NiMhurchadha, P. Gallagher, S. Hofkamp, M. MacLachlan, and S. T. Wegener, “Identifying the values and preferences of prosthetic users: a case study series using the repertory grid technique,” *Prosthet Orthot Int*, vol. 33, no. 2, pp. 157–166, Jun 2009.
- [16] B. O’Keeffe and S. Rout, “Prosthetic Rehabilitation in the Lower Limb,” *Indian J Plast Surg*, vol. 52, no. 1, pp. 134–143, Jan 2019.
- [17] P. R. Study, *Transfemoral Amputation: The Basics and Beyond*. Prosthetics Research Study, 2008.
- [18] S. Gerzeli, A. Torbica, and G. Fattore, “Cost utility analysis of knee prosthesis with complete microprocessor control (C-leg) compared with mechanical technology in transfemoral amputees,” *The European Journal of Health Economics*, vol. 10, no. 1, pp. 47–55, Feb 2009.
- [19] HCFA, *Common Procedure Coding System HCPCS 2001*, US Government Printing Office, Washington (DC), 2001.
- [20] D. Borrenpohl, B. Kaluf, and M. J. Major, “Survey of U.S. Practitioners on the Validity of the Medicare Functional Classification Level System and Utility of Clinical Outcome Measures for Aiding K-Level Assignment,” *Arch Phys Med Rehabil*, vol. 97, no. 7, pp. 1053–1063, 07 2016.
- [21] R. S. Gailey, K. E. Roach, E. B. Applegate, B. Cho, B. Cunniffe, S. Licht, M. Maguire, and M. S. Nash, “The Amputee Mobility Predictor: An instrument to assess determinants of the lower-limb amputee’s ability to ambulate,” *Arch Phys Med Rehabil*, vol. 83, no. 5, pp. 613–627, May 2002.

-
- [22] D. Podsiadlo and S. Richardson, “The timed “Up & Go”: a test of basic functional mobility for frail elderly persons,” *J Am Geriatr Soc*, vol. 39, no. 2, pp. 142–148, Feb 1991.
- [23] H. Du, P. J. Newton, Y. Salamonson, V. L. Carrieri-Kohlman, and P. M. Davidson, “A Review of the Six-Minute Walk Test: Its Implication as a Self-Administered Assessment Tool,” *Eur J Cardiovasc Nurs*, vol. 8, no. 1, pp. 2–8, Mar 2009.
- [24] B. G. A. Lambrecht and H. Kazerooni, “Design of a semi-active knee prosthesis,” in *2009 IEEE International Conference on Robotics and Automation*, 2009, pp. 639–645.
- [25] J. T. Kahle, M. J. Highsmith, and S. L. Hubbard, “Comparison of nonmicroprocessor knee mechanism versus C-Leg on Prosthesis Evaluation Questionnaire, stumbles, falls, walking tests, stair descent, and knee preference,” *J Rehabil Res Dev*, vol. 45, no. 1, pp. 1–14, 2008.
- [26] “C-Leg 4. Instructions for Use,” accessed 28 Sept 2020. [Online]. Available: <https://www.ottobockus.com/media/local-media/prosthetics/lower-limb/c-leg/files/cleg4-ifu.pdf>
- [27] E. D. Ledoux and M. Goldfarb, “Control and Evaluation of a Powered Transfemoral Prosthesis for Stair Ascent,” *IEEE Trans Neural Syst Rehabil Eng*, vol. 25, no. 7, pp. 917–924, 07 2017.
- [28] E. J. Wolf, V. Q. Everding, A. A. Linberg, J. M. Czerniecki, and J. M. Gambel, “Comparison of the Power Knee and C-Leg during step-up and sit-to-stand tasks,” *Gait Posture*, vol. 38, no. 3, pp. 397–402, Jul 2013.
- [29] D. S. Pieringer, M. Grimmer, M. F. Russold, and R. Riener, “Review of the Actuators of Active Knee Prostheses and their Target Design Outputs for Activities of Daily Living,” in *2017 International Conference on Rehabilitation Robotics (ICORR)*, vol. 2017. IEEE, 2017, pp. 1246–1253.
- [30] “Power Knee. Instructions for Use,” accessed 24 July 2020. [Online]. Available: https://media.ossur.com/image/upload/product-documents/global/PN20033/IFUS/PN20033_Power_Knee.pdf
- [31] “IntelLeg Knee. Instructions for Use,” accessed 16 Jan 2022. [Online]. Available: http://www.rbionics.com/wp-content/uploads/2021/05/Instructions_for_Use_Wearer.pdf
- [32] J. Perry and J. Burnfield, *Gait Analysis: Normal and Pathological Function*, 2nd ed. Thorofare, NJ, USA: Slack Incorporated, 2010.
- [33] D. A. Winter, *Biomechanics and Motor Control of Human Gait: Normal, Elderly and Pathological*, 2nd ed. Waterloo, Ont: Waterloo Biomechanics, 1991.
- [34] D. Halliday, R. Resnick, and J. Walker, *Physik: Bachelor-Edition*. Weinheim: WILEY-VCH, 2007.

LIST OF REFERENCES

- [35] A. Peters and L. Krumrey, “Ursachen und Korrektur von Prothesengangfehlern bei Oberschenkelamputierten,” *Rehabilitation (Stuttg)*, vol. 39, no. 4, pp. 223–230, Aug. 2000.
- [36] H. A. Varol, F. Sup, and M. Goldfarb, “Multiclass Real-Time Intent Recognition of a Powered Lower Limb Prosthesis,” *IEEE Transactions on Biomedical Engineering*, vol. 57, no. 3, pp. 542–551, 2010.
- [37] M. Tucker, J. Olivier, A. Pagel, H. Bleuler, M. Bouri, O. Lamercy, J. D. Millan, R. Riener, H. Vallery, and R. Gassert, “Control strategies for active lower extremity prosthetics and orthotics: a review,” *Journal Of Neuroengineering And Rehabilitation*, vol. 12, no. 1, 2015.
- [38] M. Ben-Ari and F. Mondada, *Elements of Robotics*. Cham: Springer, 2018.
- [39] D. B. Seifert, *Funktionelle Programmierung eines Mikroprozessor gesteuerten Prothesenkniegelenks für Geriatriker*, Diplomarbeit. Institute of Mechanics and Mechatronics of the Vienna University of Technology, 2011.
- [40] J. M. Stepien, S. Cavenett, L. Taylor, and M. Crotty, “Activity Levels Among Lower-Limb Amputees: Self-Report Versus Step Activity Monitor,” *Archives of Physical Medicine and Rehabilitation*, vol. 88, no. 7, pp. 896–900, Jul. 2007.
- [41] E. Yurtsever, J. Lambert, A. Carballo, and K. Takeda, “A Survey of Autonomous Driving: Common Practices and Emerging Technologies,” *IEEE Access*, vol. 8, pp. 58 443–58 469, 2020.
- [42] M. Wolff, *Sensor-Technologien: Band 1: Position, Entfernung, Verschiebung, Schichtdicke*, ser. De Gruyter Studium. Berlin/Boston: De Gruyter Oldenbourg, 2016.
- [43] G. A. Reider, *Photonik: Eine Einführung in die Grundlagen*, 3rd ed. Vienna: Springer Vienna, 2012.
- [44] D. C. Giancoli, *Physik: Lehr- und Übungsbuch*, 3rd ed., ser. Physik. München [u.a.]: Pearson Studium, 2010.
- [45] S. J. Rupitsch, *Piezoelectric Sensors and Actuators: Fundamentals and Applications*, ser. Topics in Mining, Metallurgy and Materials Engineering. Berlin Heidelberg: Springer Berlin Heidelberg, 2019.
- [46] P. Zanuttigh, G. Marin, C. Dal Mutto, F. Dominio, L. Minto, and G. M. Cortelazzo, *Time-Of-Flight and Structured Light Depth Cameras: Technology and Applications*. Cham: Springer International Publishing, 2016.
- [47] “CES 2020 Press Release: new pmd 3D VGA ToF modul,” accessed 18 Mar 2020. [Online]. Available: https://www.pmdtec.com/html/pdf/press_release/PR20200107_CES_VGA_module.pdf

-
- [48] M. A. Richards, *Principles of Modern Radar: 1. Basic Principles*. Edison, NJ: Scitech Publ., 2010.
- [49] J. Lien, N. Gillian, M. E. Karagozler, P. Amihoud, C. Schwesig, E. Olson, H. Raja, and I. Poupyrev, “Soli: Ubiquitous Gesture Sensing with Millimeter Wave Radar,” *ACM Trans. Graph.*, vol. 35, no. 4, 2016.
- [50] J. Webster and R. T. Watson, “Analyzing the Past to Prepare for the Future: Writing a Literature Review,” *MIS Quarterly*, vol. 26, no. 2, pp. xiii–xxiii, 2002.
- [51] D. Moher, A. Liberati, J. Tetzlaff, and D. G. Altman, “Preferred Reporting Items for Systematic Reviews and Meta-Analyses: The PRISMA Statement,” *Journal of Clinical Epidemiology*, vol. 62, no. 10, pp. 1006–1012, 2009.
- [52] B. Hu, N. E. Krausz, and L. J. Hargrove, “A Novel Method for Bilateral Gait Segmentation Using a Single Thigh-Mounted Depth Sensor and IMU,” in *2018 7th IEEE International Conference on Biomedical Robotics and Biomechatronics (Biorob)*, 2018, pp. 807–812.
- [53] M. P. Murray, “Gait as a total pattern of movement,” *American journal of physical medicine*, vol. 46, no. 1, pp. 290–333, 1967.
- [54] E. Owen, “The Importance of Being Earnest about Shank and Thigh Kinematics Especially When Using Ankle-Foot Orthoses,” *Prosthetics and Orthotics International*, vol. 34, no. 3, pp. 254–269, 2010.
- [55] H. Harms, J. Beck, J. Ziegler, and C. Stiller, “Accuracy analysis of surface normal reconstruction in stereo vision,” in *2014 IEEE Intelligent Vehicles Symposium Proceedings*, 2014, pp. 730–736.
- [56] S. M. Stigler, “Gauss and the Invention of Least Squares,” *The Annals of Statistics*, vol. 9, no. 3, pp. 465 – 474, 1981.
- [57] S. R. Balaji and S. Karthikeyan, “A survey on moving object tracking using image processing,” in *2017 11th International Conference on Intelligent Systems and Control (ISCO)*, 2017, pp. 469–474.
- [58] A. Myronenko and X. Song, “Point Set Registration: Coherent Point Drift,” *IEEE Transactions on Pattern Analysis and Machine Intelligence*, vol. 32, no. 12, pp. 2262–2275, 2010.
- [59] P. Bergström and O. Edlund, “Robust registration of point sets using iteratively reweighted least squares,” *Computational Optimization and Applications*, vol. 58, no. 3, pp. 543–561, 2014.
- [60] W.-C. Chang and C.-H. Wu, “Candidate-based matching of 3-d point clouds with axially switching pose estimation,” *The Visual Computer*, vol. 36, no. 3, pp. 593–607, 2020.

LIST OF REFERENCES

- [61] M. A. Fischler and R. C. Bolles, “Random Sample Consensus: A Paradigm for Model Fitting with Applications to Image Analysis and Automated Cartography,” *Commun. ACM*, vol. 24, no. 6, p. 381–395, 1981.
- [62] A. M. Jones and J. H. Doust, “A 1% treadmill grade most accurately reflects the energetic cost of outdoor running,” *Journal of Sports Sciences*, vol. 14, no. 4, pp. 321–327, 1996.
- [63] H. R. Batten, S. M. McPhail, A. M. Mandrusiak, P. N. Varghese, and S. S. Kuys, “Gait speed as an indicator of prosthetic walking potential following lower limb amputation,” *Prosthetics and Orthotics International*, vol. 43, no. 2, pp. 196–203, 2019.
- [64] “TDK News Release: CH101 availability,” accessed 4 April 2021. [Online]. Available: https://www.tdk.com/en/news_center/press/20190625_01.html
- [65] R. J. Przybyla, H.-Y. Tang, A. Guedes, S. E. Shelton, D. A. Horsley, and B. E. Boser, “3D Ultrasonic Rangefinder on a Chip,” *IEEE Journal of Solid-State Circuits*, vol. 50, no. 1, pp. 320–334, 2015.
- [66] “CH101 Datasheet,” accessed 5 July 2021. [Online]. Available: <https://invensense.tdk.com/wp-content/uploads/2021/01/DS-000331-CH101-v1.4.pdf>
- [67] “CH101 Evaluation Kit Users Guide,” accessed 10 Sept 2020. [Online]. Available: https://product.tdk.com/system/files/dam/doc/product/sensor/ultrasonic/tof/app_note/an-000157-ch-101-smartsonic-evaluation-kit-users-guide.pdf
- [68] F. Crenna, G. B. Rossi, and M. Berardengo, “Filtering Biomechanical Signals in Movement Analysis,” *Sensors (Basel)*, vol. 21, no. 13, p. 4580, Jul 2021.
- [69] “Genium. Instructions for Use,” accessed 10 Dec 2020. [Online]. Available: <https://shop.ottobock.us/media/pdf/647G573-INT-08-1404w.pdf>
- [70] “3D L.A.S.A.R. Posture,” accessed 10 Sept 2020. [Online]. Available: https://pe.ottobock.com/en/downloads/646d1159_3d-lasar.pdf
- [71] M. Bellmann, T. Schmalz, and S. Blumentritt, “Comparative biomechanical analysis of current microprocessor-controlled prosthetic knee joints,” *Archives of Physical Medicine and Rehabilitation*, vol. 91, no. 4, pp. 644–652, Apr 2010.
- [72] D. H. Sutherland, “The evolution of clinical gait analysis. Part II Kinematics,” *Gait Posture*, vol. 16, no. 2, pp. 159–179, Oct 2002.
- [73] D. H. Sutherland, “The evolution of clinical gait analysis part III – kinetics and energy assessment,” *Gait Posture*, vol. 21, no. 4, pp. 447–461, Jun 2005.
- [74] H. Vallery, R. Burgkart, C. Hartmann, J. Mitternacht, R. Riener, and M. Buss, “Complementary limb motion estimation for the control of active knee prostheses,” *Biomedizinische Technik. Biomedical Engineering*, vol. 56, no. 1, pp. 45–51, 2011.

-
- [75] M. Bernal-Torres, H. Medellín-Castillo, and A. González, “Development of an Active Biomimetic-Controlled Transfemoral Knee Prosthesis,” in *2016 ASME International Mechanical Engineering Congress and Exposition. Volume 3: Biomedical and Biotechnology Engineering*, 2016.
- [76] M. G. Bernal-Torres, H. I. Medellín-Castillo, and J. C. Arellano-González, “Design and Control of a New Biomimetic Transfemoral Knee Prosthesis Using an Echo-Control Scheme,” *Journal of Healthcare Engineering*, vol. 2018, 2018.
- [77] B. Su, J. Wang, S. Liu, M. Sheng, J. Jiang, and K. Xiang, “A CNN-Based Method for Intent Recognition Using Inertial Measurement Units and Intelligent Lower Limb Prosthesis,” *IEEE Transactions on Neural Systems and Rehabilitation Engineering*, vol. 27, no. 5, pp. 1032–1042, 2019.
- [78] L. Ambrozic, M. Gorsic, S. Slajpah, R. Kamnik, and M. Munih, “Wearable Sensory System for Robotic Prosthesis,” *International Journal of Mechanics and Control JoMaC*, vol. 15, no. 1, 2014.
- [79] L. Ambrozic, M. Gorsic, J. Geeroms, L. Flynn, R. M. Lova, R. Kamnik, M. Munih, and N. Vitiello, “CYBERLEGS: A User-Oriented Robotic Transfemoral Prosthesis with Whole-Body Awareness Control,” *IEEE Robotics & Automation Magazine*, vol. 21, no. 4, pp. 82–93, 2014.
- [80] M. Goršič, R. Kamnik, L. Ambrožič, N. Vitiello, D. Lefeber, G. Pasquini, and M. Munih, “Online Phase Detection Using Wearable Sensors for Walking with a Robotic Prosthesis,” *Sensors (Basel)*, vol. 14, no. 2, pp. 2776–2794, 2014.
- [81] A. Parri, E. Martini, J. Geeroms, L. Flynn, G. Pasquini, S. Crea, R. M. Lova, D. Lefeber, R. Kamnik, M. Munih, and N. Vitiello, “Whole Body Awareness for Controlling a Robotic Transfemoral Prosthesis,” *Frontiers in Neurorobotics*, vol. 11, no. 25, 2017.
- [82] B. Hu, E. Rouse, and L. Hargrove, “Fusion of Bilateral Lower-Limb Neuromechanical Signals Improves Prediction of Locomotor Activities,” *Frontiers in Robotics and AI*, vol. 5, 2018.
- [83] B. H. Hu, E. J. Rouse, and L. J. Hargrove, “Using bilateral lower limb kinematic and myoelectric signals to predict locomotor activities: A pilot study,” in *2017 8th International IEEE/EMBS Conference on Neural Engineering (NER)*, 2017, pp. 98–101.
- [84] B. Hu, E. Rouse, and L. Hargrove, “Benchmark Datasets for Bilateral Lower-Limb Neuromechanical Signals from Wearable Sensors during Unassisted Locomotion in Able-Bodied Individuals,” *Frontiers in Robotics and AI*, vol. 5, 2018.
- [85] N. E. Krausz, B. H. Hu, and L. J. Hargrove, “Subject- and Environment-Based Sensor Variability for Wearable Lower-Limb Assistive Devices,” *Sensors*, vol. 19, pp. 4887–4887, 2019.

LIST OF REFERENCES

- [86] F. Zhang, T. Yan, and M. Q. Meng, "Gait Phase Recognition Based on A Wearable Depth Camera*," in *2018 IEEE International Conference on Information and Automation (ICIA)*, Aug 2018, pp. 756–760.
- [87] G. G. Scandaroli, G. A. Borges, J. Y. Ishihara, M. H. Terra, A. F. D. Rocha, and F. A. de Oliveira Nascimento, "Estimation of Foot Orientation with Respect to Ground for an Above Knee Robotic Prosthesis," in *2009 IEEE/RSJ International Conference on Intelligent Robots and Systems*, 2009, pp. 1112–1117.
- [88] T. Ishikawa and T. Murakami, "Real-Time Foot Clearance and Environment Estimation Based on Foot-Mounted Wearable Sensors," 10 2018, pp. 5475–5480.
- [89] B. Kleiner and D. Cismeci, "D8.4 - Foresighted Control of Active Foot Prostheses," in *SENSOR+TEST Conferences 2011, Nürnberg*, ser. D8 - Medical III, vol. Proceedings SENSOR 2011, 2011, pp. 669 –672.
- [90] F. Zhang, Z. Fang, M. Liu, and H. Huang, "Preliminary Design of a Terrain Recognition System," in *2011 Annual International Conference of the IEEE Engineering in Medicine and Biology Society*, vol. 2011, 2011, pp. 5452–5455.
- [91] X. Zhang, D. Wang, Q. Yang, and H. Huang, "An Automatic and User-Driven Training Method for Locomotion Mode Recognition for Artificial Leg Control," in *2012 Annual International Conference of the IEEE Engineering in Medicine and Biology Society*, vol. 2012, 2012, pp. 6116–6119.
- [92] D. Wang, L. Du, and H. Huang, "Terrain Recognition Improves the Performance of Neural-Machine Interface for Locomotion Mode Recognition," in *2013 International Conference on Computing, Networking and Communications (ICNC)*, 2013, pp. 87–91.
- [93] M. Liu, D. Wang, and H. Huang, "Development of an Environment-Aware Locomotion Mode Recognition System for Powered Lower Limb Prostheses," *IEEE Transactions on Neural Systems and Rehabilitation Engineering*, vol. 24, no. 4, pp. 434–443, 2016.
- [94] S. Carvalho, J. Figueiredo, and C. P. Santos, "Environment-Aware Locomotion Mode Transition Prediction System," in *2019 IEEE International Conference on Autonomous Robot Systems and Competitions (ICARSC)*, April 2019, pp. 1–6.
- [95] S. Sahoo, M. Maheshwari, D. K. Pratihar, and S. Mukhopadhyay, "A Geometry Recognition-Based Strategy for Locomotion Transitions' Early Prediction of Prosthetic Devices," *IEEE Transactions on Instrumentation and Measurement*, vol. 69, no. 4, pp. 1259–1267, 2019.
- [96] H. A. Varol and Y. Massalin, "A Feasibility Study of Depth Image Based Intent Recognition for Lower Limb Prostheses," in *2016 38th Annual International Conference of the IEEE Engineering in Medicine and Biology Society (EMBC)*, 2016, pp. 5055–5058.

-
- [97] Y. Massalin, M. Abdrakhmanova, and H. A. Varol, “User-Independent Intent Recognition for Lower Limb Prostheses Using Depth Sensing,” *IEEE Transactions on Biomedical Engineering*, vol. 65, no. 8, pp. 1759–1770, 2018.
- [98] B. Laschowski, W. McNally, A. Wong, and J. McPhee, “Preliminary Design of an Environment Recognition System for Controlling Robotic Lower-Limb Prostheses and Exoskeletons,” in *2019 IEEE 16th International Conference on Rehabilitation Robotics (ICORR)*, June 2019, pp. 868–873.
- [99] T. Yan, Y. Sun, T. Liu, C. Cheung, and M. Q. Meng, “A Locomotion Recognition System Using Depth Images,” in *2018 IEEE International Conference on Robotics and Automation (ICRA)*, May 2018, pp. 6766–6772.
- [100] J. P. Diaz, R. L. D. Silva, B. Zhong, H. H. Huang, and E. Lobaton, “Visual Terrain Identification and Surface Inclination Estimation for Improving Human Locomotion with a Lower-Limb Prosthetic,” in *2018 40th Annual International Conference of the IEEE Engineering in Medicine and Biology Society (EMBC)*, 2018, pp. 1817–1820.
- [101] N. E. Krausz, T. Lenzi, and L. J. Hargrove, “Depth Sensing for Improved Control of Lower Limb Prostheses,” *IEEE Transactions on Biomedical Engineering*, vol. 62, no. 11, pp. 2576–2587, 2015.
- [102] B. Kleiner, N. Ziegenspeck, R. Stolyarov, H. Herr, U. Schneider, and A. Verl, “A Radar-Based Terrain Mapping Approach for Stair Detection Towards Enhanced Prosthetic Foot Control,” in *2018 7th IEEE International Conference on Biomedical Robotics and Biomechanics (Biorob)*, 2018, pp. 105–110.
- [103] K. Zhang, C. Xiong, W. Zhang, H. Liu, D. Lai, Y. Rong, and C. Fu, “Environmental Features Recognition for Lower Limb Prostheses Toward Predictive Walking,” *IEEE Transactions on Neural Systems and Rehabilitation Engineering*, vol. 27, no. 3, pp. 465–476, 2019.
- [104] K. Zhang, W. Zhang, W. Xiao, H. Liu, C. W. D. Silva, and C. Fu, “Sequential Decision Fusion for Environmental Classification in Assistive Walking,” *IEEE Transactions on Neural Systems and Rehabilitation Engineering*, vol. 27, no. 9, pp. 1780–1790, 2019.
- [105] I. Goodfellow, Y. Bengio, and A. Courville, *Deep learning*, ser. Adaptive computation and machine learning. Cambridge, Massachusetts London: The MIT Press, 2016.
- [106] M. A. Fischler and R. C. Bolles, “Random Sample Consensus: A Paradigm for Model Fitting with Applications to Image Analysis and Automated Cartography,” *Commun. ACM*, vol. 24, no. 6, pp. 381–395, 1981.
- [107] E. Zheng, S. Manca, T. Yan, A. Parri, N. Vitiello, and Q. Wang, “Gait Phase Estimation Based on Noncontact Capacitive Sensing and Adaptive Oscillators,” *IEEE Transactions on Biomedical Engineering*, vol. 64, no. 10, pp. 2419–2430, 2017.

LIST OF REFERENCES

- [108] F. Zhang, M. Liu, S. D. Harper, M. Lee, and H. Huang, “Engineering Platform and Experimental Protocol for Design and Evaluation of a Neurally-controlled Powered Transfemoral Prosthesis,” *Journal of Visualized Experiments*, vol. 89, 2014.
- [109] H. Huang, F. Zhang, L. J. Hargrove, Z. Dou, D. R. Rogers, and K. B. Englehart, “Continuous Locomotion-Mode Identification for Prosthetic Legs Based on Neuromuscular-Mechanical Fusion,” *IEEE Transactions on Biomedical Engineering*, vol. 58, no. 10, pp. 2867–2875, 2011.
- [110] R. Duda and P. Hart, “Use of the Hough transformation to detect lines and curves in pictures,” *Communications of the ACM*, vol. 15, no. 1, pp. 11–15, 1972.
- [111] G. Csurka, C. R. Dance, L. Fan, J. Willamowski, and C. Bray, “Visual Categorization with Bags of Keypoints,” in *Workshop on Statistical Learning in Computer Vision, ECCV, 2004*, pp. 1–22.
- [112] “Triton Vertical Shock Prosthetic Foot. Instructions for Use,” accessed 14 Sept 2021. [Online]. Available: <https://shop.ottobock.us/media/pdf/647G674-INT-11-1707w.pdf>
- [113] M. Grimmer, J. Zeiss, F. Weigand, G. Zhao, S. Lamm, M. Steil, and A. Heller, “Lower limb joint biomechanics-based identification of gait transitions in between level walking and stair ambulation,” *PLoS One*, vol. 15, no. 9, 2020.
- [114] D. Grimes, W. Flowers, and M. Donath, “Feasibility of an active control scheme for above knee prostheses,” *Journal of Biomechanical Engineering*, vol. 99, pp. 215–221, 1977.
- [115] F. Dadashi, B. Mariani, S. Rochat, C. J. Büla, B. Santos-Eggimann, and K. Aminian, “Gait and Foot Clearance Parameters Obtained Using Shoe-Worn Inertial Sensors in a Large-Population Sample of Older Adults,” *Sensors (Basel)*, vol. 14, no. 1, pp. 443–457, 2013.
- [116] “Genium. Set-up Guide,” accessed 9 Sept 2019. [Online]. Available: <https://shop.ottobock.us/media/pdf/647G868-EN-02-1210w.pdf>
- [117] J. Han, L. Shao, D. Xu, and J. Shotton, “Enhanced Computer Vision With Microsoft Kinect Sensor: A Review,” *IEEE Transactions on Cybernetics*, vol. 43, no. 5, pp. 1318–1334, 2013.
- [118] M. Scudellari, “Self-driving wheelchairs debut in hospitals and airports [News],” *IEEE Spectrum*, vol. 54, no. 10, 2017.
- [119] D. Moloney, B. Barry, R. Richmond, F. Connor, C. Brick, and D. Donohoe, “Myriad 2: Eye of the computational vision storm,” in *2014 IEEE Hot Chips 26 Symposium (HCS)*, 2014, pp. 1–18.
- [120] “CamBoard pico flexx Datasheet,” accessed 26 Sept 2019. [Online]. Available: https://pmdtec.com/picofamily/assets/datasheet/Data-sheet-PMD_RD_Brief_CB_pico_flexx_V0201.pdf

-
- [121] “SoftKinetic DS325 Datasheet,” accessed 26 Sept 2019. [Online]. Available: https://www.sony-depthsensing.com/Portals/0/Download/WEB_20120907_SK_DS325_Datasheet_V2.1.pdf
- [122] C. Zech, A. Hulsmann, M. Schlechtweg, S. Reinold, C. Giers, B. Kleiner, L. Georgi, R. Kahle, K.-F. Becker, and O. Ambacher, “A compact W-band LFMCW radar module with high accuracy and integrated signal processing,” in *2015 European Microwave Conference (EuMC)*, 2015, pp. 554–557.
- [123] U. Schneider, B. Kleiner, H. V. Rosenberg, and B. Budaker, “Aktive Prothesenvorrichtung mit Terrainerfassung und Verfahren zum Steuern einer aktiven Prothesenvorrichtung,” EP2448527B1, May 9, 2012.
- [124] N. St-Onge and A. G. Feldman, “Interjoint coordination in lower limbs during different movements in humans,” *Experimental Brain Research*, vol. 148, no. 2, pp. 139–149, 2003.
- [125] J. L. McGinley, R. Baker, R. Wolfe, and M. E. Morris, “The reliability of three-dimensional kinematic gait measurements: A systematic review,” *Gait Posture*, vol. 29, no. 3, pp. 360–369, 2009.
- [126] S. Page, M. M. Martins, L. Saint-Bauzel, C. P. Santos, and V. Pasqui, “Fast embedded feet pose estimation based on a depth camera for smart walker,” in *2015 IEEE International Conference on Robotics and Automation (ICRA)*, 2015, pp. 4224–4229.
- [127] S. Pasinetti, M. M. Hassan, J. Eberhardt, M. Lancini, F. Docchio, and G. Sansoni, “Performance Analysis of the PMD Camboard Picoflexx Time-of-Flight Camera for Markerless Motion Capture Applications,” *IEEE Transactions on Instrumentation and Measurement*, vol. 68, no. 11, pp. 4456–4471, 2019.
- [128] M. Grimmer, K. Schmidt, J. E. Duarte, L. Neuner, G. Koginov, and R. Riener, “Stance and Swing Detection Based on the Angular Velocity of Lower Limb Segments During Walking,” *Frontiers in Neurobotics*, vol. 13, p. 57, 2019.
- [129] “TDK News Release: Two new high-performance ultrasonic ToF sensors,” accessed 18 Jan 2022. [Online]. Available: https://www.tdk.com/en/news_center/press/20220106_04.html